TARGETING CD4 T CELLS WITH NANOTECHNOLOGY FOR ENHANCED CANCER IMMUNOTHERAPY

by
Ariel Isser

A dissertation submitted to Johns Hopkins University in conformity with the requirements for the degree of Doctor of Philosophy.

Baltimore, Maryland
April 2022

Abstract

Helper ($CD4^+$) T cells are pivotal to immune protection against a wide range of diseases and pathogens. They bridge the innate and adaptive immune systems, recruiting innate immune cells to sites of infection or disease and providing indispensable help signals to B cells and cytotoxic ($CD8^+$) T cells. In addition to their helper roles, they perform a variety of direct therapeutic functions, secreting immunomodulatory cytokines or even directly mediating lysis of diseased cells. Nevertheless, a current lack of synthetic platforms for harnessing antigen-specific $CD4^+$ T cell responses, hinders the widespread adoption of $CD4^+$ T cell-based therapies.

This thesis advances new nanotechnologies and methods to harness $CD4^+$ T cells, toward a variety of immunological applications. The first contribution of this thesis is to demonstrate the manufacturing benefits of $CD4^+$ T cells to enhance *ex vivo* production of $CD8^+$ T cell therapies. While $CD4^+$ T cells were initially believed to detract from production yields, I demonstrated through a series of depletion and addback studies that bystander $CD4^+$ T cells increase the throughput, purity, and yield of antigen-specific $CD8^+$ T cells during nanoparticle-based expansions.

The second contribution of this thesis is to engineer a nanoparticle platform for *ex vivo* $CD4^+$ T cell culture that mimics antigen presenting cells (APC) through display of murine major histocompatibility class II (MHC II) or human leukocyte antigen class II (HLA II) molecules. I demonstrated that MHC II and HLA II artificial APCs (aAPCs) expand cognate murine and human $CD4^+$ T cells, respectively, which uniquely display cytotoxic activity. Moreover, I engineered novel combined MHC I/II aAPCs that simultaneously engage $CD4^+$ and $CD8^+$ T cells, thereby relaying help signals that

enhance the function, memory formation, and antitumor activity of $CD8^+$ T cells. These technologies facilitated discovery of important biophysical parameters for $CD4^+$ T cell binding, activation, and enrichment, specific cues that induce cytotoxic $CD4^+$ T cells, and key helper signals provided by $CD4^+$ T cells to $CD8^+$ T cells.

Primary Adviser and Reader: Jonathan P. Schneck

Reader: Jamie B. Spangler

Thesis Committee

Jonathan P. Schneck, M.D. Ph.D. (primary adviser, *reader)*

Professor, Department of Pathology

Johns Hopkins University School of Medicine

Jamie B. Spangler, Ph.D. (*reader*)

Assistant Professor, Departments of Biomedical Engineering and Chemical &

Biomolecular Engineering

Johns Hopkins University School of Medicine

Jordan J. Green, Ph.D.

Professor, Department of Biomedical Engineering

Johns Hopkins University School of Medicine

Jay H. Bream, Ph.D.

Associate Professor, Department of Molecular Microbiology and Immunology

Johns Hopkins University Bloomberg School of Public Health

Acknowledgements

My grandfather-in-law, a physician who continued to see patients nearly up until the day he tragically passed away, used to say “If you love what you do, you’ll never work a day in your life.” I entered my PhD with a love for science that has, thankfully, not waned, despite the many challenges this process has brought. To be quite honest, I would likely have never received my PhD nor retained my passion for science, if not for the many mentors, peers, mentees, collaborators, colleagues, and family members, who have nurtured me and buoyed me up throughout this arduous journey.

First, I need to thank Dr. Jonathan Schneck for his never-ending support and faith in me. Against both my and Dr. Schneck’s better judgement, I dragged him into a high-risk project that pushed our lab far outside of its comfort zone, forced us to depend on collaborations for materials and samples, and ultimately required so much of my time and attention that I had to forego other mature, lower-risk projects. Along the way, Dr. Schneck has remained supportive, far beyond the call of duty. He has shepherded us through every MTA, NDA, and collaboration with some “dude” I saw somewhere on a paper, ever-patient and open-minded, while at the same time never missing an opportunity to deliver his patent-pending constructive feedback, critical, but in a way that somehow leaves you feeling inspired and empowered. To Dr. Schneck, thank you for fostering my love of science, for teaching me the value of keeping in touch with contacts, no matter how trivial those interactions may be, and for caring about my growth as a person and not just as a scientist.

Second, I would like to thank the members of the Schneck lab, who have contributed to a fun, nurturing, and creative work environment. The Schneck Lab has a

uniquely tight-knit rapport, thanks to Dr. Schneck and our lab “mom”, Joanie Bieler. Joanie has managed to be a scientific role model, a strong advocate and facilitator, and a true friend, all the while keeping the lab from crashing and burning (we’ve certainly had our fair share of close calls). Joanie’s motherly tendencies, in the form of baked goods, cute pictures of grandchildren, and endless enthusiasm for my latest results, have fueled my time in the lab. Thank you to Nkechi Uzoukwu, Sebastian Salathe, and Shannon Storms for supporting Joanie and the rest of the lab. I would be remiss to not mention Norma Stocker, who has held the lab together as well in many ways; she has an uncanny ability to make others feel good about themselves with her unabashed kindness, and I have learned a thesis from her about graciousness and thoughtfulness.

Thank you to all of the graduate students, post-docs, and fellows who have served as mentors. In our short time together, Alyssa Galaro “recruited” me to BME EDGE and taught me to use scientific reason to design projects and tweak protocols. Ami Bessell, the big sister I never had, focused my scatterbrained creative energies, encouraged my “pun”ctilious shenanigans, and taught me everything I know about asking meaningful scientific questions. John Hickey has been a true role model for me and helped jumpstart my research in the Schneck lab. He taught me how to identify and leverage the strengths of collaborators and how to foster the scientific curiosity of students. Bracha Avigdor and Ted Kouo have been a privilege to work with; their impressive experience and unique backgrounds have helped me reexamine my own research from completely different perspectives.

Thank you as well to my peers and mentees in the lab. Pan-am Chaisawangwong has taught me about patience and perseverance; Natalie Livingston

has demonstrated where laser-like focus and determination can get you; Mary Omotoso has been a friend, a proud BME EDGE successor, and a regular source of inspiration (both intellectual and emotional). Shuyi Li has taught me about bravery and dedication; Joseph Choy has forgotten more science as a second year student than I have learned in the last 5+ years and is a fantastic resource for bouncing around ideas; Gary Wang, an ideal collaborator, is destined to become a prominent data scientist; Si-Sim Kang, Niklas Bachmann, Sydney Shannon, and Mara Lanis are all fortunate enough to have both innate scientific talent (far more than I certainly possess) but also a strong desire to learn, grow, and discover. Sam Warner, my first rotation student and “mentorship” guinea pig, possesses a rare combination of resplendent brilliance and endless patience. I look forward to hearing about his many achievements in the years to come. Ashley Chen is resourceful and self-sufficient, requiring minimal guidance to excel. Kayla Gee made my entry into the world of undergraduate mentorship very easy, thanks to her close attention to detail. Emma Elias was a true pleasure to mentor; she is very smart, constantly brimming with energy, and has an illogical reservoir of kindness, all of which will allow her to shine as a clinician. Last, Gohta Aihara is one of the smartest, humblest, and hardest working students I have ever had the privilege to mentor, and most of the time I forget he is still an undergraduate student. I have no doubt that he will one day fulfill his dreams of becoming the CEO of a large pharmaceutical company.

I cannot proceed without thanking the many collaborators who have contributed to my progress throughout my PhD. First, thank you to Dr. Jamie Spangler for taking a gamble on my thesis project and for all of the support. You also provided me with the opportunity to learn from your preeminent postdoctoral student, Elissa Leonard, and to

“mentor” your exceptional graduate students, Mikey Mass, Aliyah Silver, and Monika Kizerwetter, who have each taught me far more than I have taught them. Thank you to Hawley Pruitt for your unwavering belief in my thesis work. You don’t back down from a challenge, which will serve you well in your pursuit of a career in academia. Thank you to Dr. Jeffrey Weber, who, despite being a prominent and exceedingly busy oncologist, has always made time to guide both my scientific and career pursuits. Thank you to Dr. Jordan Green and members of his lab for the years of guidance through often challenging collaborative projects. Thank you to Drs. Tim Chan, Ruhong Zhou, and Kris Sachsenmeier, who have each instilled confidence in me at various stages of my PhD and whom I will forever look up to as scientific role models. Lastly, thank you to Drs. Jonathan Powell and Jay Bream for your never-ending ideas to fully showcase the potential of my research, as members or former members of my thesis committee.

I’d like to thank the BME Department for all of its support, especially from Hong Lan and Drs. Michael Miller, Reza Shadmehr, and Feilim Mac Gabhann. You gave me a very much undeserved admission to this PhD program, which has transformed my life. Moreover, in such a colossal department, with so many competing interests, you made me feel heard, and I am truly grateful. I am also so fortunate to have served on the student group, BME EDGE. Chuck Montague’s harsh “bumper-guarding” but unassailable dedication to his students has completely changed my advocacy skills. Any career successes I achieve will be at least partially thanks to his constant exhortation to let others say “no”. Thank you to Alyssa Galaro for “recruiting” me to EDGE, to Chrissy O’Keefe, Joseph Yu, and David Wilson for encouraging me to stick

around, to my former co-chairs Yuan Rui and Alex Trick for honing my leadership skills, and to Mary Omotoso and Alex Hasnain for adroitly taking on the mantle.

Thank you to my family for all of your support and encouragement throughout my PhD. To my Ima and Abba, brothers David, Yonatan, and Eitan, sisters-in-law, nephews, Sabba and Savta, and extended family, you have been there with me every step of the way, encouraging me to see the light at the end of the tunnel. I have also been fortunate to grow up in the lab, having met, dated, engaged, and married my significant other. In the process, I have gained another fiercely supportive family. To Mark, Jackie, and the rest of the Horowitz family, thank you for taking me in as your own and for exaggerating my accomplishments in the most flattering of ways. You provided me with a home away from home and so much more.

Lastly and most importantly, thank you to my wife Elana for all that you have done and sacrificed for me over the last 6 years. I've put you through two long years of long-distance dating, another four years of living far away from your family, friends, or any other sources of support, and countless working weekends and late-night meetings. It was not an easy adjustment, and it certainly has not been an easy time. And yet, throughout it all, you have been my most ardent supporter. You have encouraged me to gain advocacy and professional development skills, held me to routines that transformed my productivity and health, and encouraged me just about every other day when I have doubted myself or was bummed out about another professional or scientific setback. Thank you, Elana, for putting my needs far ahead of yours for years. You are a living, breathing testament to unconditional love and true dedication.

Table of Contents

List of Tables

List of Figures

Chapter 1. Summary of the Dissertation

The organization of this dissertation is as follows:

Chapter 2 is a literature review of current biomaterial platforms that harness cancer-specific T cell responses. It provides an overview of current clinical approaches to adoptive T cell therapy (ACT), with discussions of how a wide range of *in vitro* and *in vivo* material technologies address existing limitations. This was published in the journal, Biomaterials: Isser, Ariel, Livingston, Natalie K, and Jonathan P. Schneck, “Biomaterials to enhance antigen-specific T cell expansion for cancer immunotherapy.” Biomaterials 268 (2021): 120584.

Chapter 3 is the manuscript: Hickey, J. W. and Isser, Ariel, et al., “Adaptive Nanoparticle Platforms for High Throughput Expansion and Detection of Antigen-Specific T cells.” Nano Lett. 20 (2020): 6289–6298. It describes development of multiplexed and streamlined nanoparticle-based approaches to enrich, expand, and detect murine and human antigen-specific $CD8^+$ T cells, including neoantigens. Critically, it also reveals that the presence of bystander $CD4^+$ T cells enhances the output and throughput of $CD8^+$ T cell expansions, with potential implications for cell therapy manufacturing. It also motivates the rest of the thesis work, which is focused on development of technologies to harness antigen-specific $CD4^+$ T cell responses.

Chapter 4 is an excerpt from the manuscript: Isser, Ariel and Jonathan P. Schneck, “High affinity T cell receptors for adoptive cell transfer.” J. Clin. Invest. 129 (2018): 69–71. It provides a brief overview of the important roles $CD4^+$ T cells play in the cancer immune response.

Chapter 5 is the manuscript: Isser, Ariel, et al., “A Nanoparticle Platform Mobilizes $CD4^+$ T cells for Immunotherapy.” In Review at Nature Communications. The manuscript describes development of the murine Major Histocompatibility class II (MHC II) and analogous Human Leukocyte Antigen class II (HLA II) artificial antigen presenting cells (aAPC). It demonstrates antigen-specific murine and human $CD4^+$ T cell expansion, including rare endogenous subsets. Unlike cells activated through traditional approaches, these aAPC stimulated $CD4^+$ T cells demonstrate lytic activity. The manuscript also describes a novel nanoparticle platform that relays help signals from $CD4^+$ to $CD8^+$ T cells through co-display of MHC I and MHC II molecules. The resultant $CD8^+$ T cells express higher levels of memory markers, are more functional and cytotoxic, and possess enhanced antitumor activity.

Chapter 6 is a summary of my contributions to other projects. This includes the work that I have done with others in the Schneck Lab, as well as in collaboration with Drs. Jeffrey Weber, Jordan Green, and Jamie Spangler. Here, I will summarize the major findings, without providing additional detail or data.

Chapter 7 is a general summary of my chapters and outlines several directions for potential future work.

Chapter 2. Biomaterials to Enhance Antigen-Specific T cell Expansion for Cancer Immunotherapy[1].

2.1 Introduction

Immunotherapy relies on the manipulation of the immune system to induce a potent and durable antigen-specific attack on diseased cells. Most immunotherapies to date have specifically relied on the work of effector T cells, as they accomplish many of the goals set by both personalized medicine[1] and targeted drug delivery[2]. T cells accumulate in the diseased site[3], kill diseased cells with high specificity and efficiency, and potentiate not only responses from other T cells, but from other branches of the immune system as well. In addition, while coordinated immune responses involving both the humoral and cellular arms of the adaptive immune system are important in the response to most infections, diseases such as cancer[4] and the novel SARS-CoV-2[5] specifically require strong T cell responses for lasting immunity. As a result, much work has gone into the development of therapies to replace, induce, or potentiate T cell responses in the treatment of cancer, infectious diseases, and autoimmunity.

Our native T cell repertoire provides safe and efficient protection from a range of infections and malignancies. Even before individuals have gone through puberty, they have approximately $4x10^{11}$ T cells in circulation[6]. Each of these cells has survived positive selection, ensuring the creation of billions of distinct and functional T cell

[1] This chapter is reprinted (adapted) with permission from: “Isser, Ariel, Livingston, Natalie K, and Jonathan P. Schneck. Biomaterials to enhance antigen-specific T cell expansion for cancer immunotherapy. *Biomaterials* 268 (2021): 120584”. Copyright 2020 Elsevier.

receptors (TCRs), and negative selection, which deletes any self-reactive clones. This process results in a repertoire with enough breadth to protect against future unknown pathogens while avoiding overactivity or autoimmunity. However, this system can become dysfunctional for a variety of reasons – from genetics to disease – rendering otherwise potent T cells ineffective. For instance, natural T cell responses can be suppressed in cancer through a wide range of immunoevasive tactics[7].

Strategies to replace or supplement T cell responses have been in development for decades. In this review, we will discuss the importance of biomaterials for bringing existing cellular therapies to the forefront of cancer immunotherapy, with a focus on recent advances in technologies for *ex vivo* and *in vivo* antigen-specific T cell activation and expansion. These technologies are particularly relevant for endogenous T cell therapy (ETC), an approach in which rare, naturally present, tumor-specific T cells are expanded to therapeutic levels from the peripheral blood mononuclear cells (PBMC) of cancer patients[8]. ETC is poised to provide a path toward personalized immunotherapies but comes with many challenges; biomaterials have the potential to alleviate many of these challenges, and in turn, facilitate widescale adoption of ETC. Alternative cellular therapies are also at various stages of clinical use and development. Analogously, these approaches can be further augmented through use of biomaterial platforms for control over the phenotype, function, dosing, and timing of therapeutic T cell administration. The development of biomaterial platforms for these therapies requires an in-depth understanding of T cell biology and careful consideration of design parameters that can allow for rapid expansion and fine control of T cell phenotype and function.

2.2 Endogenous T Cell Therapy: Opportunities, Challenges, and Alternatives

In the natural immune response, disease-specific antigen is taken up by antigen presenting cells (APCs), such as dendritic cells (DCs), at the site of infection or disease. When these antigens are internalized along with pathogen-associated or danger-associated molecular patterns (PAMPs and DAMPs respectively), the DCs are activated and travel to secondary lymphoid organs (SLOs) such as lymph nodes (LNs), in which naïve lymphocytes are concentrated. In the SLO, DCs travel to T cell rich zones and present three essential signals to naïve T cells. The first signal, signal 1, confers specificity in the form of the peptide-MHC (pMHC) complex which binds to the T cell receptor (TCR). The second signal, signal 2, is costimulatory and works to amplify downstream events from the TCR. The third signal, signal 3, is soluble cytokine support, secreted from DCs or other nearby cells to support cell growth and differentiation. Once activated, T cells leave the SLO and travel through systemic circulation until they encounter signals presented at the diseased site. T cells are then cued to extravasate into the tissue where they begin searching for cells expressing the cognate antigen.

The types of T cells that are targeted and their functions, are dependent on the signals they encounter during activation. For signal 1, peptide-loaded major histocompatibility complex I (pMHC I) molecules activate cytotoxic (CD8+) T cells, whose function is primarily to lyse cells infected with intracellular pathogens, whereas pMHC II molecules activate helper (CD4+) T cells, whose function is further specialized based on the cytokines they encounter upon activation. Alternatively, CD3 engagement

is an approach used commonly in the clinic to bypass antigen-specific TCR signaling and activate polyclonal populations of CD4+ and CD8+ T cells[9,10]. T cell memory is also determined early on after activation through several potential mechanisms[11]. The resulting memory state of the T cells determine whether they die off several weeks after initial activation or if they persist in the body for months to years.

Endogenous T cell therapy (ETC) seeks to mimic natural antigen-specific T cell responses *ex vivo* through the enrichment and expansion of rare, circulating tumor-reactive T cells from patients' peripheral blood, followed by reinfusion of large numbers of autologous tumor-specific T cells into cancer patients (**Figure 2-1A**). Enrichment of tumor-specific T cells can be performed in a number of ways, most commonly through fluorescent-activated cell-sorting (FACS) based on T cell binding to cognate, fluorescently-labelled, and multimerized pMHC molecules known as tetramers. Other common approaches include sorting on T cell activation or inhibitory markers, such as PD-1[12,13] or CD137[14], or immunomagnetic bead-based enrichment[15]. Expansion of tumor-specific T cells is most commonly performed using autologous APCs that are either pulsed with tumor-specific peptides or transfected with RNA encoding tumor antigens[15].

2.2.1 Opportunities

Endogenous T cell therapy has much potential as a cancer immunotherapy, as evidence by its clinical use for almost two decades (see ref[8] for a summary of ETC clinical studies). ETC has minimal requirements of clinical grade peptide or RNA and patient PBMCs to produce a cell product, and it can be easily tailored to specific antigens simply by altering which epitope(s) are pulsed onto autologous APCs. Since

only autologous cells are used, this approach presents few regulatory hurdles or complex pipelines, allowing for rapid, ad hoc targeting of patient-specific tumor antigens[8] or even neoantigens[16,17], novel epitopes that result from tumor-specific mutations[18]. The benefit of modularity in this approach is further emphasized by studies which have shown optimal antitumor responses may require simultaneous targeting of multiple tumor antigens[19,20]. Additionally, by targeting naïve T cells, ETC inherently provides flexibility over the memory phenotype of the final T cell product. This is particularly important, as there is significant evidence from mouse models and human clinical trials that less differentiated naïve, stem cell memory, or central memory T cells show significantly greater *in vivo* persistence and antitumor efficacy compared to more differentiated effector memory or terminally differentiated effector cells[21,22]. The resulting T cells tend to be relatively safe, as these endogenous cells have gone through negative selection and therefore are unlikely to cross-react with healthy cells. Patient preconditioning steps for ETC also tend to be relatively safe and can range from no[23,24] to mild lymphodepletion[25] and no[24] to low doses of IL-2[23,25], both common sources of toxicities for other cellular therapies (see section 2.2.3.1)[26]. Lastly, recent studies have shown that receptors inserted into the native TCR locus generate more potent immune responses[27], suggesting that endogenous T cells which inherently signal through their native TCR may generate more effective immune responses compared to most engineered cellular therapies.

2.2.2 Challenges

Replicating or inducing natural T cell immune responses for cancer immunotherapy has been no small feat. Despite significant advancements in T cell

culture systems, several challenges remain that prevent ETC from becoming a first-line therapy.

The identification of appropriate tumor antigens is a critical yet challenging process that must be completed iteratively as each patient has a unique human leukocyte antigen (HLA) phenotype as well as a unique tumor mutanome. Tumor associated antigens (TAAs) or neoantigens may be identified from a biopsy or resected portion of the tumor which is then digested and purified for sequencing of mutations, overexpressed antigens, and HLA expression [28]. For neoantigens, once potential epitopes are uncovered, prediction software is used to determine if the mutated epitopes are capable of being processed and presented on expressed HLA molecules[29]. Tumor specificity and immunogenicity of the resulting pool of targets can then be determined by monitoring T cell responses to peptide or cDNA libraries through a variety of methods including cytokine secretion, activation or inhibitory marker upregulation, or peptide-HLA multimer staining [29] to choose the final epitope(s) to target.

Even when an immunogenic target epitope is found, T cells against that antigen can be very rare in the naïve repertoire, especially for cancer antigens, as the numbers of T cells that recognize overexpressed self-antigen or mutated-antigen are naturally very low[30]. These extremely rare cells must be expanded to large numbers; infused cell products for ACT can be up to 10^{11} cells[16,31] to confer clinical benefit. The 4-5 weeks long culture that is required to reach these cell numbers[8,32] can often lead to T cell exhaustion due to overstimulation[33].

T cell therapy is traditionally an autologous cell therapy, meaning that patient to patient variability not only affects the response to the treatment but also the production

of the treatment. Variability in the precursor frequencies and phenotype of patient T cells, as well as the availability and function of patient antigen presenting cells, can have a significant impact on T cell expansion and resulting function. Patient age, disease status, co-infections, and drug usage all affect the outcome of the T cell product.

The autologous nature of ETC also has impacts on manufacturing, as personalized cellular products face challenges such as lack of quality control markers and high cost. The length of time in manufacturing facilities, resources required for expansion, transport of cells between facilities and hospitals, as well as any necessary sequencing of patient samples to determine the proper T cell treatment all contribute to the cost of ETC. Prices may fall as technology improves, but currently the cost excludes many patients from benefiting ETC, and even for patients who can afford it, it is still not offered as a first- or second-line treatment.

2.2.3 Alternatives

Several additional approaches to ACT have been developed including polyclonal expansion of Tumor Infiltrating Lymphocytes (TIL) (**Figure 2-1B**), and genetic engineering host cells to express antitumor TCRs or CARs (**Figure 2-1C**).

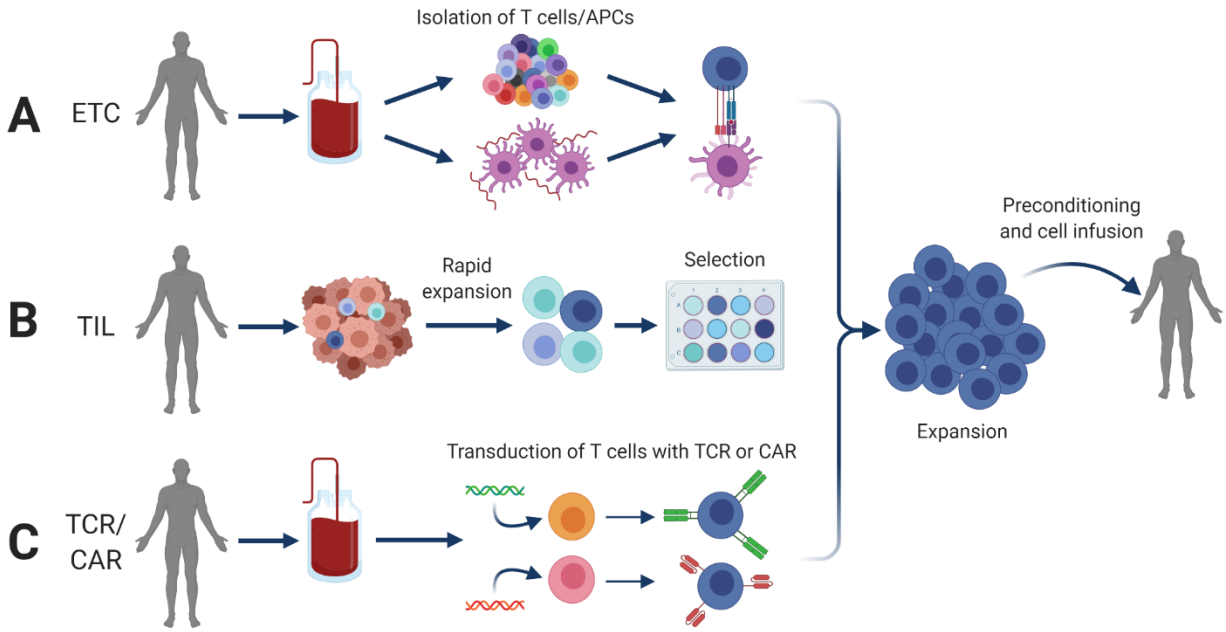

Figure 2-1. Protocols of T cell production for (A) ETC, (B) TIL, and (C) TCR/CAR T therapies.(A) For ETC, T cells and APCs are isolated from patient-sourced PBMCs. APCs are engineered to express the antigen of interest, then incubated with T cells to expand tumor-specific T cells. (B) TILs may be isolated from an excised tumor and rapidly expanded with IL-2. Tumor-reactive T cells from this pool are then selected for longer term expansion. (C) T cells for TCR and CAR T therapies are derived from patient-sourced PBMCs. T cells are transduced with genes for a tumor specific TCR or CAR, then expanded to large numbers. Created with BioRender.com.

2.2.3.1 TIL Therapy

TIL therapy, one of the earliest forms of ACT, involves isolating lymphocytes that have infiltrated the stroma of patient tumors and expanding them on irradiated allogeneic feeder layers for 5-6 weeks in the presence of an αCD3 antibody and IL-2[31]. TIL provide a source of T cells that are naturally enriched for tumor-reactivity, in comparison to PBMC[31]. The approach has shown tremendous promise as a therapy for metastatic melanoma[34] and has since been refined to include chemotherapy-based lymphodepletion immediately prior to TIL transfer[35] to improve the persistence of adoptively transferred cells, resulting in objective response rates and complete tumor regression in up to 72% and 40% of patients, respectively[36]. Despite these impressive clinical results, TIL therapy suffers from several drawbacks. Tumor-reactive TIL have

only been successfully expanded from melanoma tumors[31] limiting the applicability of this therapy to other forms of cancer. Even for melanoma, there can be wide variations in the success of expanding patient TIL[37]. The necessary preconditioning steps, including lymphodepletion and high doses of IL-2 post adoptive transfer, are associated with harsh toxicities and thus require close monitoring of patients[26]. Furthermore, the process of activating TIL, which traditionally requires 5-6 week *ex vivo* cultures with irradiated feeder cells and complex rounds of selection for cultures that show antitumor activity[31], is not easily amenable to large-scale translation. TIL also often exhibit a terminally differentiated, exhausted phenotype with impaired effector function, limiting their therapeutic efficacy[38–41].

2.2.3.2 TCR and CAR-T Immunotherapies

TCR and CAR T cell immunotherapies have been developed to widen the range of targetable cancers and produce more “off-the-shelf” alternatives to ACT. In these therapies, a patient’s endogenous T cells are genetically reprogrammed to recognize tumor antigens either through an engineered alpha-beta TCR or through a CAR, which contains an extracellular antigen-binding domain that resembles the variable region of an antibody and an intracellular signaling domain for T cell activation and co-stimulation[42]. The transduced cells are then isolated and expanded for several weeks before being reinfused into the patient. A single TCR or CAR construct can be used to treat many patients with the cognate tumor antigen. In fact, CAR T cell therapies bypass HLA restrictions, so they can treat any tumors with the target antigen and maintain therapeutic efficacy even for tumors that develop defects in antigen processing and presentation[43]. However, CAR T cell therapies are limited to surface expressed

antigens[18], while TCR therapies can target intracellular antigens presented on HLA molecules.

While the scalability of these technologies has provided tremendous translational potential, these therapies are associated with several life-threatening complications. First, CAR T cell therapies, in particular, can lead to excessive release of cytokines that require careful medical management in specialized facilities[44]. Secondly, numerous clinical trials have resulted in severe on-target off-tumor toxicities because these high affinity, exogenous receptors have not gone through negative selection[45,46] and are thus more prone than endogenous T cells to attack healthy cells that express low levels of antigen or cross-reactive epitopes[47–50]. Clinical success at minimizing toxicities by targeting tumor antigens that are only otherwise present on nonessential healthy cells have been seen for a variety of hematological malignancies[51–53]; however, an analogous approach has proven elusive for solid tumors, as many tumor-specific antigens are either expressed at levels that are too low on tumor cells or are also present on healthy cells[31]. Neoantigens are promising targets for TCR immunotherapy as they are only present on tumor cells; however, personalized neoantigen-specific TCR therapies are currently too expensive and cumbersome for widespread clinical use[54]. To further complicate matters, patients may require TCRs or CARs specific to multiple tumor antigens for optimal tumor control, as single-antigen targeting can result in escape of antigen-loss variants, especially for solid tumors[55–58]. Several recent publications have identified pan-cancer TCRs[59,60] and CAR T targets[61] which may prove to be universal cancer immunotherapies for solid tumors.

Additionally, the high affinity nature of current TCR or CAR T immunotherapies raise concerns of chronic antigen stimulation that can lead to T cell exhaustion and hyporesponsiveness[4,62]. There is ongoing work to reduce exhaustion and improve persistence of CAR T cell therapies either by including additional costimulatory domains[63,64], knocking out inhibitory molecules[65] and transcription factors[62,66], or even using lower affinity CARs[67].

2.2.3.3 Biomaterials for Antigen-specific T cell Expansion

As engineered cellular therapies continue to address current limitations of T cell-based therapies, biomaterials that can expand antigen-specific T cells also have an opportunity to play significant roles in the advancement of cancer immunotherapy (**Table 2-1**). First, they could present a path forward for ETC therapies, by providing a scalable means of identifying and targeting a patient's unique tumor-specific T cells with "off-the-shelf" platforms. One of the main barriers to personalized immunotherapies is that current clinical approaches to identification and expansion of endogenous tumor-specific T cells rely on autologous antigen presenting cells, such as monocyte derived dendritic cells (moDCs)[16,24,68]. While T cells expanded by moDCs have shown clinical efficacy[24], DC-based T cell expansion is limited by availability[69], potential dysfunction[70,71], and complex manufacturing of autologous DCs. In contrast, "off-the-shelf" and relatively inexpensive biomaterials can stably and reproducibly present all the necessary cues for T cell activation and co-stimulation. These platforms can also be modularly designed to accommodate a range of tumor antigens across multiple HLA types, providing a facile manner of identifying and targeting patient-specific tumor antigens or neoantigens[72]. Second, biomaterial-based platforms can augment existing

cancer immunotherapies by enhancing the persistence, phenotype, and function of transferred cells. In contrast to moDCs, which provide limited control over the signals T cells encounter during activation, biomaterial shape, size, stiffness, porosity, and biodegradability as well as the organization, dose, and composition of ligands and soluble factors can each have profound effects on T cell expansion, function, and phenotype[73], and be precisely tuned for optimal T cell stimulation. This in turn can allow for greater consistency in final ETC, TCR, or CAR T cell products. The flexibility and control offered by biomaterials is especially important, as the field of cancer immunotherapy continues to discover more about the most ideal targets and T cell phenotypes for achieving therapeutic responses. By example, while it has been known that cytokine secretion alone does not predict cytotoxic T cell killing ability and by extension potential clinical efficacy[74], the precise mechanisms of cytotoxic T cell killing through thrombospondin-1 dependent supramolecular attack particles were only discovered recently, motivating future biomaterial approaches that target this pathway to specifically enhance cytotoxicity[75]. Furthermore, biomaterial platforms for T cell expansion can allow for control of the dosing, timing, and localization of ETC, CAR, or TCR therapies *in vivo* to maintain antitumor immune responses and maximize their efficacy, while minimizing the risks of off-target toxicities, T cell exhaustion, or immune escape. The dynamics and localization of T cell therapies can be controlled *in vivo* by targeting specific cells such as T cells or dendritic cells, specific sites such as lymph nodes or the tumor, or specific external stimuli to control the timing of immune responses. Finally, biomaterials that can sufficiently activate and direct T cell immune responses *in vivo* could drastically streamline production processes for antigen-specific

T cell therapies. In the next two sections, we will discuss the progress that has been made as well as the specific design parameter considerations for biomaterial platforms used for *ex vivo* and *in vivo* antigen-specific T cell activation and modulation. Tables of representative biomaterials platforms for antigen-specific T cell expansion can be found in references [76–78].

Table 2-1. Summary of advantages and limitations of existing immunotherapies and how biomaterials can help overcome those limitations.

Cellular Therapy	Advantages	Limitations	Examples of How Biomaterials Can Help
ETC	Ease of personalization	HLA restricted	Adaptive aAPCs allow for simple screening of tumor antigen immunogenicity[72]
	Minimal regulatory hurdles	Complexity of identifying antigens	aAPCs[79,80] and APC-ms[81] can rapidly expand highly functional T cells from very low precursor frequencies
	Can target neoantigens	Rarity of cells	aAPCs can eliminate variability of moDC function through stable antigen-presentation on particles or scaffolds[79]
	Control over memory phenotype	Difficult to expand to therapeutic levels	Easy and inexpensive GMP production of synthetic platforms[82]
	Safe	Long culture period	
	Mild Preconditioning	Patient Variability	
	Native TCR signaling	Manufacturing Challenges	
		Cost of Treatment	
TIL	Personalized to a patient's tumor antigens or neoantigens	HLA restricted	aAPCs[79,80] and APC-ms[81] can allow for a more rapid culture period
	Enrichment of tumor-reactive T cells	Limited, mostly to melanoma	Local delivery and sustained release of T cells from scaffolds can reduce length of culture period by requiring fewer cells for therapeutic efficacy[83,84]
	Streamlined screening for tumor immunogenicity	Patient variability	aAPCs can be designed to reverse T cell exhaustion[85]
	Native TCR signaling	Harsh preconditioning steps	Easy and inexpensive GMP production of synthetic platforms[82]
		Long culture period	
		Exhausted phenotype and reduced effector function	
		Cost of treatment	
TCR	Scalable	HLA restricted	Targeted *in vivo* vaccination can maintain TCR-transduced cells
	Short culture period	Difficult to personalize	

	Can recognize intracellular antigens, such as neoantigens High affinity response Control over memory phenotype	Overstimulation can lead to exhaustion On-target, off-tumor toxicities Cost of Treatment	within the therapeutic window to reduce toxicities[54,61] Conjugation of particles with soluble factors to cells can allow controlled delivery of immunomodulatory factors to the tumor[86]
CAR T	Scalable Short culture period Not HLA restricted High affinity response Control over memory phenotype	Restricted to surface-expressed antigens Difficult to personalize Overstimulation can lead to exhaustion Cytokine-related toxicities On-target, off-tumor toxicities Cost of Treatment	Targeted *in vivo* vaccination can maintain CAR-transduced cells within the therapeutic window to reduce toxicities[54,61] Conjugation of particles with soluble factors to cells can allow controlled delivery of immunomodulatory factors to the tumor[86]

aAPCs, artificial antigen presenting cells; *APC-ms,* antigen presenting cell mimetic scaffold; *CAR,* chimeric antigen receptor; *ETC,* endogenous T cell*; GMP,* good manufacturing practices; *moDC,* monocyte derived dendritic cell; *TCR,* T cell receptor; *TIL,* tumor infiltrating lymphocyte.

2.3 *Ex Vivo* Biomaterial Platforms for Antigen-Specific T cell Activation

Much of the progress in understanding critical design parameters for T cell activation in the last 40 years has come from biomaterial-based technologies for *ex vivo* T cell expansion. In contrast to cell-based approaches for T cell expansion, these technologies provide reductionist systems to directly and independently observe how material properties, dosing, and choice of ligands and soluble factors each modulate T cell proliferation, function, and phenotype. *Ex vivo* technologies for T cell stimulation are in some ways simpler and, in others, more complex to design than *in vivo* technologies.

On the one hand, *ex vivo* platforms do not require tuning of physical or biochemical properties to meet biocompatibility requirements, to enhance *in vivo* biodistribution, or to allow for organ or cell-specific targeting; on the other hand, these technologies generally aim to replace and not simply augment or modify the function of endogenous APCs and thus, may require optimization of a large number of design parameters to show similar if not improved efficacy compared to endogenous APCs.

The most fundamental requirements for antigen-specific T cell stimulation by professional APCs include recognition through interaction between a TCR and its cognate pMHC (signal 1), co-stimulation most fundamentally through CD28 on T cells and B7.1/2 (signal 2) on antigen-presenting cells, and soluble factors known as cytokines (signal 3), which direct T cell fate and lineage[82]. In addition to the composition of these signals, the mechanical forces they transmit, their density and dose, and their spatial organization all affect T cell activation. Initial T cell activation does not only require binding of TCR to its cognate pMHC, but also the specific mechanotransduction that occurs due to this interaction[87–89]; this means that even high affinity TCR-pMHC binding events can occur without leading to T cell activation[89]. Upon initial activation, TCRs which are pre-clustered on naïve T cells into 35-70 nm nanoislands[90] begin to coalesce into microscale clusters and eventually form the central portion of an immunological synapse with an APC[91]. The cytoskeletal dynamics associated with formation of the immunological synapse exert mechanical forces at the T cell-APC interface[91]. Moreover, immobilization of intracellular cell adhesion molecule 1 (ICAM-1) on APCs during the formation of the immunological synapse is necessary for mechanically activating the integrin lymphocyte function associated antigen-1 (LFA-1)

on T cells[92]. The cytoskeletal reorganization and mechanical forces that occur at the T cell-APC interface have implications on the arrangement and density of signals as well as the mechanical properties of biomaterials that can lead to robust T cell stimulation. Thus, a wide range of APC-mimetic biomaterials have been developed to recapitulate these fundamental properties for efficient *ex vivo* T cell stimulation.

Biomaterials for antigen-specific T cell stimulation have been studied using particle and scaffold-based platforms (**Figure 2-2A,B**). Both modalities offer flexibility of ligand choice and density, with particles more closely mimicking endogenous APCs and allowing for control over the curvature of interaction with T cells, and scaffolds enabling easier and more precise ways to pattern signaling molecules and tune biophysical properties such as stiffness and porosity. As dendritic cell (DC) based T cell stimulation requires at the bare minimum signal 1 and 2 within a specific cytokine milieu, APC-mimetic particles and scaffolds minimally present pMHC and either B7.1/2 or an agonistic αCD28 monoclonal antibody[82]. Beyond those minimal requirements, each modality has its unique design considerations for antigen-specific T cell stimulation.

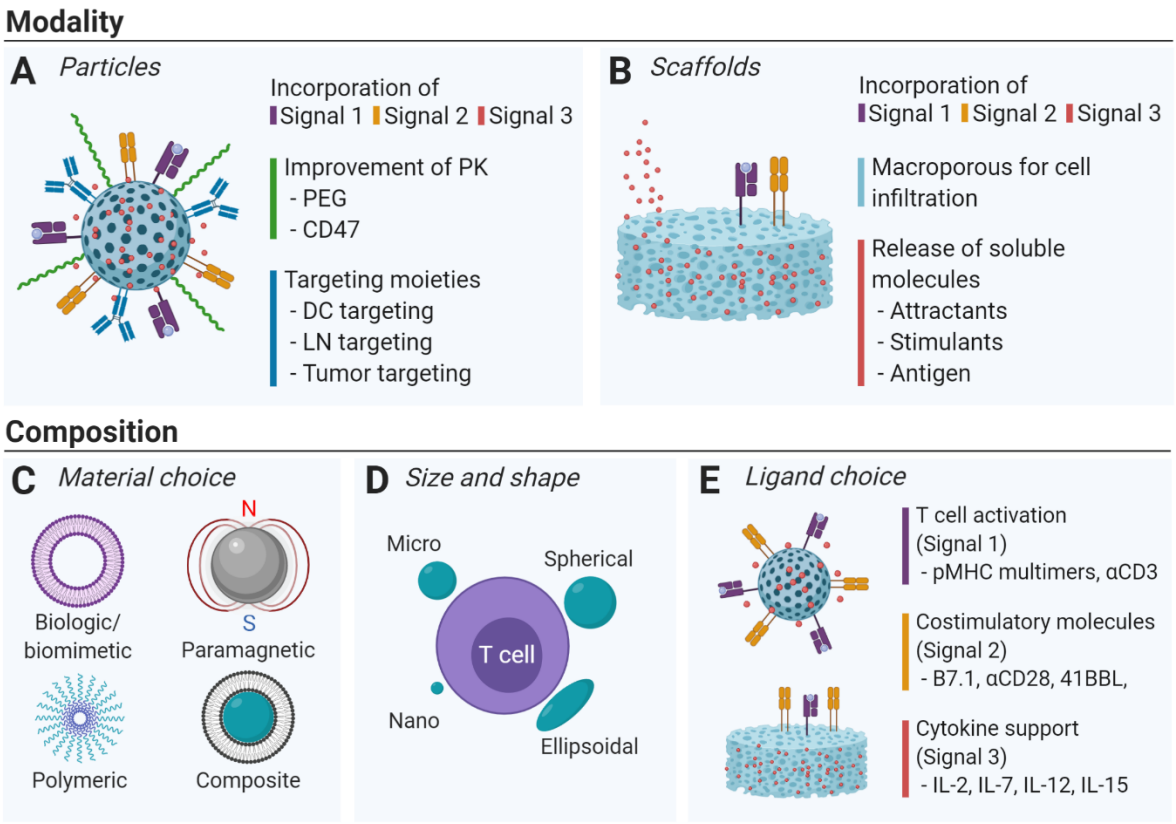

Figure 2-2. Overview of design considerations for T cell stimulating platforms. Stimulating signals may be delivered either via particles (A) or scaffolds (B). Each modality has unique interactions with T cells and with the body that influence design parameters. With both modalities, material choice (C), size and shape (D), and choice of ligands (E) all have significant effects on T cell activation, both ex vivo and in vivo. PK, pharmacokinetics. Created with BioRender.com.

2.3.1 Particles

Particles used for antigen-specific T cell stimulation are often referred to as artificial antigen presenting cells (aAPCs). Beyond the minimal requirements of presenting signals 1 and 2, the major design considerations for aAPCs include material, size and shape, and ligand choice (**Figure 2-2C-E**).

2.3.1.1 Materials

The materials which have been used for aAPCs have ranged from biomimetic or biological such as liposomes or cell membranes, to inorganic such as iron oxide or carbon nanotubes, to polymeric such as polystyrene or poly(lactic-co-glycolic acid)

(PLGA), or some combination thereof (**Figure 2-2C**). Material choice can play an integral role in determining the function of aAPCs, as it can impact particle properties such as membrane fluidity, nanoscale organization of ligands, stability, stiffness, degradability, surface area, ease of encapsulation of soluble factors, and responsiveness to magnetic fields.

Some of the first aAPCs were developed over 40 years ago, using phospholipid membranes reconstituted with cell-derived MHC molecules to induce cytotoxic T cell responses[93,94]. Liposomal aAPCs, like cell membranes, form dynamic lipid bilayers that can provide fluidity in interacting with T cells, in contrast to inorganic or polymeric particles that are rigid and therefore have constrained orientations of T cell signaling molecules bound to their surface[95]. In addition, the lateral mobility of liposomal aAPCs, especially at higher temperatures such as 37°C, can allow for migration of pMHC molecules and costimulatory ligands towards the site of formation of the immunological synapse[96], in a manner akin to endogenous T cell-APC interactions. Lipid formulations can also allow for formation of microdomains containing pre-clustered T cell ligands, mimicking the microdomains of pMHC molecules found on APCs[97]. Several studies have shown that liposomes which contain these regions of pre-clustered T cell ligands more potently stimulate T cells than liposomes with randomly distributed signaling ligands[98,99]. Capitalizing upon these findings, one group directly isolated the lipid rafts of pre-clustered MHC molecules from DCs and reconstituted them onto liposomes to form RAFTsomes[100]. Not only did these RAFTsomes lead to cytokine secretion and antigen-specific T cell proliferation *in vitro* but they also led to tumor protection in an *in vivo* immunization model[100].

Despite these benefits, liposomes tend to have lower stability than polymeric or inorganic materials and may have stiffnesses that are too low to provide the necessary mechanical cues for T cell stimulation. This has led some groups to pursue composite materials, known as supported lipid bilayers, that contain a polymeric or inorganic core surrounded by a lipid outer membrane. Some of the earliest work examining the ability of supported lipid bilayers to stimulate cytotoxic T cell responses against tumor antigens involved production of large multivalent immunogens formed through the incorporation of tumor cell plasma membrane vesicles onto silica or latex microspheres[101]. These initial studies found that the composite particles led to improved cytotoxicity against tumor antigens and significant reduction in tumor growth for several syngeneic tumor models, whereas tumor-derived liposomes had no effect on cytotoxicity or tumor growth[101]. Since these reports, several other groups have pursued analogous approaches for generating tumor-specific T cell responses using 100-200 nm supported lipid bilayers composed of a PLGA core and a cell membrane coating derived from unmodified tumor cells[102], tumor cells genetically modified to express the costimulatory molecule B7.1[103], or mature dendritic cells pulsed with tumor lysate[104]. These approaches have shown promising results both *in vitro* and *in vivo* and may provide an "off-the-shelf" antigen-agnostic approach of generating personalized tumor-specific immunotherapies.

Other commonly used materials for aAPCs are inorganic, such as iron oxide. Iron oxide microparticles have been used extensively for expansion of antigen-specific CD4+ and CD8+ T cells in both humans[95,105] and mice[106]. Clinically, they are an attractive platform for stimulating T cells for ACT, as the particles can be easily removed using a

magnet prior to infusion[82,107]. Nanoscale iron oxide aAPCs can additionally be used to enhance T cell activation by driving aggregation of aAPCs on the surface of T cells with a magnetic field[108,109]. This approach leads to enhanced TCR clustering and much greater antigen-specific CD8+ T cell expansion *ex vivo*, as well as improved antitumor efficacy *in vivo*[108]. More recently, nanoscale iron oxide aAPCs have been used to simultaneously enrich and expand rare, endogenous antigen-specific CD8+ T cells[79,80,110]. aAPCs are first incubated with a diverse population of endogenous T cells to allow rare, cognate T cells to bind to aAPCs. Next, bound T cells are enriched using a magnet, depleting non-cognate T cells and simultaneously clustering TCRs on rare cognate cells to enhance their activation[80]. Not only does this process of enrichment and expansion result in a higher frequency of antigen-specific T cells, but it also improves the expansion of cognate cells compared to aAPC-based stimulation without enrichment[79,80]. In turn, this approach allows for identification of putative neoantigens from murine tumor models, as well as greater than 1000-fold expansion of antigen-specific murine and human T cells in one week[80]. Despite this rapid expansion, which can often lead to exhaustion, endogenous tumor-specific T cells expanded with this approach showed impressive antitumor responses *in vivo*[80]. Enrichment and expansion has also been applied to melanoma patients from various immunotherapy trials and has resulted in up to 1000-fold expansion of Melanoma Antigen Recognized by T cells 1 (MART-1) tumor-specific CD8+ T cells over two weeks[79]. Even after this rapid expansion, these MART-1 CD8+ T cells displayed a predominantly “stem-like” phenotype and were highly functional based on cytokine release and cytotoxicity assays[79].

The magnetic properties of iron oxide nanoparticles have also been used to produce more modular approaches to antigen-specific T cell expansion, allowing for greater control over the phenotype and specificity of the expanded cells. For instance, signal 1 and 2 can be displayed by separate nanoparticles and then co-localized on the surface of T cells using magnetic clustering[85]. This approach can allow for the dosing and composition of signal 1 and a range of signal 2s to be varied independently of each other, allowing for rapid prototyping of an array of aAPC designs to skew toward a specific memory phenotype or to optimize T cell expansion[85] (**Figure 2-3A**). Furthermore, as naïve T cells constitutively express CD28[111], enrichment with signal 1 only particles can reduce nonspecific binding of non-cognate cells, leading to a purer enriched fraction that can subsequently be expanded through co-clustering of signal 1 and 2[85]. The magnetic properties of iron oxide aAPCs have also been utilized to produce high throughput platforms for enrichment and expansion of a range of T cell specificities[72]. In this setting, an adaptive aAPC conjugated with unloaded MHC molecules and αCD28 can be surface loaded with a range of peptides and then washed using a 96-well plate magnet, to parallelize production of aAPCs targeting a variety of T cell specificities (**Figure 2-3B**). T cells can be incubated with batches of these particles in a 96-well plate, enriched, and expanded, to allow for much wider screens of endogenous antigen-specific T cell responses in cancer immunotherapy, autoimmunity, and infectious diseases[72].

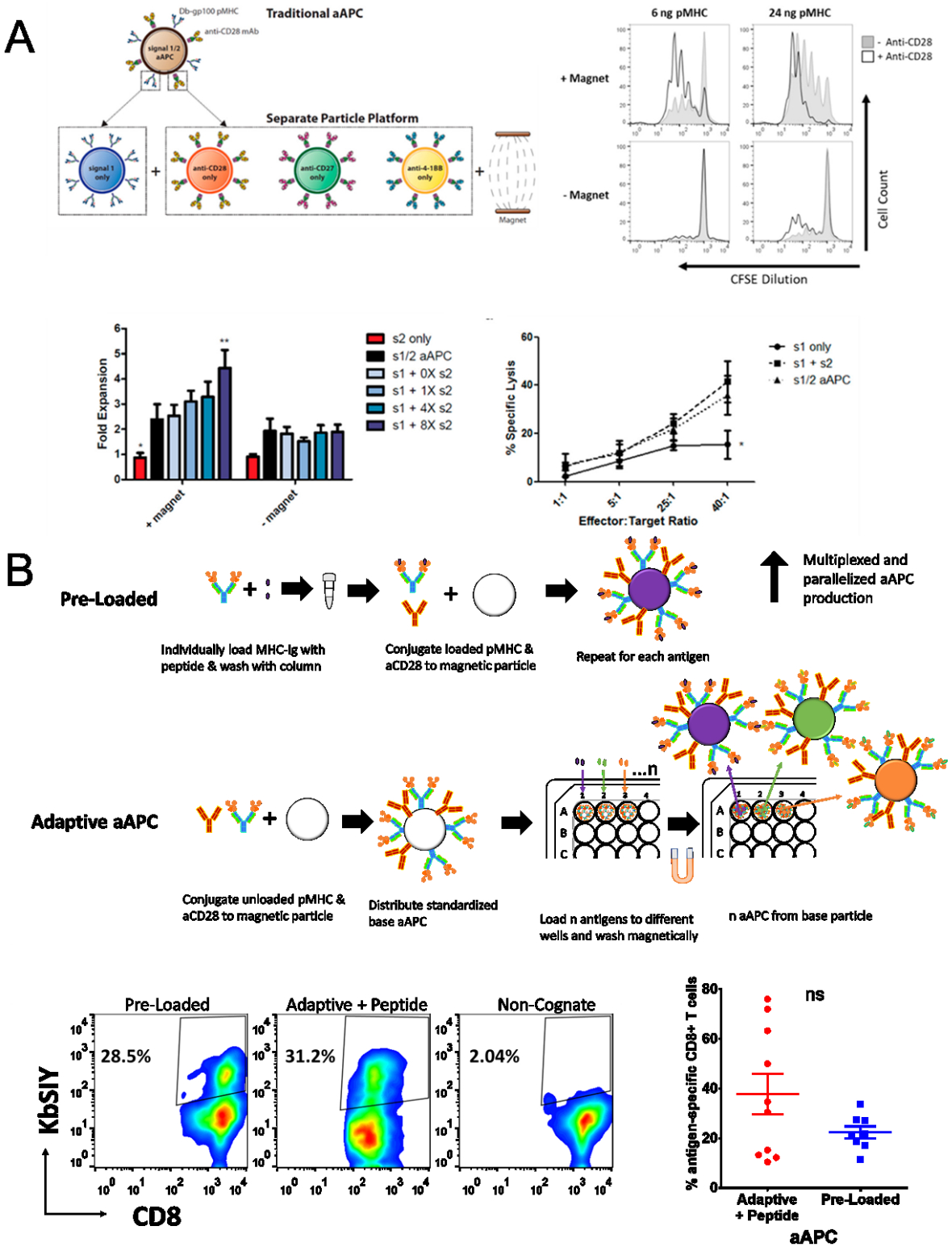

Figure 2-3. Examples of modular nanoparticle platforms for custom T cell expansion. (A) Magnetic field clustering of nanoparticles allows for separation of signal 1 and 2 to allow a wide range of ratios and combinations of signal 2s to be studied for T cell activation. (B) Plate magnets and adaptive aAPCs allow for high throughput expansion and screening of antigen-specific T cells. (A) Reprinted with permission from Kosmides, A. K., Necochea, K., Hickey, J. W. & Schneck, J. P. Separating T Cell Targeting

Components onto Magnetically Clustered Nanoparticles Boosts Activation. *Nano Lett.* 18, (2018), Copyright (2020) American Chemical Society. (B) Reprinted with permission from Hickey, J. W. *et al.* Adaptive Nanoparticle Platforms for High Throughput Expansion and Detection of Antigen-Specific T cells. *Nano Lett.* (2020). doi:10.1021/acs.nanolett.0c01511, Copyright (2020) American Chemical Society.

Carbon nanotubes are another inorganic material that has been studied for both polyclonal and antigen-specific expansion of CD8+ T cells[112,113]. Some of the advantages offered by carbon nanotubes include their clustering of signaling ligands due to their unique topography, as well as their high surface area and aspect ratio, resulting in increased multi-avidity interactions and contact with T cells[112]. In addition to conjugating signal 1 and 2 to carbon nanotube aAPCs, one study also conjugated PLGA nanoparticles loaded with IL-2 and magnetite to the nanotube, allowing for local delivery of IL-2 for enhanced *ex vivo* T cell stimulation, as well as a means of magnetically removing particles prior to adoptive transfer of T cells[112]. These composite aAPCs enhanced long-term *ex vivo* expansion of murine and human antigen-specific CD8+ T cells and delayed tumor growth in a mouse melanoma adoptive transfer model.

A variety of polymeric materials have also been used to produce aAPCs. Due to their widespread use, ease of coating, and biocompatibility, polystyrene microspheres were used commonly in the initial production of fully synthetic aAPCs[114–118]. The flexibility of size and control over ligand composition and density using polystyrene microparticles provided some of the first insights into optimal particle-based stimulation of T cells (see sections 2.3.1.2 and 2.3.1.3). PLGA aAPCs have also been explored, due to their *in vivo* biocompatibility as well as some unique properties that enable efficient *ex vivo* T cell stimulation. Since they are formed through emulsion techniques and are biodegradable, they can be used to encapsulate and slowly release soluble signals such as cytokines. A number of studies have used this property to design

aAPCs that mimic endogenous APCs in providing paracrine delivery of IL-2 when aAPCs bind to and activate cognate T cells[112,119,120]. These studies found that paracrine release of IL-2 was significantly more potent at activating antigen-specific murine and human CD8+ T cells than similar concentrations of bulk IL-2[119]. PLGA particles are also plastic, allowing them to be reshaped to alter their surface contact with CD8+ T cells[121,122].

The range of materials explored for *ex vivo* antigen-specific T cell expansion reflect the various aspects of endogenous T cell-APC interactions that researchers have sought to recapitulate synthetically. For instance, liposomes, iron oxide, and PLGA particles can each provide control over the T cell-aAPC interface in distinct manners. Liposomes mimic endogenous T cell-APC interactions through their membrane fluidity and incorporation of microdomains with pre-clustered stimulatory signals, iron oxide particles can use an external magnetic field to allow for nanoscale clustering of TCRs bound to aAPCs, and PLGA particles can be stretched to tune the number of available ligands at the T cell-aAPC interface.

The various formulations also need to satisfy important criteria for translation of aAPC technologies to the clinic, such as shelf-life, safety, and flexibility in tuning T cell specificity and optimizing T cell function for personalized cancer immunotherapies. In terms of scalability, liposomal formulations tend to be less stable and more difficult to manufacture than iron oxide or PLGA particles, somewhat hindering their “off-the-shelf” potential. In terms of biocompatibility, liposomes and PLGA aAPCs are biodegradable and safe for *in vivo* administration, whereas less is known about the *in vivo* biocompatibility of iron oxide particles[123]. On the other hand, several pre-clinical[112] and

clinical[9] studies have successfully removed iron oxide particles prior to adoptive cell transfer using an external magnet. With regards to control over T cell specificity, liposomal aAPCs can be targeted towards tumor antigens by sourcing lipid bilayers from the cell membranes of a patient's tumor cells or dendritic cells pulsed with tumor lysate. These approaches are appealing in their efforts to provide an antigen-agnostic but patient-specific cancer immunotherapy; however, they also introduce risks such as inadvertent expansion of T cell specific to antigens that are also present on healthy cells. In contrast, iron oxide aAPCs can provide control over T cell specificity through surface-loading of tumor-specific peptides and magnetic enrichment and expansion of T cells specific to these tumor antigens. This process is more labor-intensive than the antigen-agnostic approach provided by liposomes, but it is nonetheless amenable to high-throughput screens[72]; it is also safer and easier to monitor, as the T cell specificities in this case are known. Lastly, in terms of control over function and phenotype, liposomal and polymeric aAPCs present only the costimulatory molecules that were initially conjugated to their surface, whereas a range of T cell costimulatory molecules, combinations, and ratios can be co-clustered with iron oxide aAPCs within an external magnetic field[85]. On the other hand, the biodegradability of liposomes and PLGA aAPCs allows for encapsulation and paracrine release of a variety of soluble factors such as IL-2 that are vital for T cell survival, function, and phenotype.

2.3.1.2 Size and Shape

The size and shape of aAPCs can have a significant impact on T cell activation by altering the particle-cell surface contact area and, in turn, the avidity of TCR-pMHC interactions[110] (**Figure 2-2D**). Initial studies examining the effect of aAPC size on T cell

activation found that large, 4-5 μm, cell-sized polystyrene microspheres led to greater T cell stimulation than aAPCs below 4 μm[114]. These results, along with the observation that higher doses of smaller or less dense aAPCs could not rescue T cell activation, suggested that T cell activation required large contiguous regions of TCR ligation, and did not depend solely on the total number of TCR-pMHC interactions[114]. These results were corroborated in later studies with biodegradable aAPCs, that showed 8 μm microparticles led to significantly greater activation of antigen-specific CD8+ T cells than 130 nm nanoparticles[119]. That said, later studies with 30-100 nm magnetic and quantum-dot based aAPCs showed that saturating doses of low or high density nanoparticles could lead to robust antigen-specific murine and human CD8+ T cell proliferation *in vitro*[124]. Mechanistic studies varying both size and ligand density of magnetic aAPCs found that 50 nm aAPCs led to lower antigen-specific T cell stimulation at similar densities of signal and doses of total protein, compared to larger 300 nm, 600 nm, or 4.5 μm aAPCs, which each performed comparably[109]. However, the suboptimal stimulation with 50 nm particles could be overcome at saturating doses. Interestingly, as in previous studies[124], the density of signal on 50 nm aAPCs did not affect T cell stimulation at similar total doses of protein, suggesting that these smaller aAPCs had monovalent or divalent interactions with T cells. Indeed, a simple calculation showed that larger 5 μm microparticles could have up to 200 bioavailable ligands at the T cell-aAPC interface, whereas 50 nm nanoparticles may have as few as one or two, due to their significantly higher degree of local curvature[109]. In contrast to the results with 50 nm particles, T cell stimulation with particles 300 nm or larger, showed a dependency on ligand density, requiring a ligand spacing below 100 nm for robust T cell

activation[109]. Taken together, these results show a requirement for multivalent interactions between T cells and aAPCs when the particle footprint becomes large enough to otherwise preclude sufficient receptor occupancy within TCR nano-islands. Interestingly, a later study showed that even below 50 nm, pMHC-coated nanoparticles for activating antigen-specific CD4+ and CD8+ T cells depended on ligand density. The study found an agonistic threshold for T cell activation at an inter-pMHC distance of 17 nm[125], which corresponds roughly to the width of the TCR complex[126]. However, the nanoparticles used in this study did not have a costimulatory molecule conjugated to their surface, which may affect the minimum valency requirements for T cell triggering.

Another approach that has been used to modulate the contact area at the T cell-aAPC interface is changing the shape of the aAPC (**Figure 2-2D**). In one study, ellipsoidal PLGA microparticles were formed by stretching spherical PLGA microparticles to aspect ratios of up to 6.6[121]. The group found that stretched particles led to increased T cell expansion across a range of total antigen doses and ligand densities, compared to spherical particles. These differences were heightened at low doses of total protein and correlated with increased binding and contact area between stretched aAPCs and T cells[121]. A follow-up study with 200 nm nanoscale PLGA aAPCs similarly found that ellipsoidal aAPCs led to increased T cell proliferation *in vitro*, indicating the importance of the geometry of the T cell-aAPC interface even at the nanoscale[122].

2.3.1.3 Ligand Choice

Another parameter that can affect aAPC function is the choice of ligands to include. As mentioned previously, the most basic signals attached to an aAPC include

signal 1, which activates T cells, and signal 2, a costimulatory molecule (Fig. 2E). Signal 1 can be a pMHC molecule or an αCD3 antibody for antigen-specific or polyclonal T cell activation, respectively. Classically, agonistic αCD28 antibodies or B7.1 molecules have been used as signal 2[82]. However, a wide range of costimulatory molecules with immunomodulatory effects on T cell effector function, survival, and memory formation, have been characterized[127]. Many of these molecules, such as CD27, OX40, CD40L, 4-1BB, ICOS, and GITR[128,129], have been targeted directly with agonistic antibodies to stimulate T cell responses for cancer immunotherapy. The differential effects of co-stimulation through these molecules provide ample opportunity to design aAPCs that can elicit customized T cell responses. As an example, CD27 co-stimulation has been shown to produce short-lived but highly functional effector CD8+ T cells, whereas 4-1BB agonism can generate persistent memory cells[130]. In order to improve T cell survival and effector function, co-stimulation through 4-1BB has also been included as part of the TIL rapid expansion protocol[131].

Moreover, certain combinations of co-stimulatory molecules have been shown to have synergistic effects on T cell proliferation. For instance, co-stimulation of 4-1BB and OX40[132] has been shown to profoundly increase CD8+ T cell expansion. Several studies have applied these findings to produce more functional cellular aAPCs by using multiple co-stimulatory molecules[133,134]. Likewise, the ratios of these costimulatory molecules can affect T cell proliferation and function as well. For instance, one study with polystyrene microsphere aAPCs shows that a 3:1 ratio of αCD28 to α4-1BB could lead to up to five-fold higher frequencies of antigen-specific CD8+ T cells after several rounds of stimulation, compared to other ratios[135]. As discussed previously, another

study in which signal 1 and 2 were attached to separate magnetic nanoparticles and then co-clustered with a magnetic field allowed for rapid comparisons of different ratios of co-stimulation with αCD28, α4-1BB, and αCD27[85]. This study confirmed that a 3:1 ratio of αCD28 to α4-1BB particles led to increased proliferation and memory formation. Finally, a recent publication produced 11-molecule PLGA microparticle aAPCs, consisting of two MHC molecules, three costimulatory molecules, a CD47-Fc molecule for improved *in vivo* retention, and five encapsulated cytokines, chemokines, and antibodies[136]. The aAPCs showed significant expansion of endogenous tumor-specific CD8+ T cells both *ex vivo* and *in vivo* and inhibited tumor growth in a mouse melanoma model[136].

2.3.2 Scaffolds

While there have been fewer scaffolds reported for *ex vivo* expansion of antigen-specific T cells than particles, many parameters such as patterning and spacing of signaling ligands as well as material stiffness have been gleaned from studies with pMHC or αCD3 coated scaffolds.

2.3.2.1 Patterning of Signaling Ligands

One of the first studies showing how patterned surfaces could be used to study T cell activation used electron-beam lithography to produce micron sized grids on silica substrates and then patterned the support with lipid bilayers containing pMHC and ICAM-1 molecules[137]. The constraints imposed by these grids restricted ligand mobility and, in turn, prevented centralized TCR clustering and formation of immunological synapses. Analogous results were found using photolithography techniques to produce arrays of immobilized αCD3 and ICAM-1 molecules in various spatial arrangements.

The study found that αCD3 needed to be arranged into focal, as opposed to annular, patterns to enable T cells to proliferate and secrete cytokines[138]. Later studies that incorporated αCD28 onto these APC-like arrays through multiple rounds of microcontact printing demonstrated that T cells could sense both the microscale distance between and orientation of signal 1 and 2[139,140].

Several studies have also used patterned surfaces to investigate the role of ligand density in T cell activation. A common technique used in these studies is known as block copolymer micellar nanolithography[141], which can produce arrays of gold nanoparticles with nanoscale control over interparticle distance. The arrays of gold nanoparticles can then be conjugated with signal 1 to produce surfaces with controlled ligand densities[142,143]. These studies demonstrated that αCD3-based T cell activation required interparticle spacing below 60 nm[142,143], in line with the previously mentioned study that varied ligand densities on nanoparticle-based aAPCs[109]. A more recent study has used electron beam lithography on glass coverslips to allow for patterning of αCD3 and ICAM-1 onto gold-palladium nanoparticle arrays with defined intermolecular distances[144]. Some of the arrays underwent an additional etching step to produce raised 10 nm glass pedestals. Thus, these arrays allowed for precise axial and lateral positioning of αCD3 molecules. By increasing the intermembrane distance between T cells and the activating surface, the glass pedestals allowed free diffusion of CD45 phosphatases during TCR engagement, thus inhibiting a critical component of T cell activation, CD45 exclusion[145]. In turn, arrays with raised glass pedestals had different requirements for lateral spacing of signals, compared to planar arrays[144], motivating

further study of the three-dimensional patterning and spacing requirements for T cell activation.

2.3.2.2 Stiffness

Several studies have used materials with tunable bulk stiffnesses to understand the role of mechanotransduction during T cell activation. Poly(acrylamide)[146,147] or poly(dimethylsiloxane)[148] gels were produced with stiffnesses ranging from as low as 0.5 kPa to as high as 2 MPa by altering the amount of crosslinker present during formation of the gels. Gels were conjugated with αCD3 and αCD28 to activate T cells, and consistently across each of these studies, it was found that 100 kPa gels optimally stimulated T cells. Interestingly, one of the studies found through RNA microarray analysis that T cell transcriptional profiles show a graded response to substrate stiffness in the presence of CD3-based stimulation[147] (**Figure 2-4A**). Furthermore, the study found that T cells secrete cytokines across a range of stiffnesses; however, only T cells on the stiffest substrates used for this study (100 kPa) became metabolically active and began cell cycle progression[147]. In turn, T cells showed the greatest proliferation after 72 hours on the stiffest substrates[147]. The importance of stiffness in modulating T cell activation has also been shown with antigen-pulsed APCs seeded onto two and three-dimensional alginate scaffolds[149]. Analogous to these previous studies, for both two-dimensional and three-dimensional gels, stiffer 40 kPa scaffolds led to better T cell activation, proliferation, and function than softer 4 kPa scaffolds[149]. Moreover, the stiffer gels led to a significant increase in the size of immune synapses (**Figure 2-4B**).

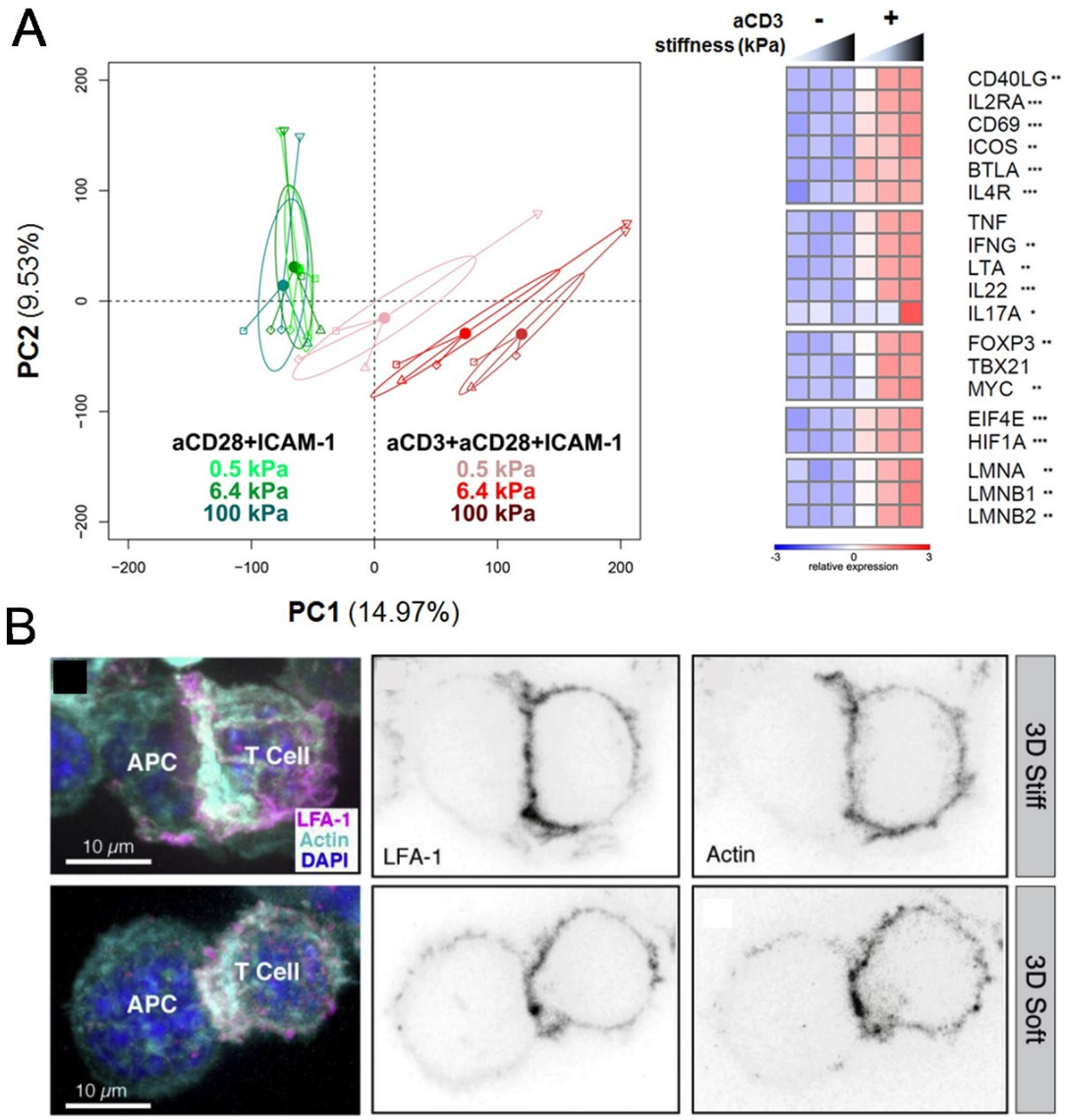

Figure 2-4. Substrate stiffness of T cell activating surfaces modulates T cell transcriptional profiled and immune synapse formation.(A) In the presence of αCD3, T cells show a graded transcriptional response to substrate stiffness. (B) Stiffness of three-dimensional substrates modulates size of immune synapses between T cells and APCs, with stiffer substrates leading to larger synapses. (A) Reprinted with permission from Saitakis, M. et al. Different TCR-induced T lymphocyte responses are potentiated by stiffness with variable sensitivity. Elife 6, e23190 (2017) under the Creative Commons Attribution License (B) Reprinted from Majedi, F. S. et al. T-cell activation is modulated by the 3D mechanical microenvironment. Biomaterials 252, 120058 (2020), Copyright (2020), with permission from Elsevier.

2.3.2.3 Applications for Cancer Immunotherapy

The findings above have been invaluable to the understanding of T cell biology and how to better create substrates for the activation of tumor-specific T cells for adoptive immunotherapy. One study synthesized a hydrogel from hyaluronic acid, a

common component of the extracellular matrix (ECM), and conjugated it with pMHC and αCD28 to form an artificial T cell stimulating matrix (aTM) for antigen-specific T cell stimulation[150]. The study investigated the effects of stiffness, ligand density, and a variety of ECM proteins on T cell proliferation, function, and phenotype. Interestingly, in contrast to some of the studies previously mentioned, this study found that softer 0.5 kPa gels led to significantly greater proliferation, function, and CD3 cluster formation than stiffer 3 kPa gels. Moreover, culturing T cells on the aTM led to an increase in expansion and polyfunctionality of endogenous antigen-specific CD8+ T cells, compared to culturing T cells on a tissue culture plate or a blank hydrogel in the presence of magnetic nano-aAPCs. Similarly, endogenous T cells expanded on the aTM and adoptively transferred into tumor-bearing mice significantly slowed tumor growth and increased mouse survival, compared to T cells stimulated with nano-aAPCs on a tissue culture plate. Another study produced a composite APC mimetic scaffold (APC-ms) by forming a supported lipid bilayer with T cell signaling cues on high-aspect ratio mesoporous silica micro-rods (MSRs)[81]. The MSRs were pre-loaded with IL-2, coated with liposomes, and then conjugated with signal 1 and 2 for T cell stimulation. *In vitro*, the MSRs self-assembled into a three-dimensional scaffold with high enough porosity to allow for cell infiltration. T cells cultured with the APC-ms formed denser clusters with the MSRs than with traditional aAPC microbeads, due in part to both the larger size (70 μm vs 4.5 μm) and higher aspect ratio of the MSRs. Moreover, paracrine release of IL-2 from the MSRs was shown to be more potent at T cell stimulation than adding the same amount of bulk IL-2, as in previous studies[112,119]. This platform was shown to be more effective than aAPC microbeads for polyclonal expansion of primary

T cells or tumor-specific CAR T cells. Similarly, the platform outperformed moDCs for expansion of rare antigen-specific CD8+ T cells. CAR T cells expanded with APC-ms showed similar antitumor efficacy compared to CAR T cells expanded with aAPC microbeads. Together, the results from these two studies show promise for future clinical studies using artificial scaffolds to expand patient-specific CD8+ T cells for ACT.

2.4 *In Vivo* Biomaterial Platforms for Antigen-Specific T cell Activation

As researchers have developed increasingly better particles and substrates for T cell activation that are efficient and avoid off-target activation, there has been a growing interest in using these materials to directly activate T cells *in vivo*. Biomaterial-based technologies for *in vivo* T cell activation are an attractive option to alleviate many of the challenges associated with adoptive cell transfer. Avoiding the *ex vivo* T cell culture step drastically lowers cost, time-to-treatment, and exhaustion of cells due to long culture periods. *In vivo* antigen-specific CD8+ T cell activation is a relatively new venture in T cell therapy, yet the field has generated a lot of interest and is propelling forward with several active clinical trials[151,152].

In vivo T cell activation strategies can broadly be divided into two categories: vaccines and direct T cell activation. Vaccines work by activating host APCs, which in turn activate host T cells (**Figure 2-5A,B**). Direct T cell activation bypasses host APCs by recruiting, directly binding to, and activating host T cells (**Figure 2-5C,D**). Each of these categories is largely approached with the use of either particle- or scaffold-based platforms. Particles typically travel via circulation or lymphatics and activate either DCs

or T cells in the periphery or in the lymph node (**Figure 2-5A,C**). Scaffolds are typically injected or implanted subcutaneously and act either through the release of soluble activating molecules to activate nearby cells or through recruitment of cells into the scaffold itself for activation through direct contact (**Figure 2-5B,D**).

General design considerations for injectable biomaterial-based particles and scaffolds have been reviewed extensively[153–155]. To summarize, particles and scaffolds must be biocompatible, biodegradable, and display favorable pharmacokinetics. Biomaterial scaffolds must also have a porous structure, be easily injectable, and avoid foreign body responses. These properties may be inherent to the chosen material or may be engineered. Biomaterials have been utilized *in vivo* to treat cancer for decades, mostly for drug delivery. Platforms specifically for T cell activation share some considerations with drug delivery vehicles, such as targeting distinct organs and cell types, but also have their own unique considerations.

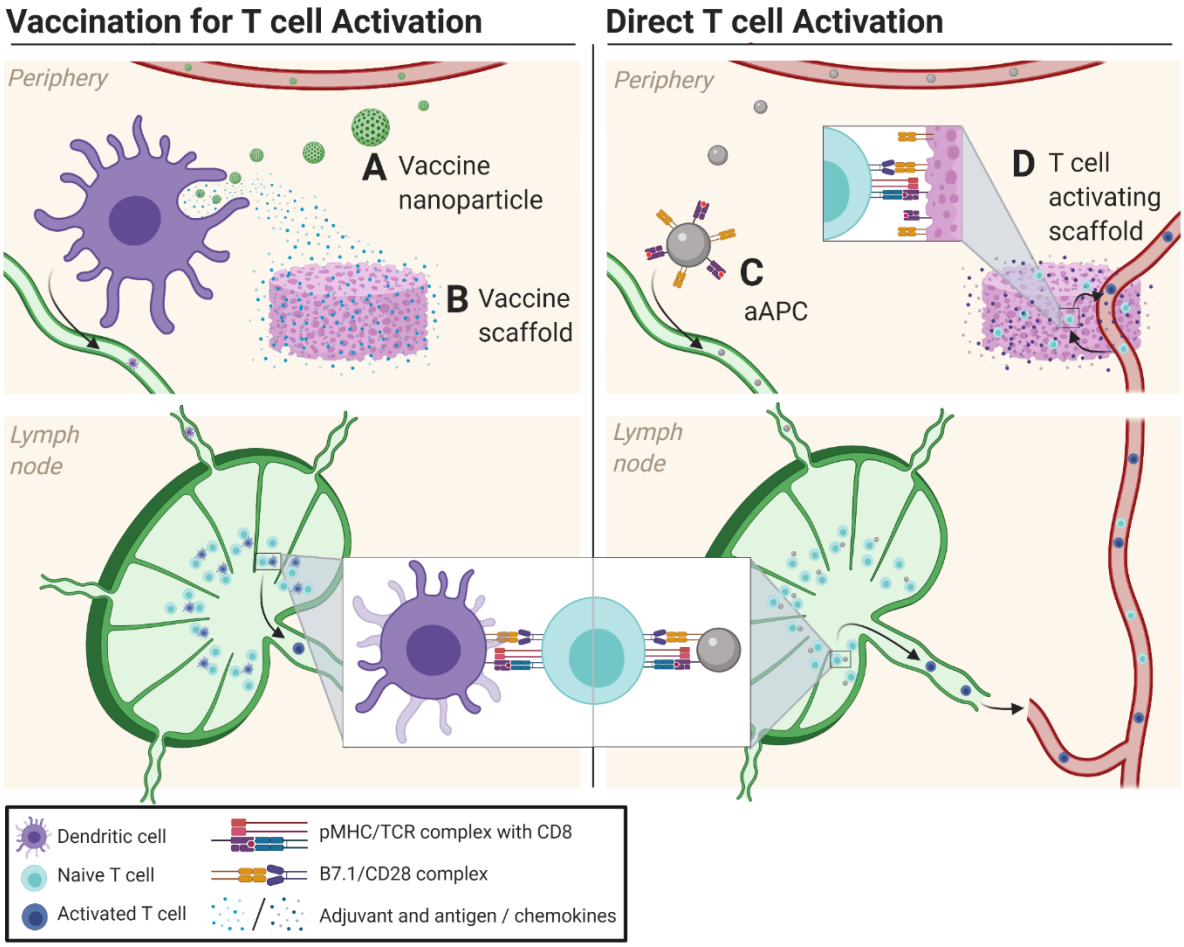

Figure 2-5. Methods for *in vivo* activation of antigen-specific T cells.(A) Vaccine particles may be injected subcutaneously or intravenously and either taken up by DCs in the periphery or travel directly to the LN where they interact with DCs. From the periphery, activated DCs will travel to T cell zones of the LN to activate cognate naïve T cells. (B) Vaccine scaffolds are typically injected or implanted subcutaneously with antigen and adjuvant encapsulated for slow release. The scaffold may either activate local tissue resident DCs or may actively recruit DCs via chemoattractants. Activated DCs leave the scaffold and travel to the LN for T cell activation. (C) aAPCs for direct T cell activation may be injected intravenously or subcutaneously. Intravenously injected particles may drain to the spleen, while subcutaneously injected particles may drain via lymphatics into the lymph node. Once in secondary lymphoid organs, particles can directly interact with and activate T cells. (D) Scaffolds for direct T cell activation are injected or implanted subcutaneously and have encapsulated or conjugated T cell stimulating molecules. Scaffolds, infused with chemokines, attract naïve T cells from systemic circulation. T cells are activated within or on the surface of the scaffold, then travel back into systemic circulation. After T cells have entered systemic circulation, they can travel to the site of infection or cancer via endogenous mechanisms to kill cells expressing the target antigen. Created with BioRender.com.

2.4.1 Vaccines

Vaccines are arguably the oldest and most successful form of immune engineering[156]. Since the first vaccine – cowpox, by Edward Jenner – numerous

pathogens have been successfully controlled by vaccines. The first vaccine for cancer can be traced to the end of the 19th century. Dr. William Coley came across a case of a patient whose malignant tumor receded after developing cellulitis, a bacterial skin infection[157]. He began treating his cancer patients with streptococcal organisms, "Coley's Toxin", in his first attempts at a therapeutic cancer vaccine[157]. Coley's results were eventually deemed irreproducible, but they sparked interest in the development of an effective, reproducible cancer vaccine.

At a minimum, vaccines must include an antigen to direct the specificity of the immune response and an adjuvant to activate the immune response. Initial vaccines typically injected these components as separate entities in one mixture. For most diseases, these early vaccines induced strong antibody development, which was enough to neutralize pathogens. However, a strong CD8+ T cell response is harder to elicit, yet necessary for cancer treatment[158]. Since vaccine components are delivered extracellularly, the antigen is by default loaded onto MHC class II molecules, stimulating CD4+ helper cells which in turn support B cell growth and maturation. CD4+ T cells are also known to support CD8+ T cell growth and differentiation, but CD8+ cells must first be activated by DCs presenting MHC class I. The process of uninfected DCs loading antigen onto MHC class I is referred to as cross-presentation, and it is often a central component of cancer vaccine design. CD4+ T cells are also thought to be necessary for anti-cancer efficacy of vaccines[159], but as MHC class II loading is the default loading pathway for exogenous antigen, it is often not necessary to add extra design considerations for eliciting CD4+ T cell responses.

Biomaterials have been invaluable to the field of vaccine development as they can not only improve trafficking of vaccine components *in vivo*, but they have been shown to induce cross-presentation of antigen by DCs. Biomaterial-based vaccine composition, delivery route, modality, timing, and dose have all been shown to have a strong impact on T cell activation, as discussed below[160,161].

2.4.1.1 Particle-based vaccines

Particle-based vaccines are designed to deliver antigen and adjuvant directly to antigen presenting cells, most commonly DCs. As mentioned, the particle must promote cross-presentation of the antigen onto MHC class I molecules in order to activate CD8+ T cells. Vaccine nanoparticles for T cell activation must be efficiently internalized by DCs, rather than other phagocytic cells which are inefficient at cross-presentation. Once taken up, the particles must release antigen and trigger DC maturation and activation. Intervention in each of these steps can be accomplished with the design of biomaterial-based vaccine carriers.

To target cross-presentation pathways, many vaccines are designed to enhance direct delivery of vaccine particles to DCs[162]. In the periphery, DCs constitutively uptake molecules through non-specific macropinocytosis and receptor-mediated endocytosis in order to survey the environment[163]. Vaccine particles less than 50 nm are internalized via macropinocytosis whereas particles larger than 500 nm are internalized via receptor-mediated pathways[162]. Passive targeting of DC uptake can be achieved through modulation of particle material, size, shape, and surface charge[164–167]. Active targeting can be achieved by directing the particles towards receptors involved in receptor-mediated endocytosis. For example, mannose and fructose moieties can interact with

membrane-bound lectins on DCs, which are involved with phagocytosis[168]. Several vaccine particles take advantage of this pathway by coating the particle surface with mannose and mannose-mimicking molecules[169–171]. Other endocytic receptors on DCs, such as DEC-205, DC-SIGN, Clec9A, DNGR-1, and Fc receptors[166,172–177], have also been targeted. However, Clec9A, DNGR-1, and DEC205 seem to be particular effective at promoting cross-presentation through endosomal pathways [176,178–180]. More complex platforms can also be designed to deliver and release vaccine components at critical moments during uptake by DCs, such as during endosomal escape, to enhance cross-presentation efficiency[162,181,182].

The two DC subtypes that are most adept at cross-presentation of antigens are CD103+ and CD8+ DCs[183]. CD103+ DCs largely reside in nonlymphoid tissue, and the above DC targeting methods can be used to increase vaccine accumulation in these DCs. Targeting these populations is made easier by the fact that they exist throughout the body, in mucosal surfaces, the skin, and the lungs primarily. However, an alternative approach is to target CD8+ DCs, which reside in lymphoid tissue. In the spleen, these cells are located in the marginal zone or the red pulp, making them easily accessible to circulating particles. In the lymph node, CD8+ DCs have been found to line the subcapsular sinus along with macrophages[184] and are therefore the first cells that vaccine particles may interact with upon reaching the lymph node. In addition to high concentrations of CD8+ DCs being accessible to circulating particles, DCs in lymphoid tissue have the added benefit of already being in close proximity to T cells. Properties of biomaterials to enhance lymphatic drainage to the LN have been reviewed extensively[185]. Particle size, shape, charge, hydrophobicity, rigidity, and targeting

ligands all have significant effects on not only LN drainage but also retention, which directly affects the T cell response[161]. Beyond modifying these particle surface properties, unique biomaterials designs can enhance vaccine particle delivery even further. One approach involves so-called “albumin hitchhiking”, linking vaccine cargo to albumin, which has been shown to efficiently drain to lymph nodes[54,186]. One barrier to efficient delivery to LNs is the differing size requirements for each stage of transport. Particles between 25 and 100 nm demonstrate enhanced direct lymphatic drainage; however, once in the LN, only particles less than 70kDa (~5nm) can penetrate deeply into the LN into T cell zones[185]. To overcome these opposing design considerations, one group has developed a multistage delivery platform[187]. The vaccine particles, which are 27 nm, preferentially drain through the lymphatics as they are too large for free diffusion through the vascular endothelial layer[188]. The individual vaccine components within the particles are initially sequestered within the nanoparticle by linkage to larger molecules. The linker degrades in the approximate time that it takes for the particles to reach the LN, allowing for the vaccine components to be released from the nanoparticle and passively diffuse into the interior of the LN[187]. Another recent study has shown that clodronate-mediated depletion of subcapsular sinus macrophages, the main barrier to the LN interior, can improve vaccine accumulation[189]. However, this method has only been tested for its effects on inducing a humoral response rather than a T cell response.

To efficiently facilitate activation and cross-presentation, it is important that DCs receive both components of the vaccine – antigen and adjuvant – simultaneously in order to avoid a tolerizing effect[190]. One group has avoided premature release of vaccine components with a pH switch[191]. The pH switch helps circumvent burst release

and minimizes off-target effects. However, again, the real barrier that has plagued cancer vaccines is the lack of systems that can effectively promote cross-presentation. In the most common pathway of cross-presentation, exogenous antigen is phagocytosed or otherwise internalized, then can escape from the phagosome into the cytosol where it follows traditional loading onto MHC I in the ER [181,192]. Cytosolic exportation from the phagosome or endosome is a key mechanism through which vaccines may induce cross-presentation. Indeed, methods to induce endosomal rupture upon vaccine particle uptake have shown robust results[181]. Another popular approach is the use of liposomal carriers, which may fuse with the endosome membrane to release antigen into the cytosol[181]. Most notably, the RNA-Lipoplex system has shown robust T cell responses for cancer[61,152]. In this system, liposomes carrying RNA encoding tumor antigens were targeted to DCs throughout the body by altering the lipid composition to obtain a net positive charge on the liposome surface, leading to efficient uptake and expression of the target antigen on DCs and subsequent activation of effector T cells. This platform is currently in clinical trials for malignant melanoma[152]. More recent studies are working to elucidate how details of the particle synthesis affect antigen-specific responses. For example, one study has shown that both the peptide modifications and crosslinking chemistry used to encapsulate antigen affect DC maturation and T cell activation[193]; this study along with future mechanistic studies will be vital to the optimization of cancer vaccines.

2.4.1.2 Vaccine Scaffolds

Despite advancements, vaccine particles still struggle to overcome barriers such as efficient delivery to DCs and retention of vaccine components in cell-rich areas like

lymph nodes[194]. An alternative approach is to inject or implant a biomaterial scaffold that will attract peripheral DCs to the implant site for activation. This approach may also allow for single-shot vaccines, a highly coveted standard of vaccination, as it can provide controlled and sustained release of its components. In addition to providing the two critical components of a vaccine, antigen and adjuvant, vaccine scaffolds must also release a DC attractant to enhance cell infiltration from the periphery (**Figure 2-2B**). Activated DCs must then leave the scaffold to travel to the LN as they would after being activated endogenously.

The first step in the vaccine scaffold approach is recruitment of naïve DCs to the site. This has most commonly been accomplished using cytokine granulocyte–macrophage colony-stimulating factor (GM-CSF)[194–197]. Inclusion of a cell adhesion motif such as Arg-Gly-Asp (RGD) has also been shown to help recruit and retain DCs[198]. Vaccine scaffolds may be used solely as a depot for the release of adjuvant and antigen, but more recent designs are macroporous or otherwise assembled in such a way that allows the entry of immune cells into the scaffold, where they may access cytokines and other vaccine components. The pore size required for cell infiltration makes encapsulating small vaccine components challenging. One approach to address this issue is to create dual-porous scaffolds. For example, cryogelation may be used to create the large pores required for cell influx, while the base gel component maintains a smaller pore size that allows for sustained release of encapsulated components[196]. Another dual-porosity approach is to take advantage of self-assembling structures like mesoporous silica rods[195,198]. The rods themselves have pore sizes for small-molecule loading, while *in vitro* and *in vivo* they spontaneously assemble into structures that

maintain large enough pore sizes for immune cell infiltration. Finally, researchers have combined scaffolds and particles to ensure sustained delivery of vaccines (**Figure 2-6A**)[197,199]. In this study, MSRs carrying GM-CSF are loaded with mesoporous silica nanoparticles (MSNs) that contain with antigen (OVA) and adjuvant (Toll-like receptor 9 agonist). This approach takes advantage of the benefits of nanoparticle vaccines – controlled, simultaneous delivery of vaccine components into phagocytic cells – while improving on the limitations of particles by allowing them to activate cells efficiently in the periphery. While this study uses OVA as a model antigen, like many *in vivo* platforms to date, the technology is highly modular and can theoretically be adapted for loading of TAAs or neoantigens. Using defined antigens such as these has the benefit of being both personalizable and predictable. However, TAAs are only relevant for patients whose tumors express them at high enough levels and neoantigens can be challenging and time consuming to discover. Multiple antigens must also be targeted simultaneously to more effectively treat highly heterogeneous tumors. As an alternative, many studies have attempted to use tumor cell lysate in cancer vaccines[200], with several recent reports of clinical efficacy [201,202]. Vaccine scaffolds using tumor lysate have also shown efficacy with limited toxicities for a range of mouse tumor models [196,203,204], and one such scaffold is currently in Phase I clinical trials[205]. However, the approach of targeting undefined antigens *in vivo* carries a risk of inadvertently expanding autoreactive T cells, without the ability to pre-screen for self-reactivity of the expanded T cells, as is done with *ex vivo* expansions. As a result, extensive characterization of the T cell response in humans will be necessary for translation.

While vaccine adjuvants may be loaded into the structures described above, the biomaterial itself may also act as an adjuvant. For example, it has been shown that mesoporous silica has adjuvant properties by stimulating pattern recognition receptors (PRRs)[195,198]. Other biomaterials may increase in immunogenicity as degradation occurs, such as poly(beta-amino ester) (PBAE), as the material experiences changes in surface properties, size, and shape[206]. In addition to the material having inherent adjuvant activity, it is also possible to modify surface properties of the material, such as charge, to increase immunogenicity[207].

Vaccines are an attractive approach for stimulating an antigen-specific T cell response as they avoid the difficulty of expanding rare T cell clones *ex vivo*. Several biomaterial-based cancer vaccines are currently in clinical trials, summaries of which can be found in references [208] and [209]. However, despite advances, it is still challenging to elicit a cellular response from vaccines. Furthermore, cancer patients often have dysfunctional DCs[210], rendering vaccine approaches ineffective.

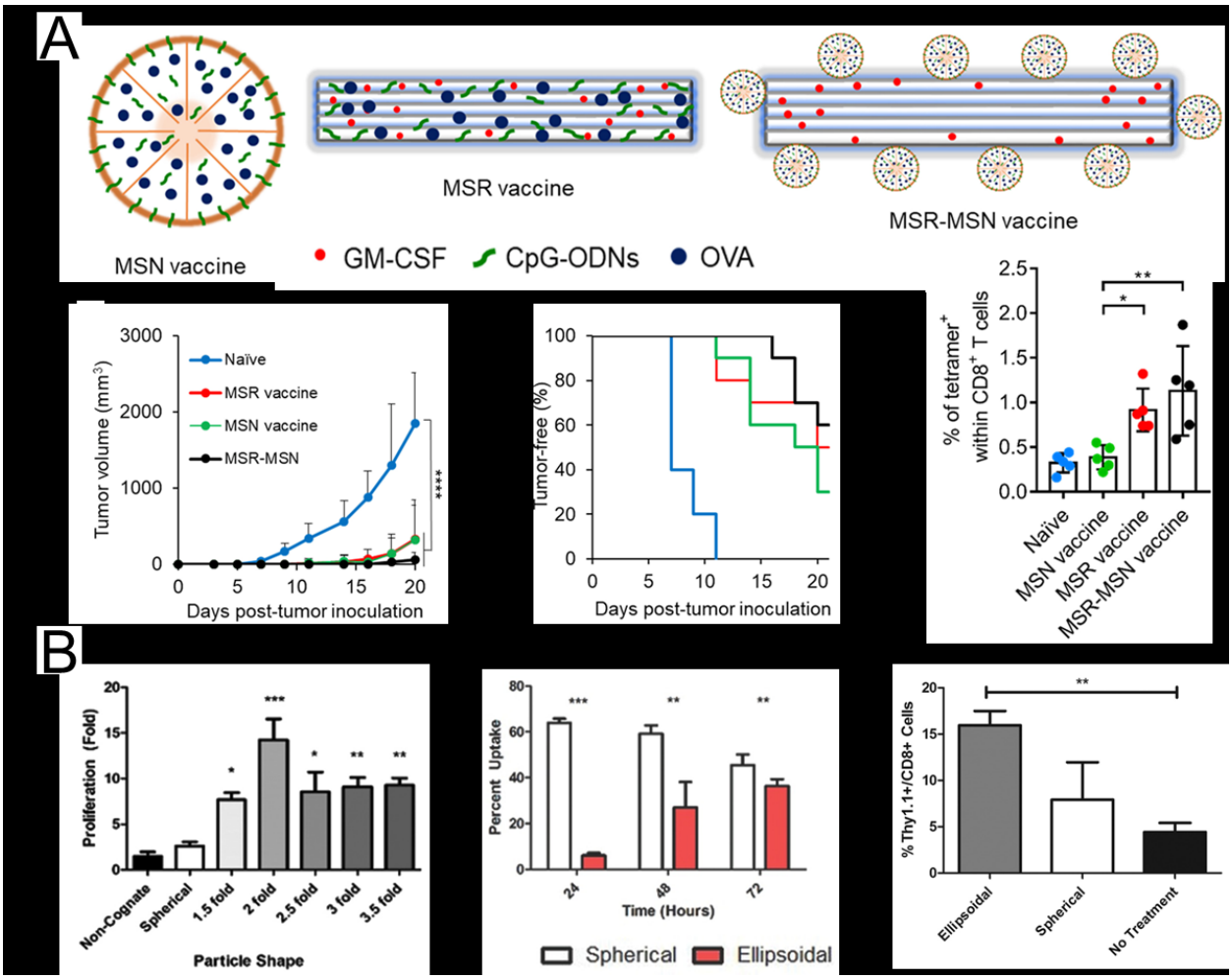

Figure 2-6. Biomaterials-based nanoparticles for vaccines and aAPCs can elicit strong antigen-specific CD8+ T cell responses *in vivo*.(A) A combination vaccine approach containing mesoporous silica microrods (MSRs) coupled with mesoporous silica nanoparticles (MSNs) increases the population of antigen-specific CD8+ T cells and improves the anti-tumor response compared to particles or scaffolds alone. (B) Altering the shape of biodegradable aAPCs improves antigen specific T cell activation *in vitro* as well as decreases non-specific uptake by macrophages, resulting in enhanced T cell activation *in vivo* as well. (A) Reproduced with permission from Nguyen, T. L., et al. Injectable dual-scale mesoporous silica cancer vaccine enabling efficient delivery of antigen/adjuvant-loaded nanoparticles to dendritic cells recruited in local macroporous scaffold. Biomaterials 239, 119859 (2020). (B) Reproduced with permission from Meyer, R. et al. Biodegradable Nanoellipsoidal Artificial Antigen Presenting Cells for Antigen Specific T-Cell Activation. Small 11, 1519–1525 (2014).

2.4.2 Direct T cell Activation

While still a relatively new area of exploration, *in vivo* direct T cell activation may offer solutions to the problems that plague both adoptive T cell transfer and vaccination. Compared to *ex vivo* activation of T cells, *in vivo* activation saves time and money and moves the field closer to “off-the-shelf” treatments[82]. Compared to vaccination, direct T

cell activation offers more direct control over the specificity and phenotype of the immune response as it avoids relying upon intermediary players, such as endogenous antigen presenting cells. It may also avoid adverse events that are experienced from current cancer vaccines[211,212] while reducing the number of injections necessary for efficacy[213].

This approach to expand endogenous antigen specific cells *in vivo* shares many design considerations with aAPCs used for *ex vivo* T cell expansion described above. However, with *in vivo* stimulation, there is increased concern of activating off-target cells, without the advantage of being able to characterize the cell product prior to infusion, as in *ex vivo* expansion systems. Platforms must include signals 1, 2, and 3 for T cell stimulation, activate cells without over-stimulating them, and avoid activating non-specific T cells.

As mentioned with vaccine design, considerations like biocompatibility, biodegradability, and pharmacokinetics exist here as with any other pharmaceutical agent. However, there are several important distinctions between the vaccine approach and the direct T cell activation approach. First, unlike with vaccine platforms, T cell activators must avoid being internalized by phagocytic cells as they need to directly interact with T cells. Second, it is disadvantageous for the material itself to induce an immune response as this will likely attract innate immune cells rather than naïve T cells. Finally, the platform must be designed with a specific patient in mind, as endogenous T cell activation is HLA restricted. Here, we will discuss current technologies that enable *in vivo* T cell activation and how they are designed to enable antigen-specific activation without activating off-target effector cells.

2.4.2.1 Particle-based T cell activation

aAPCs were originally evaluated for their ability to expand T cells *ex vivo* for ACT but are now being adapted for *in vivo* applications for both CD4+ cells and CD8+ T cells[106,214]. Similar to aAPCs for *ex vivo* use, the minimum requirements for aAPC use *in vivo* are the incorporation of signals 1 and 2 for T cell activation. Particles with pMHC complexes and αCD28 for co-stimulation have been shown to be at least partially effective at treating tumors upon either intravenous or subcutaneous co-injection of aAPCs and naïve T cells[106,124,213,214] and an intraperitoneal injection of IL-2 (signal 3) to support T cell growth. These initial studies provided the proof of concept that aAPC particles can in fact support T cell growth *in vivo*. Improvements to these base aAPC designs have focused on particle circulation, LN drainage, and interaction with and activation of T cells.

One challenge with injectable aAPCs is directing accumulation to secondary lymphoid organs, where naïve T cells are concentrated. Since T cells continuously cycle through the LN, it is an ideal target for aAPC accumulation. Unlike vaccine particles, which can target DCs in the subcapsular sinus, aAPCs have to penetrate deeper into the T cell zone within the paracortex of the LN. If aAPCs are injected subcutaneously, small particles (< 5 nm) will enter the blood stream while large particles (~50 - 100 nm) will enter lymphatics[188]. While targeting lymphatic drainage is an attractive solution for vaccine accumulation in the LN, larger aAPCs would likely not be able to pass the subcapsular sinus barrier and thus would not interact with T cells. Instead, delivery via vasculature may be better as it more closely mimics native T cell trafficking[215]. Particles can even be functionalized to target draining LN High Endothelial Venules (HEVs), which are the same channel of entry used by T cells[216].

Several aAPC properties have been shown to impact *in vivo* T cell activation (**Figure 2-2**). One study investigated PLGA-based aAPCs of different shapes with pMHC and aCD28 conjugated to the surface[122] . The study found that ellipsoidal aAPCs not only enhanced T cell activation but also reduced uptake by macrophages thus improving *in vivo* half-life over spherical particles (**Figure 2-6B**)[122]. Research into the effect of ligand positioning on aAPCs *in vitro* has been extended to *in vivo* results, demonstrating that both lateral and axial control of ligand positioning has an impact on T cell expansion *in vivo*[217]. Using red blood cells as the base material for the aAPC with DNA linkers to attach pMHC and aCD28 proteins, researchers found that pre-forming clusters of pMHC and using shorter linkers for pMHC conjugation improves the performance of injectable aAPCs[217].

As described previously, many aAPC properties have been studied *in vitro* and these findings will likely be relevant *in vivo* as well. However, tradeoffs exist for injectable aAPC design as biocompatibility and pharmacokinetics must be balanced with aAPC properties that optimize T cell activation and expansion. As an example, the most efficient size for effective LN drainage may be at odds with the size necessary for enhanced T cell contact; it has been shown that effective LN drainage occurs with particles around 50 nm[185] whereas effective T cell activation occurs with particles above 300 nm[109].

Finally, as discussed for *ex vivo* technologies, ligand choice is an important aspect of injectable aAPC design (**Figure 2-2**). The pivotal work that has been done to characterize contributions of various stimulating receptors on T cell activation has been extended *in vivo*; for example one group that incorporated pMHC, αCD28, and α4-1BB

molecules onto a latex-based aAPC[218] showed enhanced *in vivo* T cell activation. One concern of *in vivo* T cell activation is the activation of off-target T cells through the costimulatory molecules on aAPCs[219]. In the study mentioned previously, the group did observe some non-specific activation of T cells due to the co-stimulatory molecules; however, for cancer applications it may be advantageous, as delivery of these molecules alone has been shown to have anti-tumor effects[220]. Beyond improving the specificity and efficiency of T cell activation itself, researchers may consider adding ligands to aAPCs to improve the pharmacokinetic profile of the particle, for example by reducing uptake of particles by the reticuloendothelial system (RES). In an 11-molecule aAPC, previously discussed in section 2.3.1.3, the group added CD47-Fc, the "don't eat me signal," to the surface of the particle. Addition of this signal improved accumulation in the spleen and LN, presumably through reduced phagocytosis, and enhanced the anti-melanoma immune response as compared to particles without CD47-Fc. There has been a large body of work describing methods to create so called "stealth" particles that show improved circulation in the body, which can be extended to the field of aAPCs[136,221].

2.4.2.2 Scaffolds

As with vaccine development, the difficulty of efficient accumulation of aAPCs in secondary lymphoid organs gave rise to a second approach for *in vivo* T cell activation – the T cell stimulating scaffold. This goal of this approach is to create an injectable or implantable biomaterial scaffold that incorporates chemokines and T cell stimulating signals that can recruit and expand T cells at the peripheral site; in other words, the creation of an "artificial lymph node" that recreates some or all of the functions of a LN.

Thus far, this goal has not been fully realized, but the field is growing with many promising pre-clinical studies.

There have been several scaffolds developed to support pan-T cell expansion and subsequent *in vivo* delivery. One group demonstrated that T cells activated overnight with αCD3 and αCD28 antibodies can be embedded in a polyisocyanopeptide (PIC) hydrogel with IL-2 for subcutaneous delivery into mice[222]. The group was able to see continued T cell activation and slow release from the gel, indicating suitability of the platform for sustained local delivery of pre-activated T cells. The sustained release itself is a significant contribution to the field of ACT, as persistence of transferred cells has been a challenge in humans[223]. Another group has developed chitosan gels to co-encapsulate TIL with tumor fragments, which promote the expansion of TILs[83]. The group achieved a linear release of encapsulated TILs over time, which could then kill target cancer cells[83]. However, the approach is still in development and more *in vivo* testing is needed. Similarly, a group has developed an alginate scaffold to encapsulate tumor reactive T cells, which can be implanted at the tumor resection bed or at the site of an inoperable tumor[84]. The scaffold included a synthetic collagen-mimetic peptide for T cell adhesion. T cell activation was mediated by encapsulated silica microparticles coated with lipid bilayers including αCD3, αCD28 and α4-1BB and encapsulated IL-15 superagonist. The T cells were steadily released as the biomaterial degraded and treated mice showed enhanced survival after tumor challenge[84]. To further reduce the manufacturing burden of T cell therapy, eventually the goal of this approach would be to attract host T cells rather than co-delivering isolated T cells. One step that has been taken towards this end is the encapsulation of chemokine CCL21 into PEG hydrogels

containing αCD3/αCD28 microparticles[224]. The platform was only tested for *ex vivo* T cell activation, but future experiments may use CCL21 to attract host cells into the scaffold for subsequent activation and release.

Another avenue of research has been to fully construct artificial lymph nodes by co-implanting biomaterial scaffolds with LN stromal cells. Efforts here were started in the early 2000s with formation of LN-like organoids that reconstitute some functions of the LN like B and T cell retention[225,226]. More recent research has produced much more sophisticated systems that are capable of enhanced functionality without the need to co-implant stromal cells. One group created artificial lymph node-like tertiary lymphoid organs (artTLOs) by implanting collagen sponge scaffolds with beads that facilitated the slow release of lymphorganogenic chemokines (lymphotoxin-α1β2, CCL19, CCL21, CXCL12, CXCL13, and soluble RANK ligand)[227]. The platform showed the capacity to produce an antigen-specific immune response to immunizations in SCID mice[227]. Another group created a bone-marrow mimicking alginate cryogel (BMC) to enhance T cell regeneration after hematopoietic stem cell transplantation (HSCT)[228]. These technologies that restore lymphoid function could be used in patients whose cancer has rendered them immunosuppressed, to allow them access to immunotherapy treatments.

2.4.2.3 Biomaterials that enhance ACT or the natural T cell response

In working towards developing technologies for *in vivo* endogenous antigen-specific T cell expansion, some platforms are currently acting as support mechanisms to traditional forms of ACT, such as ETC, TCR, or CAR T therapies. One challenge with ACT, either with endogenous cells or with engineered cells, is the persistence of transferred cells[229,230]. In order to potentiate the efficacy of the immunotherapy by

extending the persistence, groups have developed various systems to support injected cells. One group has created a nanogel “backpack” that contains IL-15 superagonist (IL15sa)[86]. This approach not only supports the cells *in vivo*, but it potentiates the immune response in an antigen-specific manner, as the release of IL-15sa is local and is only triggered upon T cell recognition of its target[86]. Another method has been the co-injection of T cells and a vaccine. For example, in one study DCs were pretreated with the adjuvant monophosphoryl lipid A[231]. Vesicles from these cells were isolated and co-injected into recipients with pre-activated CD8+ T cells. The vesicles acted as a vaccine to activate DCs *in vivo* which in turn activated antigen-specific T cells *in vivo*, potentially both transferred and endogenous cells[231]. Vaccines have also been co-delivered with CAR T cells to re-stimulate cells after transfer[54,61]. Another group used a non-specific vaccine to augment ACT; biopolymer scaffolds delivering stimulator of IFN genes (STING) agonists could expand tumor-specific T cells that recognize other tumor epitopes that the transferred cells did not, broadening the anti-cancer immune response[232]. Besides enhancing the persistence of adoptively transferred cells, one group has enhanced ACT by improving the accumulation of transferred cells in the tumor site. Prior to injection, T cells were decorated with magnetic APCs so that upon transfer, cells could be driven to the tumor by MRI and magnetic guidance[233].

There have also been developments in the enhancement of the endogenous T cell response without the need for ACT. These technologies use biomaterials to engineer tumor cells *in situ* to induce them to secrete or express molecules that support T cell growth and function within the tumor microenvironment. One group has developed a PBAE nanoparticle that delivers both IL-12 and 4-1BBL DNA into the

tumor, turning tumor cells into APC-like cells, which restored function to tumor-specific T cells[234]. Another group has created tumor-targeting lipid-dendrimer-calcium-phosphate (TT-LDCP) nanoparticles that deliver IL-2 DNA and PD-L1 siRNA to induce tumor cells to support T cell growth while removing T cell inhibition [235]. Because these approaches work to enhance the endogenous T cell response, they can be antigen agnostic which circumvents many of the challenges faced by ETC. However, their efficacy is limited in settings where tumors inherently have poor T cell infiltration.

Finally, T cell therapies have been greatly enhanced by the advent of immune checkpoint blockade (ICB) where antibodies against “immune brakes” potentiate anti-cancer T cell responses *in vivo*. ICB has already seen great success clinically, alone and in conjunction with ACT[236,237]. In a murine model, ICB has also been shown to synergize with aAPCs; upon co-delivery of aAPCs with αPD-1, the group saw enhanced IFN-γ secretion by CD8+ T cells as well as tumor regression in a melanoma model[213]. Biomaterials may also have a role in improving ICB delivery. For example, ICB may be coated onto nanoparticles to enhance their accumulation in the tumor microenvironment[238–241]. Another group has taken this idea further with the development of the “immunoswitch”[242], a nanoparticle conjugated with αPD-L1 and α4-1BB to not only block the checkpoint blockade signal, but also replace it with a co-stimulatory signal[242]. As technologies for *in vivo* T cell activation continue to advance, they will likely be used in conjunction with technologies like those mentioned here. Combination immunotherapies are already used in the clinic today and are rapidly becoming the standard of care[243,244].

In vivo generation of a cytotoxic, antigen-specific T cell response is an active field of research with growing excitement. Biomaterial-based therapeutic cancer vaccines are currently the closest to market, with many active clinical trials. However, there has been a long history of cancer vaccines failing to show anti-tumor efficacy in humans[209]. Significant progress has been made in improving the immunogenicity of these formulations through targeting neoantigens; nevertheless, the efficacy of such technologies may be inherently capped for patients with dysfunctional APCs. In these cases, biomaterials that directly activate T cells *in vivo* may be more effective. The approach of using aAPCs and scaffolds *in vivo* benefits from decades of *ex vivo* characterization and optimization of these technologies; however, the safety of direct T cell activation in humans has yet to be studied and may prove to be problematic. In patients who already have underlying antitumor T cell responses but have yet to "break" tolerance within the immunosuppressive tumor microenvironment, technologies that enhance the natural immune response may be the most effective and have the added benefit of being the closest to "off-the-shelf" technologies. As with direct T cell activation, these biomaterial technologies are still largely pre-clinical.

2.5 Summary and Conclusions

T cells play an integral role in directing immune responses against infected or cancerous cells. Biomaterial platforms that can mimic these natural immune responses can not only enhance our understanding of T cell biology, but can be harnessed towards design of immunotherapies tailored towards a variety of cancers and infectious diseases. Clinically, ACT-based therapies show great promise but are still not first-line

therapies. The use of biomaterials for *ex vivo* manipulation of T cells, *in vivo* delivery of immunomodulatory agents, or *in vivo* activation of T cells has the potential to drastically change the landscape of cancer immunotherapy and bring the benefits of T cell therapy to more patients.

Cost, manufacturing difficulty, time-to-treatment, and patient variability all prevent the widespread use of ETC in the clinic. Mass-producible biomaterials that can provide the modularity necessary to induce robust T cell responses against a wide range of cancer antigens, with the flexibility to skew towards unique functional and phenotypic profiles, could translate into the next-generation of immunotherapies. “Off the shelf” aAPCs can help reduce the cost and length of *ex vivo* culture for personalized cell therapies while smart material choices can potentially simplify regulatory approval when the materials can be separated from T cell products prior to infusion. Cost reduction, customizability, streamlined regulatory proceedings, and lack of dependence on the availability and quality of patient-derived APCs can all help widen the pool of patients who can benefit from ACT.

Use of biomaterials in patients has been explored in depth in fields such as regenerative medicine and tissue engineering. However, biomaterials for *in vivo* activation of antigen-specific T cells is a relatively new, alternative approach to cancer immunotherapy. Vaccines have been around for a century, but rarely stimulate cytotoxic T lymphocytes. Biomaterials that enhance the vaccine’s ability to elicit a cellular response by increasing host APC cross-presentation of cancer antigens have renewed interest and hope in a cancer vaccine[152]. Alternatively, direct activation of host T cells *in vivo* may be particularly helpful for patients who have deficient APCs, a common

occurrence in many cancers. The path towards translation of technologies for *in vivo* T cell activation has been partially paved by decades of biomaterials characterization. Many materials have defined toxicities, immune interactions, and degradation profiles that will alleviate some of the regulatory hurdles that exist for new therapies. However, materials for in vivo T cell activation have their own translational concerns, such as potential for on-target off-tumor effects. These risks can be mitigated through thoughtful materials design as discussed throughout this review, as well as careful monitoring of patient responses.

Several endogenous T cell therapies using iron oxide aAPCs for *ex vivo* expansion are currently in clinical trials[245,246]. As for *in vivo* expansion technologies, cancer vaccines are the most well studied platform in the clinic, with more than a dozen active clinical trials[208,209]. Biomaterials for direct T cell activation is a newer approach, with most research in pre-clinical stages. However, a novel antibody fusion protein designed for direct antigen-specific T cell activation in vivo is currently being investigated in clinical trials, providing evidence that the concept of direct T cell activation is translatable[219]. Continued development of these biomaterials-based technologies for endogenous antigen-specific T cell activation may offer a truly universal, “off-the-shelf” treatment for many cancer patients. As many studies have shown, there is great synergy between T cell-based therapies and other immunotherapies such as ICB. The future of cancer immunotherapy will likely involve intensive screening of the patient’s genome and mutanome to create a comprehensive treatment plan that includes targeted stimulation of a range of innate and adaptive

immune cells in tandem with administration of immunomodulatory agents, such as ICB, to fight cancer cells in the tumor's immunosuppressive microenvironment.

Chapter 3. Adaptive Nanoparticle Platforms for High Throughput Expansion and Detection of Antigen-Specific T cells[2]

3.1 Introduction

T cells are immune cells which play critical roles in carrying out and bolstering immune responses against pathogens, self, allergens, and cancer[73]. Each T cell recognizes antigenic peptide sequences presented in major histocompatibility complexes (MHC) through their unique T cell receptor (TCR). Identification of antigen-specific T cells is critical to understanding disease[73,125,247–250] and creating therapies[251,252].

Despite their known roles in immunity, identification of antigen-specific T cells can be challenging. Unique TCRs are generated through VDJ recombination with 10^{14} possible unique TCRs[253], and the frequency of any one specific clonotype is between 1 in 10^4 to 10^6 of T cells[30,254]. This diversity and frequency requires conventional methods of cellular identification, like flow or mass cytometry, to be adapted[255]. Several approaches have been used to increase detection sensitivity, such as multimerizing MHC[256], co-evaluation with inflammatory markers (e.g. cytokines)[257–260], and magnetic enrichment by peptide-loaded MHC (pMHC)[80,261]. However, these techniques also suffer from low throughput. To improve throughput, researchers have developed UV-

[2]This chapter is reprinted (adapted) with permission from: "Hickey J. W., Isser Ariel, et al., Adaptive Nanoparticle Platforms for High Throughput Expansion and Detection of Antigen-Specific T cells. *Nano Letters* 20 (2020): 6289-6298". Copyright 2020 American Chemical Society.

cleavable peptides[262], combinatorial fluorescent labeling[263,264], and pMHC yeast displays[265]. However, the high degree of complexity of these procedures renders them difficult to use.

Here we build on previous techniques to enrich and expand (E+E) rare antigen-specific T cells with pMHC and co-stimulatory molecules (such as anti-CD28)[80,85,110]. We demonstrate the versatility of this platform by eliminating the requirement of costly cell isolation kits, which simultaneously enhances CD8+ T cell activation from the presence of additional immune cells. We adapt this technology to be higher throughput with the capability of processing multiple antigen-specific T cells in parallel. Similarly, we use fluorescent magnetic nanoparticles to create a new adaptive detection bead that enables parallelized detection reagent production. We highlight the utility of our system through multiplexed expansion of murine antigen-specific T cells including commensal bacterial cross-reactive CD8+ T cells (SVY), detection of rare, low affinity neoantigen CD8+ T cells, and expansion of human viral and tumor-specific CD8+ T cells. The simplicity of these technologies makes them easy to adopt by non-specialists and provides a high-throughput workflow for identification and analysis of antigen-specific T cell responses.

3.2 Results

3.2.1 Antigen-specific T Cell Enrichment and Expansion from Splenocytes

The current Enrichment and Expansion (E+E) protocol requires CD8+ isolation prior to adding magnetic nanoparticle aAPCs for enriching T cells[80]. To streamline this process, we enriched and then expanded antigen-specific CD8+ T cells directly from unpurified splenocytes (**Figure 3-1a, Figure 3-2a**). Interestingly, the E+E from

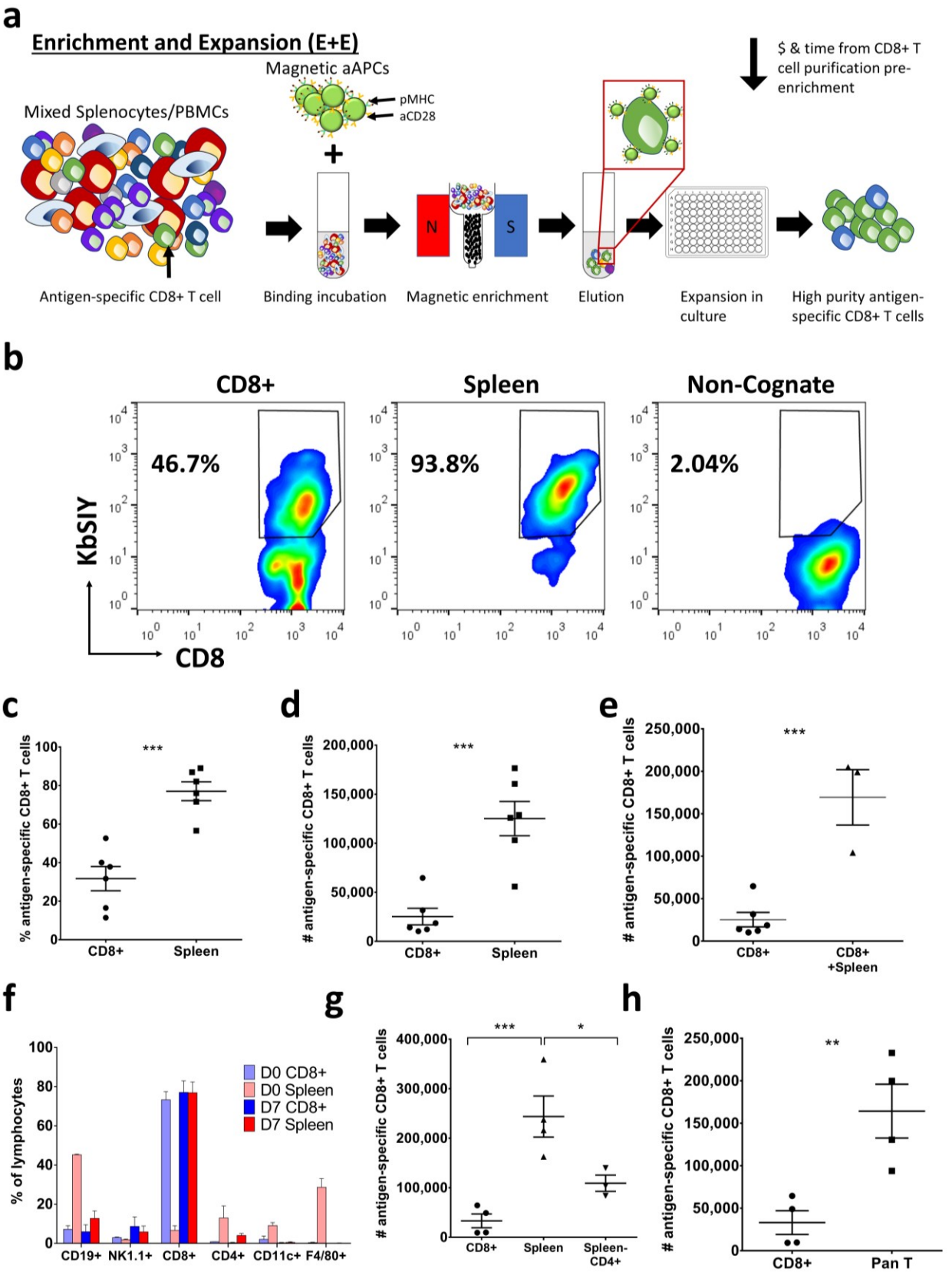

Figure 3-1. Boosting activation of antigen-specific CD8+ T cells with co-culture of non-CD8+ T cells in E+E.(a) Schematic of eliminating CD8+ T cell isolation from protocol for using artificial antigen-presenting

cells (aAPCs) for enrichment and expansion of antigen-specific T cells which represents cost, time and technical advantages. (b) Representative flow plot of CD8+ T cells (from B6 mouse) 7 days post enrichment and expansion from CD8+ T cells vs. splenocytes. (c) Percent and (d) number of antigen-specific T cells resulting from aAPC enrichment and expansion of two different starting populations of cells (purified CD8+ T cells vs. splenocytes) on day 7 (error bars show s.e.m.; **p < 0.01, n = 6, Student's t-test, two-tailed). (e) Number of antigen-specific T cells resulting from aAPC enrichment and expansion of CD8+ T cells, splenocytes, or isolated CD8+ T cells added back to splenocytes post-enrichment (error bars show s.e.m.; **p < 0.01, ***p < 0.001, n = 3 – 6). (f) Cellular composition of post-enrichment fractions on days 0 and 7 during the culture (error bars show s.e.m; n = 3). (g) Number of antigen-specific T cells 7 days after aAPC enrichment and expansion following depletion of CD4+ cells from splenocytes compared to isolated CD8+ T cells (error bars show s.e.m.; *p < 0.05, ***p < 0.001, n = 3 – 4, one-way ANOVA with Tukey's post test). (h) Number of antigen-specific T cells resulting from aAPC enrichment and expansion from two different starting populations of cells (CD8+ T cell purified, Pan T cell purified) on day 7 (error bars show s.e.m.; **p < 0.01, n = 6, Student's t-test, two-tailed).

splenocytes dramatically improved the purity of the expanded population post-expansion (**Figure 3-1b**). Specifically, the percent and number of SIY-specific CD8+ T cells increased by two- (**Figure 3-1c**) and five-fold (**Figure 3-1d**), respectively, after seven days of expansion while phenotype and function were conserved (**Figure 3-2b,c**). This was not due to differences in efficiency of enrichment (**Figure 3-2d**) or percent recovery (**Figure 3-2e**) between purified CD8+ T cell and splenocyte populations; nor was it unique to SIY, as we found similar results when expanding for endogenous antigen TRP2 (**Figure 3-2f,g**). As with E+E from CD8+ T cells[85], optimal E+E from splenocytes required anti-CD28 to be present on aAPCs (**Figure 3-3a,b**).

We hypothesized that this boost in output was driven by presence of non-CD8+ T cells. To investigate this view, we first enriched SIY-specific CD8+ T cells from a purified CD8+ population with our aAPCs and then added splenocytes post-enrichment, functionally diluting CD8+ T cells back to their initial frequency with non-CD8+ T cells. This approach increased the number of antigen-specific cells by six-fold on day 7 (**Figure 3-1e**), confirming our hypothesis.

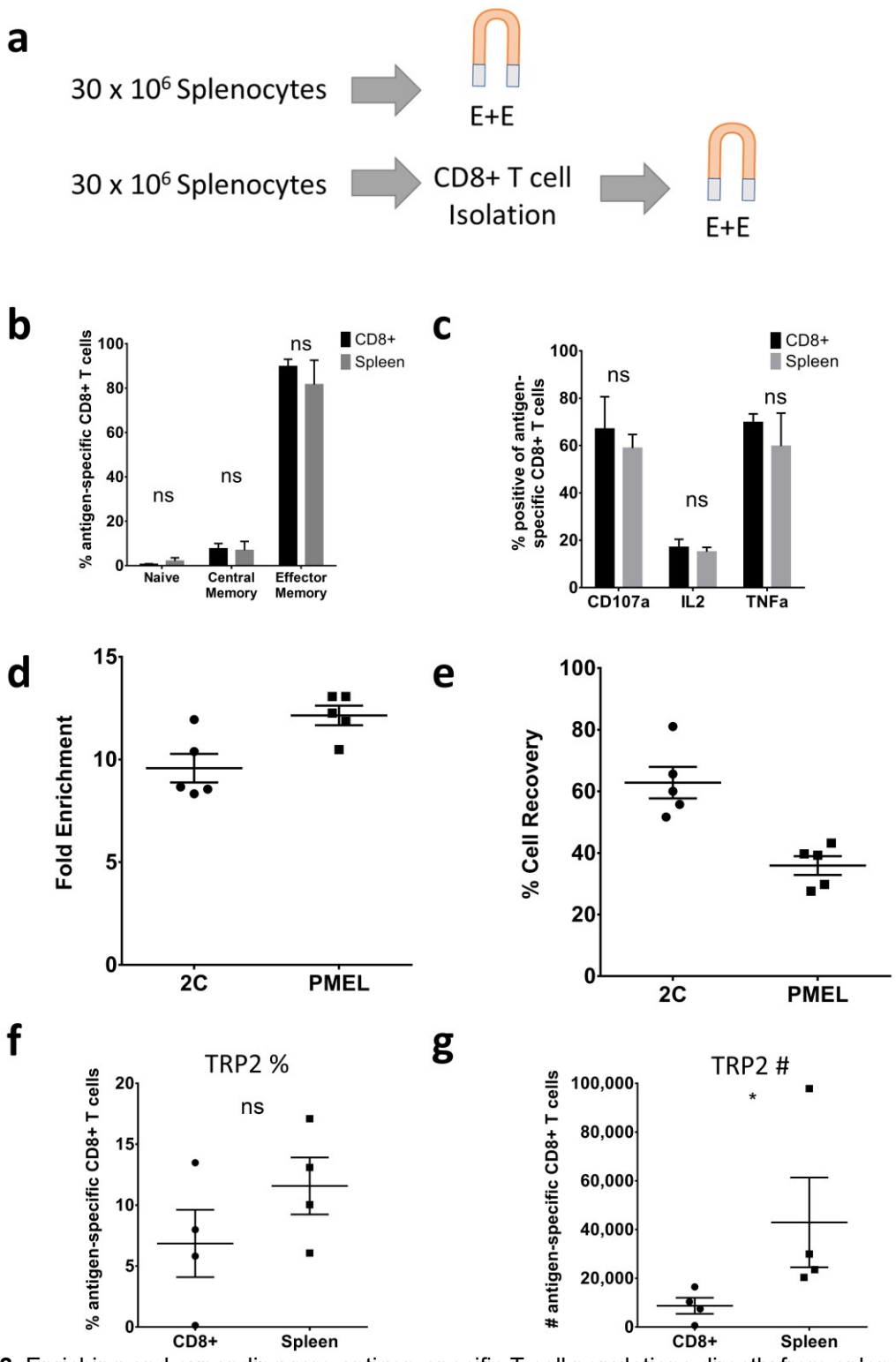

Figure 3-2. Enriching and expanding rare antigen-specific T cell populations directly from splenocytes and comparing to starting from purified CD8+ T cell populations.(a) Schematic of experimental set up for comparing different starting populations (splenocyte vs. purified CD8+ T cells). We divided harvested splenocytes into two equal parts: one population that went through a step for CD8+ T cell isolation and the other that did not. Enriching from splenocytes does not alter antigen-specific (b) phenotype or (c) cytokine production on day 7 (error bars show s.e.m.; ns $p > 0.05$, $n = 3$, one-way ANOVA with Tukey's

post test). (d-e) Enhancements in enrichment and expansion of antigen-specific CD8+ T cells from splenocyte starting populations do not come from increases in levels of fold enrichment or percent cell recovery of antigen-specific T cells on day 0. Doping fluorescently-labeled (CFSE) antigen-specific CD8+ T cells (2C or PMEL CD8+ T cells) at ($1:10^4$) in endogenous splenocytes allow comparison of (e) fold enrichment and (e) percent cell recovery of 50 nm aAPCs that are not different from fold enrichment and cell recovery in CD8+ T cell populations (error bars show s.e.m.; n = 5). (f) Percent and (g) number of antigen-specific T cells (TRP2+) resulting from aAPC enrichment and expansion two different starting populations of cells (CD8+ T cell purified, splenocytes) at day 7 (error bars show s.e.m.; *p < 0.05, n = 4, Student's t-test, two-tailed).

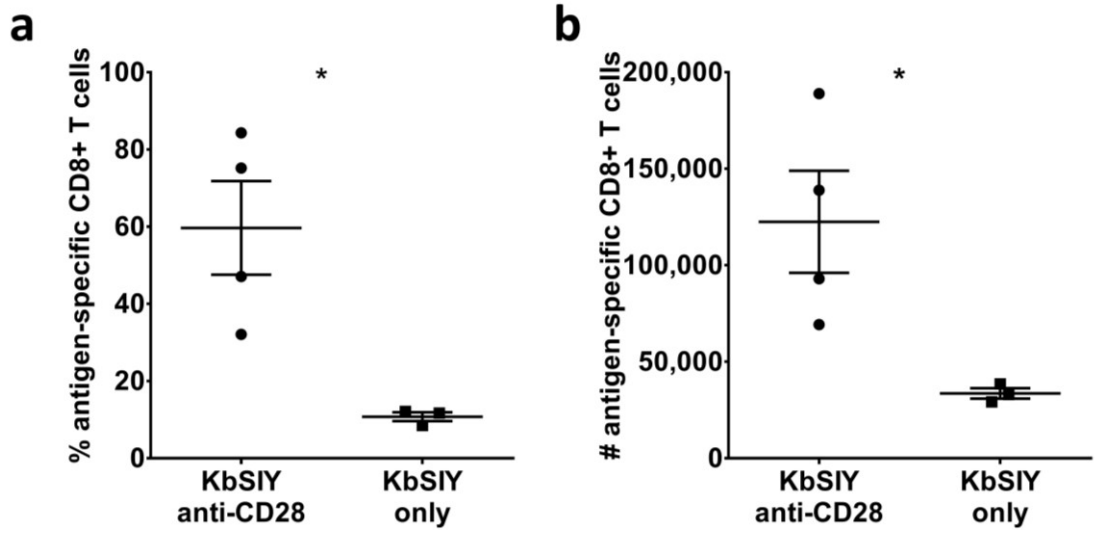

Figure 3-3. Importance of anti-CD28 for enrichment and expansion of CD8+ T cells from splenocytes.(a) Percentage and (b) number of KbSIY specific CD8+ T expanded with KbSIY+anti-CD28 vs. KbSIY-only aAPCs (error bars represent s.e.m.; *p < 0.05, n = 3 – 4, Student's t-test, two-tailed).

We next began investigating which non-CD8+ T cell populations contributed to enhanced CD8+ T cell expansion because splenocyte E+E starting populations (post-aAPC enrichment) also included B cells (CD19+), NK cells (NK1.1+), CD4+ T cells, dendritic cells (CD11c+), and macrophages (F4/80+), despite converging to a relatively homogenous CD8+ population by day 7 (**Figure 3-1f**). Amongst endogenous antigen presenting cells such as B cells, macrophages, and dendritic cells, only depletion of dendritic cells pre-enrichment significantly reduced the output from splenocyte E+Es (**Figure 3-4a,b**). Additionally, we suspected that the presence of CD4+ T cells could drive this boost, considering their natural roles in the priming of naïve CD8+ T cells[266,267]. To address this theory, we depleted CD4+ T cells (**Figure 3-5a**) pre-

enrichment from splenocytes. We found that depletion of CD4+ T cells significantly decreased the number of antigen-specific cells on day 7 (**Figure 3-1g**). Finally, we examined if CD4+ T cells alone were sufficient to improve the output by performing E+E on a cell population purified with a Pan T cell isolation kit. Interestingly, we found that using a Pan T cell isolate (**Figure 3-5a**) significantly boosted the frequency (**Figure 3-5b**) and number (**Figure 3-1h**) of antigen-specific T cells.

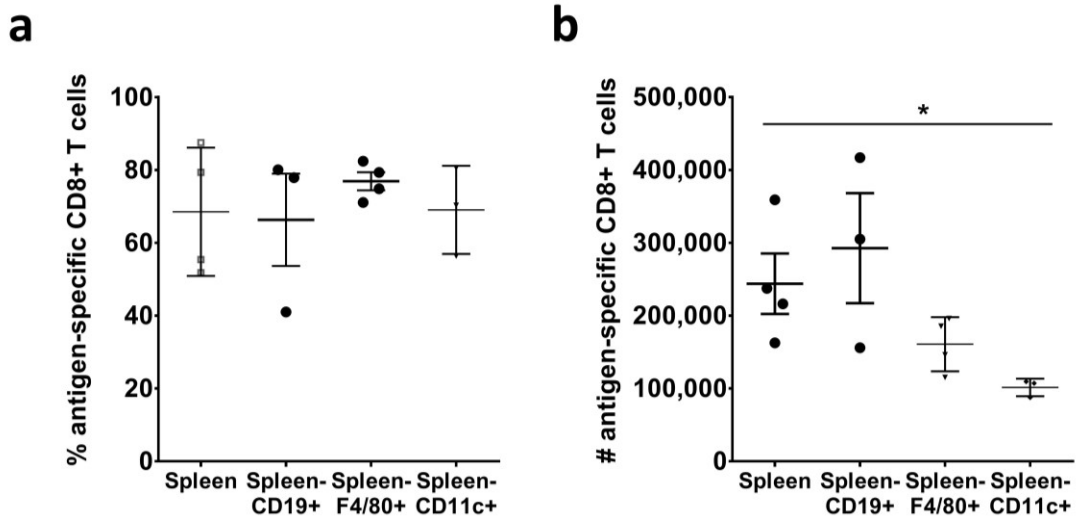

Figure 3-4. Contribution of endogenous antigen presenting cells to enhanced output from Splenocyte E+E.(a) Percent and (b) Number of antigen-specific T cells resulting from aAPC enrichment and expansion of splenocytes depleted of B cells (CD19+) macrophages (F4/80+) and dendritic cells (CD11c+) (error bars show s.e.m.; *$p < 0.05$, n = 3 – 4, one-way ANOVA).

Thus, this approach of isolating from splenocytes, represents not only a cost, time, and technical advantage but also demonstrates the importance of additional CD4+ T cell support during CD8+ activation. Since MHC class I aAPCs only stimulate CD8+ T cells *ex vivo*, the presence of CD4+ T cells was not expected to provide significant benefit[80]. Our results here suggest the opposite and future work is warranted to fully understand this interaction. Finally, this finding also supports the need for development of MHC class II aAPCs, where simultaneous expansion of antigen-specific CD4+ and CD8+ T cells may be mutually beneficial to *ex vivo* expansion.

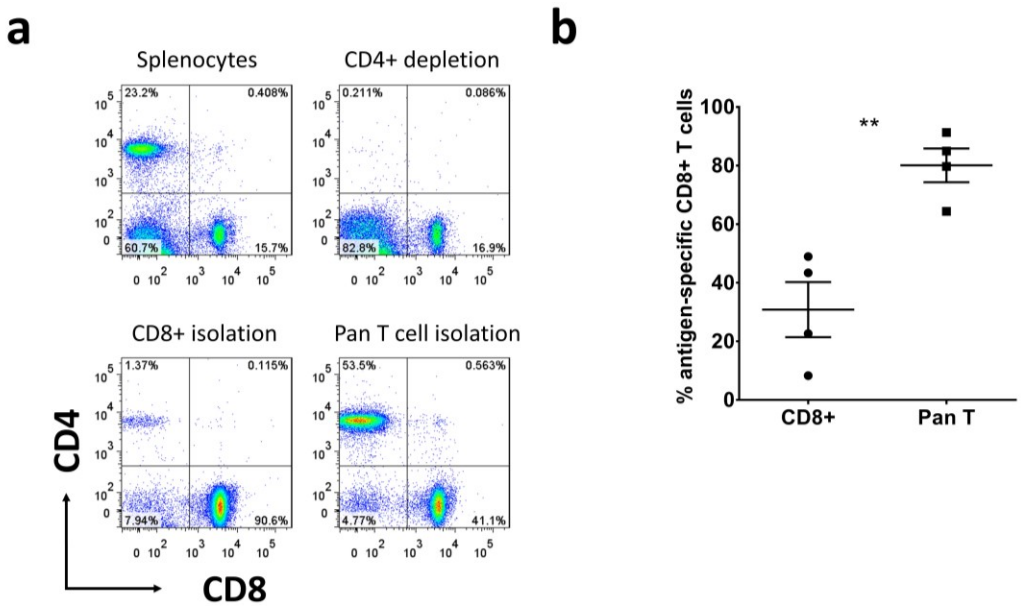

Figure 3-5. Understanding the contribution of CD4+ T cells in enhancing antigen-specific CD8+ T cell activation.(a) Comparison staining of populations of splenocytes, Pan T cells, CD8+ isolation, and CD4+ depletion used for E+E experiments. (b) Percent of antigen-specific T cells resulting from aAPC enrichment and expansion from two different starting populations of cells (CD8+ T cell purified, Pan T cell purified) on day 7 (error bars show s.e.m.; **$p < 0.01$, $n = 4$, Student's t-test, two-tailed).

3.2.2 High Throughput Enrichment and Expansion

Previous efforts for enrichment and expansion of antigen-specific T cells have included the use of 50-nm aAPCs[80], which require specially-produced magnetic columns to produce magnetic fields strong enough to retain labeled cells. This limits the throughput and adaptability of the protocol. Previously, we studied how the size of the aAPC impacts both T cell activation[109] and enrichment[110] and found that particles close to 300 nm were most efficient at activating and enriching antigen-specific T cells. These 300-nm aAPCs can be magnetically isolated with weaker magnetic fields such as conventional neodymium magnets and thus can be adapted to a 96-well plate format (**Figure 3-6a**).

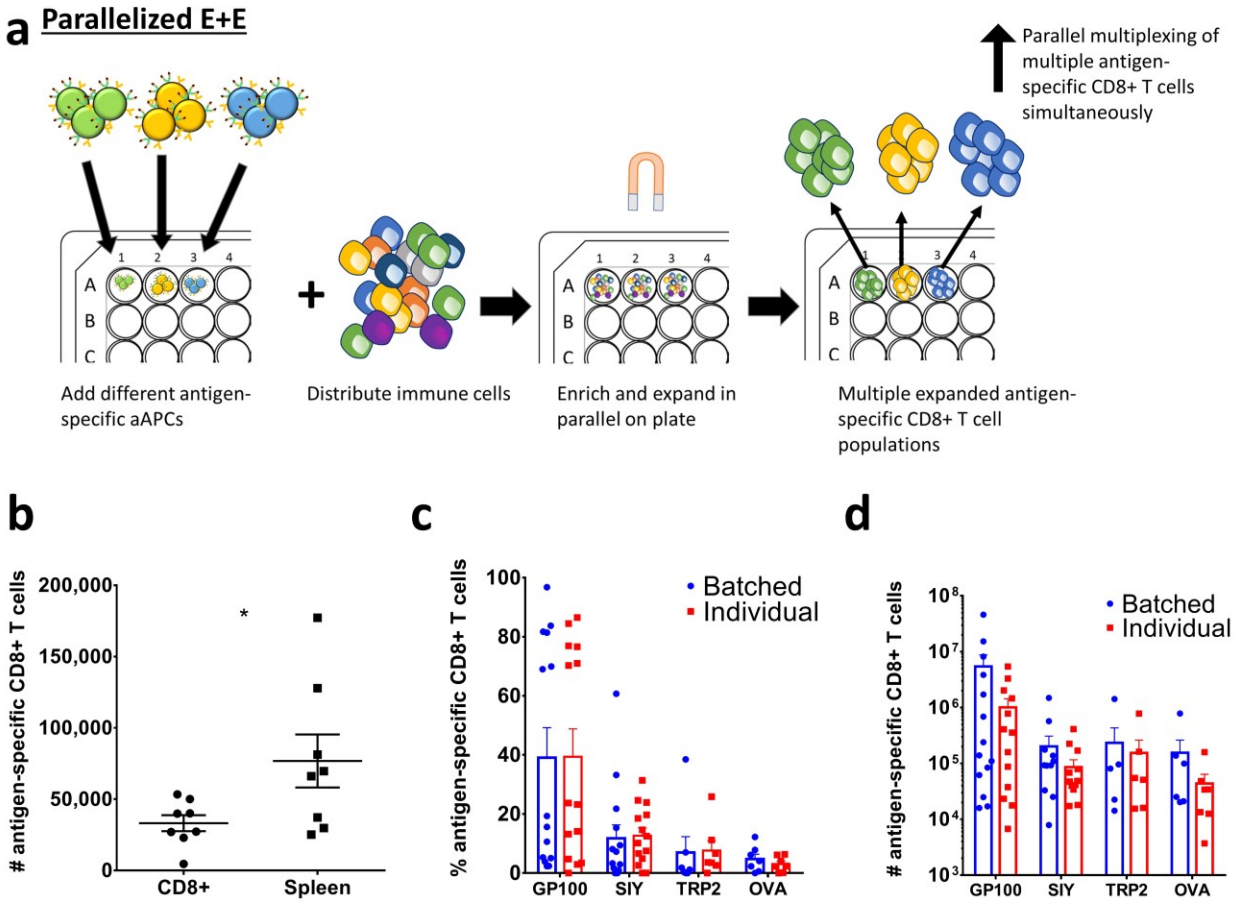

Figure 3-6. Increasing the throughput of enrichment and expansion of antigen-specific CD8+ T cells by increasing simultaneous parallel processing.(a) Schematic illustrating limitations of current approach to enrich rare cells by magnetic columns with 50–100-nm magnetic particles and increasing throughput by adapting a 96-well plate magnet approach with 300-nm magnetic nanoparticles. (b) Efficient enrichment and expansion from a starting population of splenocytes on a plate magnet in comparison to the CD8+ T cell isolated starting population (error bars show s.e.m.; *p < 0.05, n = 8, Student's t-test, two-tailed). (c-d) Comparison of (c) percentages and (d) numbers of four different antigen-specific T cell populations and comparing having the aAPCs batched versus processing individually in parallel (error bars show s.e.m.; n = 7 – 14).

We have also found that nanoparticle concentration is a key factor influencing the optimal E+E of antigen-specific T cells[110]. We thus optimized concentrations of aAPC E+E with this new particle size (300 nm), starting cell populations (splenocytes), and magnet format (96-well plate neodymium magnet) for enrichment (**Figure 3-7a**), cell recovery (**Figure 3-7b**), and cell expansion (**Figure 3-7c**). We then used this 96-well plate set-up to perform E+Es on endogenous antigen-specific T cells from a wild-type B6 mouse, and confirming our previous results where we observe similarly observe an

increase in expansion of antigen-specific T cells by starting from a population of splenocytes compared to purified CD8+ T cells (**Figure 3-6b, Figure 3-7d**). We thus conducted all of our following E+E experiments with 96-well plate from a starting population of splenocytes.

To test its ability for parallel processing, we generated four distinct antigen-loaded aAPCs (gp100, SIY, TRP2, OVA) and performed E+Es on endogenous T cells with the 96-well plate format. We compared batched versus separate enrichments (**Figure 3-8**) and found both conditions produced similar percentages (**Figure 3-6c**) with slightly higher numbers of antigen-specific T cells in batched conditions, though not statistically significant (**Figure 3-6d**). This suggests that either configuration could be used to identify antigen-specific T cells depending on the availability of samples or number of combinatorial staining reagents.

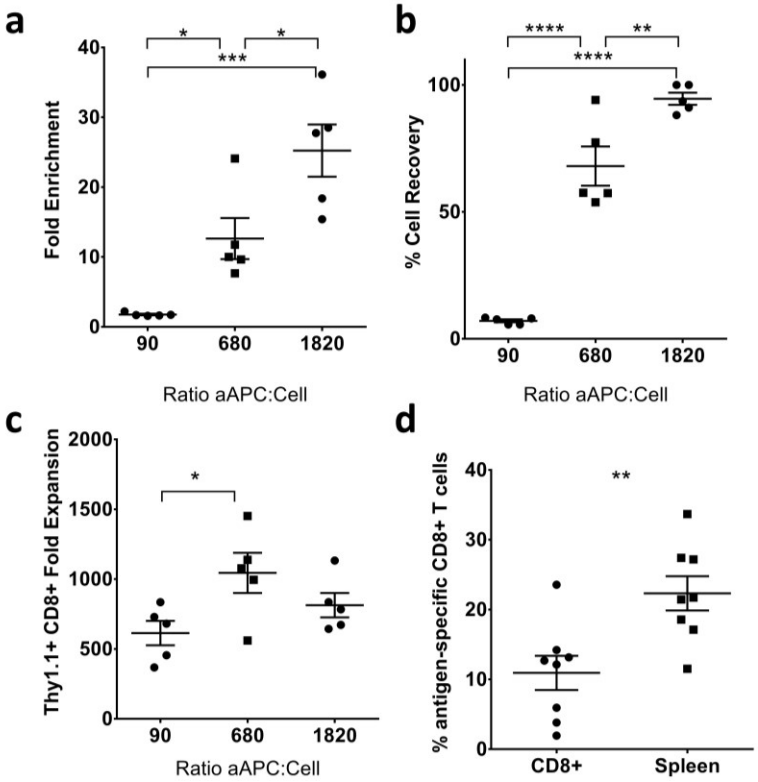

Figure 3-7. Establishing the proper dose of 300 nm aAPCs to use to enrich antigen-specific T cells.(a-b) Doping antigen-specific CD8+ T cells at ($1:10^4$) in endogenous splenocytes allow comparison of (a) fold

enrichment and (b) percent cell recovery of 300-nm aAPCs at different ratios of aAPCs to cells (error bars show s.e.m.; *p < 0.05, **p < 0.01, ***p < 0.001, n = 5, one-way ANOVA with Tukey's post test). (c) By doping in Thy1.1+, transgenic PMEL CD8+ T cells into Thy1.2+ mice at a 1:1000 ratio, we determine effective aAPC:Cell ratios needed for the new enrichment and expansion protocol (error bars show s.e.m.; *p< 0.05, n = 5, one-way ANOVA with Tukey's post test). (d) Comparing antigen-specific T cell frequency on day 7 from a 96-well plate format starting population of splenocytes or purified CD8+ T cells (error bars show s.e.m.; **p < 0.01, n = 8, Student's t-test, two-tailed).

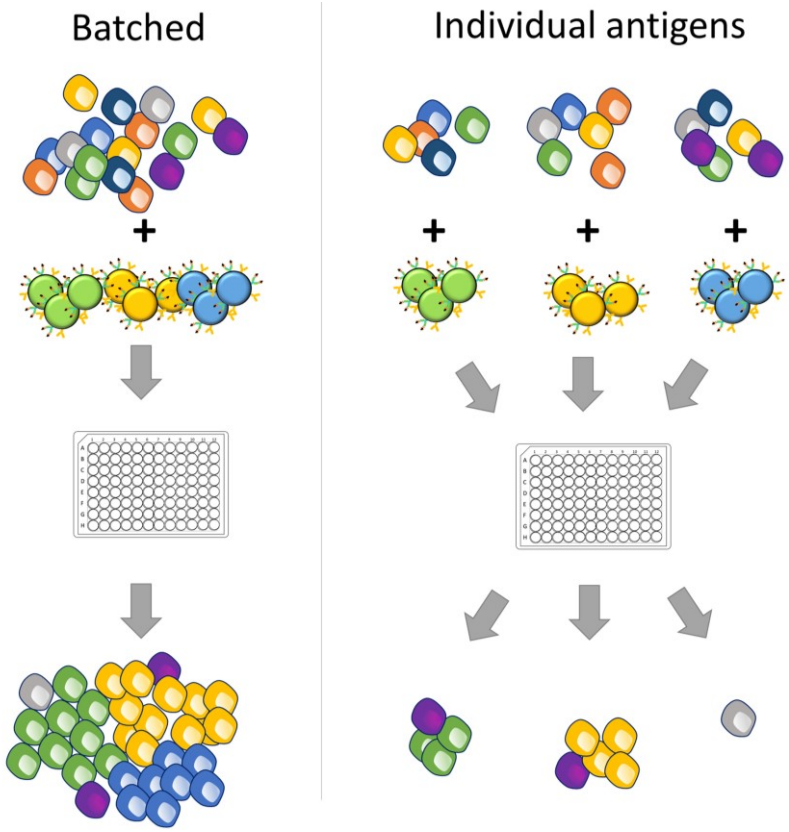

Figure 3-8. Schematic for comparing experimental set-up for comparing batched to individual antigen-specific CD8+ T cell enrichment and expansions.

3.2.3 Adaptive aAPCs to Enrich and Expand T cells with Multiple Antigen Specificities

While the 96-well plate format provides a convenient, high-throughput approach to enrich antigen-specific T cells, creating individual, antigen-specific aAPCs can be labor- and reagent-intensive. Rather than loading and then coupling dimeric MHC-Ig (pre-loaded), we conjugated unloaded dimeric MHCs directly to magnetic nanoparticles creating an adaptive aAPC that requires a one-step particle synthesis and standardizes

aAPC reagents (**Figure 3-9a**). These peptide-less aAPCs can be aliquoted into individual wells on 96-well plates and efficiently loaded through incubation with peptides for multiplexing the number of antigens that can be probed at a time.

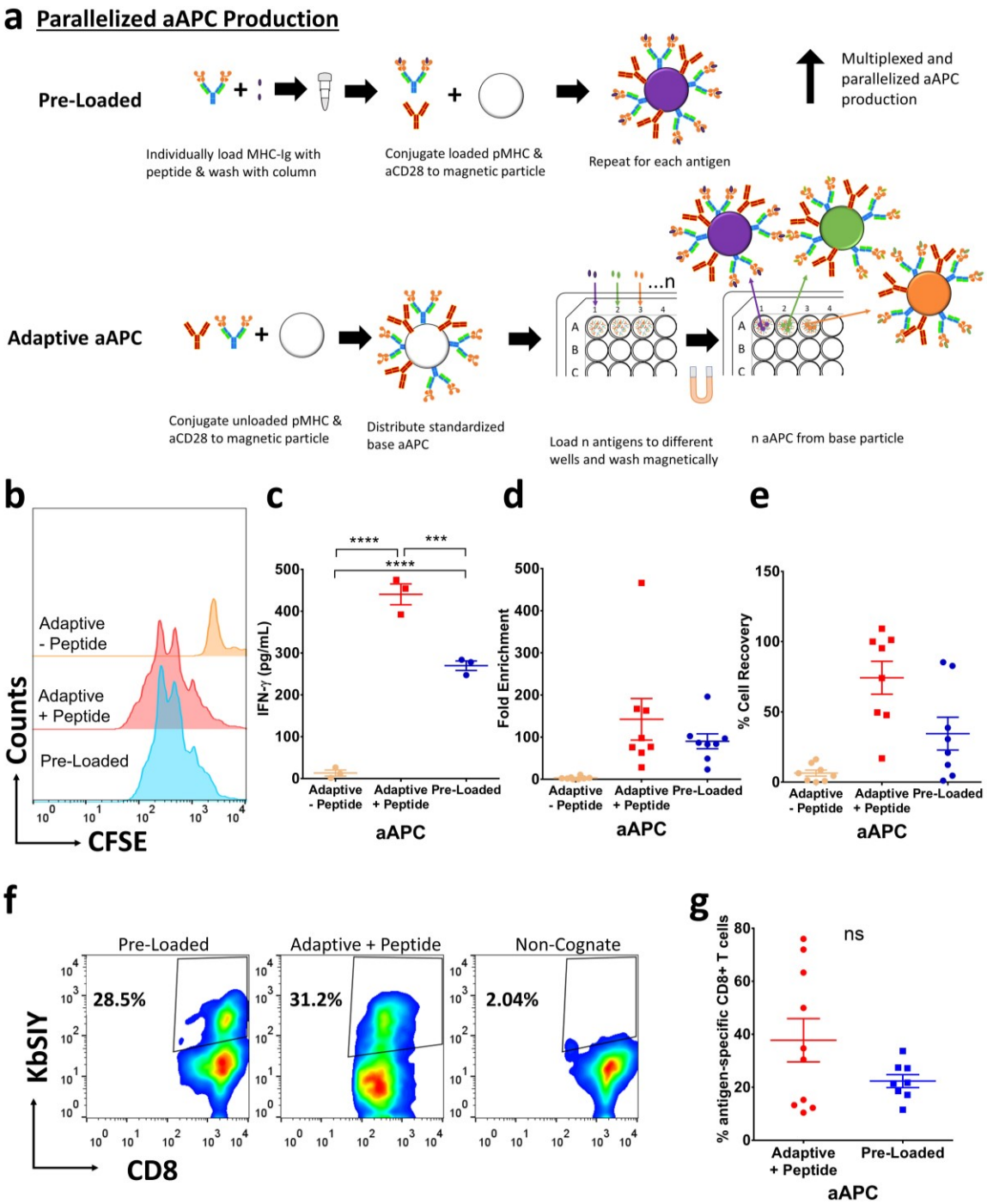

Figure 3-9. Increasing the throughput of E+E of antigen-specific CD8+ T cells through development of adaptive aAPCs.(a) Schematic illustrating limitations of current approach where individualized antigen-specific aAPCs require individual processing. It illustrates the concept of increasing throughput by

creating adaptive aAPCs and then loading antigens post-conjugation and using a magnetic field for parallel processing. (b) CFSE dye dilution demonstrates effective antigen-specific activation of adaptive aAPCs compared to pre-loaded aAPCs. (c) IFN-γ secretions demonstrate functional responses after re-stimulating activated T cells with adaptive aAPCs compared to pre-loaded aAPCs (error bars show s.e.m; ***$p < 0.001$, ****$p < 0.0001$, n = 3, one-way ANOVA with Tukey's post test). (d-e) Comparing the (d) fold enrichment and (e) percent cell recovery from adaptive aAPCs - peptide, adaptive aAPCs + peptide, and pre-loaded aAPCs in a doped Thy1.1+ system (error bars show s.e.m; n = 8). (f-g) Cognate and non-cognate staining of antigen-specific cells enriched and expanded for 7 days by adaptive aAPCs compared to pre-loaded aAPCs (error bars show s.e.m.; $p > 0.05$, n = 8–10).

To confirm the function of adaptive aAPCs, we evaluated their efficiency in stimulating antigen-specific T cells. T cells proliferated at comparable rates with both adaptive (+peptide) and pre-loaded aAPCs by CFSE dilution assay after 3 days of culture (**Figure 3-9b**). In contrast, unloaded adaptive aAPCs (-peptide) did not result in any measurable activation, demonstrating both the specificity and efficiency of the adaptive peptide loading process. Additionally, the functional response of 2C cells to adaptively loaded aAPCs as measured by IFN-g secretion was significantly higher as compared to pre-loaded KbSIY aAPCs or unloaded adaptive aAPCs (**Figure 3-9c**).

In addition, we tested the ability of these peptide-loaded adaptive aAPCs to bind and enrich antigen-specific T cells. In a doped enrichment experiment, we observed similar to higher levels of fold enrichment (**Figure 3-9d**) and recovery (**Figure 3-9e**) of target cells with the peptide-loaded adaptive aAPCs compared to pre-loaded aAPCs, while unloaded adaptive aAPCs produced no measurable antigen-specific enrichment. Additionally, after E+E of endogenous antigen-specific T cells, peptide-loaded adaptive aAPCs generated comparable levels of expansion of antigen-specific T cells by day 7 to pre-loaded aAPCs (**Figure 3-9f,g**). Together, these results demonstrate that adaptive aAPCs provide a facile method for parallel production of multiple antigen-specific aAPCs in a single process, all while using smaller amounts of costly pMHC.

3.2.4 Adaptive Detection Beads for High-throughput Antigen-specific T Cell Detection

A multiplexed process for enriching and expanding T cells with many antigen specificities, necessitates new technologies to increase multiplexing of detecting antigen-specificity post-expansion. Current methods to produce detection pMHC complexes require biotinylation of dimeric or tetrameric MHC before loading and washing with each individual antigen. This is a labor-intensive process, resulting in losses of expensive MHC protein. We produced an adaptive detection bead using fluorescently labelled magnetic particles conjugated with unloaded MHC-Ig (**Figure 3-10a**). This builds off of the results shown in **Figure 3-6**, confirming that peptide-loaded adaptive aAPCs work well for antigen-specific binding, and our previous work showing multivalent pMHC on the aAPC surface has high cognate affinity interactions with CD8+ T cells[110].

To test the efficacy of these adaptive detection beads, we incubated them with SIY peptide and then used them to identify endogenous antigen-specific T cells at low, intermediate, and high antigen-specific frequencies post E+E. Compared to a traditional biotinylated dimeric pMHC, the adaptive detection beads efficiently detected antigen-specific T cells with relatively low background (**Figure 3-10b**). Optimal fluorescent bead dose was found at a bead to cell ratio of 3,000 for each of the antigen-specific frequencies (**Figure 3-11, Figure 3-12, Figure 3-13**). Thus, these fluorescent magnetic detection beads can be customized with target peptides and easily added for sensitive staining of antigen-specific T cells. Compared to traditional staining reagents like dimers

or tetramers, this establishes a universal base particle that enables adaptation to antigens of interest, as well as 96-well plate-based parallel processing.

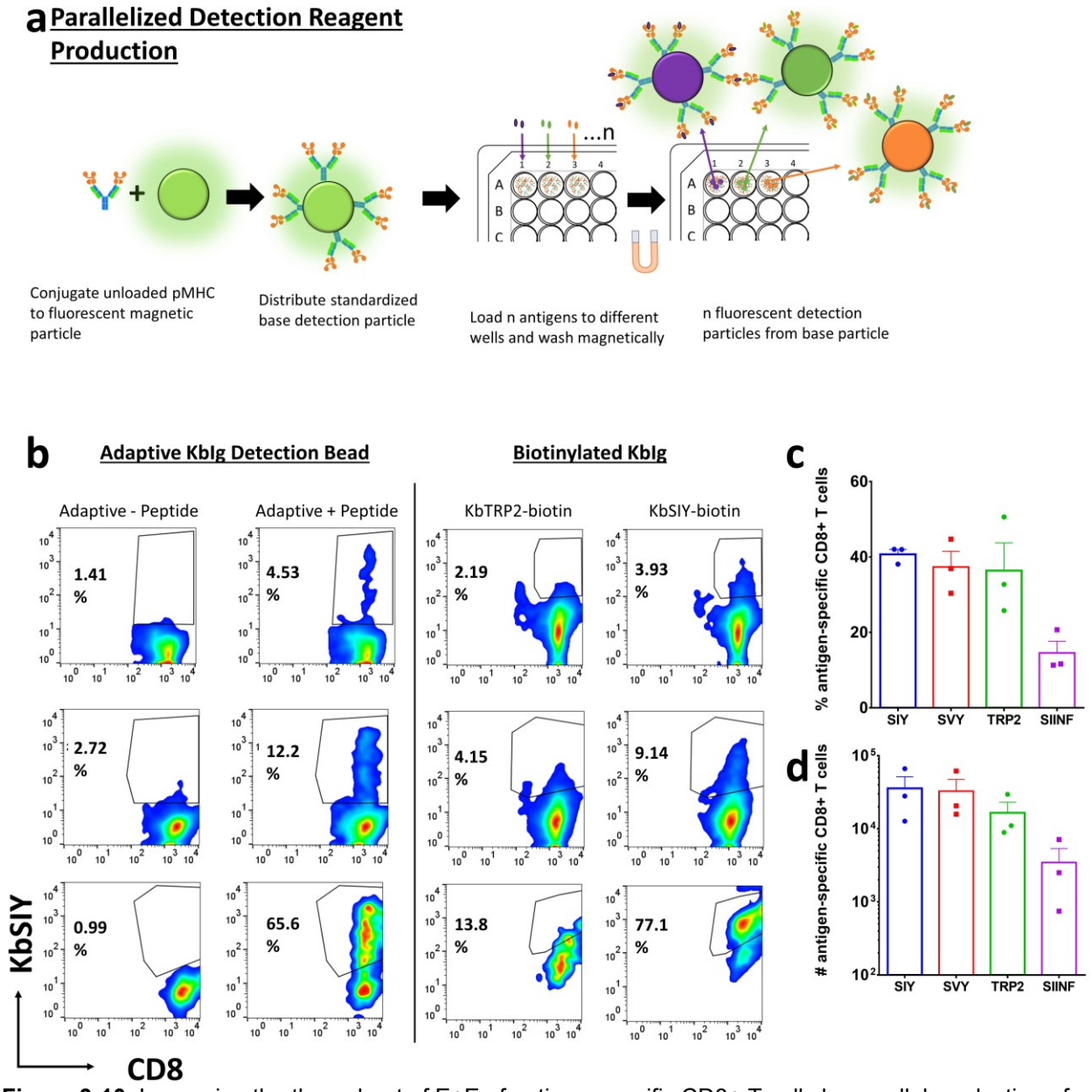

Figure 3-10. Increasing the throughput of E+E of antigen-specific CD8+ T cells by parallel production of different detection beads.(a) Schematic illustrating limitations of current approaches which require creating individualized detection dimers/tetramers. It also illustrates how we increased the throughput by developing adaptive detection beads which are loaded with peptide post-conjugation for parallel processing. (b) Adaptive detection beads are at least as sensitive as current detection technology for antigen-specific T cells at low, intermediate, and high frequencies at day 7 of the E+E protocol. (c) Percent and (d) number of antigen-specific CD8+ T cells enriched and expanded by peptide-loaded Adaptive aAPCs and detected on day 7 by adaptive detection beads (n = 3).

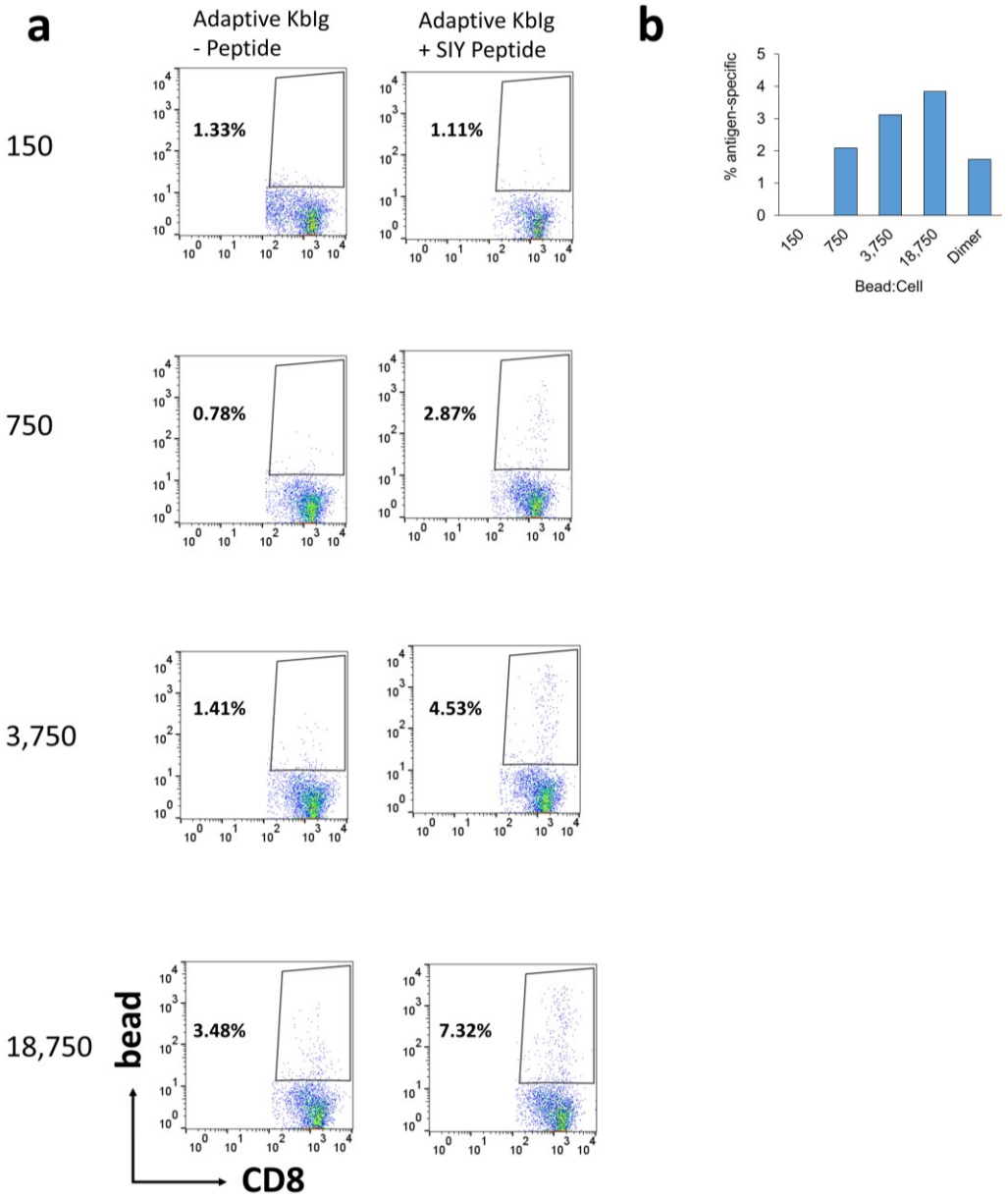

Figure 3-11. Titration of detection bead:cell ratios to evaluate optimal staining concentration for staining antigen-specific T cells on day 7 of the enrichment and expansion protocol with a low final percentage of antigen-specific T cells.(a) Flow cytometry plots of peptide-loaded Adaptive aAPCs (Adaptive + Peptides) and unloaded (Adaptive - Peptides) detection beads (b) Percentage of control staining (Adaptive - Peptide/non-cognate) were subtracted to evaluate final percentage of antigen-specific T cells on day 7 and compare to traditional biotinylated dimer staining reagents.

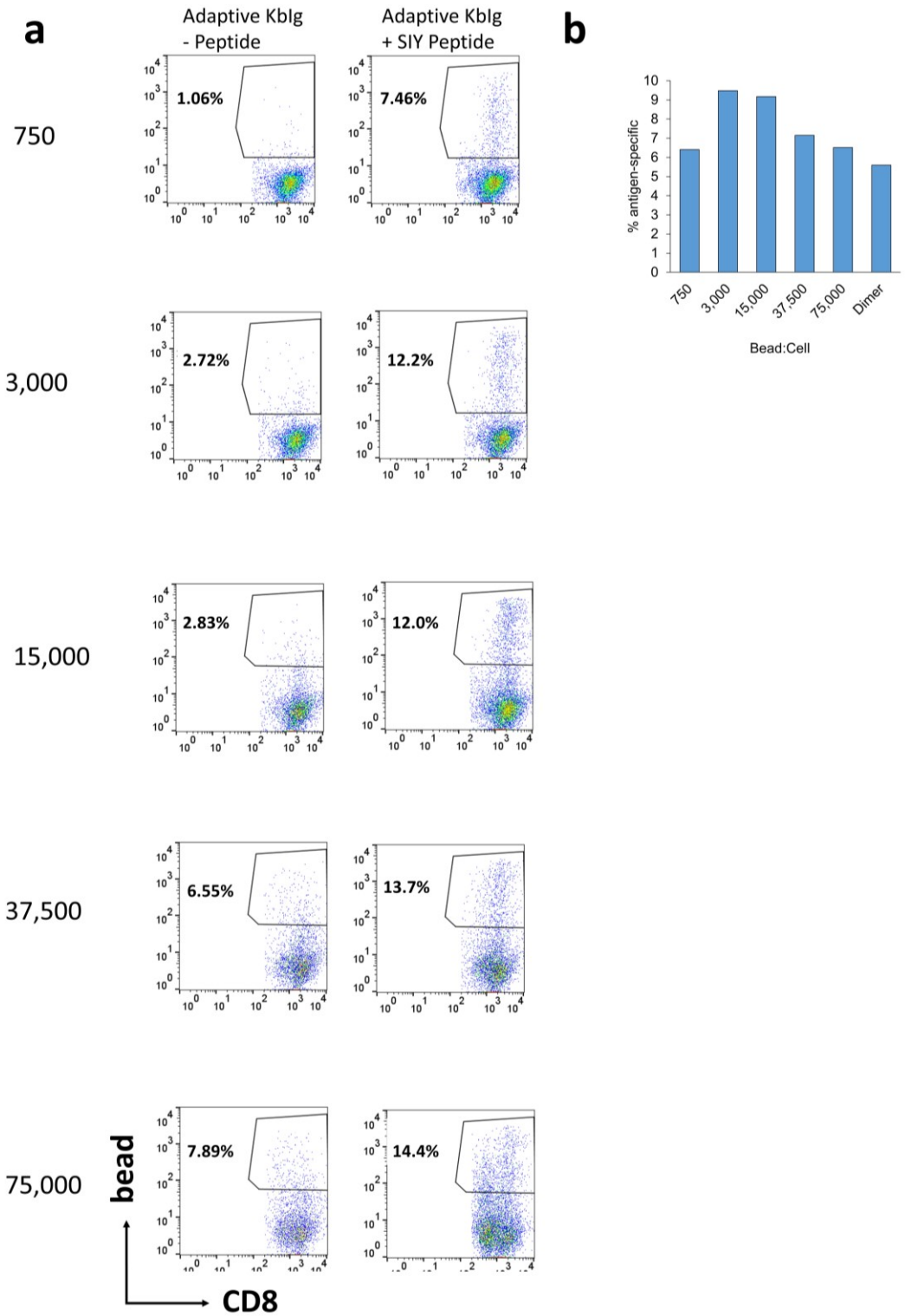

Figure 3-12. Titration of detection bead:cell ratios to evaluate optimal staining concentration for staining antigen-specific T cells on day 7 of the enrichment and expansion protocol with an intermediate final percentage of antigen-specific T cells.(a) Flow cytometry plots of both peptide-loaded Adaptive aAPCs (Adaptive + Peptides) and unloaded aAPCs (Adaptive - Peptides) detection beads (b) Percentage of control staining (Adaptive - Peptide/non-cognate) were subtracted to evaluate final percentage of antigen-specific T cells on day 7 and compare to traditional biotinylated dimer staining reagents.

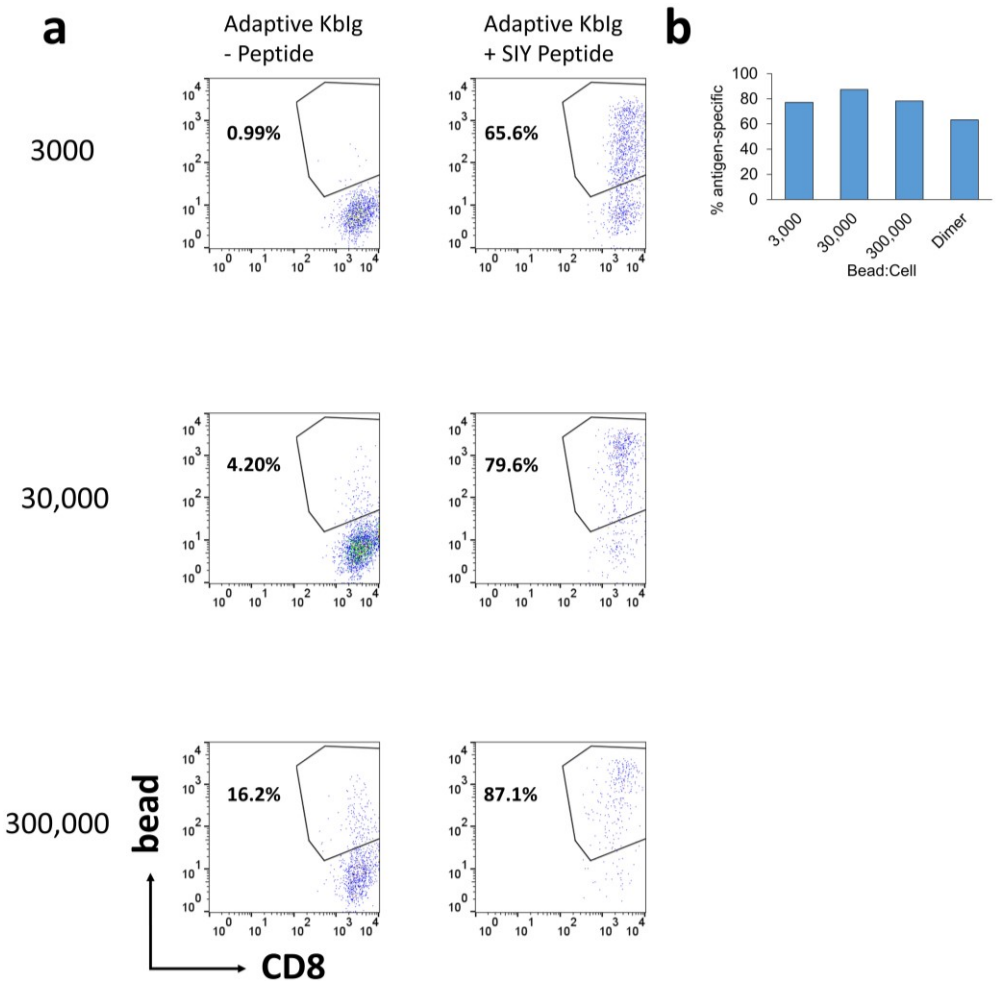

Figure 3-13. Titration of detection bead:cell ratios to evaluate optimal staining concentration for staining antigen-specific T cells on day 7 of the enrichment and expansion protocol with a high final percentage of antigen-specific T cells.(a) Flow cytometry plots of both peptide-loaded Adaptive aAPCs (Adaptive + Peptides) and unloaded (Adaptive - Peptides) detection beads (b) Percentage of control staining (Adaptive - Peptide/non-cognate) were subtracted to evaluate final percentage of antigen-specific T cells on day 7 and compare to traditional biotinylated dimer staining reagents.

One area of increasing interest is CD8+ T cell cross-reactivity. We have previously studied how a gut microbiota-derived antigen SVY leads to expansion of CD8+ T cells cross-reactive for the SIY antigen, with demonstrated increased SIY+ tumor killing[268]. Investigation of CD8+ T cell cross-reactivity would benefit from a platform that enables simultaneous identification of multiple antigen-specific T cells, including antigenic controls. Further, having only one variable changing as the antigen that is loaded would provide a more reliable comparison and reproducible evaluation of

properties of cross-reactivity, where there may be variability between batches of individually produced staining reagents.

To demonstrate this capability, we loaded adaptive aAPCs on Day 0 with SIY (antigen of B16-SIY melanoma tumor), SVY (cross-reactive Bifido bacterium antigen), TRP2 (B16 endogenous melanoma antigen), and SIINF (ovalbumin model antigen). Following E+E, on Day 7, we loaded adaptive detection beads with the same four peptide and successfully detected T cells specific to all four antigens simultaneously, with antigen-specific percentages between 10 and 40% (**Figure 3-10c-d, Figure 3-14**). In conclusion, we have developed an adaptive nanoparticle platform for detection of CD8+ T cells with a range of antigen-specificities, which complements our adaptive aAPCs that allow for multiplexed E+E.

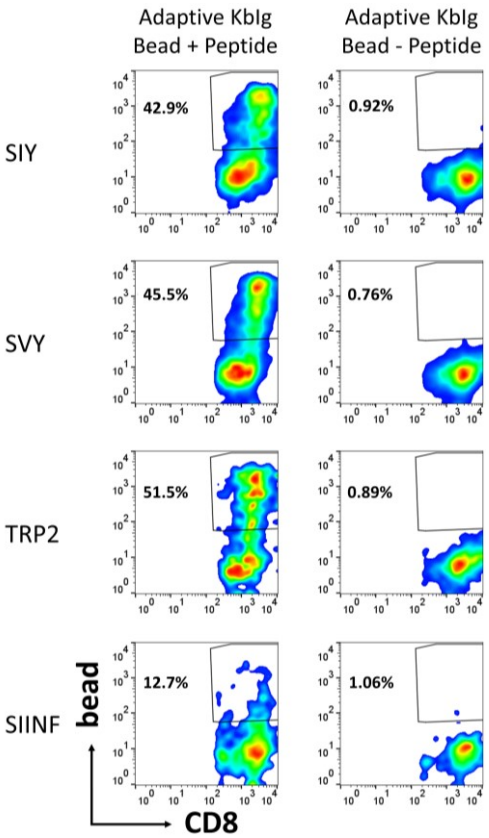

Figure 3-14. Combination of multiplexed Adaptive aAPC, 96-well plate enrichment and expansion starting from a population of splenocytes, and detection by Adaptive detection beads. Representative staining on

day 7 by detection bead of antigen-specific T cells after enrichment and expansion for each antigen using unloaded adaptive detection beads (Adaptive-Peptide) as a negative control.

3.2.5 Adaptive aAPC Platform for Cancer Neoantigens and Human Antigen-specific T cells

Our high-throughput and adaptive detection platform for identifying antigen-specific T cells extends our ability to investigate multiple candidate antigens, which will be beneficial for cancer neoantigens. Neoantigens are processed and presented peptides derived from mutated tumor proteins that the immune system has not been tolerized to; thus, they represent unique and specific immune cell targets for the tumor[269,270]. Treatments targeting neoantigens have led to dramatic clinical results in both adoptive immunotherapy and tumor vaccines[271,272]. However, neoantigen-specific therapies have been limited because of challenges in identifying antigen-specific T cell responses. With hundreds to thousands of potential antigen candidates for each patient, current techniques can only examine a few antigen-specific responses at one time and thus rely primarily on imperfect prediction algorithms[273–275] and are labor intensive. Adaptive nanoparticle platforms overcome many of these challenges and are therefore poised to identify neoantigen-specific cells for understanding these responses and for designing better, more targeted, immunotherapies.

To study whether our platform could be used to detect neoantigen-specific CD8+ T cells, we analyzed the efficacy of staining a B16-F10-derived neoepitope, *Kif18b*$_{735\text{-}745}$, *VDWE**N**VSPEL* (VDW), that was previously shown to be immunogenic[276]. In comparison to the SIY peptide, VDW has low affinity for Kb (**Figure 3-15**), allowing us to assess whether our detection platform can be used for staining low affinity peptides. To expand VDW-specific T cells, we vaccinated mice with poly I:C and SIY and VDW

peptide (**Figure 3-16a**)[276]. Comparison of dimer staining for KbSIY and KbVDW pre- and post-vaccination showed significant increases in both SIY and VDW-specific CD8+ T cells (**Figure 3-17**). We then compared particle stains for SIY and VDW from splenocytes of vaccinated mice and found that there was significantly greater particle staining of SIY and VDW specific T cells over background (**Figure 3-16b,c**). These results confirmed that our adaptive detection beads were capable of staining neoantigen-specific CD8+ T cells.

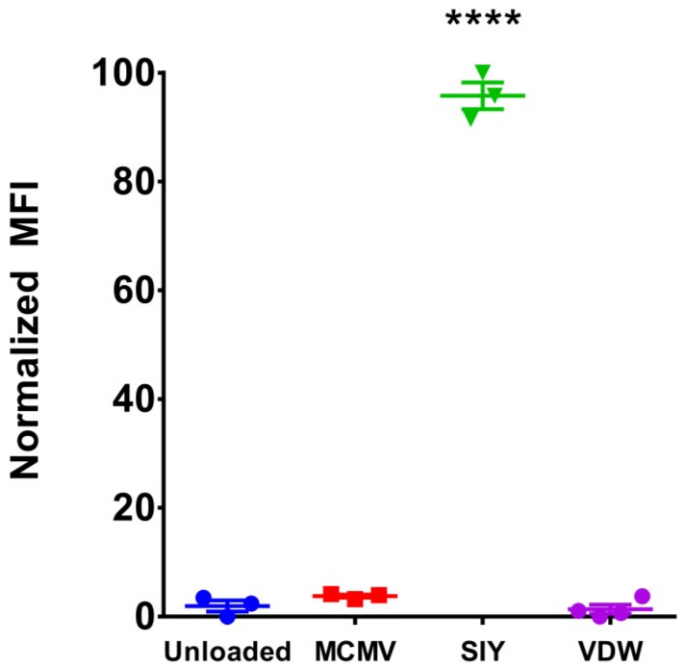

Figure 3-15. Peptide Stabilization Assay to Determine Relative Binding Affinity of SIY and VDW for Kb MHC molecule.RMA-S cells have significantly more Kb protein stabilized and expressed on their surface when pulsed with 1 μg of high affinity SIY peptide, compared to no peptide, 1 μg of Db-restricted MCMV peptide, or 1 μg neoantigen VDW peptide (error bars show s.e.m; ****$p < 0.0001$, n = 3, one-way ANOVA with Tukey's post test).

To understand the clinical utility of these platforms, we applied our multiplexed adaptive aAPCs and detection beads to human antigen-specific CD8+ T cells. We observed effective expansion with both 100- and 300-nm adaptive aAPCs pulsed with viral antigens (CMV and M-1) as well as melanoma antigens (MART-1) (**Figure 3-16d, Figure 3-18**).

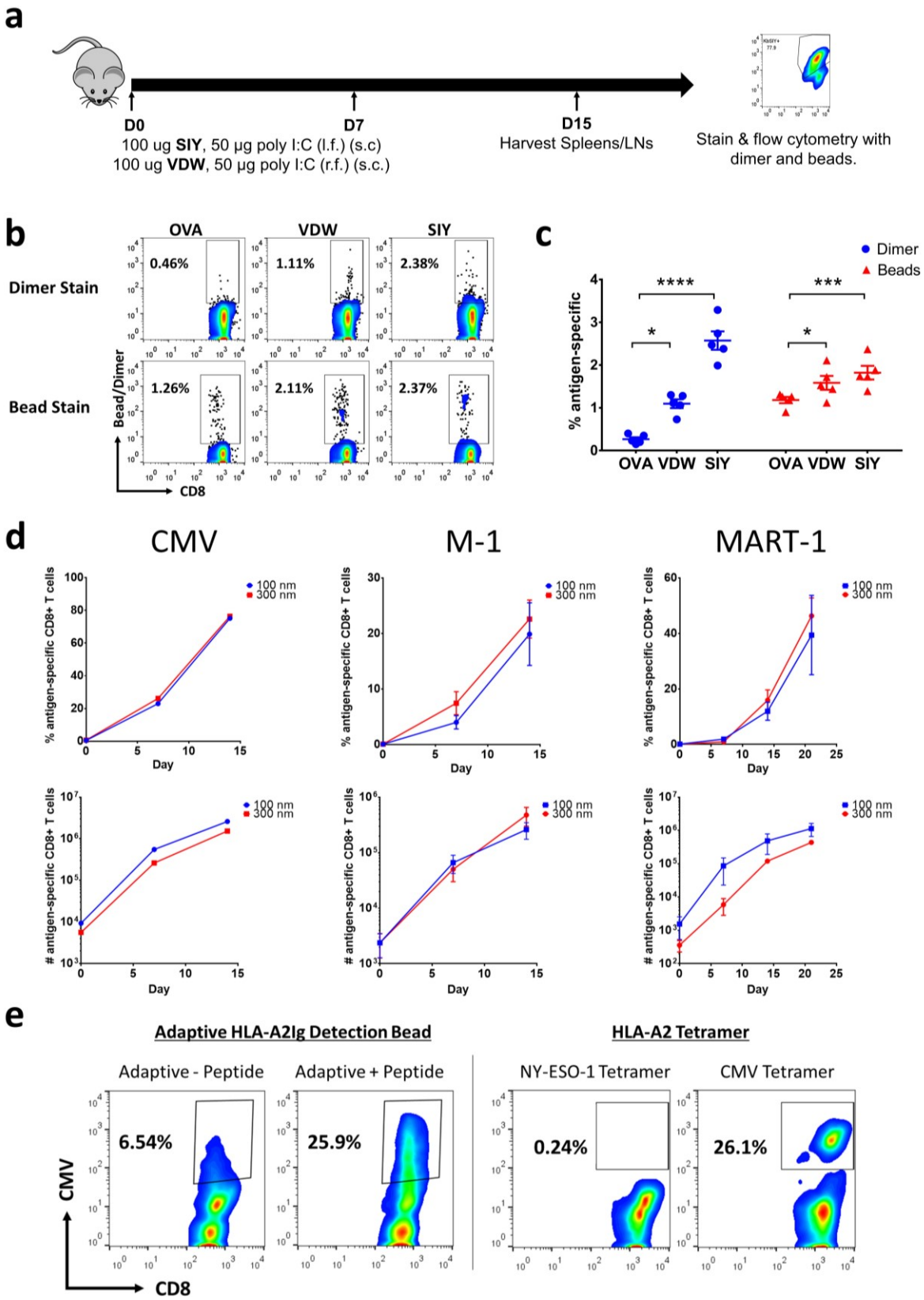

Figure 3-16. Application of developed adaptive nanoparticle platforms to isolate and identify neoantigen-specific and human antigen-specific CD8+ T cells.(a) Schematic of *in vivo* vaccination protocol for both SIY and VDW peptides. (b) Representative flow plots and (c) summary of results from staining

splenocytes of vaccinated B6 mice with SIY and VDW-loaded dimer and adaptive detection beads (error bars represent s.e.m; *p < 0.05, ***p < 0.001, ****p < 0.0001, n = 5, one-way ANOVA with Tukey's post test). (d) Replicates of staining of CMV, M-1 and MART-1 specific CD8+ T cells for antigen-specific (top panel) frequency and (bottom panel) number on Day 0 pre-enrichment and Days 7, 14, and 21 (for MART-1) following E+E (error bars represent s.e.m.; n = 1 – 5). (e) Representative staining of endogenous CMV-specific CD8+ T cells with adaptive detection beads compared to tetramer stains.

Specifically, we observed precursor frequencies increasing from 0.02–0.5% to 20–70% by Days 14 and 21 (**Figure 3-16d, top, Figure 3-18**). Similarly, we obtained log-fold number increases in total antigen-specific CD8+ T cells by Days 14 and 21, ending up with 10^5–10^6 antigen-specific CD8+ T cells from precursor numbers between 100 and 1,000, representing nearly a 200-300-fold increase by Day 14 for CMV and M-1 and a 500–2000-fold-increase by Day 21 for MART-1 (**Figure 3-16d, bottom**). Finally, to determine if we could apply our detection platform for endogenous human-specific CD8+ T cells, we followed a similar approach to synthesize fluorescent HLA-A2Ig detection beads and then load with peptide of interest. We found that the detection beads had similar efficacy at staining endogenous CMV-specific CD8+ T cells as CMV-specific tetramers (**Figure 3-16e**). This indicates our developed system can be applied in studying and discovering human antigen-specific CD8+ T cells.

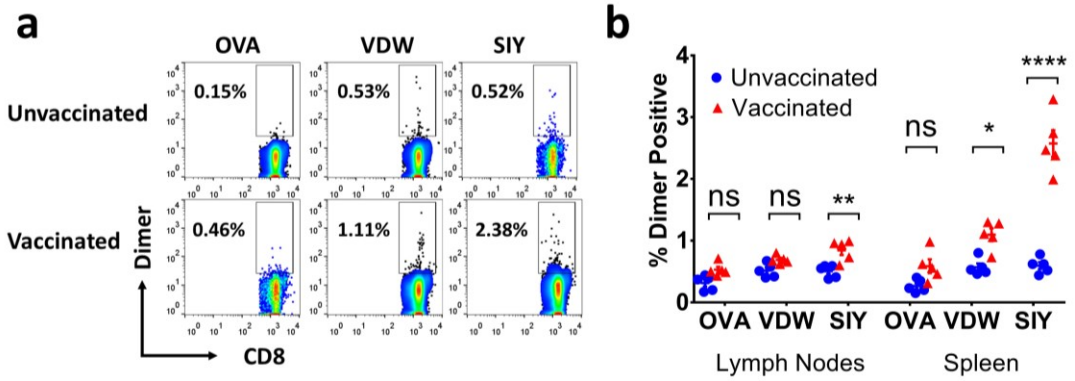

Figure 3-17. *In Vivo* Peptide vaccination with VDW and SIY peptide.(a) Representative and (b) summary of non-cognate OVA and cognate SIY and VDW dimer staining of spleens and lymph nodes of unvaccinated and vaccinated mice. The frequency of SIY and VDW specific CD8+ T cells is significantly increased by D15 in the spleens of vaccinated mice (error bars show s.e.m; *p < 0.05, **p < 0.01,****p < 0.0001, n = 5, one-way ANOVA with Tukey's post test).

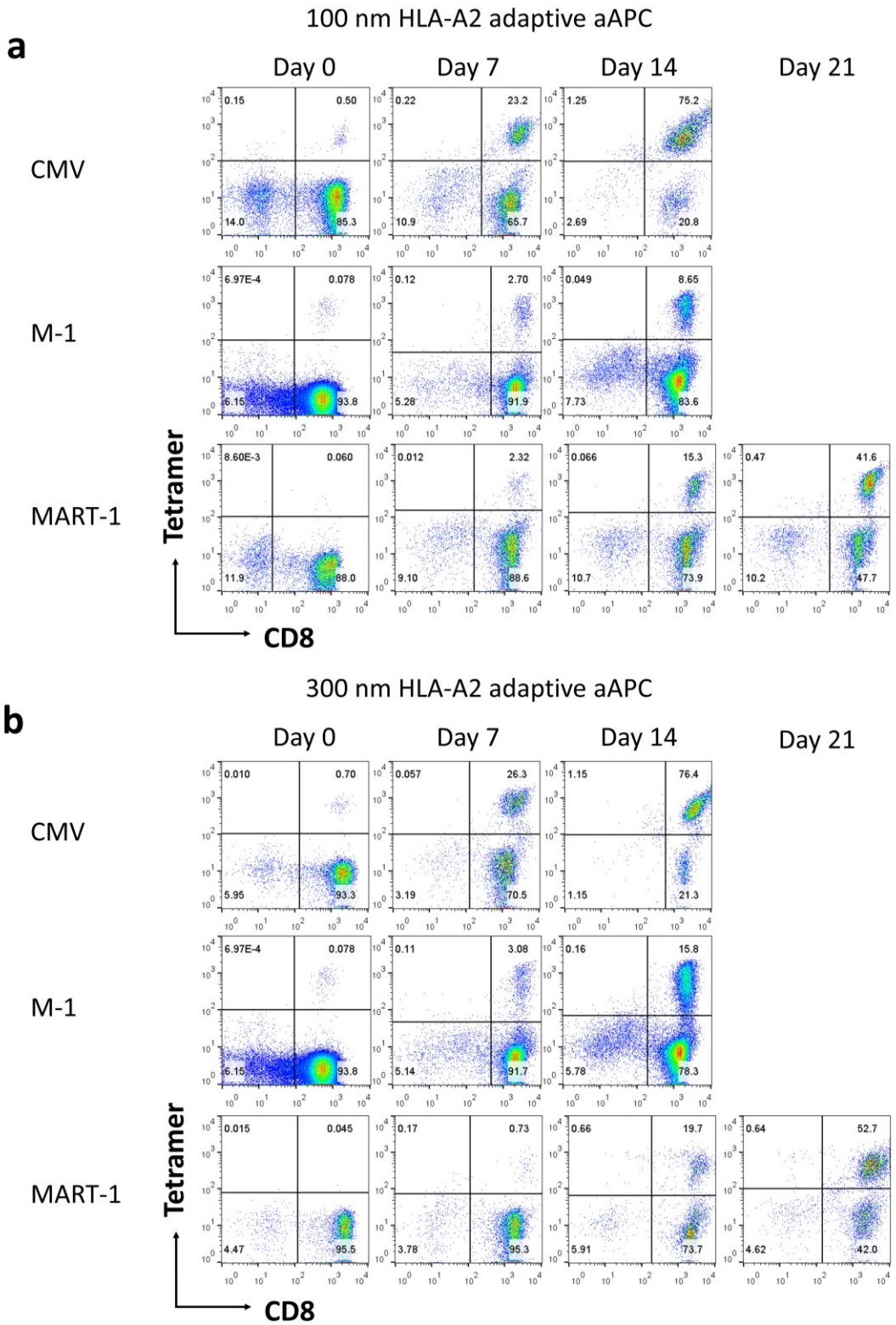

Figure 3-18. Enrichment and Expansion of antigen-specific CD8+ T cells for viral (M-1 and CMV) and tumor (MART-1) antigens using Adaptive aAPCs.(a) Representative expansion data with 100 nm Adaptive aAPCs. (b) Representative expansion data with 300 nm Adaptive aAPCs.

3.3 Conclusions

We engineered magnetic nanoparticle platforms to substantially improve expansion and detection of antigen-specific T cells and extended the process throughput and adaptability. First, we eliminated the need to enrich and expand antigen-specific T cells from purified CD8+ T cell populations. This decreased the total cost and time needed to perform the assay and resulted in significant increases in both the numbers and percentages of antigen-specific CD8+ T cells. Second, we modified the size of the aAPCs to 300 nm to enable parallel processing of multiple antigen-specific aAPC enrichments on a 96-well plate. Third, to further increase multiplexing and to create a standardized base particle, we created an adaptive aAPC where the MHC-Ig was conjugated to the surface of the particle and subsequently divided and loaded with a range of peptides. Fourth, we created a fluorescent, magnetic adaptive detection bead that can be loaded with a range of peptides to parallelize antigen-specific staining reagent production. Each of these engineered technologies and streamlined processes for E+E of antigen-specific T cells overcomes critical difficulties in processing and identifying antigen-specific T cells. Particularly, this technique is (a) sensitive, as it amplifies signal from both expanding and staining rare antigen-specific CD8+ T cells; (b) high-throughput, as the combination of the 96-well plate E+E format, adaptive aAPCs, and adaptive detection beads allow multiplexing for isolation and analysis of antigen-specific T cells; and (c) easy to use, as CD8+ T cell isolation kits are removed and nanoparticle reagents are easily customizable.

We applied this technology to isolate and identify a range of antigen-specific CD8+ T cells across disease, species, TCR affinity, and number of unique antigens. We

looked at CD8+ T cells specific for low-affinity cancer neoantigens, which demonstrates its versatility and ability to discover unknown antigen-specific CD8+ T cells to new antigens. We evaluated CD8+ T cells specific towards several antigens simultaneously, which facilitates the ability to examine cross-reactivity in the same sample. Finally, we evaluated this tool in respect to human infectious disease and melanoma antigens, which demonstrates direct clinical relevance either as a diagnostic or therapeutic. We anticipate that the throughput and parallel processing capabilities of our adaptive nanoparticle system will lend it to be adopted into other high-throughput assays such as single-cell RNA sequencing that would enable unique TCR-antigen combination analysis. In summary, our work facilitates adoption of both the platform and process to study unprecedented numbers and types of antigen-specific T cell responses in infectious disease, autoimmunity, allergy, and cancer.

3.4 Experimental Section

3.4.1 Mice

B6, 2C, and PMEL transgenic mice were maintained per guidelines approved by the Johns Hopkins University's Institutional Review Board. C57BL/6J mice were purchased from Jackson Laboratories (Bar Harbor, ME, USA). 2C T cell receptor transgenic mice were kept as heterozygotes by breeding on a C57BL/6J background.

3.4.2 MHC-Ig and Peptides

Soluble MHC-Ig dimers loaded with peptides ("Pre-loading") including DbIg, KbIg, and A2Ig were produced in-house as described[85,277]. Peptides for experiments used include: GP100: KVPRNQDWL, SIY: SIYRYYGL, SVY: SIYRYYGL, OVA: SIINFEKL,

TRP2: SVYDFFVWL, VDW: VDWENVSPEL, MCMV: YPHFMPTNL, CMV: NLVPMVATV, M1: GILGFVFTL, MART-1: ELAGIGILTV. Peptides were purchased from GenScript (New Jersey, USA). 2C T cell transgenic mice are cognate for SIY peptide loaded into KbIg and PMEL transgenic mice are cognate for GP100 peptide loaded into DbIg.

3.4.3 Pre-loaded Artificial Antigen Presenting Cells Production

Artificial antigen presenting cells (aAPC) were produced in-house as described[110,277]. Briefly, loaded antigen-specific dimeric MHC-Ig and equimolar anti-CD28, clone 37.51 (BioXCell. West Lebanon, NH, USA) were conjugated to the surface of magnetic particles functionalized with NHS surface groups at a based particle size of 200 nm (Ocean Nanotech, Springdale, AR, USA) per the manufacturer's recommendations.

3.4.4 Adaptive Artificial Antigen Presenting Cells Production

For Adaptive aAPCs, MHC-Ig was conjugated to particles (with the same method as pre-loaded) except without previously loading in a specific peptide.

3.4.5 Detection Bead Production

For detection beads, BNF-Starch-greenF 100-nm magnetic particles with amine surface groups (Micromod, Rostock, Germany) were functionalized with Sulfo-SMCC (Proteochem, Hurricane, UT, USA) and dimeric MHC-Ig was thiolated with Traut's reagent (2-iminothiolane) (Sigma Aldrich, St. Louis, MO, USA) and then mixed with the functionalized particles per the manufacturer's recommendations. For adaptive

detection beads, MHC-Ig was conjugated to particles without previously loading in a specific peptide.

3.4.6 Artificial Antigen Presenting Cell Characterization

The amount of protein conjugated successfully to the surface of the particles was quantified through fluorescent staining. The amount of MHC-Ig was quantified by staining with FITC-conjugated rat anti-mouse Ig λ1, λ2, λ3 light chain, clone R26-46 (BD Biosciences, San Jose, CA, USA), and the amount of anti-CD28 was quantified by staining with FITC-conjugated mouse anti-Armenian Syrian hamster IgG, clone G192-1 (BD Biosciences). Particles were stained with 1 µL of the antibody for 1 h at 4°C, washed three times, and then fluorescence was read on Synergy HTX Multi-mode florescent plate reader (BioTek, Winooski, VT, USA). Protein was quantified by comparison to fluorescent standard curve of staining antibodies, and particle number was quantified by absorbance using a spectrophotometer at a wavelength of 405 nm.

3.4.7 Adaptive aAPCs and Detection Bead Peptide Loading

To load Adaptive aAPCs or Detection Beads, an aliquot of aAPCs (1.5×10^{10} particles) or Detection Beads (3.8×10^{10} particles) was aliquoted into a final volume of 100 µL of PBS in a 96-U bottomed plate. Then 1 µg of peptide was added to the particles overnight at 4°C. The particles were washed three times on the “Ring” magnet with 200 µL of PBS and immediately used.

3.4.8 Supplemented Media and T Cell Growth Factor

Supplemented media (B’ Media) was made with PBS buffer and 0.5% bovine serum albumin (BSA) (Gemini, Sacramento, CA) and 2 mM EDTA. The T cell growth

factor (TCGF) was made with RPMI 1640 media with glutamine, 1x non-essential amino acids, 1 mM sodium pyruvate, 0.4× vitamin solution, 92 μM 2-mercaptoethanol, 10 μM ciprofloxacin and 10% fetal bovine serum (FBS) (Atlanta Biologicals, Flowery Branch, GA).

3.4.9 Specific Cell Isolation and Depletion

Murine cells were obtained from adult female and male mouse lymph nodes and spleens. Obtained cells were treated with ACK lysing buffer to lyse red blood cells and filtered through cell strainers to isolate splenocytes. PBMCs from healthy human donors were isolated by Ficoll-Paque PLUS gradient centrifugation (GE Healthcare, Chicago, IL, USA). For isolating CD8+ T lymphocytes, CD4+ T lymphocytes, Pan T cells, these cells were isolated from splenocytes or PBMCs by negative selection using CD8+, CD4+, and Pan T cell isolation kits and magnetic columns from Miltenyi Biotech (Auburn, CA, USA) according to the manufacturer's protocol. Memory CD8+ T cells were not depleted for all CD8+ isolations, in order to maintain consistency with CD8+ populations we would encounter in isolating antigen-specific T cells from splenocyte or PBMC sources. To deplete specific cell populations, biotinylated antibody was added to splenocytes for 5 min at 4°C, followed by ratio of anti-biotin magnetic beads consistent with previous manufacturer recommended amounts from isolation kits (Miltenyi Biotech); for CD4+ T cells, clone Gk1.5 (eBioscience), for CD11c+ cells, clone N418 (BioLegend, San Diego, CA, USA). PBMCs were obtained from blood drawn from healthy males and females per JHU IRB approved protocols.

3.4.10 Enrichment and Expansion for Small (50–100 nm) Nanoparticle aAPCs

All E+E conditions received the same number of initial splenocytes going into the various isolation conditions. Following cell isolation, the nanoparticle aAPCs were added to cells based on the ratio of 10^{11} aAPC-bound, peptide-loaded MHC-Ig for every 1×10^7 splenocytes or for every 10^6 CD8+ T cells. Similarly, E+Es with KbSIY-only aAPCs or from Pan-T isolate were performed at a ratio of 10^{11} aAPC-bound peptide-loaded class I MHC-Ig for every $1x10^6$ CD8+ T cells. The aAPC particle and cell mixtures were incubated for 1 h at 4°C with continual mixing in a PBS buffer with 2 mM EDTA and 0.5% Bovine Serum Albumin (BSA) (*Termed Running Buffer*). The magnetic particle aAPC:cell mixtures were then separately washed in a Miltenyi MS magnetic column three times. The magnetic column was wet with 0.5 mL of PBS, then the particles/cells were added to the column and washed using two separate washes of B' Media and third wash using B' Media with 1% TCGF. The cells were counted using a hemocytometer and plated in a 96 U-bottomed plate in 160 µL per well of B' Media with 1% TCGF at a concentration of 1×10^6 splenocytes/mL or 2.5×10^5 CD8+ T cells/mL. The aAPC:cell mixtures were cultured in a humidified 5% CO_2 37°C incubator for 3 days. On day 3, the cells were fed with 80 µL per well of B' Media with 2% TCGF and placed back into the incubator until day 7. On day 7, the stimulated cells were harvested into a 5-mL round bottom tube for counting and analyzed for antigen specificity by flow cytometry.

3.4.11 96-well Plate-based Enrichment and Expansion for 300-nm aAPCs

A similar protocol to the E+E for small aAPCs, as described above, was followed, with an alternate washing process. Following the 1 h incubation at 4°C, the aAPC:cell mixtures were added to a 96 U-bottomed well plate and placed on a magnet for 5 min. Two different kinds of magnets were used for the experiments the “Ring” magnet—“MAGNUM™ EX Adaptive Magnet Plate” (Alpaqua, Beverly, MA)–and the “Bottom” magnet—“EasyPlate Easy Sep Magnet” (STEM-cell, Vancouver, Canada). The buffer was carefully removed from the wells with an angled multichannel pipette to not disrupt the magnetic pellet on the bottom or in the ring. The plate was removed from the magnet, and the pellet was resuspended in 200 µL of B’ Media. The plate was placed on the magnet for 2 min. The supplemented media was then carefully removed from the wells. The plate was removed from the magnet, and the pellet was resuspended in 200 µL of B’ Media with 1% TCGF. Then the plate was placed on the magnet for 2 min. The plate was removed from the magnet, and the pellet was resuspended in 160 µL of B’ Media with 1% TCGF. The plate was placed in a humidified 5% CO_2 37°C incubator for 3 days. On day 3, the cells were fed with 80 µL per well of B’ Media with 2% TCGF and placed back into the incubator until day 7. On day 7, the stimulated cells were harvested into a 5-mL round bottom tube for counting and analyzed with antigen-specific staining for flow cytometry.

For batched versus individual E+E comparisons, the splenocytes were divided into 8 equal portions in sterile FACS tubes. The respective four types of antigen-specific aAPCs were added to two different FACS tubes. To form the batched condition, four of

the individual conditions were combined into one tube and then processed together from then on.

In the case of human T cell expansion, 10% AB serum was used instead of 10% fetal bovine serum. On day 3 of culture, cells were fed with half the volume of the initial T cell culture media with twice the concentration of T cell growth factor cocktail. On day 7 cells were harvested counted and re-plated at a density of 50,000 cells per well with an additional dose of aAPCs, while a subset was taken for antigen-specific staining. On day 10 of culture, cells were fed with half the volume of the initial T cell culture media with twice the concentration of T cell growth factor cocktail. Cells were harvested on day 14, counted, and stained for antigen-specificity.

3.4.12 Antigen Specific Staining

On day 7 of culture, the number of cells were counted using a hemocytometer. After counting, less than 500,000 cells were collected and placed into two 5-mL round bottom tubes for antigen-specific staining. One tube was used for the cognate peptide-MHC stain, and the other tube was used for the non-cognate stain to determine background staining. To the two conditions, 1 µg of cognate or non-cognate biotinylated MHC-Ig in 100 µL of PBS with 0.05% sodium azide and 2% FBS (FWB) for 1 h at 4°C. The excess biotinylated MHC-Ig with PBS was washed through centrifugation. The samples were then stained with a 1:350 ratio of PE-labeled streptavidin, with 1:100 APC-conjugated rat anti-mouse CD8a, clone 53-6.7 (BioLegend, San Diego, CA, USA), and with 1:1000 ratio of LIVE/DEAD® Fixable Green Dead Cell Stain (ThermoFisher) for 15 min at 4°C. Excess secondary and live/dead stain were washed by centrifugation and resuspended with 150 µL of PBS buffer with FWB to read on a BD FACSCalibur

flow cytometer. To determine the percent of antigen-specific cells, the following gates were used in the respective order: live+, lymphocyte+ (forward scatter by side scatter), CD8+, and Dimer+. The Dimer+ gate was determined by comparing non-cognate to the cognate stain. To determine the percentage of antigen-specific cells, the percentage of Dimer+ of the cognate MHC-Ig stain was subtracted from the non-cognate MHC-Ig stain. To obtain the number of antigen-specific cells, this number was multiplied by the percentage of CD8+ T cells and the number of cells counted.

Detection of antigen-specific human cells was done similarly, except instead of staining with biotinylated dimer, the antigen-specific cells were stained with purchased PE-labeled tetramer (MBL International, Woburn, MA) for 30 min at room temperature, then washed and stained with APC-conjugated anti-human CD8a, clone SK-1 (BioLegend), and 1:1000 of LIVE/DEAD® Fixable Green Dead Cell Stain for 15 min at 4 °C.

3.4.13 Fluorescent Magnetic Bead Antigen-specific Staining

On day 7 of culture, the number of cells were counted using a hemocytometer. After counting, less than 500,000 cells were collected and placed into two 5-mL round bottom tubes for antigen-specific staining. To either tube, pre-loaded MHC-Ig fluorescent beads or adaptive detection beads +/- peptides were added at the indicated amounts and allowed to bind for 45 min at 4°C. Then a solution of 1:100 APC-conjugated rat anti-mouse CD8a, clone 53-6.7 (BioLegend, San Diego, CA, USA) (for mouse stains) and with 1:1000 ratio of LIVE/DEAD® Fixable Red Dead Cell Stain (ThermoFisher) was added to samples to stain for an additional 15 min at 4°C. Cells were washed and read on a BD FACSCalibur and antigen-specificity was determined

similar to biotinylated dimer-MHC staining, while unloaded adaptive detection beads were used as the background staining.

Particle staining of human cells was done using a similar protocol except an APC-conjugated mouse anti-human CD8a, clone SK-1 (Biolegend), was substituted for the rat anti-mouse CD8a stain.

3.4.14 *In Vivo* Peptide Vaccination

Naïve 8-week-old female mice were injected subcutaneously with a mixture of 100 µg SIY peptide and poly I:C diluted into 200 µL PBS on their left rear flanks, and 100 µg VDW peptide and poly I:C diluted into 200 µL PBS on their right rear flanks on both Day 0 and Day 7. On Day 15, mouse spleens and lymph nodes were harvested for dimer and particle staining, following similar protocols described above.

3.4.15 Splenocyte Immune Cell Flow Cytometry Panel

Less than 500,000 cells were collected and stained with a 1:100 PBS solution of Pe/Cy7-conjugated rat anti-mouse CD19, clone 6D5 (Biolegend), APC-conjugated rat anti-mouse NK-1.1, clone PK136 (BD Pharmingen), APC/Cy7-conjugated rat anti-mouse CD8a, clone number 53-6.7 (Biolegend), PE-conjugated rat anti-mouse CD4, clone H129.19 (Biolegend), PerCP-conjugated rat anti-mouse CD11c, clone N418 (Biolegend), AmCyan-conjugated F4/80, clone 605 (Biolegend), and 1:1000 of LIVE/DEAD® Fixable Green Dead Cell Stain (ThermoFisher) for 15 min at 4°C. Cells were then washed with FACS wash buffer to be read on BD LSRII flow cytometer and analyzed using FlowJo to measure the population of B cells (CD19+), NK cells (NK1.1+), CD4+ T cells, dendritic cells (CD11c+), and macrophages (F4/80+).

3.4.16 T Cell Proliferation Assay

CD8+ T cells were isolated as previous described and resuspended in 1 mL T cell culture media. Cells were mixed with 1 µL CellTrace™ carboxyfluorescein succinimidyl ester (CFSE) dye (ThermoFisher) in 1 mL of T cell culture media per 3 million cells and incubated at 37 °C for 20 min. CFSE stained cells were washed with 50 mL of T cell culture media to remove unstained dye and plated. On day 3 of culture, cells were harvested and stained with a 1:100 PBS solution of APC-conjugated rat anti-mouse CD8a, clone 53-6.7 (Biolegend) for 15 min at 4 °C. The CFSE fluorescence intensity was measured using BD FACSCalibur flow cytometer. Cell proliferation was analyzed using FlowJo with diluted CFSE fluorescence peaks signifying population after each round of cell division. A subset of the cells was allowed to expand for 7 days and viable cells were counted with a hemocytometer to determine fold expansion.

3.4.17 T Cell Phenotype Assay

On day 7 of culture, the numbers of cells were counted using hemocytometer. After counting, less than 500,000 cells were collected and stained with a 1:100 PBS solution of APC-conjugated rat anti-mouse CD8a, clone 53-6.7 (Biolegend), PE-conjugated rat anti-mouse CD62L, clone MEL-14 (BD Biosciences), PerCP-conjugated rat anti-mouse CD44, clone IM7 (Biolegend), and 1:1000 of LIVE/DEAD® Fixable Green Dead Cell Stain (ThermoFisher) for 15 min at 4 °C. Cells were then washed with FACS wash buffer to be read on BD FACSCalibur flow cytometer and analyzed using FlowJo to measure the population of naïve T cells (CD62L+CD44-), effector T cells (CD62L-CD44+), and memory T cells (CD62L+CD44+).

3.4.18 T Cell Cytokine Functionality Assay

On day 7 of culture, approximately 500,000 CD8+ T cells were isolated from each condition and separated into cognate or noncognate groups. Cells were stained with 1 µg of either cognate or non-cognate biotinylated pMHC-Ig dimer for 1 h at 4°C. After washing, samples were stained with a 1:350 ratio of PE-labeled streptavidin (BD Pharmingen, San Diego, CA, USA). Then 10 µL solution of 1:50 FITC anti-CD107a, 1:350 BD GolgiStop Protein Transport Inhibitor (BD Biosciences), and 1:350 BD GolgiPlug Protein Transport Inhibitor (BD Biosciences) in PBS was added to the samples and incubated with 100 µL of complete media for 37 °C for 6 h. Cells were then washed and stained with 1:100 PBS solution of PerCP-conjugated anti-mouse CD8a, clone 53-6.7 (Biolegend) and 1:1000 of LIVE/DEAD® AmCyan Fixable Aqua Dead Cell Stain (ThermoFisher) at 4 °C for 30 min. Cells were then fixed and permeabilized with 100 µL BD Cytofix/Cytoperm Fixation and Permeabilization Solution (BD Biosciences) overnight. Cells were then washed with 1× BD PERM/Wash buffer with 2% BSA and stained with 1:100 solution of APC-conjugated rat anti-mouse IFN-γ, clone XMG1.2 (BD Pharmingen) and PE-Cy7-conjugated rat anti-mouse TNFα, clone MP6-XT22 (Biolegend) in PERM/Wash buffer with 2% BSA at 4 °C for 1 h. Stained cells were read on BD LSR II flow cytometer.

3.4.19 IFN-γ Release Assays

On day 7 of culture, 25,000 2C CD8+ T cells were re-stimulated with 300-nm pre-loaded vs. Adaptive aAPCs pre- vs. post-loaded KbSIY/anti-CD28 particles for 18 h at 37°C, and then the supernatants were collected. IFN-γ was measured by ELISA using the eBioscience murine IFN-γ Ready-SET-Go! Kit (San Diego, CA, USA)

3.4.20 Peptide Stabilization Assays

RMA-S cells were left at 25° overnight and pulsed for 2 h with 1 μg peptide and put at 37° for 2 h to degrade unstable MHC molecules. Cells were then stained with anti-Kb clone M1/42 and analyzed by flow cytometry for MHC expression.

3.4.21 Doped Enrichment Experiments

PMEL CD8+ T cells were obtained by using a mouse CD8+ T cell negative isolation kit from Miltenyi Biotech and following the manufacturer's instructions. PMEL transgenic mice have CD8+ T cells with the same T cell receptor that recognizes the mouse MHC Db loaded with the gp100 peptide. The PMEL CD8+ T cells were counted with a hemocytometer and added at a 1:1000 ratio to wildtype B6 CD8+ T cells and mixed thoroughly in running buffer. Particle aAPCs were added to this mixture at the indicated amounts per 1×10^6 total CD8+ T cells and allowed to bind at 4 °C for 1 h. The particle cell-mixture was then washed magnetically as previously described within the "Enrichment and Expansion" experiments. All particle-cell mixtures counted via a hemocytometer and stained with the APC-conjugated rat anti-mouse CD8a, clone 53–6.7, (Biolegend) for 15 min at 4°C, washed and read on a BD FACSCalibur.

Fold enrichment was determined by dividing the percent of PMEL positive cells in the eluted particle-cell mixture by the percent of PMEL positive the native 1:1000 doped mixture. Percent cell recovery was calculated by dividing the number of PMEL positive cells in the eluted particle-cell mixture by the number of PMEL positive in the native 1:1000 doped mixture. The PMEL cell counts were calculated by multiplying the number of cells in each mixture by the measured percentages from flow cytometry.

3.4.22 Particle and Bead Binding

Particle aAPCs were allowed to bind with cognate transgenic CD8+ T cells at 4°C for 1 h at various ratios of particle aAPCs to T cells. This mixture was washed and stained with a 1:350 ratio of PE labeled rat-anti-mouse IgG for 15 min at 4°C. PE labeled polyclonal goat-anti-mouse IgG1 (ThermoFisher) recognizes the mouse IgG of the dimeric Kb-Ig on the particles to discriminate the quantitate particles on the surface. Excess antibody was washed away and then stained with a 1:100 PBS solution of APC-conjugated rat anti-mouse CD8a, clone 53-6.7 (Biolegend). Cells were washed and read on a BD FACSCalibur to determine the percent of cells bound with respect to the non-particle bound and non-cognate CD8+ T cells of background staining. Fluorescent magnetic detection bead binding and analysis was performed similarly, except that there is no need for secondary antibody staining since the particles themselves are fluorescent.

Chapter 4. Antitumor Roles of CD4+ T cells[3]

Recent studies show that CD4+ T cells have important effector roles in the anti-tumor response including: superior recognition of tumor neoantigens in both mouse [278] and human[272] systems, MHC II-dependent tumor cell lysis [279], and MHC II-independent but INF-γ-dependent recruitment and activation of macrophages and NK cells[280] (**Figure 4-1**). In fact, autologous transfer of NY-ESO-1 reactive CD4+ T cells alone has been shown to mediate durable remission in a patient with refractory metastatic melanoma[24]. Moreover, there is significant evidence that combined CD4+ and CD8+ cell-based therapies may have synergistic effects, as CD4+ T cells play important helper roles in enhancing CD8+ activation[281], memory formation[282], and antigen-spreading to non-targeted tumor epitopes [283,284].

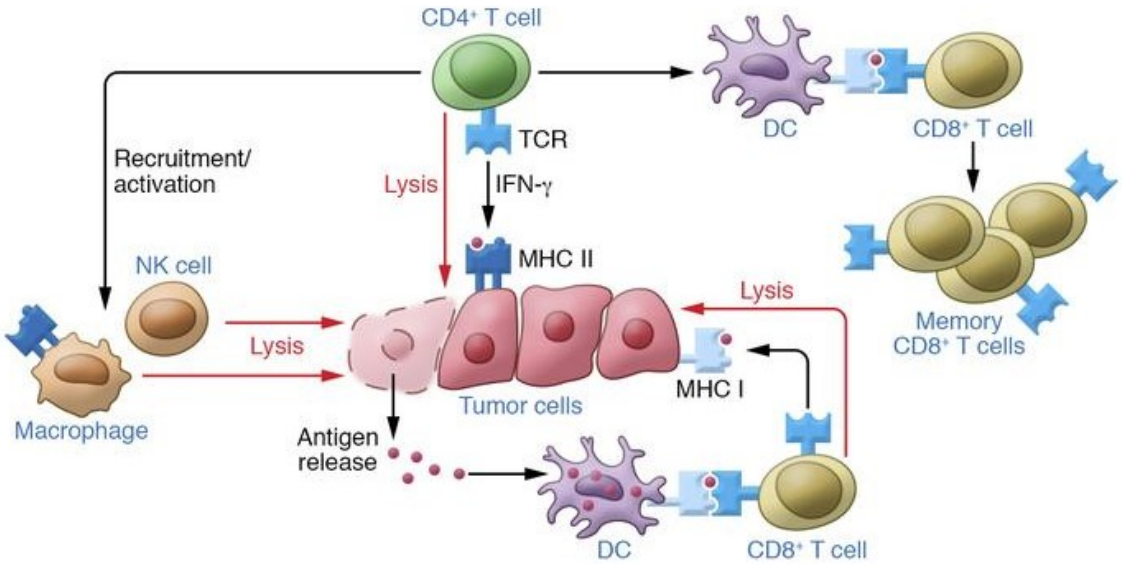

Figure 4-1. The wide range of effector and helper roles of CD4⁺ T cells in the antitumor response.CD4⁺ T cells can directly lyse tumor cells that have constitutive or inducible MHC II expression. Additionally, they can indirectly lead to tumor cell lysis by recruiting and activating macrophages and NK cells, which can release tumor antigens that can be presented by professional antigen-presenting cells such as dendritic cells to CD8⁺ T cells. Finally, they can also license dendritic cells, enhancing the activation and memory formation of tumor-specific CD8⁺ T cells.

[3] This chapter is excerpted (adapted) with permission from: "Isser, Ariel and Jonathan P. Schneck, High affinity T cell receptors for adoptive cell transfer. *J. Clin. Invest.* 129 (2018): 69–71. Copyright 2019 American Society for Clinical Investigation.

Chapter 5. A Nanoparticle Platform Mobilizes CD4$^+$ T Cells for Immunotherapy

5.1 Introduction

Clinical successes of adoptive cell transfer (ACT) therapies across a wide range of hematologic malignancies[285,286] and solid tumors[16,24] have propelled T cell therapies to the forefront of treatment options for a variety of cancers and other diseases. Despite their promise, some of the largest hurdles these therapies face in moving towards widespread translation are the associated time, costs, and complexities of *ex vivo* T cell expansion[287], as well as the variability of the resulting clinical products.

A range of approaches have been developed for *ex vivo* expansion of tumor-specific T cells, including polyclonal T cell stimulation with plate- or bead-bound anti-CD3 (αCD3) antibodies or antigen-specific T cell stimulation with peptide-pulsed autologous antigen presenting cells (APCs). To simultaneously address the lack of specificity of αCD3 stimulation as well as the manufacturing challenges and variability of donor-derived APCs, biomimetic artificial APCs (aAPCs) that include MHC proteins and co-stimulatory molecules have been produced[105]. Thus far, these synthetic platforms have focused almost exclusively on CD8$^+$ T cells, whereas little progress has been made for CD4$^+$ targeted technologies.

CD4$^+$ T cells serve several critical functions in the antitumor immune response, including recognizing neoantigens that result from tumor-specific mutations[278,288], recruiting and activating innate immune cells[280,289,290], directly lysing MHC II positive

tumor cells[279], and relaying indispensable “help” signals to $CD8^+$ T cells to enhance their antitumor function and memory formation[291]. A simplified system that modulates these functions could pave the way toward scalable, consistent $CD4^+$ T cell or “helped” $CD8^+$ T cell cancer therapies, while also providing mechanistic insight into $CD4^+$ T cell tumor biology.

Herein, we describe a novel platform for antigen-specific $CD4^+$ T cell expansion, consisting of iron-dextran nanoparticles coated with MHC II and co-stimulatory proteins. These MHC II aAPCs lead to expansion of cognate murine $CD4^+$ T cells that display high levels of effector cytokine production and demonstrate robust lytic capacity *in vitro* and *in vivo*. MHC II aAPCs also relay help signals from $CD4^+$ T cells to tumor-specific $CD8^+$ T cells, which, in turn, enhance $CD8^+$ T cell cytokine production, memory formation, and *in vitro* and *in vivo* antitumor activity. Lastly, murine MHC II and human counterpart HLA II aAPCs can expand rare subsets of endogenous murine and human $CD4^+$ T cells, respectively for a variety of research and therapeutic applications.

5.2 Results

5.2.1 MHC II aAPCs stimulate functional antigen-specific murine $CD4^+$ T cells

T cells require two signals to become activated: T cell receptor (TCR) stimulation known as signal 1 (S1) through cognate peptide-loaded MHC (pMHC) interactions, and co-stimulation, termed signal 2 (S2), most commonly through the CD28 receptor. TCR-pMHC interactions tend to be lower affinity for $CD4^+$ T cells than for $CD8^+$ T cells[292]. Based on this premise, we formulated two aAPC designs for *ex vivo* activation of

antigen-specific murine CD4$^+$ T cells: one that, similar to traditional MHC I aAPCs[105], co-presents MHC II I-A^b proteins and anti-CD28 (αCD28) antibodies (S1/2) and a second that presents only I-A^b proteins, with addition of soluble αCD28 (S1+S2), to maximize MHC II valency on aAPCs (**Figure 5-1a**). To synthesize the aAPCs, signals were conjugated to 200 nm iron oxide nanoparticles, a size which corresponds to the pre-formed TCR clusters found on naïve T cells[90] and which we have previously shown is optimal for CD8$^+$ T cell engagement[109]. Post fabrication, the aAPCs were approximately 300 nm in size (**Figure 5-2a-b**), with around 100 I-A^b molecules per S1/2 bead and 200 I-A^b molecules per S1 bead (**Figure 5-1b**). Through titration of the S1/2 aAPCs into culture with TCR transgenic OT-II ovalbumin (OVA) specific CD4$^+$ T cells, we found that a concentration of 80 ng/mL I-A^b loaded with the OVA$_{329-337}$ peptide (I-A$^b_{OVA}$) led to similar percentage of T cells dividing at day 3 (**Figure 5-2c-d**) and fold proliferation at day 7 (**Figure 5-1c**) compared to control αCD3/αCD28 microbeads. The stimulation was antigen-specific, as I-A^b aAPCs loaded with an irrelevant CLIP$_{87-101}$ peptide (I-A$^b_{CLIP}$) did not induce OT-II proliferation (**Figure 5-1c, Figure 5-2c-d**). For S1 aAPCs, increasing the amount of soluble S2 added into culture did not impact the percentage of cells dividing at day 3 (**Figure 5-2e-f**) but did increase fold proliferation at day 7 to levels similar to αCD3/αCD28 microbeads and S1/2 aAPCs (**Figure 5-1d**). As certain CD4$^+$ T cell subsets can either promote or inhibit antitumor responses[293] (e.g. Th1 versus regulatory T cells), we next analyzed CD4$^+$ T cell polarization, by activating OT-II CD4$^+$ T cells with MHC II aAPCs in the presence of various cytokine mixes. In comparison to treatment with interleukin-2 (IL-2) only and no cytokines, a Th1 mix (IL-2, IL-12p70, and IFN-γ) led to higher T-bet expression (**Figure 5-1e-f**) and IFN-γ

production (**Figure 5-1g, Figure 5-2g**), hallmark transcription factors and cytokines of the Th1 lineage, respectively. Interestingly, a standard T cell growth factor (TF) cytokine cocktail for $CD8^+$ T cell culture[294], led to a similar increase in T-bet levels but not IFN-γ production. We also compared the impact of different types of T cell stimulation on OT-II cell proliferation and function when cultured in the Th1 mix. We found that optimal doses of S1/2 and S1+S2 aAPCs led to equivalent proliferation as αCD3/αCD28 microbeads, OT-II splenocytes pulsed with $OVA_{323-339}$ peptide, or bone marrow derived dendritic cells (BMDCs) (**Figure 5-2h**). Additionally, S1+S2 aAPC stimulation led to IFN-γ production equivalent to peptide-pulsed splenocytes or αCD3/αCD28 microbeads, whereas cells cultured with S1/2 aAPCs or BMDCs produced less IFN-γ **Figure 5-1h, Figure 5-2i**). To assess the impact of signal density on aAPC-mediated OT-II proliferation and function, we mixed I-A^b_{OVA} proteins at 1:1 and 1:3 molar ratios with isotype antibodies (S1/I) or bovine serum albumin (S1/B), detecting lower conjugation of I-A^b at higher ratios of these additional proteins (**Figure 5-2j**). We found that at equivalent doses of S1 (80 ng/mL), aAPCs with lower S1 density led to similar percentages of OT-II cells dividing at day 3 (**Figure 5-2k**), but lower overall proliferation at day 7 compared to higher density S1 or S1/2 aAPCs (**Figure 5-2l**). That said, the density of S1 did not impact OT-II function at day 7 (**Figure 5-2m**). We performed similar analyses using 4.5 μm S1/2 aAPCs that more closely mimic the size of endogenous APCs, observing no significant differences in OT-II proliferation or IFN-γ and TNF-α secretion compared to nano-aAPCs, but higher frequencies of IL-2 producing cells (**Figure 5-2k-m**). Together, these results demonstrate robust expansion

of functional, antigen-specific CD4⁺ T cell is achieved by both S1/2 and S1+S2 MHC II aAPCs and that the extent of expansion is directly dependent upon S1 density.

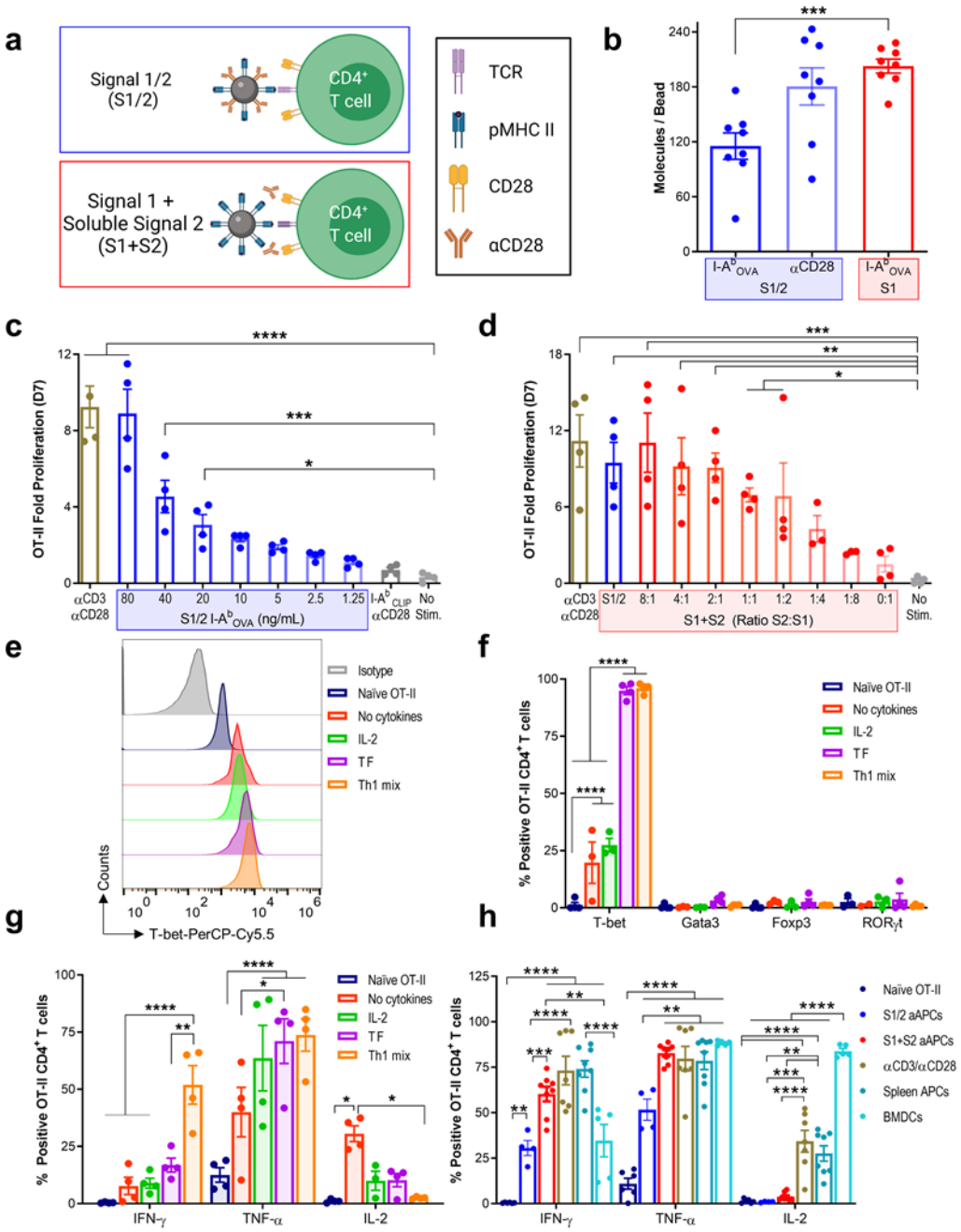

Figure 5-1. MHC II aAPCs stimulate functional antigen-specific murine CD4⁺ T cells.(**a**) Design of MHC II aAPCs with MHC II molecules (MHC II) as Signal 1 (S1) and anti-CD28 antibodies (αCD28) as Signal 2 (S2). S2 is attached to aAPCs (S1/2) or delivered solubly (S1+S2). Created with BioRender.com. (**b**) Fluorescent quantification of I-A$^b_{OVA}$ and αCD28 conjugated to S1/2 and S1 aAPCs. (**c**) OT-II CD4⁺ T cell fold proliferation after 7-day stimulation with I-A$^b_{OVA}$ S1/2 aAPCs compared to polyclonal αCD3/αCD28 or I-A$^b_{CLIP}$ aAPCs. (**d**) Day 7 OT-II fold proliferation following treatment with S1 aAPCs and a titration of S2, compared to S1/2 or αCD3/αCD28 aAPCs. (**e**) Day 7 T-bet staining, (**f**) CD4⁺ lineage transcription factor staining, and (**g**) cytokine production of OT-II cells stimulated with S1/2 aAPCs in media containing: no

cytokines, IL-2, T cell growth factor (TF), or a Th1 mix (IL-2, IL-12p70, IFN-γ). (**h**) Day 7 cytokine production of OT-II cells stimulated with S1/2, S1+S2, or αCD3/αCD28 aAPCs versus peptide pulsed splenocytes or bone-marrow derived dendritic cells (BMDCs). Data in (**b-d, f-h**) represent mean ± standard error of the mean (s.e.m.) from three or more independent experiments. (**b**) n = 8 analyzed using an unpaired Student's *t* test, two-tailed, (**c-d**) n = 3-4 mice analyzed using a one-way ANOVA compared to 'no stim.' with Dunnett's post-test, and (**f-h**) n = 3-5 mice analyzed using a two-way ANOVA with Tukey's multiple-comparisons test, *p < 0.05, **p < 0.01, ***p < 0.001, ****p < 0.0001.

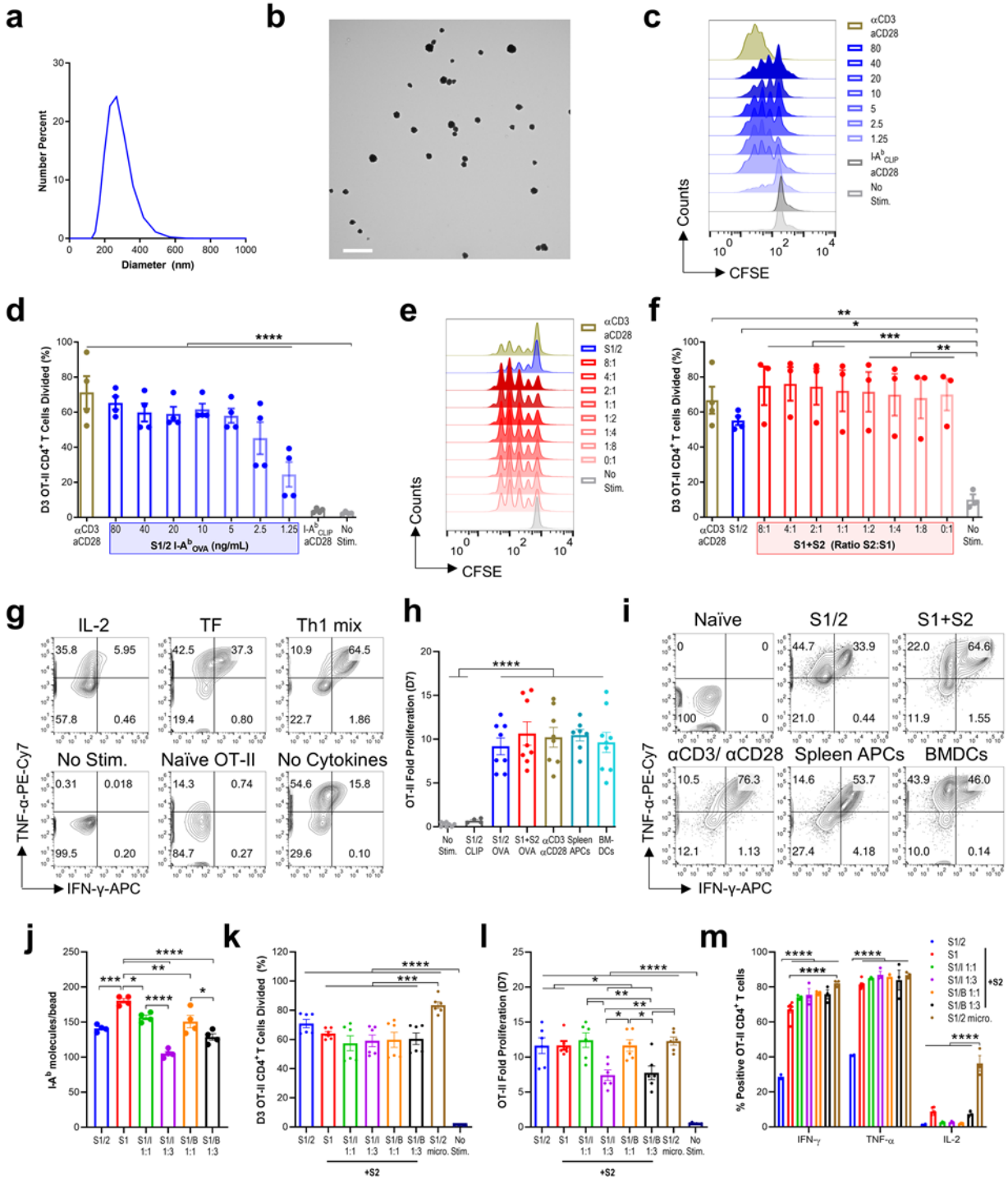

Figure 5-2. Characterization and function of MHC II aAPCs.(**a**) Size distribution of MHC II aAPCs as measured by dynamic light scattering (DLS). (**b**) Transmission electron imaging of MHC II aAPCs. Scale

bar: 500 nm. (**c**) CFSE dilutions and (**d**) percentage of OT-II CD4$^+$ T cells divided after 3 days of stimulation with a titration of I-A$^b_{OVA}$ S1/2 aAPCs compared to polyclonal αCD3/αCD28 or I-A$^b_{CLIP}$ aAPCs. (**e**) CFSE dilutions and (**f**) percentage of OT-II cells divided after 3 days of stimulation with I-A$^b_{OVA}$ S1 aAPCs and a titration of S2, compared to S1/2 or αCD3/αCD28 aAPCs. (**g**) Representative day 7 cytokine staining of OT-II cells stimulated with S1/2 aAPCs in media containing: no cytokines, IL-2, T cell growth factor (TF) cytokine cocktail, or a Th1 mix (IL-2, IL-12p70, IFN-γ). (**h-i**) Fold proliferation and representative day 7 cytokine staining of OT-II cells stimulated with saturating doses of S1/2, S1+S2, or αCD3/αCD28 aAPCs versus peptide pulsed OT-II splenocytes or bone-marrow derived dendritic cells (BMDCs). (**j**) Fluorescent quantification of I-A$^b_{OVA}$ on 300 nm nanoparticles conjugated with S1, S1 and αCD28 (S1/2) at a 1:1 ratio, S1 and isotype antibodies (S1/I), or S1 and BSA (S1/B) at 1:1 and 1:3 ratios. (**k**) Day 3 CFSE, (**l**) day 7 fold proliferation, and (**m**) day 7 cytokine secretion of OT-II CD4$^+$ T cells stimulated with S1/2, S1, S1/I, and S1/B nanoparticles with soluble S2, or S1/2 4.5 μm microparticles. Data in (**a**) represents mean size distribution of two independent samples. Data in (**d,f,h,j-m**) represent mean ± standard error of the mean (s.e.m.) from three or more independent experiments.(**d,f**) n = 3-4 mice analyzed using a one-way ANOVA compared to no stim. condition with Dunnett's multiple-comparisons test, (**j**) n = 4 and (**h, k-m**) n = 3-6 mice analyzed using a (**h,j-l**) one-way or (**m**) two-way ANOVA with Tukey's multiple-comparisons test, *p < 0.05, **p < 0.01, ***p < 0.001, ****p < 0.0001.

5.2.2 MHC II aAPCs expand rare murine CD4$^+$ T cell subsets

To explore whether MHC II aAPCs could be used to expand rare antigen-specific CD4$^+$ T cells, we employed an analogous approach to our previous work with murine[80,110] and human[79] CD8$^+$ T cells, following a three-step process that includes aAPCs binding to T cells, magnetic enrichment of aAPC-bound T cells, and expansion of the enriched T cell product (**Figure 5-3a**). For S1 aAPCs, excess soluble S2 was added to the enriched product to facilitate T cell expansion. To optimize the enrichment and expansion system, we diluted CFSE labelled OT-II CD4$^+$ T cells at a ratio of 1:1000 into a background of C57BL/6 (B6) CD4$^+$ T cells. Mimicking MHC II tetramer binding protocols[295], we incubated the mixed cell population with aAPCs at 37°C for 2 hours, followed by magnetic enrichment of aAPC-bound cells using a 96 well plate magnet compatible with our 300 nm aAPCs[72]. Immediately post enrichment, we found that S1 aAPCs led to significantly higher fold enrichment than S1/2 aAPCs (**Figure 5-3b**). To understand why this was, we tracked aAPC binding to cognate OT-II CD4$^+$ T cells compared to non-cognate B6 CD4$^+$ T cells. S1 aAPCs bound with significantly greater specificity to cognate CD4$^+$ T cells across a range of doses (**Figure 5-3c-d**).

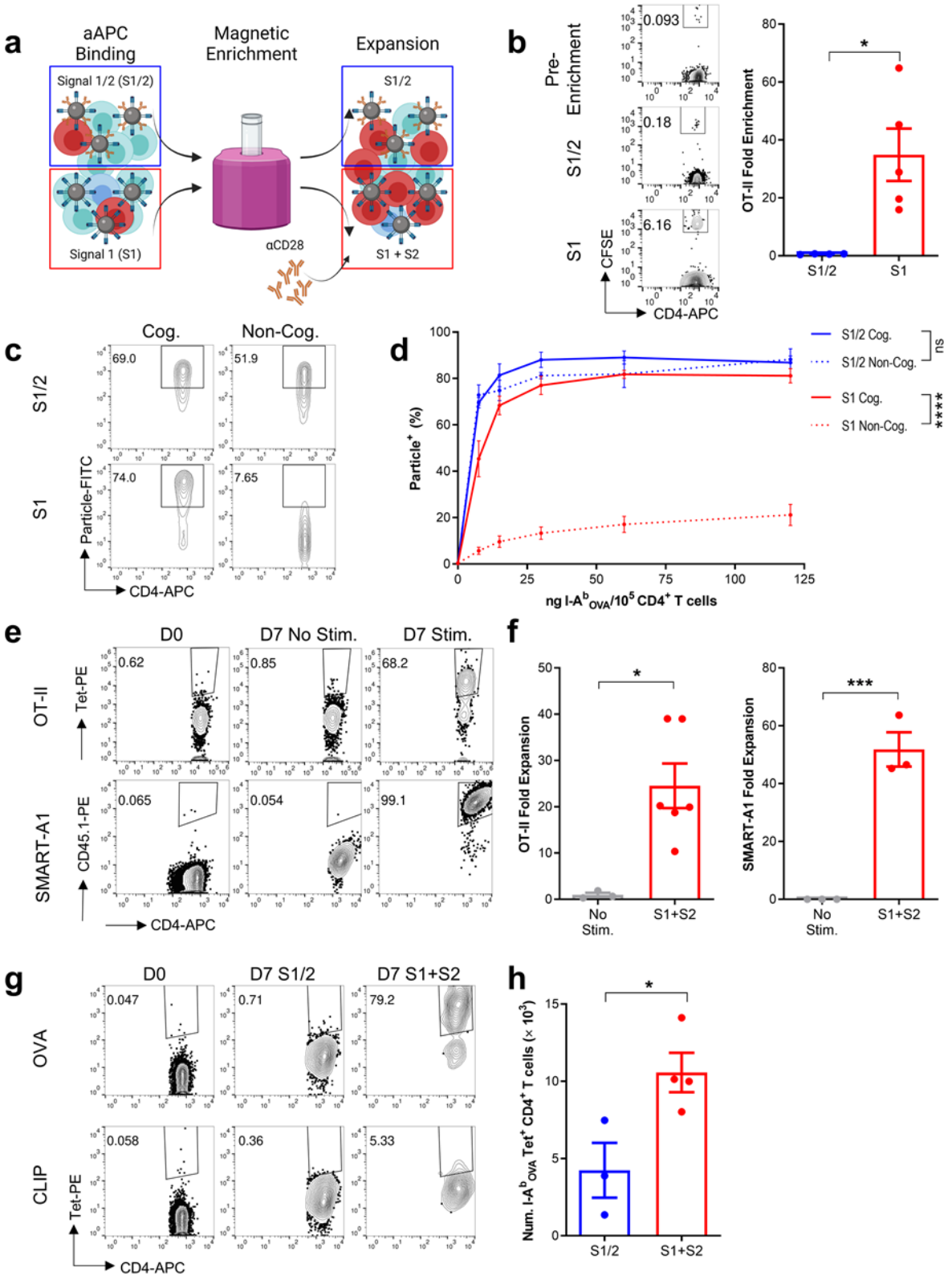

Figure 5-3. MHC II aAPCs expand rare murine CD4⁺ T cell subsets.(**a**) Schematic of magnetic enrichment of rare CD4⁺ T cells with aAPCs. Created with BioRender.com. (**b**) Representative flow plots (left) and fold enrichment (right) of OT-II cells diluted into a B6 background at a ratio of 1:1000 after magnetic enrichment with S1/2 or S1 aAPCs. (**c**) Representative flow plots and (**d**) percent of OT-II

(cognate) and B6 (non-cognate) $CD4^+$ T cells bound to particles after 2 hours of incubation at 37°C with S1/2 versus S1 aAPCs across a range of doses. (**e**) Representative flow plots and (**f**) fold expansion of OT-II and SMART-A1 cells diluted 1:1000 into a B6 background, as measured 7 days after S1+S2 enrichment and expansion. (**g**) pMHC Tetramer staining and (**h**) quantified number of I-A^b_{OVA} $CD4^+$ T cells 7 days after S1/2 or S1+S2 enrichment and expansion. Data in (**b,d,f,h**) represent mean ± standard error of the mean (s.e.m.) from two or more independent experiments. (**b,f,h**) n = 3-4 mice analyzed using an unpaired Student's *t* test, two-tailed and (**d**) n = 2-4 mice analyzed using a two-way ANOVA with Tukey's multiple-comparisons test, *p < 0.05, ***p < 0.001, ****p < 0.0001.

The temperature of incubation as well as active cellular processes both affected the enrichment and recovery of diluted OT-II cells, as binding at 4°C or metabolic inhibition with sodium azide (NaN_3) each impaired the enrichment process (**Figure 5-4a-b**). To understand these findings, we tracked nanoparticle internalization over time by incubating cells with 200 nm particles conjugated with PE-labelled I-A^b_{OVA} tetramers. Particles remaining on the surface of cells were subsequently detected with an anti-MHC II antibody. Interestingly, OT-II cells remained positive for the tetramer-labelled particles regardless of incubation time, temperature, or metabolic inhibition (**Figure 5-4c**); however, within the tetramer positive cell populations, two hours of incubation at 37°C in the absence of NaN_3 led to a significant reduction in cells staining positive for MHC II, indicating internalization of the particles (**Figure 5-4d-e**). Loss of MHC II staining coincided with downregulation of TCRs, suggesting the particle internalization was TCR-mediated; indeed, non-cognate B6 $CD4^+$ T cells that were incubated with particles in the same manner non-specifically bound to but did not internalize aAPCs (**Figure 5-4d-e**). We confirmed aAPC internalization through confocal microscopy, observing a significant drop in the spatial correlation between particle and MHC II fluorescence at 37°C in the absence of NaN_3 (**Figure 5-4f-g**).

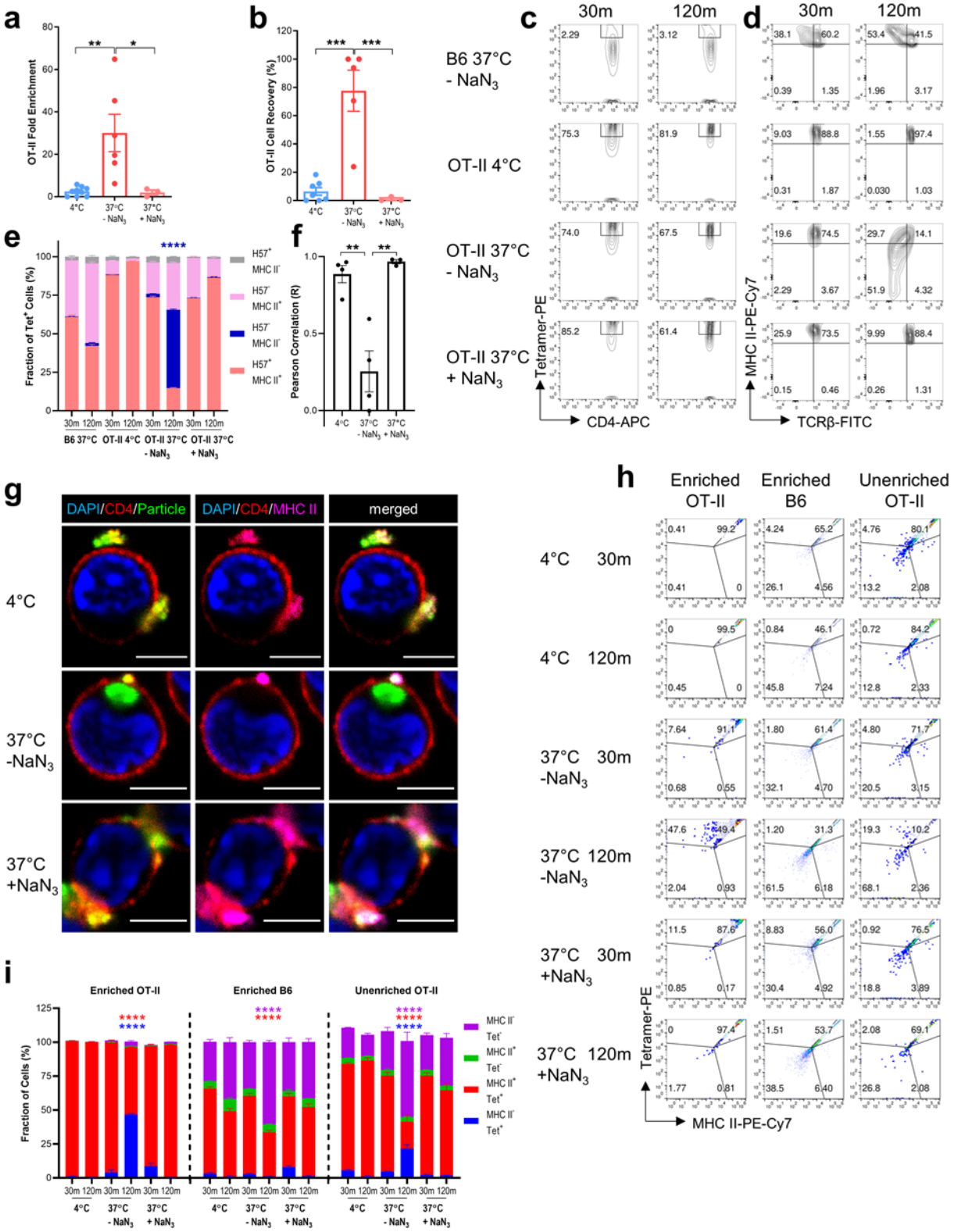

Figure 5-4. Antigen-specific MHC II aAPC internalization enhances CD4⁺ T cell magnetic enrichment.(**a**) Fold enrichment and (**b**) percent cell recovery of OT-II cells diluted into a B6 background at a ratio of 1:1000 after magnetic enrichment with S1 aAPCs after 2 hours of incubation at various temperatures with

and without sodium azide (NaN_3) uptake inhibitor. (**c-e**) Binding and internalization of PE-labelled S1 aAPCs by OT-II (cog.) and B6 (non-cog) $CD4^+$ T cells after incubation for 30 minutes and 2 hours at various temperatures with and without NaN_3. $CD4^+$ T cells with particles on their surface are $Tet^+MHC\ II^+$, whereas cells with internalized particles are $Tet^+MHC\ II^-$. (**c**) Representative flow plots of $CD4^+$ T cells that have either bound or internalized particles, (**d**) Representative flow plots and (**e**) overall MHC II and TCRβ staining of the Tet^+ $CD4^+$ T cells from (**c**). (**f**) Pearson's correlation of MHC II detection and particle fluorescence from (**g**) confocal imaging of OT-II $CD4^+$ T cells incubated with AF488-labelled S1 aAPCs after incubation for 2 hours at various temperatures with and without NaN_3. Scale bar: 4 μm. (**h-i**) Particle internalization tracking after magnetic enrichment of OT-II cells diluted into a B6 background at a ratio of 1:1000 with PE-labelled S1 aAPCs after incubation for 30 minutes and 2 hours at various temperatures with and without NaN_3. (**h**) Representative flow plots and (**i**) overall MHC II and PE staining of enriched OT-II, enriched B6, or unenriched OT-II $CD4^+$ T cell populations from the enrichment experiments. Data in (**a-b, e-f, i**) represent mean ± standard error of the mean (s.e.m.) from three or more independent experiments. (**a-b**) n = 3-5 mice, (**e**) n = 3 mice, (**f**) n = 3-4, (**i**) n = 3 mice, analyzed using a one-way (**a-b,f**) or two-way ANOVA (**e,i**) with Tukey's multiple-comparisons test, *$p < 0.05$, **$p < 0.01$, ***$p < 0.001$, ****$p < 0.0001$.

To more closely assess the impact of aAPC internalization on enrichment of rare $CD4^+$ T cell populations, we performed an enrichment study as above with CFSE labelled OT-II $CD4^+$ T cells, analyzing the surface binding versus internalization patterns of cognate $CFSE^+$ OT-II and non-cognate $CFSE^-$ B6 $CD4^+$ T cells. We found that a two-hour incubation period at 37°C in the absence of NaN_3 allowed for enrichment of OT-II cells with either surface-bound or internalized aAPCs (**Figure 5-4h-i, left**)**.** In contrast, all other incubation conditions only enriched OT-II cells with surface-bound aAPCs. Moreover, enriched B6 cells from this incubation condition showed minimal particle internalization, despite non-specifically binding to the aAPCs (**Figure 5-4h-i, middle**), demonstrating the antigen-specificity of internalization, even in mixed samples. Finally, unlike other conditions where OT-II $CD4^+$ T cells were lost in the enrichment process even when bound at high levels with aAPCs, the majority of unenriched OT-II $CD4^+$ T cells from samples incubated at 37°C without metabolic inhibition, were tetramer negative (**Figure 5-4h-i, right**), suggesting that aAPC interaction is more likely to lead to cell recovery in this condition.

To examine whether poor specific binding and enrichment of OT-II CD4$^+$ T cells with S1/2 aAPCs was due to lower TCR-pMHC avidity compared to S1 aAPCs or non-specific CD28/αCD28 interactions, we examined the binding of lower density S1/I and S1/B aAPCs (**Figure 5-2j**) to cognate OT-II and non-cognate B6 CD4$^+$ T cells. We found that while lower S1 density aAPCs bound less effectively to OT-II cells, their specific binding still remained significantly higher than their non-specific binding, unlike S1/2 aAPCs (**Figure 5-5a-b**). Indeed S1/I aAPCs yielded similar fold enrichment of diluted OT-II cells, as S1 aAPCs (**Figure 5-5c**), despite having a slightly lower density of I-A^b (**Figure 5-2j**). In contrast, 4.5 μm S1/2 aAPCs bound poorly to, and failed to enrich, cognate cells (**Figure 5-5a-c**).

The dose of aAPCs also affected the efficiency of enrichment and recovery of TCR transgenic OT-II and SMART-A1 lymphocytic choriomeningitis virus glycoprotein (I-A^b LCMV GP$_{61-80}$) specific CD4$^+$ T cells, with optimal cell enrichments and recoveries being achieved at 30 ng I-A^b/10^6 CD4$^+$ T cells (**Figure 5-5d-f**). Using S1+S2 aAPCs with this optimized enrichment protocol, we observed 30-50-fold expansion of OT-II and SMART-A1 CD4$^+$ T cells after 7 days (**Figure 5-3e-f**). Likewise, the optimized protocol allowed us to expand a nearly 80% specific population of endogenous I-A$^b_{OVA}$ specific CD4$^+$ T cells from a naïve B6 background in 7 days (**Figure 5-3g-h, Figure 5-5g-h**). Based on estimated precursor frequencies of I-A$^b_{OVA}$ CD4$^+$ T cells in B6 mice[296], this corresponds to approximately 1000-fold expansion. In contrast, S1/2 aAPCs yielded a higher total number of CD4$^+$ T cells at day 7, but both the percentage and number of antigen-specific CD4$^+$ T cells were significantly reduced (**Figure 5-3g-h, Figure 5-5g-**

h), illustrating that separation of S1 and S2 can dramatically increase the frequency of rare antigen-specific CD4⁺ T cell populations.

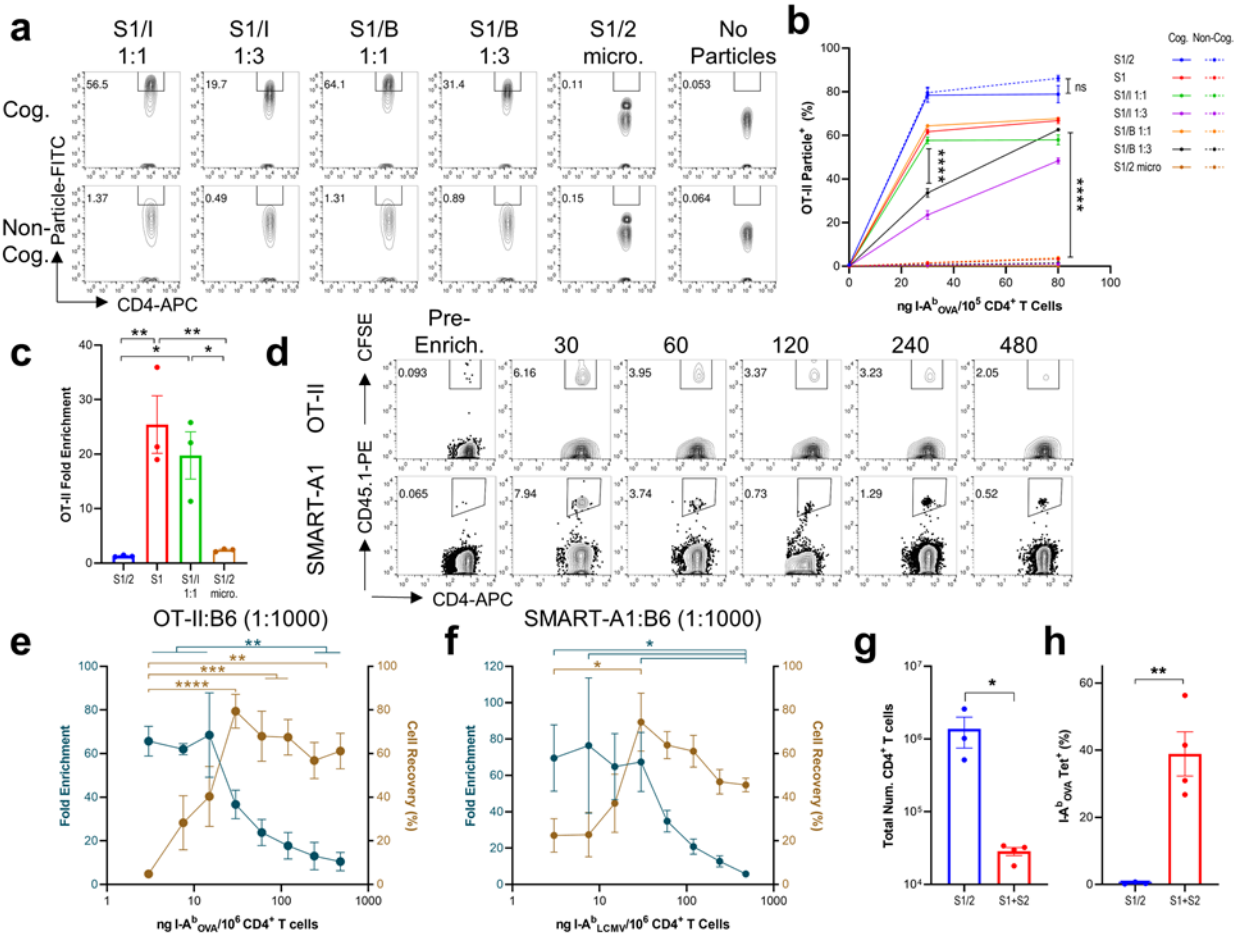

Figure 5-5. Impact of MHC II aAPC size, ligand density, and dosing on antigen-specific CD4⁺ T cell binding and enrichment.(**a-b**) Particle binding to OT-II (cog.) and B6 (non-cog.) CD4⁺ T cells after incubation at 30 minutes and 37°C with 300 nm nanoparticles conjugated with S1, S1 and αCD28 (S1/2) at a 1:1 ratio, S1 and isotype antibodies (S1/I) or BSA (S1/B) at 1:1 or 1:3 ratios, or with S1/2 4.5 μm microparticles. (**a**) Representative flow plots at 30 ng I-A^b/10^5 CD4⁺ T cells, and (**b**) Percent cells bound across a range of doses. (**c**) OT-II CD4⁺ T cells were diluted 1:1000 into a B6 background and incubated for 2 hours at 37°C with 30 ng I-A^b/10^6 CD4⁺ T cells of S1/2, S1, or S1/I 1:1 nano-aAPCs versus S1/2 micro-aAPCs. Fold enrichment of magnetically enriched samples relative to baseline. (**d**) Representative flow plots of OT-II (top) and SMART-A1 CD4⁺ T cells (bottom) pre- and post-enrichment, (**e-f**) fold enrichment and percent cell recovery of (**e**) OT-II and (**f**) SMART-A1 cells post-enrichment with a titration of cognate S1 nano-aAPCs. (**g**) Total number of CD4⁺ T cells and (**h**) percentage of I-A^b_{OVA} tetramer positive CD4⁺ T cells 7 days after S1/2 or S1+S2 enrichment and expansion. Data in (**b,c,e-h**) represent mean ± standard error of the mean (s.e.m.) from three or more independent experiments. (**b-c**) n = 3 mice, (**e-f**) n = 3-6 mice, and (**g-h**) n=3-4 mice analyzed using a (**b**) two-way or (**c,e-f**) one-way ANOVA with Tukey's multiple-comparisons test, or (**g-h**) an unpaired Student's *t* test, two-tailed, *p < 0.05, **p < 0.01, ***p < 0.001, ****p < 0.0001.

5.2.3 MHC II aAPCs promote CD4$^+$ T cell cytotoxicity

There have been published reports of CD4$^+$ T cell acquisition of cytotoxic functions[279,297–299] in various disease states but there is no consistent method for producing them or studying them *ex vivo*. To assess the impact of MHC II aAPCs on CD4$^+$ T cell cytotoxicity, we monitored production of the serine protease Granzyme B (GzmB) and associated lytic capacity of aAPC activated CD4$^+$ T cells (**Figure 5-6a**). We found that induction of CD4$^+$ T cell cytotoxicity was sensitive to both TCR engagement and the cytokine milieu. We observed a dramatic increase in GzmB levels when aAPC-activated CD4$^+$ T cells were cultured in Th1 media compared to TF or cytokine-free media (**Figure 5-6b, Figure 5-7a**). In Th1 media, S1+S2 stimulation induced significantly higher levels of GzmB production than αCD3/αCD28 stimulation or the use of splenocytes or BMDCs pulsed with peptide (**Figure 5-6c, Figure 5-7b**). GzmB production increased over the course of S1+S2 stimulation (**Figure 5-6c**) and was specifically dependent on the presence of IL-2 in the Th1 mix (**Figure 5-7d-e**). Additionally, we found that GzmB induction depended on soluble, as opposed to conjugated S2, and nano-, as opposed to micro-particles, but did not depend on S1 density (**Figure 5-7f**). Consequently, S1+S2 stimulated OT-II CD4$^+$ T cells were able to lyse B16-OVA tumor cells *in vitro* when cultured in Th1 media (**Figure 5-6d, Figure 5-7g**) in a GzmB and MHC II dependent manner (**Figure 5-6e**).

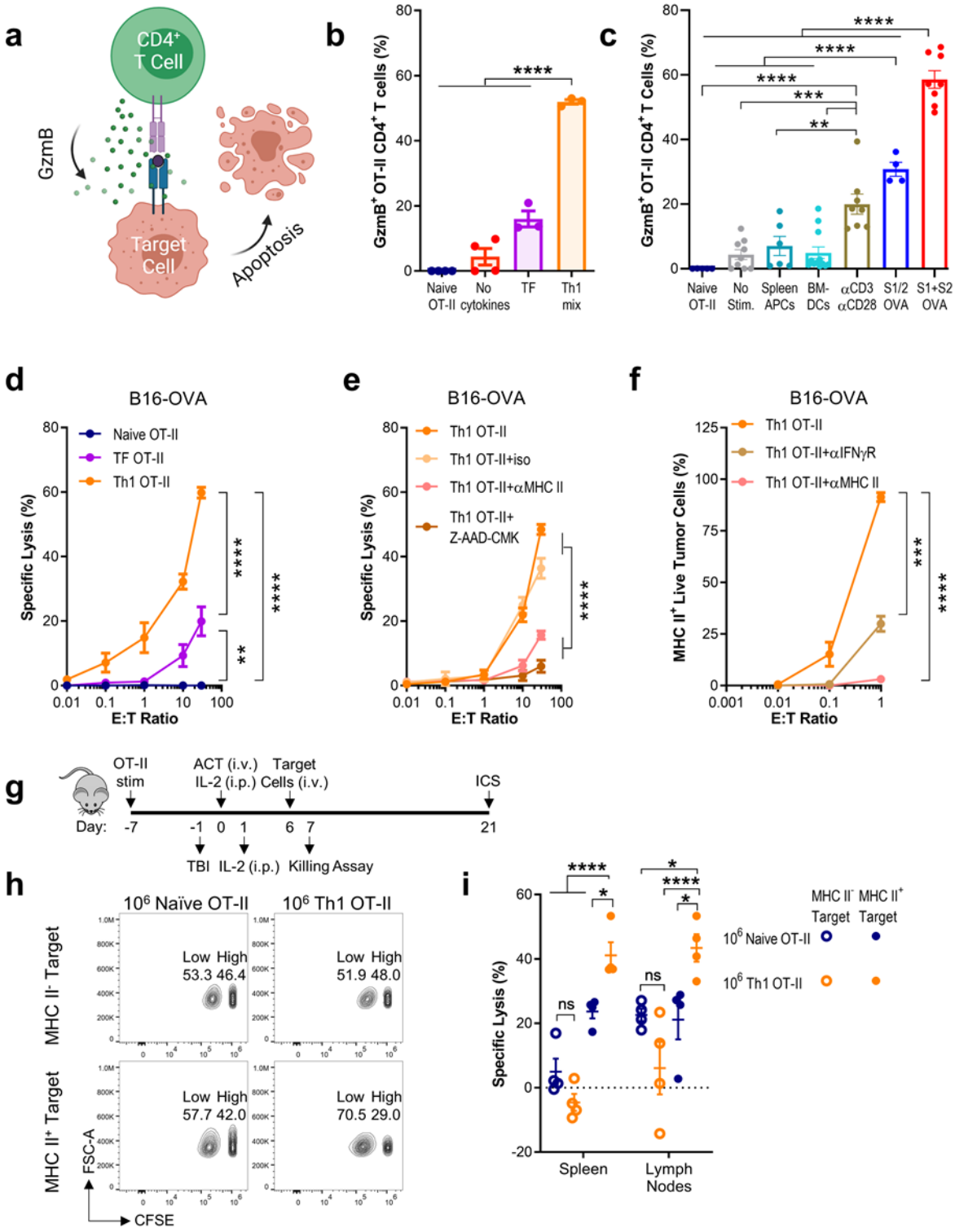

Figure 5-6. MHC II aAPCs promote CD4⁺ T cell cytotoxicity.(**a**) Schematic of direct CD4⁺ T cell lysis of target cells. Created with BioRender.com. (**b**) Granzyme B (GzmB) staining in OT-II cells stimulated with S1+S2 aAPCs for 7 days in media containing: no cytokines, TF, or a Th1 mix. (**c**) Day 7 GzmB levels of OT-II cells stimulated in Th1 media with S1/2, S1+S2, or αCD3/αCD28 aAPCs versus peptide pulsed OT-II splenocytes or bone-marrow derived dendritic cells (BMDCs). (**d**) Specific lysis of B16-OVA tumor cells after overnight incubation with naïve or aAPC stimulated OT-II cells (cultured in TF or Th1 media). Various effector to target (E:T) ratios are presented. (**e**) Specific lysis of B16-OVA cells after overnight

incubation with aAPC-stimulated and Th1-skewed OT-II cells with MHC II antibody blocking or Z-AAD-CMK GzmB inhibition. (**f**) Percentage of MHC II-expressing live B16-OVA cells after overnight incubation with aAPC-stimulated Th1 OT-II cells and MHC II or IFN-γR antibody blocking. (**g**) Experimental overview of *in vivo* killing and cytokine production assays on naïve vs. aAPC activated Th1 OT-II cells. (**h-i**) Specific lysis of $OVA_{323-339}$ pulsed splenocytes six days after adoptive T cell transfer (ACT) of naïve or Th1 OT-II cells. Data in (**b-f,i**) represent mean ± standard error of the mean (s.e.m.) from two or more independent experiments. (**b-c**) n = 3-5 mice, (**d-f**) n = 3-4 mice, and (**i**) n = 4 mice/group analyzed using a (**b-c**) one-way or (**d-f,i**) two-way ANOVA with Tukey's multiple-comparisons test, *p < 0.05, **p < 0.01, ***p < 0.001, ****p < 0.0001.

To elucidate how OT-II recognition of B16-OVA tumor cells was occurring, given that most tumors do not constitutively express MHC II, we monitored MHC II expression on live B16-OVA cells after co-culture with S1+S2 aAPC activated OT-II cells, finding that the $CD4^+$ T cells induce MHC II expression on B16-OVA in an IFN-γ dependent manner (**Figure 5-6f, Figure 5-7h**). We next assessed the *in vivo* functional activity of S1+S2 aAPC activated OT-II $CD4^+$ T cells by examining their lytic capacity and cytokine production 7 and 21 days post adoptive transfer into CD45.1 B6 mice (**Figure 5-6g**). At day 7, aAPC activated cells specifically lysed $OVA_{323-339}$ pulsed target cells in an MHC II-restricted manner (**Figure 5-6h-i**). Activated cells persisted through day 21, remaining T-bet positive (**Figure 5-7i-j**) and continuing to secrete IFN-γ and TNF-α (**Figure 5-7k-l**). Collectively, *in vitro* and *in vivo* cytotoxicity studies revealed that aAPCs can activate lytic programs in $CD4^+$ T cells.

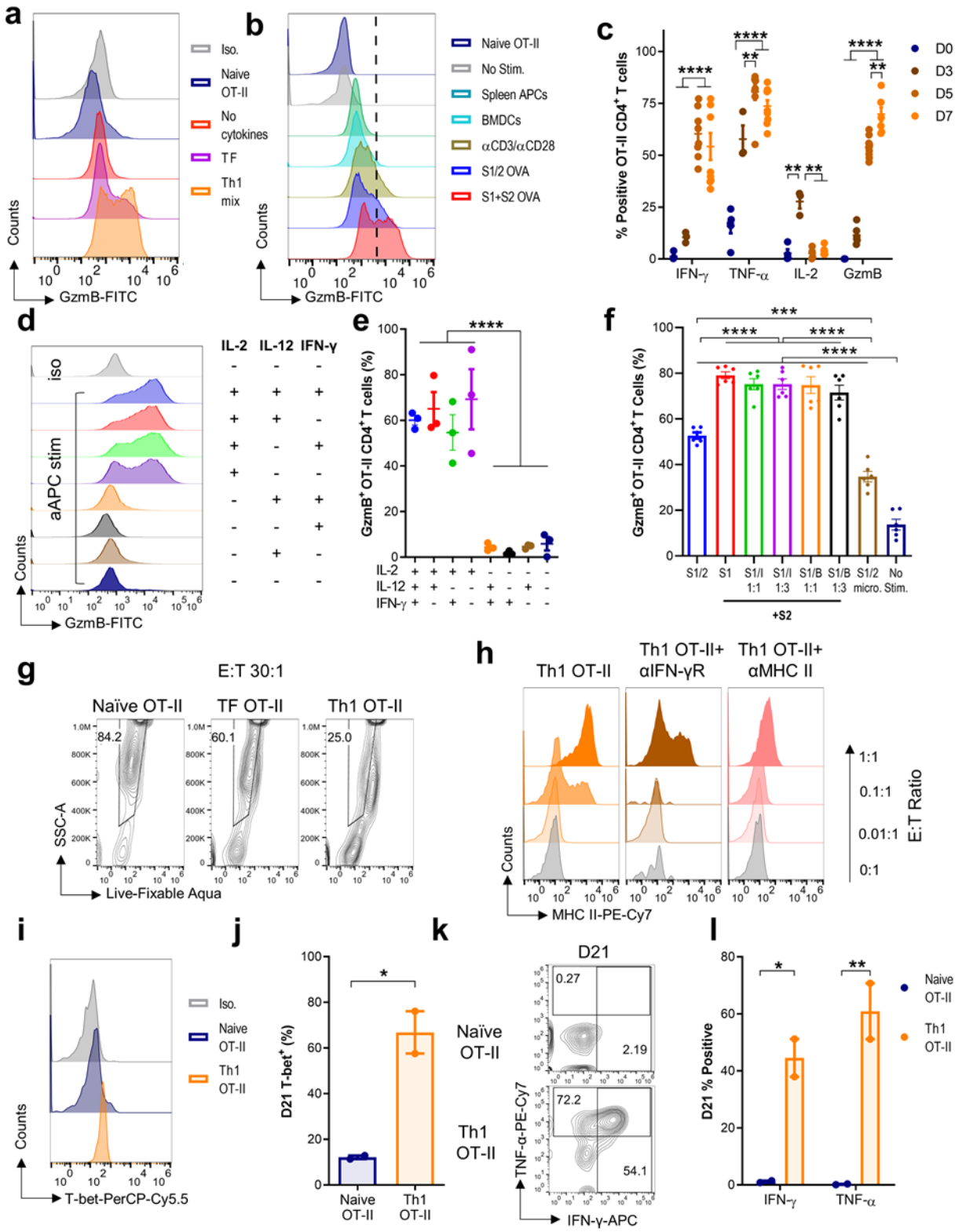

Figure 5-7. Extended Data: MHC II aAPCs promote CD4⁺ T cell cytotoxicity.(**a**) Day 7 GzmB levels of OT-II cells stimulated with S1+S2 aAPCs in media with: no cytokines, TF, or a Th1 mix (IL-2, IL-12p70, IFN-γ). (**b**) Day 7 GzmB levels of OT-II cells stimulated in Th1 media with S1/2, S1+S2, or αCD3/αCD28 aAPCs versus peptide pulsed splenocytes or bone-marrow derived dendritic cells (BMDCs). (**c**) OT-II cytokine production on days 0, 3, 5, 7 of stimulation with S1 aAPCs in Th1 media. (**d**) GzmB staining and

(**e**) percent positive of OT-II cells after 7 days of S1+S2 stimulation in the various components of the Th1 mix. (**f**) Percentage of GzmB$^+$ OT-II cells after 7 days of stimulation with 300 nm nanoparticles conjugated with S1, S1 and αCD28 (S1/2) at a 1:1 ratio, S1 and isotype antibodies (S1/I) or BSA (S1/B) at 1:1 or 1:3 ratios, or S1/2 4.5 μm microparticles. (**g**) B16-OVA tumor cell viability after overnight incubation at an effector-to-target (E:T) ratio of 30:1 with naïve or aAPC stimulated OT-II cells cultured in TF or Th1 media. (**h**) Live B16-OVA MHC II expression after overnight incubation with aAPC stimulated Th1 OT-II cells and MHC II or IFN-γR antibody blocking. (**i**) T-bet staining and (**j**) percentage, (**k**) IFN-γ and TNF-α staining and (**l**) percentage of naïve versus Th1 OT-II CD4$^+$ T cells 21 days post adoptive cell transfer (ACT). Data in (**c,e,f,j,l**) represent mean ± standard error of the mean (s.e.m.). (**c,f**) n = 6 mice and (**e**) n = 3 mice analyzed using a (**c**) two-way or (**e-f**) one-way ANOVA with Tukey's multiple-comparisons test, (**j,l**) n = 2 mice/group analyzed using an (**j**) unpaired Student's *t* test, two-tailed or (**l**) two-way ANOVA with Tukey's multiple-comparisons test, *p < 0.05, **p < 0.01, ***p < 0.001, ****p < 0.0001.

5.2.4 MHC II aAPCs modulate CD4$^+$ T cell helper function

One objective in developing MHC II aAPCs was to produce a scalable approach for generating CD4$^+$ T cells that could enhance the memory formation, function, and cytotoxicity of tumor-specific CD8$^+$ T cells[291]. To do so, CD4$^+$ and CD8$^+$ T cells were co-activated either with separate MHC I and MHC II aAPCs (MHC I+II) or with a novel aAPC made by coupling nanoparticles with both MHC I and MHC II (MHC I/II) (**Figure 5-8a**). In all cases, αCD28 was delivered in solution. We first assessed the impact of CD4$^+$ and CD8$^+$ co-activation on CD8$^+$ T cell memory formation and function by co-culturing TCR transgenic K^b OVA$_{257-264}$ specific OT-I CD8$^+$ T cells (OT-I) at a 1:1 ratio with either naïve OT-II CD4$^+$ T cells or OT-II CD4$^+$ T cells activated with S1+S2 aAPCs (Th1 OT-II). We found that co-stimulation of OT-I with Th1 OT-II cells using separate MHC I+II aAPCs led to an increase in effector memory CD8$^+$ T cells that also expressed significantly higher levels of IL-7 receptor-alpha (IL-7Rα or CD127), a marker associated with long-lasting memory T cells (**Figure 5-8b, Figure 5-9a-c**). The addition of Th1 OT-II cells also increased OT-I production of GzmB (**Figure 5-8c-d**) and IFN-γ (**Figure 5-8d, Figure 5-9d**). This effect was dependent on restimulation of the Th1 OT-II cells with either MHC I/II or MHC I+II aAPCs (**Figure 5-9e-g**). Furthermore, co-culture with Th1 OT-II cells significantly boosted the *in vitro* cytotoxicity of TCR Transgenic OT-I, 2C

K^b SIY, and PMEL D^b $gp100_{25-33}$ specific $CD8^+$ T cells against B16-OVA (**Figure 5-8e, Figure 5-9h**), B16-SIY (**Figure 5-9i**), and B16-F10 tumor cells (**Figure 5-9j**), respectively.

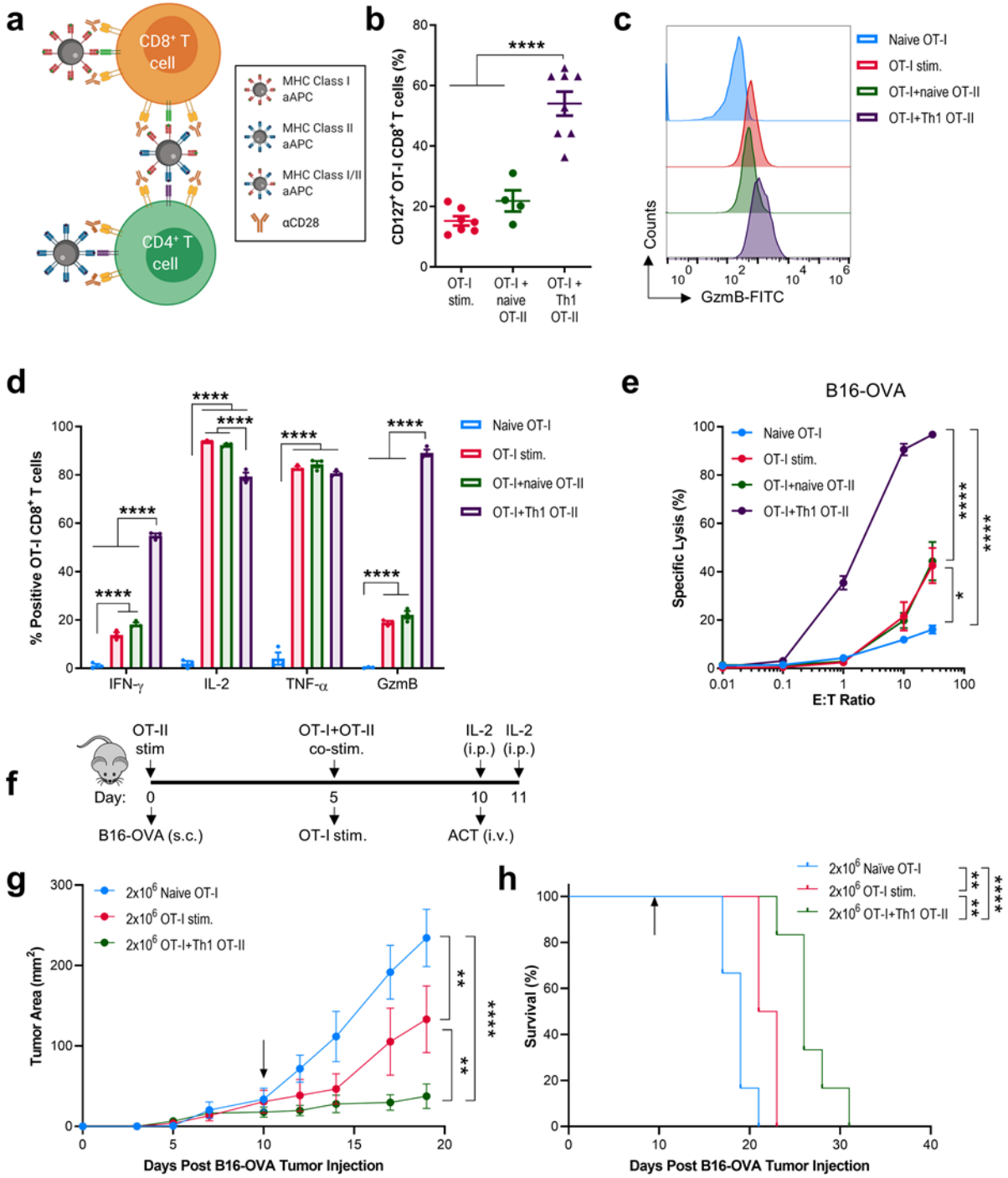

Figure 5-8. MHC II aAPCs modulate $CD4^+$ T cell helper function.(**a**) Schematic showing separate (I+II) or joint presentation (I/II) of MHC I and MHC II on aAPCs to $CD4^+$ and $CD8^+$ T cells to facilitate cell-cell crosstalk. Created with BioRender.com. (**b-h**) OT-I $CD8^+$ T cells were activated with MHC I K^b_{OVA} aAPCs

in TF supplemented media either alone or in co-culture with naïve or aAPC-stimulated Th1 OT-II cells and MHC II I-A^{b}_{OVA} aAPCs. On day 7, (**b**) IL-7Rα (CD127) surface expression, (**c**) intracellular Granzyme B, (**d**) cytokine production, and (**e**) specific lysis of B16-OVA tumor cells after overnight incubation with $CD8^+$ T cells were compared between stimulation cohorts. (**f**) Experimental overview of subcutaneous (s.c.) B16-OVA melanoma adoptive transfer model. (**g**) Tumor growth and (**h**) survival in mice subjected to adoptive transfer of OT-I $CD8^+$ T cells that were either freshly harvested, activated in isolation, or co-activated with Th1 OT-II $CD4^+$ T cells. The black arrows indicate time of ACT. Data in (**b,d-e**) represent mean ± standard error of the mean (s.e.m.) or (**g**) mean ± standard deviation (s.d.) from three or more independent experiments. (**b**) n = 4 mice, (**d**) n = 3 mice, and (**e**) n = 4 mice analyzed using a (**b**) one-way or (**d-e**) two-way ANOVA with Tukey's multiple comparisons test, (**g-h**) n = 6 mice/group analyzed using (**g**) a repeated measure two-way ANOVA with Tukey's multiple-comparisons test or (**h**) log-rank test, *p < 0.05, **p < 0.01, ****p < 0.0001.

To determine whether $CD4^+$ T cell help led to superior *in vivo* antitumor efficacy of $CD8^+$ T cell therapies, we used an adoptive transfer model of pre-established murine melanoma (**Figure 5-8f**). In this model, B6 mice were injected subcutaneously with B16-OVA tumor cells and then treated 10 days later with either naïve OT-I $CD8^+$ T cells, aAPC-activated OT-I $CD8^+$ T cells, or OT-I $CD8^+$ T cells co-activated with Th1 OT-II $CD4^+$ T cells using MHC I+II aAPCs. By the day of treatment, all of the cells in the co-culture condition were $CD8^+$, allowing direct comparisons of the antitumor function of $CD8^+$ T cells across these three conditions (**Figure 5-9k-l**). We found that treatment with OT-I $CD8^+$ T cells that had been co-cultured with $CD4^+$ T cells resulted in significantly improved B16-OVA antitumor control **Figure 5-8g, Figure 5-9m**) and enhanced survival (**Figure 5-8h**) compared to both naïve or aAPC-activated OT-I $CD8^+$ T cells. Hence, both *in vitro* assays and *in vivo* disease models corroborated the beneficial role of aAPC-stimulated $CD4^+$ T cells in boosting $CD8^+$ T cell function.

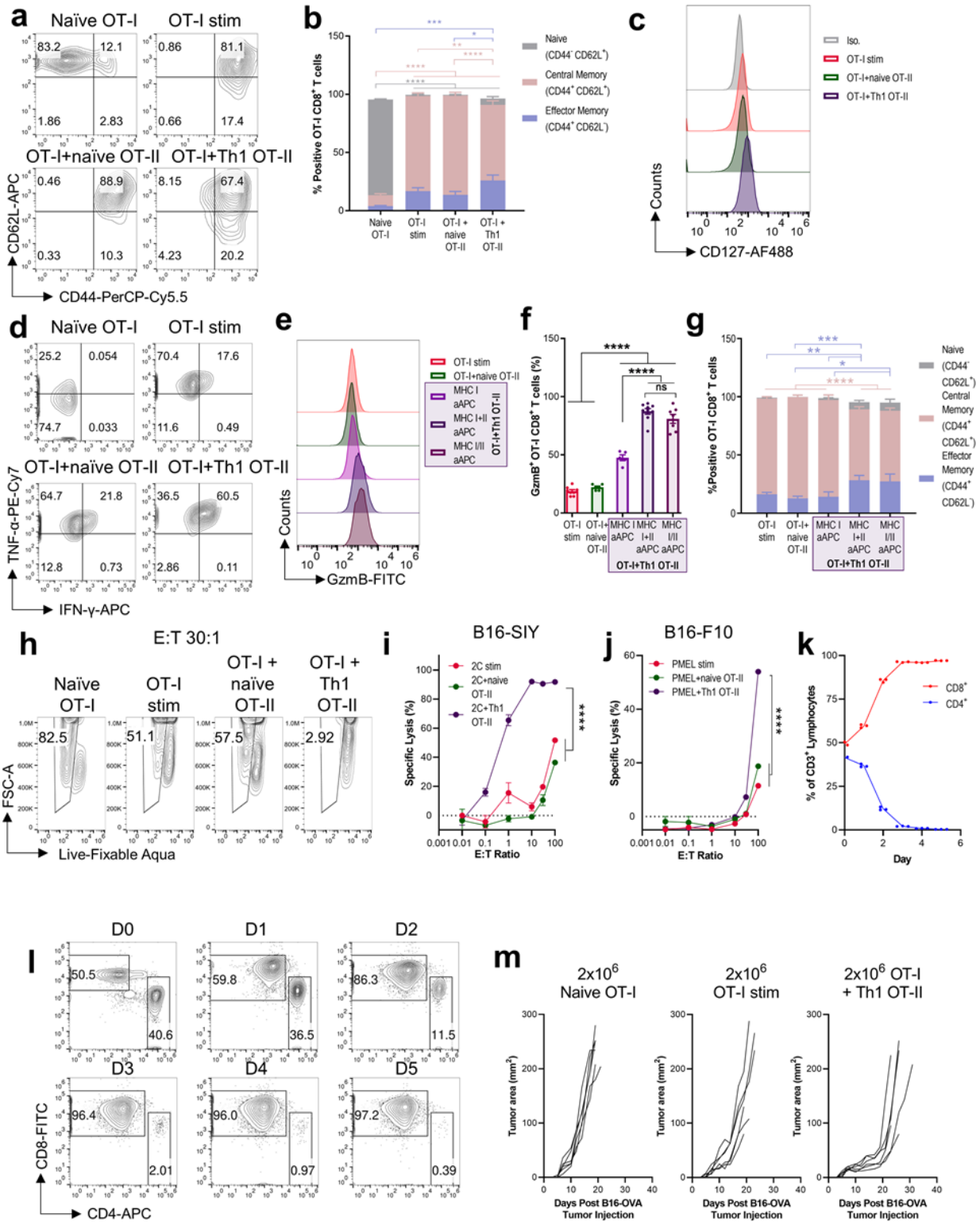

Figure 5-9. Extended Data: MHC II aAPCs modulate CD4⁺ T cell helper function.(**a-d**) OT-I cells in TF supplemented media were activated with MHC I K^{b}_{OVA} aAPCs either alone or in co-culture with naïve or aAPC activated Th1 OT-II cells and MHC II I-A^{b}_{OVA} aAPCs. Day 7 (**a-b**) memory phenotype, (**c**) CD127 expression, and (**d**) cytokine staining from the various stimulations. (**e-f**) OT-I cells were cultured as above but with different stimuli: K^{b}_{OVA} only (MHC I), separate (MHC I+II), and co-presenting (MHC I/II) aAPCs. Day 7 (**e-f**) intracellular GzmB levels and (**g**) memory phenotype of OT-I cells stimulated under

these various conditions. (**h**) B16-OVA viability after overnight incubation at an E:T ratio of 30:1 with OT-I cells stimulated alone or co-cultured with naïve or Th1 OT-II cells. (**i**) B16-SIY and (**j**) B16-F10 specific lysis after overnight incubation with 2C or PMEL $CD8^+$ T cells, respectively, stimulated alone or co-cultured with naïve or Th1 OT-II cells. (**k-l**) Percentage of $CD3^+$ lymphocytes that are $CD4^+$ or $CD8^+$ T cells over five days of OT-I and Th1 OT-II co-culture. (**m**) Spider plots depicting tumor growth of B16-OVA in B6 mice subjected to adoptive transfer of OT-I cells that were either freshly isolated, activated alone, or co-activated with Th1 OT-II $CD4^+$ T cells. Data in (**b,f,g,i-k**) represent mean ± standard error of the mean (s.e.m.) from two or more independent experiments. (**b**) n = 3-6 mice, (**f-g**) n = 3-5 mice, (**i-j**) n = 2 mice, and (**k**) n = 3, analyzed using a (**f**) one-way or (**b,g**) two-way ANOVA with Tukey's multiple-comparisons test, *p < 0.05, **p < 0.01, ***p < 0.001, ****p < 0.0001.

5.2.5 aAPC mediated T cell help is driven by soluble factors and extends to endogenous $CD8^+$ T cells

To better understand the mechanisms underlying bolstered activity of $CD8^+$ T cells co-cultured with $CD4^+$ T cells, we performed epifluorescent imaging of OT-I cells mixed with naïve or Th1 OT-II $CD4^+$ T cells. After 24 hours of co-incubation in the presence of MHC I/II aAPCs, OT-I $CD8^+$ T cells had significantly more cell-cell interactions with Th1 OT-II than with naïve OT-II cells (**Figure 5-10a-b**). Accordingly, Th1 OT-II cells induced significantly greater transmigration of OT-I than naïve OT-II cells (**Figure 5-10c**). To assess whether this enhanced cell-cell interaction was complementary to or a requirement for improving OT-I function, we performed transwell assays, wherein OT-I and Th1 OT-II cells were either mixed together in the same well or separated by a 0.4 μm membrane. Interestingly, separation of OT-I and Th1 OT-II did not affect $CD8^+$ memory skewing (**Figure 5-11a**) or function (**Figure 5-10d, Figure 5-11b-c**), suggesting that MHC II aAPC mediated $CD4^+$ help occurred through soluble factors. Based on these results, we analyzed the supernatants of Th1 OT-II cells using a cytokine protein array (**Figure 5-10e, Figure 5-11d**). The results indicated that the most highly abundant cytokines and chemokines were IL-10, TNF-α, CCL3, CCL4, and

CCL5. Since chemokines CCL3, CCL4, and CCL5 primarily affect T cell migration, we focused on analyzing the impact of IL-10 and TNF-α.

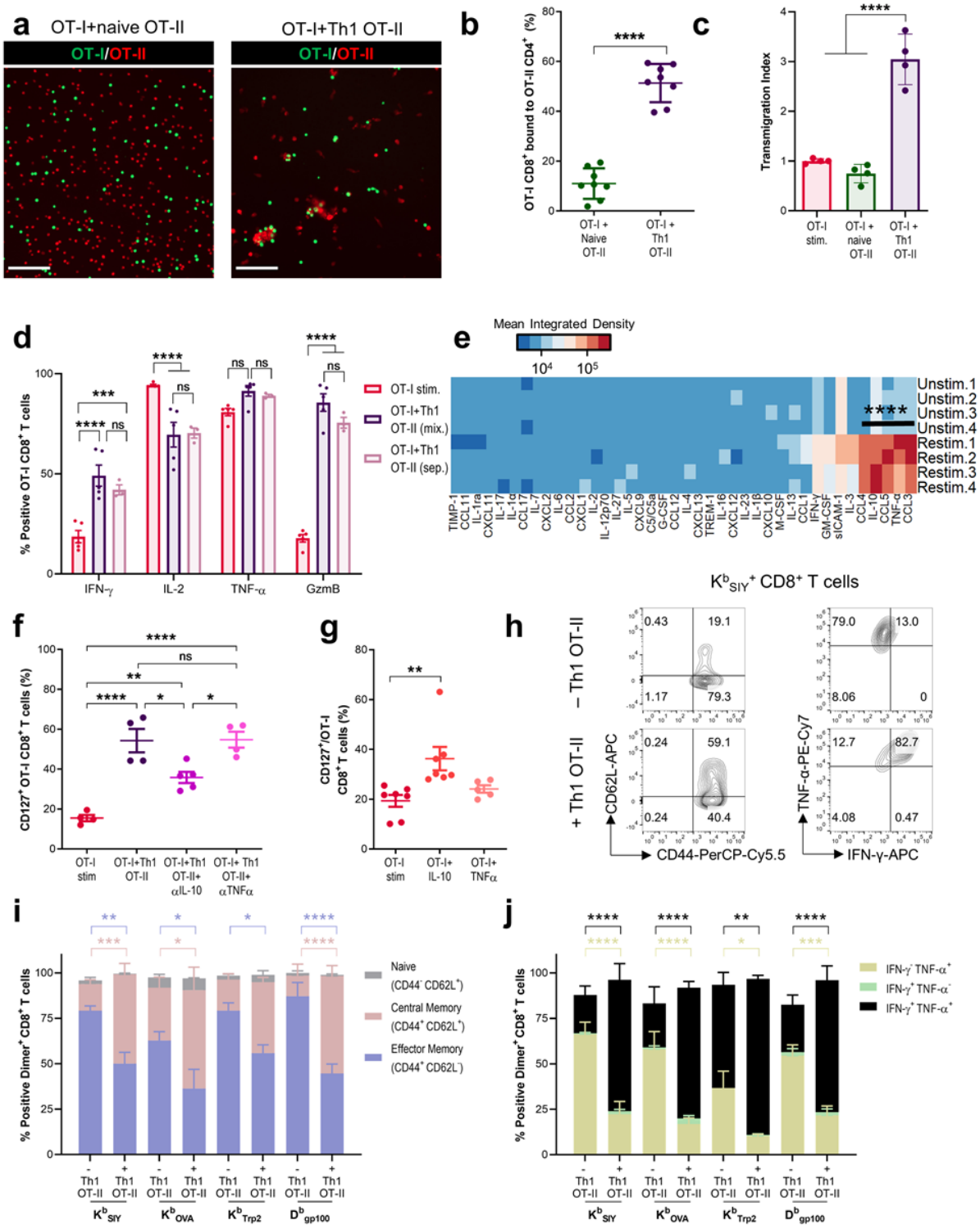

Figure 5-10. aAPC mediated T cell help is driven by soluble factors and extends to endogenous CD8⁺ T cells.(**a**) Epifluorescent imaging and (**b**) co-localization analysis of OT-I cells (green) with naïve or Th1

OT-II cells (red) and MHC I/II aAPCs 24 hours post co-incubation. Scale bar: 100 μm. (**c**) Transmigration of OT-I cells towards naïve or Th1 OT-II cells relative to basal medium. (**d**) Day 7 intracellular cytokine production of OT-I cells activated alone, separated (sep.) from, or mixed (mix.) with Th1 OT-II cells in a transwell plate. (**e**) Cytokine array heatmap depicting secreted proteins from unstimulated or re-stimulated Th1 OT-II cells. (**f**) CD127 expression of OT-I cells co-cultured with Th1 OT-II cells with blocking antibodies targeting IL-10 and TNF-α. (**g**) CD127 expression of OT-I cells stimulated in IL-10 or TNF-α supplemented media. (**h-j**) K^b_{SIY}, K^b_{OVA}, K^b_{Trp2}, and D^b_{gp100} specific $CD8^+$ T cells were enriched from B6 mice and then expanded either alone or in co-culture with Th1 OT-II cells. (**h**) Representative flow plots, (**i**) memory phenotype, and (**j**) overall cytokine production of antigen-specific $CD8^+$ T cells on day 7. Data in (**b-d**, **f-g, i-j**) represent mean ± standard error of the mean (s.e.m.) from two or more independent experiments. (**b**) n = 3, (**c**) n = 2, (**d**) n = 3-5, (**e**) n = 2, (**f**) n = 4-5, (**g**) n = 5-7, and (**i-j**) n=3 mice analyzed using an (**b**) unpaired Student's *t* test, two-tailed, (**c,f-g**) one-way, or (**d-e,i-j**) two-way ANOVA with Tukey's multiple-comparisons test, mice, *p < 0.05, **p < 0.01,***p < 0.001, ****p < 0.0001.

We found through blocking IL-10 and TNF-α in co-culture experiments and adding exogenous IL-10 and TNF-α to OT-I only cultures, that IL-10 specifically impacts OT-I GzmB production (**Figure 5-11e-f**) and CD127 expression (**Figure 5-10f-g**). Since help signals were observed to be delivered in solution, we next assessed how they would impact the memory phenotype and function of endogenous antigen-specific $CD8^+$ T cells. To answer this question, we followed our existing protocol[72] for enrichment and expansion of $CD8^+$ T cells from naïve B6 mice, with or without Th1 OT-II $CD4^+$ T cells added to the enriched fractions. We found that the addition of $CD4^+$ T cells did not significantly alter the number of antigen-specific $CD8^+$ T cells on day 7 (**Figure 5-11g-h**), but enhanced the central memory phenotype of antigen-specific CD8+ T cells (**Figure 5-10h-i**), their IFN-γ production (**Figure 5-10h,j**), and CD127 expression (**Figure 5-11i**).

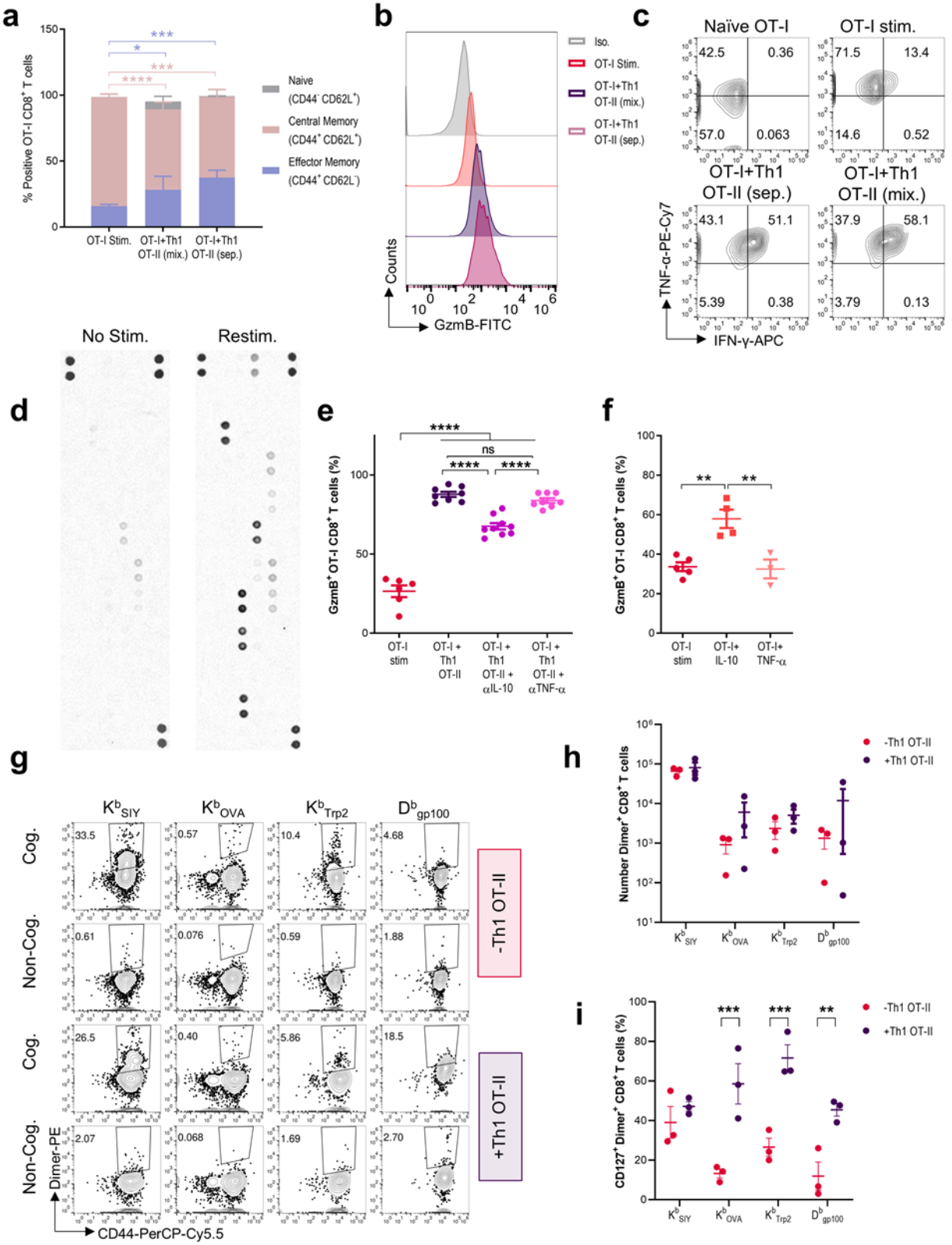

Figure 5-11. Extended Data: aAPC mediated T cell help is driven by soluble factors and extends to endogenous CD8+ T cells.(**a**) Memory phenotype, (**b**) intracellular GzmB levels, and (**c**) cytokine staining of OT-I cells activated alone, separated (sep.) from, or mixed (mix.) with Th1 OT-II cells in a transwell plate. (**d**) Cytokine arrays of supernatants harvested from unstimulated or re-stimulated Th1 OT-II cells.

(**e**) Flow cytometry detection of GzmB expression in OT-I cells co-cultured with Th1 OT-II cells in the presence of blocking antibodies to IL-10 and TNF-α. (**f**) Flow cytometry detection of GzmB in OT-I cells stimulated in media supplemented with IL-10 or TNF-α. (**g-i**) K^b_{SIY}, K^b_{OVA}, K^b_{Trp2}, and D^b_{gp100} specific $CD8^+$ T cells were enriched from B6 mice and then expanded either alone or in co-culture with Th1 OT-II cells. (**g**) Dimer staining and (**h**) numbers of $CD8^+$ T cells of corresponding antigenic specificities at day 7. (**i**) Percent of antigen-specific $CD8^+$ T cells that were CD127 positive. Data in (**a,e-f,h-i**) represent mean ± standard error of the mean (s.e.m.) and three or more independent experiments. (**a**) n = 3-6 mice, (**e**) n = 6-7 mice, (**f**) n = 3-6 mice, and (**h-i**) n = 3 mice analyzed using a (**e-f,h-i**) one-way or (**a**) two-way ANOVA with Tukey's multiple-comparisons test, *p < 0.05, **p < 0.01, ***p < 0.001, ****p < 0.0001.

5.2.6 HLA II aAPCs stimulate functional antigen-specific human $CD4^+$ T cells

To establish whether the MHC II aAPC technology could be translated for human $CD4^+$ T cell culture, we designed and expressed HLA class II monomers following a previously described system[261] (**Figure 5-12a-b**). We then covalently attached these HLA molecules and αCD28 proteins to iron dextran particles which could then be adapted to a range of target antigens through thrombin cleavage and peptide exchange (**Figure 5-13a**). To assess the function and specificity of peptide-exchanged aAPCs, we exchanged HLA DR1 aAPCs overnight with the hemagglutinin $HA_{306-318}$ peptide and then monitored their ability to activate Jurkat cells transfected overnight with the $HA_{306-318}$-recognizing HA 1.7 TCR (**Figure 5-12c**). DR1 aAPCs loaded with the cognate HA peptide (DR1 HA) upregulated CD69, a T cell activation marker, specifically on the HA 1.7 positive Jurkat cells; Moreover, unlike αCD3 based stimulation, which also activated HA 1.7 negative Jurkat cells, DR1 HA aAPCs were specific for the HA 1.7 expressing

Jurkats (**Figure 5-13b, Figure 5-12d**). We next assessed whether we could expand HA specific CD4⁺ T cells from healthy DR4 donors, using DR4/αCD28 aAPCs.

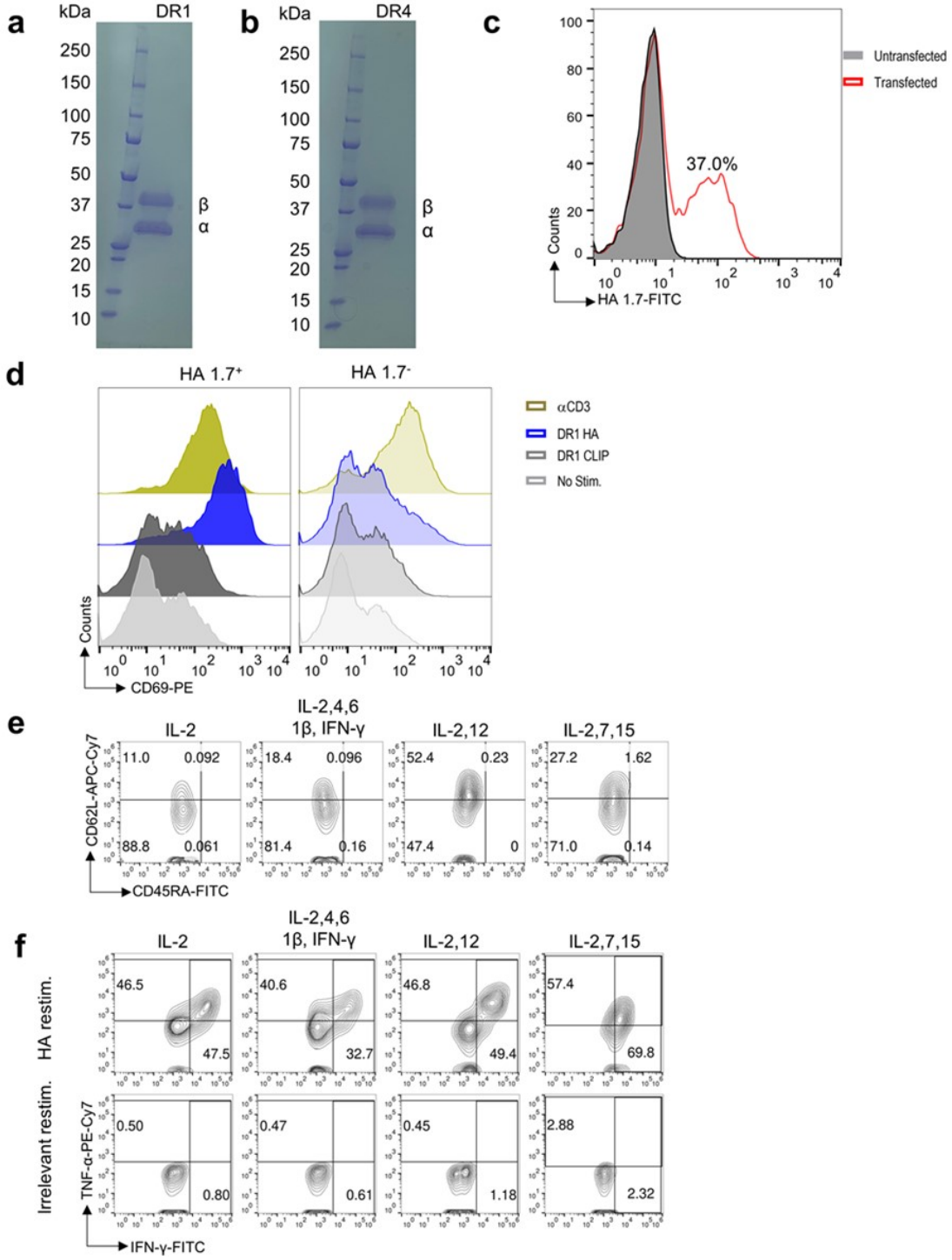

Figure 5-12. Extended Data: HLA II aAPCs stimulate functional antigen-specific human CD4+ T cells.(**a-b**) SDS-PAGE analysis of human embryonic kidney (HEK) 293-F cell-secreted (**a**) DR1 and (**b**) DR4 monomers. (**c**) Detection of HA 1.7 TCR on Jurkat cells after overnight transfection and (**d**) comparison of CD69 induction on HA1.7 TCR positive and negative Jurkat cells following stimulation with either

αCD3/αCD28 microparticles or a titration of DR1/αCD28 aAPCs loaded with cognate hemagglutinin (DR1 HA) or non-cognate CLIP (DR1 CLIP) peptides. (**e**) Memory phenotype and (**f**) intracellular cytokine production after cognate (HA) and irrelevant (NY-ESO-1) peptide stimulation of DR4 HA tetramer positive $CD4^+$ T cells expanded from healthy donor peripheral blood mononuclear cells (PBMC) using DR4 HA aAPCs and four cytokine mixes: (i) IL-2 only; (ii) IL-2, IL-4, IL-6, IL-1β, and IFN-γ; (iii) IL-2 and 12; and (iv) IL-2, IL-7, and IL-15.

We compared expansion in four different cytokine mixes: IL-2 expansion media; IL-2, IL-4, IL-6, IL-1β, and IFN-γ human $CD8^+$ culture media[79]; IL-2 and IL-12 Th1 skewing media; and IL-2, IL-7, and IL-15 memory skewing media. We found that both IL-2 media and IL-2,4,6,1β, and IFN-γ media resulted in robust expansion of HA specific $CD4^+$ T cells from nearly undetectable precursor frequencies (**Figure 5-13c**) to approximately 30% of the cell mixture (**Figure 5-13d**), leading to nearly 100,000-fold expansion over the course of 21 days (**Figure 5-13e**). Unlike with murine $CD4^+$ T cells, this antigen-specific expansion was achieved without needing to separate S1 and S2. In contrast, IL-2 and 12 media and IL-2, 7, and 15 media only yielded modest expansions that declined after day 14. The resulting phenotype of the HA-specific $CD4^+$ T cells from IL-2 or IL-2, 4, 6, 1β, and IFN-γ media was predominantly effector memory-like (**Figure 5-13f, Figure 5-12e**) and approximately 30-40% of the cells were IFN-γ and TNF-α positive after antigen-specific restimulation (**Figure 5-13g, Figure 5-12f**). Taken together, these results demonstrate that in the optimized cytokine milieu, HLA II aAPCs can expand rare antigen-specific human $CD4^+$ T cells from endogenous repertoires.

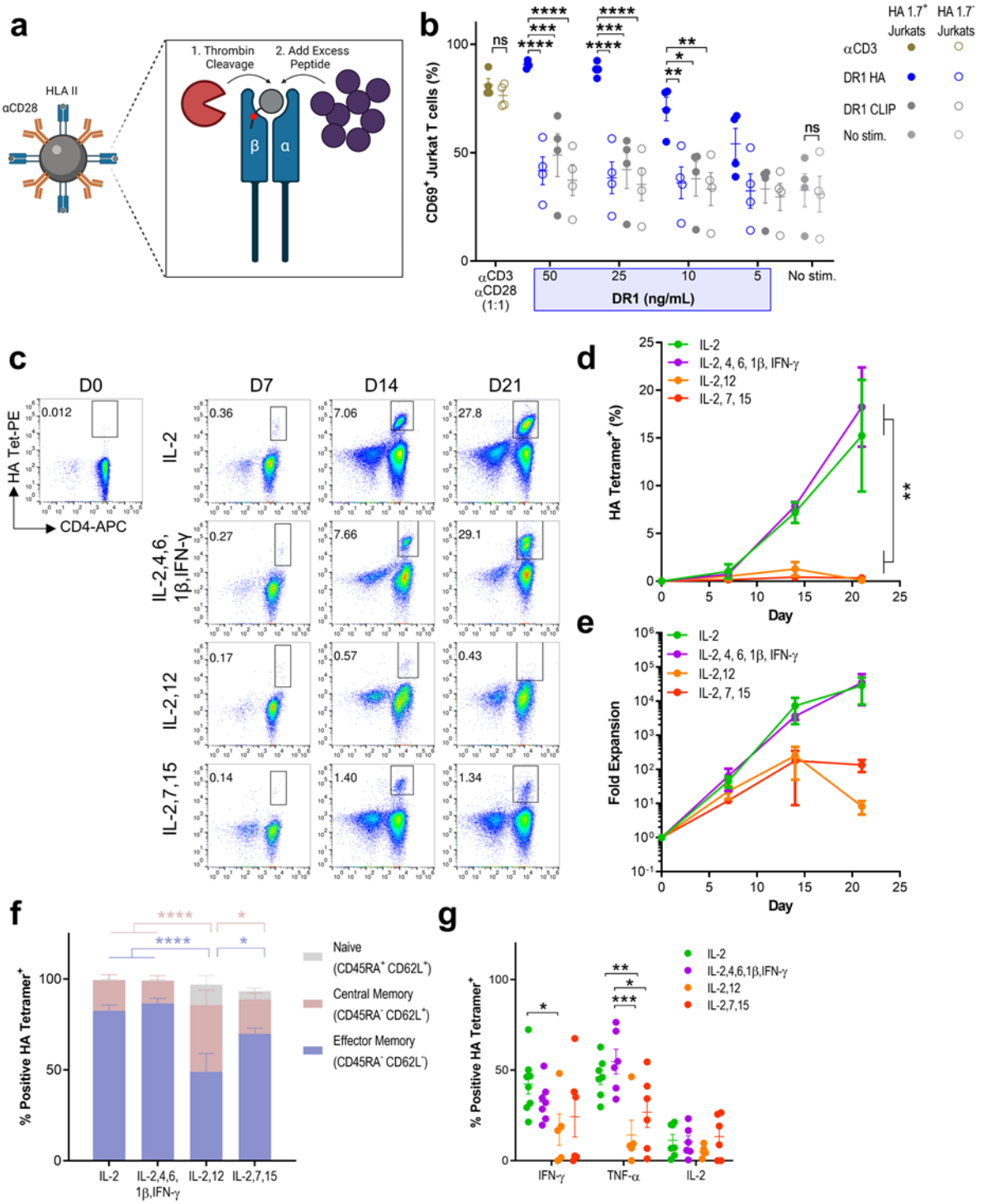

Figure 5-13. HLA II aAPCs stimulate functional antigen-specific human CD4⁺ T cells.(**a**) HLA II aAPC design includes HLA II molecules with cleavable thrombin linkers to facilitate peptide exchange. Created with BioRender.com. (**b**) CD69 induction on HA1.7 TCR transfected Jurkat cells following stimulation with αCD3/αCD28 microparticles or a titration of DR1/αCD28 aAPCs loaded with cognate hemagglutinin (DR1 HA) or non-cognate CLIP (DR1 CLIP) peptides. (**c-g**) Expansion of HA-specific CD4⁺ T cells from DRB1*04:01 healthy donor peripheral blood mononuclear cells (PBMC) treated with DR4 HA aAPCs in media supplemented with four different cytokine mixes: (i) IL-2; (ii) IL-2, IL-4, IL-6, IL-1β, and IFN-γ; (iii) IL-2 and IL-12; and (iv) IL-2, IL-7, and IL-15. (**c**) Representative tetramer staining, (**d**) frequency and (**e**)

fold expansion of DR4 HA $CD4^+$ T cells on days 0,7,14, and 21. (**f**) Memory phenotype and (**g**) intracellular cytokine production of HA-specific $CD4^+$ T cells on days 14 and 21. Data in (**b**, **d-g**) represent mean ± standard error of the mean (s.e.m.) from three or more independent experiments. (**b**) n = 4 and (**d-g**) n = 3-4 analyzed using a (**d-e**) repeated measure or (**b, f-g**) ordinary two-way ANOVA with Tukey's multiple-comparisons test, *p < 0.05, **p < 0.01, ***p < 0.001, ****p < 0.0001.

5.3 Discussion

Synthetic technologies for *ex vivo* expansion of T cells have continued to evolve over the past several decades to incorporate the breadth of biophysical and chemical cues that have been shown to affect T cell function[287]. These tools have thus far focused primarily on polyclonal T cell stimulation or expansion of antigen-specific $CD8^+$ T cells[21,26,210–32]. However, for many disease or pathogen-specific applications, $CD8^+$ T cells may play a less dominant role than other T cell subsets, particularly $CD4^+$ T cells. Even in cancer, where $CD8^+$ T cells are central to the therapeutic immune response, the antitumor function of these cells may be suboptimal without the addition of $CD4^+$ T cell help at both the priming[301] and effector[288] stages. pMHC II-coated beads have been developed for *in vivo* induction of regulatory T cells in autoimmunity[125,248]. However, technologies that harness effector or helper roles of $CD4^+$ T cells have yet to be explored. To address these limitations, here we developed the MHC II aAPC, a nanoparticle platform for *ex vivo* expansion of antigen-specific murine and human $CD4^+$ T cells. The platform confers several advantages over existing approaches to $CD4^+$ T cell expansion such as αCD3/αCD28 microparticles and peptide-pulsed autologous dendritic cells (DCs). αCD3/αCD28 microparticles provide non-specific stimulation that can result in potential expansion of irrelevant or even pathogenic T cells[79,134], presenting a hurdle for expansion of rare subsets of antigen-specific T cells. Autologous DCs provide antigen-specific stimulation; however, they require complex manufacturing

steps, their availability is limited[69], and the level and composition of signals they present to T cells are minimally controllable, which is of particular concern for cancer patients whose DCs are often dysfunctional[70,302] or even immunosuppressive[303]. Here we showed that MHC II aAPCs could be used off the shelf to activate murine and human $CD4^+$ T cells at levels similar to non-specific αCD3/αCD28 stimulation, while maintaining specificity for cognate $CD4^+$ T cells. Furthermore, MHC II aAPCs were able to specifically expand initially undetectable antigen-specific murine and human $CD4^+$ T cells from endogenous T cell repertoires. MHC II aAPCs could additionally be used in conjunction with existing synthetic platforms for *ex vivo* $CD8^+$ T cell activation to relay crucial help signals from $CD4^+$ T cells to a wide range of $CD8^+$ T cells. These help signals, in turn, boosted the memory formation, IFN-γ production, cytotoxicity, and *in vivo* antitumor control of antigen-specific $CD8^+$ T cells. Thus, the MHC II aAPC presents a streamlined approach for *ex vivo* generation of personalized $CD4^+$ T cell and the provision of helper signals to $CD8^+$ T cell therapies.

In addition to the clinical applications of the MHC II aAPC, it also provides a bottom-up approach for exploring $CD4^+$ T cell biology. For instance, here we show that MHC II aAPC stimulation results in generation of cytotoxic $CD4^+$ T cells, a phenotype which, thus far, has been observed primarily *in vivo*[279,297–299]. While confirming the importance of IL-2 in this process[304], we also observed that differentiation of $CD4^+$ T cells into cytotoxic T lymphocytes (CTL) occurred after stimulation with artificial and not endogenous APCs. Further comparisons of the signals presented by endogenous and artificial APCs may uncover the precise cues required for $CD4^+$ CTL generation. Similarly, here we utilized the MHC II aAPC platform to study which $CD4^+$ T cell cues

directly enhance $CD8^+$ T cell cytotoxicity and memory formation, in the absence of confounding DC intermediaries. Interestingly, these studies revealed an immunostimulatory effect of IL-10 on $CD8^+$ T cell cytotoxicity and effector function, in contrast with many studies that demonstrate IL-10 elicits T cell immunosuppression and anergy[305]. Our findings and other reported results[306,307] indicate that the anti-inflammatory functions of IL-10 occur indirectly through suppression of APC function, whereas the direct effects of IL-10 on $CD8^+$ T cells are stimulatory[308–311]. By providing stable presentation of MHC and costimulatory molecules, aAPCs are uniquely poised to exploit the direct effects of IL-10 on enhancing $CD8^+$ T cell antitumor function. In addition to the therapeutic implications of these findings, they are demonstrative of how a simplified approach using aAPCs can uncover additional aspects of the T cell help process that are difficult to study using traditional cellular approaches.

5.4 Methods

5.4.1 Mice

All mice used were 8−12 weeks of age and were maintained according to Johns Hopkins University's Animal Care and Use Committee under Protocol Number: MO20M349. C57BL/6 (B6), CD45.1, SMARTA-1, and OT-II mice were purchased from Jackson Laboratories (Bar Harbor, ME, USA). PMEL TCR transgenic mice were a gift from Nicholas Restifo (National Institutes of Health, MD, USA), and OT-IxRag2-/- mice were a gift from Jonathan Powell (Johns Hopkins University, MD, USA). 2C TCR transgenic mice were maintained as heterozygotes by breeding on a B6 background.

5.4.2 Human Subjects

This study was approved by the ethical committee of the Johns Hopkins University, and all healthy volunteers gave written informed consent (Human IRB protocol number: NA_00027947). HLA DR4 typing was performed on donor PBMC using an NFLD.D.1 antibody[312].

5.4.3 Cells

B16-SIY was a gift from Thomas Gajewski (The University of Chicago, IL, USA), B16-F10 was a gift from Charles Drake (Johns Hopkins University, MD, USA), and B16-OVA was a gift from Jonathan Powell (Johns Hopkins University, MD, USA). Lymphoblastoid Cell Lines (LCL) were a gift from the Johns Hopkins Human Immunogenetics Laboratory (Johns Hopkins University, MD, USA). Human Jurkat T cells clone E6-1 (ATCC no. TIB-152) was a gift from Jamie Spangler (Johns Hopkins University, MD, USA). B16 cell lines were cultured in RPMI 1640 medium (Fisher Scientific) containing 10% FBS (Atlanta Biologicals) and 10 μM ciproflaxin (Serologicals). B16-OVA and B16-SIY additionally received 400 μg/mL geneticin (Gibco). LCLs were cultured in RPMI 1640 medium containing 20% FBS, 200 mM L-glutamine (Gibco), 2mM HEPES (Quality Biologicals), and 1X Pen/Strep (Gibco). Jurkat T cells were grown in RPMI 1640 media with 10% FBS and 100 U/ml penicillin-streptomycin (Sigma). Primary murine T cells were cultured in T cell media consisting of RPMI 1640 supplemented with L-glutamine, 1X non-essential amino acids (Gibco), 1 mM sodium pyruvate (Gibco), 0.4X MEM vitamin solution (Gibco), 92 μM 2-mercaptoethanol (Gibco), 10 μM ciprofloxacin, and 10% FBS - supplemented with a previously described T cell growth factor cocktail[294], unless otherwise indicated. Primary

human T cells were cultured in the described T cell culture media containing 10% AB serum (Gemini Bio) instead of FBS and supplemented with additional indicated cytokines. All cells and cell lines were maintained at 37ºC in a humidified atmosphere with 5% CO_2.

5.4.4 Reagents

Recombinant murine IL-2, IL-12p70, IFNγ, CCL3, CCL4, CCL5, IL-10, and TNFα and human IL-1β, IL-2, IL-4, IL-6, IL-7, IL-12, IL-15, and IFN-γ were purchased from Peprotech (Cranbury, NJ, USA). Recombinant human IL-2 used in adoptive cell transfer studies (Proleukin) was a gift from Prometheus Laboratories. I-A^b $OVA_{323-339}$ (AAHAEINEA), I-A^b $CLIP_{87-101}$ (PVSKMRMATPLLMQA), and I-A^b LCMV GP_{66-77} (DIYKGVYQFKSV) monomers and tetramers were provided by the NIH Tetramer Core Facility (Emory University, GA, USA). DR1 Plasmid was a gift from Luc Teyton (Scripps Research, CA, USA). Soluble DR1 and DR4 monomers were produced in-house, as described below[261]. Soluble Class I MHC-Ig dimers were purified, biotinylated, and loaded with peptides according to previously described approaches[105]. The murine/human chimera HA1.7 T cell receptor was produced in-house, as described below. The HLA DR4-restricted NFLD.D.1 hybridoma supernatant was a gift from Sheila Drover (Memorial University of Newfoundland, St. John's, Canada)[312]. Unlabeled murine and human monoclonal antibodies (anti-CD3 clones 145-2C11 and OKT-3, anti-CD28 clones 37.51 and 9.3, anti-OX40 clone OX-86, anti-IFNγR clone GR-20, anti-I-A/I-E clone M5/114, anti-TNFα clone XT3.11, and anti-IL-10 clone JES5-2A5) were purchased from BioXCell (West Lebanon, NH, USA). Fluorescently labeled monoclonal antibodies were purchased from BioLegend (San Diego, CA, USA), BD Biosciences

(Franklin Lakes, NJ, USA), or eBioscience™ (San Diego, CA, USA), as indicated below. $OVA_{323-339}$ peptide was purchased from the Synthesis and Sequencing Facility (Johns Hopkins University, MD, USA). $OVA_{257-264}$ (SIINFEKL), $Trp2_{180-188}$ (SVYVFFDWL), SIY (SIYRYYGL), $gp100_{25-33}$ (KVPRNQDWL), $HA_{306-318}$ (PKYVKQNTLKLAT), and NY-ESO-$1_{157-170}$ (SLLMWITQCFLPVF) peptides were purchased from Genscript (Piscataway, NJ, USA).

5.4.5 Expression of human HLA DR monomers

HLA DR1 and DR4 monomers were produced following a previously described approach[261]. Briefly, HLA-DR1 and DR4 α and β chains were cloned into the gWiz mammalian expression vector (Genlantis) using Gibson Assembly® methods (New England Biolabs). The shared DRα chain vector consisted of the DRα gene (DRA*01:01) linked to a Fos leucine zipper dimerization domain that was further linked to a C-terminal hexahistidine tag. The distinct β chain vectors consisted of the Class II-associated invariant chain peptide (CLIP) followed by a thrombin cleavage site which was linked to the appropriate DRβ gene (DRB1*01:01 for HLA-DR1 or DRB1*04:01 for DR4). The DRβ gene was further linked to a Jun leucine zipper dimerization domain and C-terminal hexahistidine tag. Plasmids were purified using ZymoPURE™ II Plasmid Midiprep Kit (Zymo Research). All constructs were verified by Sanger sequencing. HLA-DR1 and DR4 MHC proteins were expressed in a human embryonic kidney (HEK) 293-F mammalian cell expression system (Thermo Invitrogen). HEK 293-F cells were cultivated in Freestyle 293 Expression Medium (Thermo Invitrogen), supplemented with 10 U/mL penicillin-streptomycin (Gibco). All cell lines were maintained at 37ºC in a

humidified atmosphere with 5% CO_2. HEK 293F cells were maintained on a shaker set to 125 rpm.

HLA-DR1 and DR4 monomers were expressed recombinantly in human embryonic kidney (HEK) 293-F cells via transient co-transfection of plasmids encoding the respective DRα and DRβ chains. DRα and DRβ chain plasmids were titrated in small-scale co-transfection tests to determine optimal DNA ratios for large-scale expression. HEK 293F cells were grown to 1.2×10^6 cells/mL and diluted to 1.0×10^6 cells/mL on the day of transfection. Plasmid DNA (filter sterilized though a 0.22 μm PES filter [Corning]) and polyethyleneimine (PEI, Polysciences) were independently diluted to 0.05 and 0.1 mg/mL, respectively, in OptiPro medium (Thermo Invitrogen), and incubated at 20°C for 15 min. Equal volumes of diluted DNA and PEI were mixed and incubated at 20°C for an additional 15 min. Subsequently, the DNA/PEI mixture (40 mL per Liter cells) was added to a flask containing the diluted HEK cells, which was then incubated at 37ºC with shaking for 3-5 days. Secreted protein was harvested from HEK 293F cell supernatants by via Ni-NTA (Expedeon) affinity chromatography, followed by size-exclusion chromatography on an ÄKTA™ fast protein liquid chromatography (FPLC) instrument using a Superdex 200 column (Cytiva). All proteins were stored in HEPES-buffered saline (HBS, 150 mM NaCl in 10 mM HEPES pH 7.3). Purity was verified by SDS-PAGE analysis.

5.4.6 Biotinylation, thrombin cleavage, peptide exchange, and tetramerization of human HLA DR monomers

For preparation of biotinylated HLA-DR1 and DR4, a C-terminal biotin acceptor peptide (BAP) GLNDIFEAQKIEWHE sequence was added to the previously described HLA-DR expression vectors. Following transfection and Ni-NTA affinity chromatography, the HLA-DR monomers were biotinylated with the soluble BirA ligase enzyme in 0.5 mM Bicine pH 8.3, 100 mM ATP, 100 mM magnesium acetate, and 500 mM biotin (Sigma). After overnight incubation at 4ºC, excess biotin was removed by size-exclusion chromatography on an ÄKTA™ FPLC instrument using a Superdex 200 column (Cytiva). To confirm covalent attachment of biotin, at least 1µg of each biotinylated HLA-DR protein was incubated with 2 mL of streptavidin (5mg/mL, MilliporeSigma) at 20°C for 5 min followed by SDS-PAGE analysis to confirm a shift in molecular weight.

CLIP peptides were cleaved by incubating DR proteins with 20 U of thrombin (Novagen, Madison WI) per milligram of monomer at 37°C for 2 hours. Peptide exchange was then performed by adjusting the concentration of monomer to 3.3 µM in a peptide exchange buffer consisting of 50 mM sodium citrate pH 5.2, 1% octylglucoside (ThermoFisher), 100 mM NaCl and 1X protease inhibitor cocktail (Roche) and incubating with 50 µM of peptide overnight at 37°C. To remove excess peptide, monomers were then washed three times in PBS with a 10 kDA MWCO concentrator (Sigma) and then frozen in small aliquots at -80°C.

Multimerization reactions were performed through incremental addition of fluorescent streptavidin molecules (Agilent) to biotinylated monomer at 20°C to reach a final streptavidin to monomer ratio of 1:3.5.

5.4.7 Synthesis of aAPCs

Murine I-A^b CLIP and I-A^b OVA and murine and human αCD3/αCD28 microparticles (Dynal, Lake Success, New York) were synthesized according to the manufacturer's instructions and as previously described[105]. Murine and human nanoparticle aAPCs were synthesized as previously described[72] and in accordance with the manufacturer's instructions by incubating 200 nm NHS-activated magnetic beads (Ocean Nanotech, Springdale, AR, USA) with either I-A^b, DR1, DR4, K^b-Ig or D^b-Ig monomers, dimers, or fluorescently labelled tetramers. Combined Signal 1 and Signal 2, Signal 1 and Isotype, or Signal 1 and BSA aAPCs were produced by pre-mixing monomers or dimers at a 1:1 or 1:3 molar ratio, as indicated, with mouse or human αCD28, isotype Armenian hamster IgG antibodies Clone HTK888 (Biolegend), or Bovine Serum Albumin (GeminiBio). Combined MHC I and MHC II aAPCs were produced by pre-mixing I-A^b monomers with K^b-Ig dimers at a 1:1 molar ratio.

Human aAPCs underwent thrombin cleavage and peptide exchange post conjugation of DR-CLIP proteins. Briefly, aAPCs were incubated with 40 units of thrombin per milligram of conjugated DR protein at 37°C for 2 hours. Particles were then magnetically washed and resuspended at 30 nM conjugated protein in peptide exchange buffer and then incubated overnight at 37°C with 3 μM peptide. Finally, particles were washed and resuspended either in storage buffer (1X PBS and 0.05% BSA) or human T cell culture media.

5.4.8 Characterization of aAPCs

Nanoparticle were sized using a Zetasiser DLS and imaged using Transmission Electron Microscopy (TEM). For TEM, iron dextran nanoparticles were allowed to adhere on carbon coated copper support grids (EMS CF400-Cu-UL) for 2 minutes, rinsed three times with deionized water, and allowed to dry at 20°C. The grids were mounted and imaged on a transmission electron microscope (Hitachi 7600) at an acceleration voltage of 80 kV.

Protein conjugation to Dynal microparticles was characterized by staining microparticles with FITC labelled secondary antibodies and then comparing them to a standard curve based on a Quantum™ FITC-5 MESF fluorescence quantification kit (Bangs Laboratories). Protein conjugation to nanoparticle aAPCs was performed as previously described[242] by staining particles with FITC labelled secondary antibodies, magnetically washing the particles, and then comparing their absorbance at 405 nm (Beckman Coulter AD340) and fluorescence at 485 nm (FisherScientific Varioskan LUX) to standard curves of known bead and protein concentrations, respectively. The following secondary antibodies were used: FITC anti-hamster IgG clone G94-56 (BD Biosciences) for murine αCD3, FITC anti-hamster IgG clone G192-1 (BD Biosciences) for murine αCD28, FITC anti-mouse I-A/I-E clone M5/114.15.2 (BioLegend) for murine I-A^b, FITC anti-mouse Ig λ1 λ2 λ3 light chain clone R26-46 (BD Biosciences) for murine K^b-Ig and D^b-Ig , FITC anti-mouse IgG2a clone R19-15 (BD Biosciences) for human αCD3 and αCD28, and FITC anti-human HLA DR clone L243 (BioLegend) for human DR1 and DR4. For fluorescent tetramer-labelled nanoparticles, the protein

concentration per nanoparticle was determined by comparing the fluorescence of the particles to a standard curve of unconjugated fluorescent tetramer.

5.4.9 T cell isolation

OT-II, SMART-A1, or B6 mice were used for $CD4^+$ expansions, and OT-I, 2C, PMEL, and B6 mice were used for $CD8^+$ expansions. Spleens and lymph nodes were harvested from 8 to 12-week-old mice and processed through a 70 μm cell strainer. Then, $CD4^+$ and $CD8^+$ T cells were isolated using corresponding no-touch isolation kits and magnetic columns from Miltenyi Biotech (Auburn, CA, USA) according to the manufacturer's instructions.

For human isolations, blood was drawn from healthy donors per JHU IRB approved protocols and PBMC were isolated by Ficoll-Paque PLUS (GE Healthcare) density gradient centrifugation. Cells were cryopreserved in a 90% FBS, 10% DMSO solution at 10^7 cells/mL and stored in liquid nitrogen. Prior to use, cryopreserved PBMC were thawed with 50 U/mL benzonase Nuclease HC (EMD Millipore), washed, and then incubated overnight in T cell culture medium at 37°C. The following morning, $CD4^+$ T cells were purified using no-touch $CD4^+$ isolation kits and magnetic columns (Miltenyi).

5.4.10 Bone Marrow Derived Dendritic Cell Isolation

Bone marrow derived dendritic cells (BMDC) were generated following a well-established approach[313]. Marrow was flushed from femurs and tibia of B6 mice, filtered, red blood cells lysed, washed, and cultured in non-treated 6 well plates at $1x10^6$ cells/mL in DC media containing RPMI 1640 media (Gibco) supplemented with 10% FBS, 1% Pen/Strep (Gibco), 50 μM 2-mercaptoethanol (Gibco), and 20 ng/mL GM-CSF (Peprotech). On day 3, cells were refed with DC media containing 40 ng/mL GM-CSF.

On day 6, 50% of cell supernatant was replaced with DC media containing 20 ng/mL GM-CSF. On day 8, non-adherent or loosely adherent cells were harvested and matured overnight by replating cells at $1x10^6$ cells/mL in DC media containing 100 ng/mL lipopolysaccharide (Sigma Aldrich), 20 ng/mL GM-CSF, and 1 μM of peptide. Prior to stimulation of $CD4^+$ T cells, DC maturation was confirmed via flow cytometry by staining for FITC anti-mouse CD11b clone M1/70 (BD Biosciences), PerCP-Cy5.5 anti-mouse CD11c clone N418 (BioLegend), APC anti-mouse CD86 clone GL-1 (BioLegend), Live/Dead Fixable Violet (Invitrogen), BV605 anti-mouse F4/80 clone BM8 (BioLegend), PE anti-mouse CD80 clone 16-10A1 (BioLegend), and PE-Cy7 anti-mouse I-A/I-E clone M5/114.15.2 (BioLegend).

5.4.11 Ex vivo T cell expansion

Isolated murine $CD4^+$ T cells were cultured in T cell culture media with the addition of either a previously described optimized T cell growth factor cocktail (TF)[294], IL-2 (10 ng/mL), or various combinations of a Th1 skewing media composed of IL-2, IL-12p70, and IFN-γ (each at 10 ng/mL). Cells were plated on day 0 at 10^5 cells/mL and refed on day 3 of culture, with half of the initial volume of T cell culture media and twice the concentration of cytokines. On day 0, micro-aAPCs were added at a 1:1 particle to cell ratio, whereas nano-aAPCs were added at a concentration of 80 ng/mL of conjugated $I\text{-}A^b$, unless otherwise indicated. For aAPCs lacking Signal 2 on their surface, soluble αCD28 was added at a concentration of 1 μg/mL unless otherwise indicated. For peptide-based stimulations, isolated splenocytes were plated at $8x10^5$ cells/mL in T cell culture media with the addition of 1 μg/mL of peptide. For BMDC-

based stimulations, murine $CD4^+$ T cells were plated at 10^5 cells/mL and at a 1:1 ratio with mature BMDCs in T cell culture media.

Murine $CD4^+$ T cell proliferation was assessed by labelling a subset of isolated $CD4^+$ T cells on day 0 with carboxyfluorescein succinimidyl ester (CFSE, Invitrogen). Cells were incubated with 5 μM dye in T cell culture media at 37°C for 20 minutes, washed and plated as above, and on day 3 of culture harvested and assessed for CFSE dilutions on a BD FACSCalibur flow cytometer. Another subset of unlabeled cells was plated as above and, on day 7, harvested, stained with Trypan blue to exclude dead cells, and then manually counted with a hemocytometer. Fold expansion was calculated as the ratio of live cells at days 7 and 0. Cell phenotype and function was assessed, as described below.

Isolated murine $CD8^+$ T cells were cultured as above in T cell culture media supplemented with TF. Class I aAPCs were added at a concentration of 30 ng/mL of conjugated K^b or D^b and 1 μg/mL soluble αCD28 unless otherwise indicated. Cells were refed as above on day 3 and then harvested and counted on day 7 for functional and phenotypic analyses. For some experiments, T cell culture media was additionally supplemented at day 0 with 25 ng/mL IL-10 or 5 ng/mL TNF-α, and then refed with double these concentrations and half the initial volume on day 3.

For murine $CD4^+$ and $CD8^+$ co-culture experiments, $CD8^+$ T cells were mixed at a 1:1 ratio with either freshly isolated $CD4^+$ T cells or $CD4^+$ T cells activated with S1+S2 aAPCs (80 ng/mL conjugated I-A^b and 1 μg/mL αCD28) for 5 days in Th1 media. The CD4:CD8 mixture was then plated at 10^5 cells/mL in T cell culture media supplemented with TF, MHC I aAPCs (30 ng/mL), MHC II aAPCs (80 ng/mL), and soluble αCD28 (1

μg/mL), unless otherwise indicated. For some experiments, T cell culture media was additionally supplemented at days 0 and 3 with 1 μg/mL IL-10 or TNF-α blocking antibodies. Cells were refed as above on day 3 and harvested and counted on day 7 for further functional and phenotypic analyses. The relative ratios of $CD4^+$ and $CD8^+$ T cells over the co-culture period was tracked via flow cytometry by staining cells with APC anti-mouse CD4 clone GK1.5 (Biolegend), PE anti-mouse CD3 clone 17A2 (Biolegend), FITC anti-mouse CD8a clone 53-6.7 (BD Biosciences), and Live/Dead Fixable Violet (Invitrogen). $CD4^+$ and $CD8^+$ co-culture experiments were also performed in 0.4 μm pore-size polycarbonate membranes transwell plates (Costar). 10^5 OT-I $CD8^+$ T cells were placed in the lower compartment in 0.75 mL of T cell culture media supplemented with T cell growth factor, MHC I aAPCs (30 ng/mL conjugated K^b) and 1 μg/mL αCD28. 10^5 Day 5 Th1 OT-II $CD4^+$ T cells were either separated in the upper or mixed with the $CD8^+$ T cells in the lower compartment in an additional 0.75 mL of T cell culture media supplemented with TF, MHC II aAPCs (80 ng/mL conjugated $I\text{-}A^b$), and 1 μg/mL αCD28. Cells were refed as above on day 3 and harvested and counted on day 7 for further functional and phenotypic analyses.

For human T cell expansions, the day 0 precursor frequencies of $HA_{306\text{-}318}$ $CD4^+$ T cells was assessed through tetramer staining. Isolated $CD4^+$ T cells were then seeded at 10^6 cells/mL in human T cell culture medium with indicated cytokines, and peptide exchanged Class II aAPCs were added at a concentration of 30 ng/mL of conjugated DR4. On days 3, 5, 10, 12, 17, and 19, cells were refed with one quarter of the initial volume of T cell culture media and twice the concentration of cytokines, and on days 7, 14, and 21, cells were harvested, counted, and assessed for antigen specificity,

phenotype, and function. On days 7 and 14 cells were additionally re-plated with fresh media, cytokines, and aAPCs at $5x10^5$ cells/mL and 100 ng/mL DR4 (day 7) and $3x10^5$ cells/mL and 100 ng/mL DR4 (day 14), respectively. Fold proliferation at days 7, 14, and 21 was calculated as the ratio of live tetramer positive $CD4^+$ T cells (total number of cells multiplied by the percentage of live lymphocytes that were both CD4 and tetramer positive) at the current and previous time points.

5.4.12 Ex vivo T cell phenotypic studies

Lineage specific transcription factors of naïve or expanded murine $CD4^+$ T cells were analyzed by washing cells and staining them for 15 minutes at 4°C with Live/Dead Fixable Aqua (Invitrogen) and APC-Cyanine7 anti-mouse CD4 clone GK1.5 (BioLegend). Cells were then washed, fixed, and permeabilized using the Foxp3 Transcription Factor Staining Buffer Set (eBioscience™), and then stained for FITC anti-mouse Foxp3 clone FJK-16s (eBioscience™), PerCp-Cyanine5.5 anti-mouse/human T-bet clone eBio4B10 (eBioscience™), APC anti-mouse/human RORγT clone AFKJS-9 (eBioscience™), and PE/Cyanine7 anti-mouse/human Gata3 clone TWAJ (eBioscience™), or their corresponding isotypes. Finally, cells were washed and resuspended in FACS wash buffer (1X PBS, 2% FBS, 0.5% sodium azide) and then analyzed on an Attune NxT Flow Cytometer.

The memory phenotype of naïve or expanded murine $CD4^+$ or $CD8^+$ T cells was analyzed by harvesting cells, and then washing and staining them for 15 minutes at 4°C with Live/Dead Fixable Violet (Invitrogen), PE anti-mouse CD3 clone 17A2 (BioLegend), APC/Cyanine 7 anti-mouse CD4 clone GK1.5 (BioLegend) or APC/Cyanine 7 anti-mouse CD8a clone 53-6.7 (BioLegend), Alexa Fluor 488 anti-mouse CD127 clone

A7R34 (BioLegend), PerCP-Cy5.5 anti-mouse CD44 clone IM7 (BioLegend), APC anti-mouse CD62L clone MEL-14 (BioLegend), Brilliant Violet 605™ anti-mouse/human KLRG1 clone 2F1/KLRG1 (BioLegend), and PE/Cyanine7 anti-mouse CD197 (CCR7) clone 4B12 (BioLegend), or their corresponding isotypes. For rare T cell analysis, PE-labelled multimer staining was substituted for anti-CD3 (see below) and performed prior to other surface marker staining.

The memory phenotype of human $CD4^+$ T cells was analyzed by first staining cells with PE labelled tetramers (see below), and then staining them for 15 minutes at 4°C with Live/Dead Fixable Aqua, PE/Cyanine 7 anti-human CD4 clone A161A1 (BioLegend), FITC anti-human CD45RA clone HI100 (BioLegend), APC/Cyanine7 anti-human CD62L clone DREG-56 (BioLegend), PerCP-Cyanine5.5 anti-human CD69 clone FN50 (BioLegend), APC anti-human CD103 clone Ber-ACT8 (BioLegend), and Brilliant Violet 421™ anti-human CD122 clone TU27 (BioLegend), or their corresponding isotypes.

5.4.13 Ex vivo T cell functional studies

Intracellular cytokine staining of murine $CD4^+$ and $CD8^+$ T cells was performed by diluting them to approximately $2x10^6$ cells/mL in T cell culture media and incubating them at 37°C for 6 hours with 1X cytokine activation cocktail (BioLegend) and GolgiPlug (BD Biosciences). No stimulation controls received only GolgiPlug. Following incubation, cells were washed and stained with PerCP anti-mouse CD4 clone RM4-5 (BioLegend) or PerCP anti-mouse CD8 clone 53-6.7 (Biolegend) and Live/Dead Fixable Aqua (Invitrogen) for 15 minutes at 4°C. Cells were then fixed and permeabilized overnight with the Cytofix/Cytoperm Fixation/Permeabilization kit (BD Biosciences),

washed, and stained with APC anti-mouse IFN-γ clone XMG1.2 (BioLegend), PE/Cyanine7 anti-mouse TNF-α clone MP6-XT22 (BioLegend), PE anti-mouse IL-2 clone JES6-5H4 (BioLegend), and FITC anti-mouse/human Granzyme B clone GB11 (BioLegend). Cells were then washed and resuspended in FACS wash buffer and analyzed on an Attune NxT Flow Cytometer.

For cytokine analysis of antigen-specific murine $CD8^+$ T cells, a similar assay was used with the following modifications. Prior to stimulation, T cells were stained with cognate and non-cognate biotinylated pMHC-Ig dimers (see below), washed, and then re-stimulated. After the 6-hour incubation, cells were washed and stained with or PerCP anti-mouse CD8 clone 53-6.7 (BioLegend), PE-labeled streptavidin (BD Biosciences), and Live/Dead Fixable Aqua (Invitrogen) for 15 minutes at 4°C. Cells were then fixed and permeabilized and stained with APC anti-mouse IFN-γ clone XMG1.2 (BioLegend), PE/Cyanine7 anti-mouse TNF-α clone MP6-XT22 (BioLegend), and FITC anti-mouse/human Granzyme B clone GB11 (BioLegend). Cells were then washed and resuspended in FACS wash buffer and analyzed on an Attune NxT Flow Cytometer. Antigen-specific human $CD4^+$ T cell cytokine analysis was performed by pulsing LCLs with 10 μg/mL cognate ($HA_{306-318}$) or irrelevant (NY-ESO-$1_{161-180}$) peptide for 1 hour at 20°C, washing, and then incubating them 1:1 with T cells in human T cell culture media containing GolgiPlug for 5 hours at 37°C. Tetramer staining was begun 50 minutes prior to the end of the 5-hour incubation (see below). Afterwards, cells were washed and stained for APC anti-human CD4 clone OKT4 (BioLegend) and Live/Dead Fixable Aqua (Invitrogen). Cells were then fixed and permeabilized as above and stained for FITC anti-human IFN-γ clone 4S.B3 (BioLegend), PerCP-Cy5.5 anti-human IL-2 clone MQ1-

17H12 (BioLegend), Pacific Blue anti-mouse/human Granzyme B clone GB11 (BioLegend), and PE/Cyanine7 anti-human TNF-α clone MAb11 (BioLegend). Cells were then washed and resuspended in FACS wash buffer and analyzed on an Attune NxT Flow Cytometer.

In vitro killing assays of murine $CD4^+$ and $CD8^+$ T cells were performed as previously described[79] by labelling $5x10^6$ B16 tumor cells with 5 μM CFSE dye (Invitrogen) at 37°C for 20 minutes in 1 mL PBS. The reaction was quenched by adding 5 mL FBS and incubating cells at 37°C for 5 minutes. Tumor cells were plated at $5x10^4$ cells/mL in ultra-low cluster 96 well plates (Costar) co-incubated with T cells at varying effector to target ratios (30:1, 10:1, 1:1, 0.1:1, 0.01:1, and 0:1) at 37°C for 16 hours. For blocking studies, anti-I-A/I-E clone M5/114 (BioXcell) or anti-IFNγR clone GR-20 (BioXcell) as well as their corresponding isotype controls were added at 10 μg/mL, while Granzyme B inhibitor Z-AAD-CMK (Calbiochem) was added at 25 μM. Cells were then treated with trypsin to detach plate-bound tumor cells, stained for 15 minutes at 4°C with Live/Dead Fixable Aqua (Invitrogen) and APC anti-mouse CD4 clone GK1.5 (BioLegend) or APC anti-mouse CD8a clone 53-6.7 (BioLegend), washed, and then run analyzed on an Attune NxT Flow Cytometer. To monitor MHC II expression on live tumor cells, cells were instead stained with Live/Dead Fixable Violet (Invitrogen), APC anti-mouse CD4 clone GK1.5 (BioLegend), and PE/Cyanine7 anti-mouse I-A/I-E clone M5/114.15.2 (BioLegend).

5.4.14 Multimer staining

Murine $CD4^+$ T cell tetramer staining was performed by incubating $1x10^5$ cells at 37°C for 2 hours with 60 μg/mL cognate and non-cognate $I\text{-}A^b$ tetramers (NIH Tetramer

Core Facility) in T cell culture medium. Cells were then washed in PBS, stained with APC anti-mouse CD4 clone GK1.5 (BioLegend) and Live/Dead Fixable Green (Invitrogen) for 15 minutes at 4°C, washed and resuspended in FACS Wash Buffer, and then analyzed on an Attune NxT Flow Cytometer.

Murine $CD8^+$ T cell dimer staining was performed by incubating $1x10^5$ cells at 4°C for 1 hour with 10 μg/mL cognate and non-cognate biotinylated K^b-Ig or D^b-Ig dimers (in-house) in FACS Wash Buffer. Cells were then washed in PBS, stained with APC anti-mouse CD8a clone 53-6.7 (BioLegend) and Live/Dead Fixable Green (Invitrogen) for 15 minutes at 4°C, washed and resuspended in FACS Wash Buffer, and then analyzed on an Attune NxT Flow Cytometer.

Human $CD4^+$ T cell tetramer staining was performed by incubating $1x10^5$ cells at 20°C for 5 minutes with 40μL/mL Human TruStain FcX™ Fc Receptor Blocking Solution (BioLegend) in T cell culture medium. An additional 20-minute incubation at 37°C with 50 nM dasatinib (Axon Medchem) followed by a 30-minute incubation at 37°C with 20 μg/mL cognate and non-cognate tetramers (in-house) was then done. Cells were then washed in PBS, stained with APC anti-human CD4 clone OKT4 (BioLegend) and Life/Dead Fixable Green (Invitrogen) for 15 minutes at 4°C, washed and resuspended in FACS Wash Buffer, and then analyzed on an Attune NxT Flow Cytometer.

5.4.15 T cell binding, internalization, enrichment, and combined enrichment and expansion

Murine $CD4^+$ T cell binding studies were performed by incubating $1x10^5$ recently isolated OT-II, SMART-A1, or B6 $CD4^+$ T cells for 30 minutes at 37°C in T cell culture media with varying concentrations of nano- and micro-aAPCs. Cells were then washed,

stained for 15 minutes at 4°C in FACS Wash Buffer with FITC anti-mouse I-A/I-E clone M5/114.15.2 (BioLegend) and APC anti-mouse CD4 clone GK1.5 (BioLegend) to detect aAPC-bound $CD4^+$ T cells, washed again, and then analyzed on a BD FACSCalibur Flow Cytometer.

Murine $CD4^+$ T cell internalization studies were performed as above using nanoparticles coated with PE-labelled $I\text{-}A^b_{OVA}$ tetramers at 80 ng $I\text{-}A^b/10^5$ $CD4^+$ T cells. The incubation time was varied between 30 and 120 minutes, incubation temperature between 4°C and 37°C, and incubation media between T cell culture with and without 0.5% sodium azide (NaN_3) supplementation. Cells were then washed and stained for 15 minutes at 4°C in FACS Wash Buffer with FITC anti-mouse TCR β chain clone H57-597 (BioLegend), APC anti-mouse CD4 clone GK1.5 (BioLegend), and PE-Cy7 anti-mouse I-A/I-E clone M5/114.15.2 (BioLegend). Samples were then washed again and analyzed on an Attune NxT flow cytometer for the percentage of cells with surface-bound ($Tetramer^+MHC\ II^+$) versus internalized ($Tetramer^+MHC\ II^-$) aAPCs.

OT-II doped enrichment studies were performed by CFSE labelling recently isolated OT-II $CD4^+$ T cells with 5 μM CFSE (Invitrogen) in T cell culture medium for 20 minutes at 37°C and then diluting them 1:1000 with recently isolated, unlabeled B6 $CD4^+$ T cells. Cells were then incubated for 2 hours with micro- or nano-aAPCs at 37°C in T cell culture media and then magnetically enriched using a 96-well ring magnet[72]. For some experiments, the incubation was performed at 4°C or with T cell culture media supplemented with 0.5% sodium azide (NaN_3). The enriched fraction was then counted with a hemocytometer, washed, and stained at 4°C for 15 minutes with APC anti-mouse CD4 clone GK1.5 (BioLegend) in FACS Wash Buffer. Cells were then washed and

analyzed on a BD FACSCalibur Flow Cytometer. Fold enrichment and percent cell recovery were calculated by taking the ratio of both the frequency and number of CFSE+ $CD4^+$ T cells pre and post enrichment. To track aAPC internalization during the enrichment process, diluted cells were incubated with nano-aAPCs conjugated with PE-labelled tetramers at 30 ng I-A^b/10^6 $CD4^+$ T cells, as above. Both the enriched and unenriched fractions were collected, counted with a hemocytometer, washed, and stained at 4°C for 15 minutes with PerCP anti-mouse CD4 clone RM4-5 (Biolegend), PE-Cy7 anti-mouse I-A/I-E clone M5/114.15.2 (BioLegend), and Alexa Fluor 647 anti-mouse TCR β chain clone H57-597 (BioLegend). Samples were then washed and analyzed on an Attune NxT Flow Cytometer, monitoring, as above, the percentage of cognate ($CFSE^+$) and irrelevant ($CFSE^-$) cells with surface-bound (Tetramer$^+$MHC II^+) versus internalized (Tetramer$^+$MHC II^-) aAPCs. SMART-A1 doped enrichment studies were performed analogously, except unlabeled SMART-A1 cells were used instead and detected with a PE anti-mouse CD45.1 clone A20 (Biolegend) antibody.

Doped enrichment and expansion studies were performed by diluting freshly isolated, unlabeled OT-II or SMART-A1 $CD4^+$ T cells into recently isolated, unlabeled B6 $CD4^+$ T cells. Cells were then incubated for 2 hours with 30 ng conjugated I-A^b/10^6 $CD4^+$ T cells of S1 aAPCs at 37°C in T cell culture media and then magnetically enriched using a 96-well ring magnet[72]. The enriched fractions were plated at $2.5x10^5$ cells/mL in T cell culture media supplemented with Th1 skewing cytokines and 1 μg/mL soluble αCD28. Cells were refed on day 3 with half of the initial volume of T cell culture media and twice the concentration of cytokines. On day 7, the frequency and number of OT-II and SMART-A1 T cells were determined by harvesting and counting samples,

staining them with tetramers or PE anti-mouse CD45.1 clone A20 (Biolegend) antibodies, respectively, and analyzing them on a BD FACSCalibur flow cytometer.

Endogenous murine $CD4^+$ T cell enrichment and expansion studies were performed analogously to the doped enrichment and expansion studies, using freshly isolated B6 $CD4^+$ T cells. On day 7, the frequency and number of antigen-specific $CD4^+$ T cells was determined by harvesting and counting samples, staining them with cognate and non-cognate tetramers, and then analyzing them on a BD FACSCalibur flow cytometer.

Endogenous murine $CD8^+$ T cell enrichment and expansion studies were performed as previously described[72], by isolating B6 $CD8^+$ T cells, and then incubating them for 1 hour with MHC I aAPCs (30 ng conjugated K^b-Ig or D^b-Ig per 10^6 $CD8^+$ T cells) at 4°C in AutoMACS Running Buffer (1X PBS with 2 mM EDTA and 0.5% Bovine Serum Albumin). Cells were then magnetically enriched on a 96-well ring magnet and plated at $2.5x10^5$ cells/mL in T cell culture media supplemented with an optimized $CD8^+$ cytokine mix[294] and 1 µg/mL soluble αCD28. For endogenous co-culture experiments, the enriched fractions were additionally supplemented with an equal number of Day 5 Th1 skewed $CD4^+$ T cells (see above) and S1 aAPCs (80 ng/mL conjugated I-A^b). Cells were refed on day 3 with half of the initial volume of T cell culture media and twice the concentration of the $CD8^+$ cytokine mix. On day 7, cells were harvested and counted, and then analyzed for specificity, phenotype, and function of dimer positive $CD8^+$ T cells.

5.4.16 Imaging studies

OT-I/OT-II imaging studies were performed by labeling freshly isolated OT-I $CD8^+$ T cells at 37°C for 20 minutes with 5 μM CellTracker™ green dye (Invitrogen) in T cell culture media without serum and then quenching at 37°C for 5 additional minutes with 5 mL FBS. Analogously, freshly isolated or Day 5 Th1 skewed OT-II $CD4^+$ T cells were labeled with 5 μM CellTrace™ Far Red dye (Invitrogen). Labeled OT-II $CD4^+$ T cells were then pre-incubated with MHC I/II aAPCs at 80 ng conjugated $I\text{-}A^b/10^5$ $CD4^+$ T cells for two hours at 37°C, prior to mixing them 1:1 with labeled OT-I $CD8^+$ T cells. T cell mixtures were incubated on gelatin coated (0.1%) plates and imaged using a Zeiss AxioObserver epifluorescent microscope with an incubation chamber at 37°C and 5% CO_2. Images at 24 hours were analyzed using a custom protocol in CellProfiler. $CD4^+$ and $CD8^+$ T cells within 5 pixels of each other were considered bound.

OT-II internalization imaging studies were performed by incubating freshly isolated OT-II $CD4^+$ T cells with nanoparticles conjugated with Alexa Fluor 488-labelled $I\text{-}A^b_{OVA}$ tetramer at a concentration of 80 ng $I\text{-}A^b/10^6$ cells for 2 hours at 37°C. Cells were then washed in PBS and stained with Alexa Fluor 594 anti-mouse CD4 clone GK1.5 (BioLegend) and Alexa Fluor 647 anti-mouse I-A/I-E clone M5/114.15.2 (BioLegend) antibodies for 15 minutes at 4°C. Cells were then washed in PBS and fixed overnight in 1% paraformaldehyde. The following morning, cells were washed in PBS and stained with DAPI (ThermoFisher) at 0.1 μg/mL for 10 minutes at 20°C. Cells were then washed and imaged in a #1.5 chambered coverglass slide (Cellvis) using an LSM980 confocal microscope with Airyscan super-resolution. Airyscan processing was performing using

Zen software, and the Pearson Correlation between Alexa Fluor 488 and Alexa Fluor 647 fluorescent signals was calculated in ImageJ.

5.4.17 Transwell migration assays

Transwell migration assays were performed as previously described[314] using transwell plates (Costar) with 5.0 μm pore-size polycarbonate membranes. Day 7 stimulated OT-I $CD8^+$ T cells were labelled at 37°C for 20 minutes with 5 μM CFSE dye (Invitrogen) in T cell culture media without serum and then quenched at 37°C for 5 additional minutes with 5 mL FBS. Analogously, freshly isolated or Day 5 Th1 skewed OT-II $CD4^+$ T cells were labeled with 5 μM CellTrace™ Far Red dye (Invitrogen). The bottom compartments of the transwell plates received 600 μL of control medium (RPMI 1640 with 0.5% BSA) with or without $1x10^6$ labelled naïve or Th1 OT-II $CD4^+$ T cells at a 1:1 ratio with αCD3/αCD28 Dynal microbeads, while the top compartments received $1x10^6$ OT-I $CD8^+$ T cells in 100 μL control medium. Plates were incubated at 37°C for 3 hours and then the upper and lower compartments were harvested, manually counted with a hemocytometer, and stained with Live/Dead Fixable Violet (Invitrogen), PE anti-mouse CD4 clone H129.19 (BioLegend), and PE/Cyanine7 anti-mouse CD8 clone 53-6.7 (BD Biosciences). Cells were washed, resuspended in FACS Wash Buffer and analyzed on an Attune NxT Flow Cytometer. The transmigration index was calculated as the ratio of the number of $CD8^+$ T cells transmigrated in a given sample to the number of $CD8^+$ T cells transmigrated in control medium.

5.4.18 Protein arrays

Day 5 Th1 OT-II $CD4^+$ T cells were either left unstimulated or were re-stimulated overnight with MHC II aAPCs (80 ng I-A^b/10^5 $CD4^+$ T cells) and soluble αCD28 (1

μg/10^5 $CD4^+$ T cells). Cell supernatants were then collected and filtered through Spin-X™ Centrifuge Tube filters (Corning). Cytokines in the cell supernatants were then analyzed with the Proteome Profiler Mouse Cytokine Array Kit A (R&D Systems). The blots were visualized with chemiluminescence using an iBright 1500 imaging system and quantified using the Protein Array Analyzer plugin in ImageJ.

5.4.19 Cloning of HA1.7 TCR

The native signal sequence and α and β variable domains of TCR HA1.7[315] (IMGT ID 1FYT) were cloned into the AbVec mammalian expression vector[316] containing the murine constant domains—to promote pairing of the exogenous α and β TCR chains—and human transmembrane domains. The α and β chains were separated by a P2A peptide. Plasmid was purified using ZymoPURE™ II Plasmid Midiprep Kit (Zymo Research).

5.4.20 HA1.7 expression and activation in Jurkat cells

10^7 Jurkat cells per transfection were centrifuged at 250 x *g* for 5 minutes, resuspended in 5 mL of OptiMEM (Gibco), and incubated at 20°C for 8 minutes. Cells were centrifuged as before, resuspended in 400 μl of OptiMEM and 20 μg HA1.7 plasmid, and transferred to a 4-mm electroporation cuvette (BioRad). Cells were incubated for 8 minutes before pulsing exponentially with 250 V, 950 μF, and ∞ ohms resistance on a Bio-Rad GenePulser Xcell with PC and CE modules. After an 8-minute recovery period, cells were rescued with 10 mL of pre-warmed Jurkat culture media (RPMI 1640 + 10% FBS + 100 U/mL penicillin-streptomycin), and kept at 37°C, 5% CO_2.

In vitro stimulation of HA1.7 TCR-transfected Jurkat cells was performed 12-16 hours after transfection. αCD3/αCD28 microbeads or titrations of nanoscale DR1 HA peptide exchanged and DR1 CLIP unexchanged aAPCs were incubated at 37°C with $5x10^4$ transfected Jurkat T cells per stimulation in Jurkat culture media. At 24 hours post-transfection, samples were washed and stained for 15 minutes at 4°C in FACS Wash Buffer with APC anti-mouse TCR β chain clone H57-597 (BioLegend) and FITC anti-human CD69 clone FN50 (BioLegend) to detect the HA1.7 TCR and activation, respectively. Cells were then washed again and analyzed on a BD FACSCalibur Flow Cytometer.

5.4.21 *In vivo* killing assay

One day prior to adoptive cell transfer (ACT), CD45.1 B6 mice received 500 cGy of irradiation to induce transient lymphopenia and promote T cell engraftment[317]. On the day of adoptive transfer, OT-II $CD4^+$ T cells were either freshy isolated (naïve) or harvested after 7 days of stimulation with MHC II aAPCs (80 ng/mL conjugated I-A^b and 1 μg/mL soluble αCD28) in Th1 skewing media (Th1). Naïve and Th1 $CD4^+$ T cells were labeled with 5 μM CellTrace™ Violet (CTV, Invitrogen) in 1mL PBS for 20 minutes at 37°C. The reaction was quenched with 5 mL FBS at 37°C for 5 minutes, and then cells were washed twice in PBS. 10^6 CTV labelled naïve or Th1 $CD4^+$ T cells were then injected intravenously in volumes of 100 μL per recipient mouse. On the day of and the day after adoptive transfer, mice received intraperitoneal injections of 30,000 U IL-2 (Prometheus Labs) in a volume of 100 μL.

To analyze *in* vivo killing, six days post adoptive transfer, freshly isolated spleens from B6 mice were brought to a single cell suspension. Cells were then labeled either

with 5 μM or 0.5 μM CFSE (Invitrogen) to generate $CFSE^{hi}$ and $CFSE^{lo}$ populations. $CFSE^{hi}$ splenocytes were then loaded for 1 hour at 37°C with 1 μg of $OVA_{323-339}$ peptide per 10^7 cells in T cell culture media, washed twice in PBS, and mixed 1:1 with unloaded $CFSE^{lo}$ splenocytes. 10^7 cells of the mixture were then injected intravenously in 100 μL volumes per recipient mouse. The following day, spleens and lymph nodes of recipient mice were harvested, processed, and stained for Live/Dead Fixable Aqua (Invitrogen), PE anti-mouse CD45.2 clone 104 (BioLegend), APC anti-mouse CD4 clone GK1.5 (BioLegend), and PE/Cyanine7 anti-mouse I-A/I-E clone M5/114.15.2 (BioLegend) for 15 minutes at 4°C. Cells were then washed, resuspended in FACS Wash Buffer, and analyzed on an Attune NxT Flow Cytometer. Specific lysis was calculated as 100% x (1-[($CFSE^{lo,pre\text{-}injection}$/$CFSE^{hi,pre\text{-}injection}$)/($CFSE^{lo,post\text{-}injection}$/$CFSE^{hi,post\text{-}injection}$)]).

To analyze *in vivo* phenotypic and functional markers, 21 days post adoptive transfer, spleens and lymph nodes were harvested from recipient mice, processed, resuspended at 10^7 cells/mL in T cell culture media and incubated at 37°C for 6 hours with 1x cytokine activation cocktail (BioLegend) and GolgiPlug (BD Biosciences). No stimulation controls received only GolgiPlug. Following incubation, cells were washed and stained with Live/Dead Fixable Aqua (Invitrogen), PE anti-mouse CD45.2 clone 104 (BioLegend), and APC anti-mouse CD4 clone GK1.5 (BioLegend). Cells were then washed, fixed and permeabilized overnight with the Foxp3 Transcription Factor Staining Buffer Set (eBioscience™), and then stained with APC anti-mouse IFN-γ clone XMG1.2 (BioLegend), PE/Cyanine7 anti-mouse TNF-α clone MP6-XT22 (BioLegend), and PerCp-Cyanine5.5 anti-mouse/human T-bet clone eBio4B10 (eBioscience™) or its corresponding isotype. Finally, cells were washed and resuspended in FACS wash

buffer (1X PBS, 2% FBS, 0.5% sodium azide) and then analyzed on an Attune NxT Flow Cytometer.

5.4.22 Adoptive transfer melanoma model

The *in vivo* therapeutic efficacy of OT-I $CD8^+$ T cells co-cultured with Th1 OT-II $CD4^+$ T cells was compared to traditionally stimulated OT-I $CD8^+$ T cells using a B16-OVA murine melanoma model. On day 0, B6 mice received a subcutaneous injection of $2x10^5$ tumor cells on the left flank. On that same day, OT-II $CD4^+$ T cells were activated in Th1 skewing media with MHC II aAPCs (80 ng/mL conjugated I-A^b and 1 µg/mL soluble αCD28). On day 5, OT-I $CD8^+$ T cells were stimulated with MHC I aAPCs (30 ng/mL conjugated K^b and 1 µg/mL soluble αCD28) in T cell culture media supplemented with TF. Co-cultured OT-I $CD8^+$ T cells were additionally mixed at a 1:1 ratio with the day 5 Th1 OT-II $CD4^+$ T cells and MHC II aAPCs (80 ng/mL conjugated I-A^b). On day 10, $2x10^6$ OT-I $CD8^+$ T cells that were freshly isolated, stimulated alone, or stimulated in co-culture with Th1 OT-II $CD4^+$ T cells, were injected intravenously in 100 µL volumes into B16-OVA tumor bearing mice. On the day of and the day after adoptive transfer, mice received intraperitoneal injections of 30,000 U IL-2 (Prometheus Labs) in 100 µL volumes. Tumor size was measured with digital calipers every 2-3 days until tumors became necrotic or reached 200 mm^2, after which mice were sacrificed with CO_2 asphyxiation and cervical dislocation.

5.4.23 Statistical Analysis

Error bars in graphs represent the standard error of the mean (s.e.m.) unless otherwise stated. All *n* values are given in the Figure legends. Statistical analyses were performed in GraphPad Prism software version 8.4.3. Two-tailed Student's *t* tests were

used for comparisons between two groups. One and two-way ANOVAs with Tukey's multiple comparisons test were used for comparisons between multiple groups. One-way ANOVAs with Dunnett's post-hoc test was used for comparison of multiple groups to a control group. Repeated measure two-way ANOVAs with Tukey's multiple comparisons test were used for comparing tumor growth curves, and log-rank tests were used for comparing survival curves.

Chapter 6. Contributions to Additional Research

6.1 Introduction

During my PhD, I have been fortunate enough to have had the opportunity to contribute to other projects both within and outside of the Schneck Lab. Broadly speaking, these contributions have focused on mathematical or computational tools to understand T cell responses or how biomaterial properties such as material, shape, and stiffness influence T cell activation and function. I will summarize the main findings from these projects as well as my contributions to them.

6.2 Mathematical and Computational Tools for Understanding T Cell Responses

Others in the lab had previously observed that particle size[109], shape[121,122], and ligand density[109] impact upon aAPC-based T cell activation. To understand the relevance of these parameters, I developed a kinetic model of T cell: aAPC interactions, by modeling aAPCs as multivalent pMHC complexes. This allowed us to predict the binding kinetics of cell: aAPC T cells to aAPCs, simply by calculating the number of TCR: pMHC interactions based on the aAPC contact area and ligand density[110]. I further validated the mathematical model for a variety of aAPC sizes and ligand densities.

A former student in the lab had developed a computational approach to cluster TCRs based on their sequence homology[318]. The first iteration of this software was written in MATLAB, slow, and required very strict TCR frequency thresholds, thus

excluding rarer TCRs from the analyses. Additionally, it was only designed to perform pairwise comparisons, restricting the breadth of TCR repertoires that could simultaneously be analyzed. To address these limitations, I migrated and optimized the software in R, drastically accelerating the computing time, and allowing us to both loosen the frequency cutoffs and simultaneously compare multiple TCR repertoires. These modifications allowed us to study the immunological impacts of cross-reactivity between commensal bacteria epitopes and tumor antigens[268] as well as between the influenza M1 antigen and SARS-COV-2. Lastly, this software allowed us to identify a highly conserved MART-1 TCR motif[79], that appears to be enriched in responders compared to non-responders, prior to checkpoint blockade immunotherapy[319].

6.3 Impact of Biomaterial Properties on T cell Activation

As part of an ongoing collaboration with Dr. Jordan Green's laboratory, I conducted both *in vitro* and *in vivo* proliferation and functional assays to assess how a poly (lactic-co-glycolic acid)/poly (beta amino ester) (PLGA/PBAE) blend aAPC impacted $CD8^+$ T cell activation, compared to traditional PLGA particles. I demonstrated that T cells activated with these particles proliferated significantly more *in vitro* and *in vivo* and had enhanced lytic function *in vivo*[300].

Additionally, I assisted with projects in the Green lab examining the *in vitro* and *in vivo* activity of prolate (one dimensional stretched) versus oblate ellipsoidal (two dimensional stretched) aAPCs. The oblate ellipsoidal aAPCs were more functional *in vitro* due to enhanced contact area with T cells but were significantly less functional *in vivo* due to poor biodistribution properties. I assisted another graduate student in the

Green lab with *in vitro* and *in vivo* assessments of how particle stiffness modulates T cell proliferation and function using poly (ethylene glycol) (PEG) aAPCs.

In addition to the collaborations with the Green lab, I have also collaborated with graduate students in the Spangler and Schneck labs. I have helped a graduate student in the Spangler lab to develop a process for orienting binding of proteins on aAPCs. We have incorporated site-directed chemistries into peptide-MHC molecules, costimulatory molecules, and immunocytokines and are examining how controlled orientation compares to random orientation. I have collaborated with another graduate student in the Spangler lab on developing microvesicles to encapsulate, activate, and capture cytokines from T cells, to enable secretome based T cell sorting. Lastly, I have helped a graduate student in the Schneck lab with *in vivo* assessments of a particulate version of the hyaluronic acid artificial T cell stimulating matrix[150]. We have shown that gels conjugated with tumor-specific pMHC and anti-CD28 lead to slower tumor growth than blank gels, in adoptive transfer melanoma models.

6.4 Incomplete Projects

There have been a number of projects which I have made headway on during my PhD but still require more work. In this section, I will briefly summarize the progress that has been made and the additional work to be done.

After developing the adaptive aAPC technology[72] (see Chapter 3), one of the outstanding questions was whether this technology could be used for loading heterologous peptides. Specifically, I asked whether I could pulse adaptive aAPCs with tumor derived peptides to generate antigen-agnostic but tumor-specific T cell responses. I developed a protocol for recovering and purifying peptides from tumor

cells, and, in several proof-of-concept studies, I demonstrated recovery of specific peptides from tumor cell lines through either mass spectrometry or lacZ reporter assays. Furthermore, aAPCs pulsed with these heterologous peptide mixtures were able to activate transgenic mice from corresponding tumor models, such as 2C mice for B16-SIY and OT-I mice for B16-OVA. The stimulations were antigen-specific, as aAPCs pulsed with B16-F10 derived peptides did not activate either transgenic model. For this project, some additional studies remain, such as activation of tumor infiltrating lymphocytes (TIL) with corresponding aAPCs, and expansion of endogenous tumor-specific T cells, particularly T cells specific to well-characterized neoantigens.

As mentioned previously, I identified a TCR motif that is highly conserved in HLA A2/MART-1 specific T cell repertoires. Yet, this same motif is five-fold more abundant in responders than non-responders prior to checkpoint blockade immunotherapy. The results here are promising but also unexpected. Hence, additional surveys of larger cohorts of patients, as well as single cell RNA-seq and follow-up mechanistic studies, would be required to both validate and understand the intriguing finding.

Lastly, additional studies are required to better understand how aAPCs induce $CD4^+$ cytotoxic T lymphocytes (CTL) as well as what $CD4^+$ T cell derived factors enhance the memory formation and function of CD8+ T cells. Some progress has been made to examine both of these questions. However, additional *in vitro* mechanistic studies and *in vivo* functional studies would benefit our understanding and validate both of these findings. Additionally, further work remains to determine how well these findings translate to the human system. Future studies examining if HLA II aAPCs

induce human $CD4^+$ CTL or if combined HLA I/II aAPCs enhance the memory formation and function of human $CD8^+$ T cells, could have immediate translational relevance.

Chapter 7. Conclusions

7.1 Summary of Work

Through close control of material properties, biomaterials can provide insights into T cell biology in ways that cellular approaches for T cell engagement cannot. Moreover, biomaterials can be used off-the-shelf and are amenable to mass production (see Chapter 2). In the course of developing high-throughput approaches for endogenous antigen-specific $CD8^+$ T cell expansion, I observed that the mere presence of bystander $CD4^+$ T cells dramatically enhances antigen-specific $CD8^+$ T cell expansion (see Chapter 3). This prompted me to look more closely at the relevance of $CD4^+$ T cells for cancer immunotherapy (see Chapter 4). As a result, I developed nanoparticle platforms to expand murine and human antigen-specific $CD4^+$ T cells and to relay help signals from $CD4^+$ to a wide range of $CD8^+$ T cell specificities (see Chapter 5). Unlike conventional approaches for T cell stimulation, MHC II aAPCs uniquely induce $CD4^+$ T cell cytotoxicity, a phenotype that up until now has almost exclusively been observed *in vivo*. As such, this platform may yield insight into the specific biophysical and molecular cues necessary for cytotoxic $CD4^+$ T cell induction. Likewise, combined MHC I/II aAPCs provide a means of promoting $CD4^+$/$CD8^+$ T cell crosstalk and, in turn, enhancing $CD8^+$ T cell function and memory formation. As this technology does not rely on confounding DC intermediaries, it can help uncover mechanisms of direct $CD4^+$ T help to $CD8^+$ T cells. Together, both technologies may pave the way toward next-generation cellular therapies using $CD4^+$ CTL or “helped” $CD8^+$ T cells.

7.2 Future Directions

In murine doped enrichment studies, I observed that aAPC internalization by $CD4^+$ T cells appeared to be TCR mediated and was significantly more specific to cognate cells than aAPC binding (see **Figure 5-4**). I capitalized off of this specificity to magnetically enrich rare populations of T cells. However, this same finding suggests we could use an analogous approach to identify or even nonvirally deliver genes to antigen-specific T cells, akin to several recent technologies that have used psuedotyped lentiviruses[320,321]. Such studies would be a natural collaboration between the Schneck and Green labs and would provide a unique engineering opportunity to study the parameter space of TCR-mediated particle internalization.

Additionally, while much of the $CD4^+$ T cell studies have been performed using Th1 skewing cytokines and anti-CD28 costimulatory molecules, both the cytokine milieu and the choice of costimulatory molecules could be manipulated to tune both $CD4^+$ T cell lineage and memory phenotype. For instance, Si-Sim Kang, a graduate student in the Schneck Lab is collaborating with Dr. Erika Darrah's lab to generate antigen-specific human regulatory T cells with HLA II aAPCs for a variety of autoimmune diseases.

Similarly, while much of my work has focused on nano- or microparticle formulations for acellular $CD4^+$ T cell stimulation, there are ongoing efforts between the Schneck lab and Dr. Luo Gu's lab to engineer alginate hydrogels of varying stiffnesses to assess how substrate stiffness impacts $CD4^+$ T cell phenotype and function.

Lastly, while I have validated that combined MHC I/II aAPCs enhance $CD4^+$ and $CD8^+$ T cell cross-talk *in vitro*, I am working with Sydney Shannon, a graduate student in the Schneck and Green Lab, to implement this technology for *in vivo* applications.

These T-Cell Help Redirectors (T-CHRs) could present a new class of technologies to piggyback off of endogenous T cell help processes (**Figure 7-1**) to generate optimal $CD8^+$ T cell therapeutic responses.

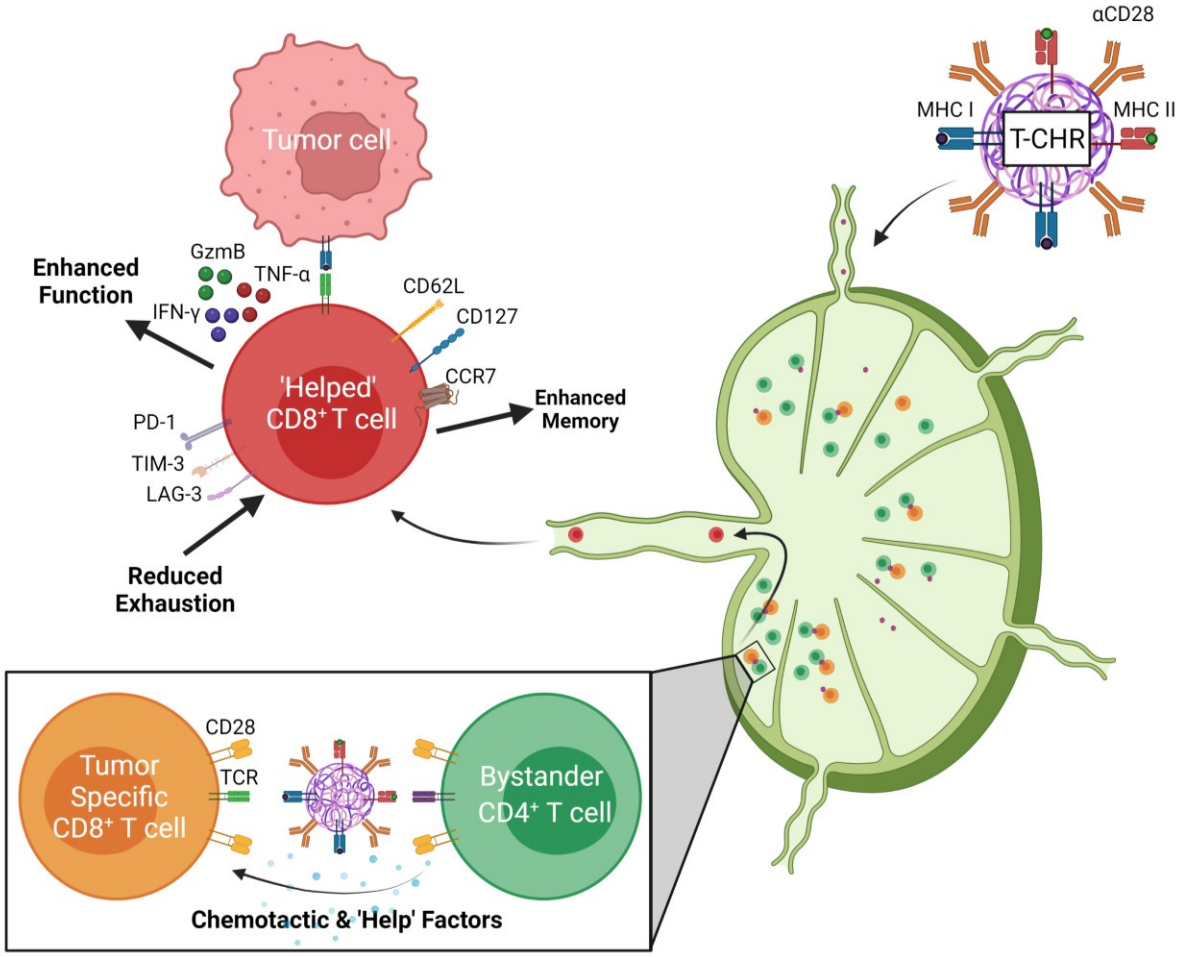

Figure 7-1. Schematic for *in vivo* T-Cell Help Redirector (T-CHR) platform. Created with BioRender.com.

Bibliography

1. Goetz, L. H. & Schork, N. J. Personalized medicine: motivation, challenges, and progress. *Fertility and Sterility* **109**, 952–963 (2018).
2. Yun, Y. H., Lee, B. K. & Park, K. Controlled Drug Delivery: Historical perspective for the next generation. *J. Control. Release* **219**, 2–7 (2015).
3. Sackstein, R., Schatton, T. & Barthel, S. R. T-lymphocyte homing: An underappreciated yet critical hurdle for successful cancer immunotherapy. *Lab. Investig.* **97**, 669–697 (2017).
4. Thommen, D. S. & Schumacher, T. N. T Cell Dysfunction in Cancer. *Cancer Cell* **33**, 547–562 (2018).
5. Grifoni, A. *et al.* Targets of T Cell Responses to SARS-CoV-2 Coronavirus in Humans with COVID-19 Disease and Unexposed Individuals. *Cell* **181**, 1489-1501.e15 (2020).
6. Lythe, G., Callard, R. E., Hoare, R. L. & Molina-París, C. How many TCR clonotypes does a body maintain? *J. Theor. Biol.* **389**, 214–224 (2016).
7. Anderson, K. G., Stromnes, I. M. & Greenberg, P. D. Obstacles Posed by the Tumor Microenvironment to T cell Activity: A Case for Synergistic Therapies. *Cancer Cell* **31**, 311–325 (2017).
8. Yee, C., Lizee, G. & Schueneman, A. J. Endogenous T-Cell Therapy: Clinical Experience. *Cancer J.* **21**, (2015).
9. Laport, G. G. *et al.* Adoptive transfer of costimulated T cells induces lymphocytosis in patients with relapsed/refractory non-Hodgkin lymphoma following CD34+-selected hematopoietic cell transplantation. *Blood* **102**, 2004–

2013 (2003).

10. Dudley, M. E., Wunderlich, J. R., Shelton, T. E., Even, J. & Rosenberg, S. A. Generation of tumor-infiltrating lymphocyte cultures for use in adoptive transfer therapy for melanoma patients. *J. Immunother.* **26**, 332–342 (2003).
11. Kaech, S. M. & Cui, W. Transcriptional control of effector and memory CD8+ T cell differentiation. *Nat. Rev. Immunol.* **12**, 749–761 (2012).
12. Gros, A. *et al.* Recognition of human gastrointestinal cancer neoantigens by circulating PD-1+ lymphocytes. *J. Clin. Invest.* **129**, 4992–5004 (2019).
13. Gros, A. *et al.* PD-1 identifies the patient-specific CD8+ tumor-reactive repertoire infiltrating human tumors. *J. Clin. Invest.* **124**, 2246–2259 (2014).
14. Ye, Q. *et al.* CD137 accurately identifies and enriches for naturally occurring tumor-reactive T cells in tumor. *Clin. Cancer Res.* **20**, 44–55 (2014).
15. Bodinier, M. *et al.* Efficient detection and immunomagnetic sorting of specific T cells using multimers of MHC class I and peptide with reduced CD8 binding. *Nat. Med.* **6**, 707–710 (2000).
16. Tran, E. *et al.* Cancer Immunotherapy Based on Mutation-Specific CD4+ T Cells in a Patient with Epithelial Cancer. *Science (80-.).* **344**, 641 LP – 645 (2014).
17. Zacharakis, N. *et al.* Immune recognition of somatic mutations leading to complete durable regression in metastatic breast cancer. *Nat. Med.* **24**, 724–730 (2018).
18. Klebanoff, C. A., Rosenberg, S. A. & Restifo, N. P. Prospects for gene-engineered T cell immunotherapy for solid cancers. *Nat. Med.* **22**, 26–36 (2016).
19. Kaluza, K. M. *et al.* Adoptive transfer of cytotoxic T lymphocytes targeting two

different antigens limits antigen loss and tumor escape. *Hum. Gene Ther.* **23**, 1054–1064 (2012).

20. Ruella, M. *et al.* Dual CD19 and CD123 targeting prevents antigen-loss relapses after CD19-directed immunotherapies. *J. Clin. Invest.* **126**, 3814–3826 (2016).
21. Klebanoff, C. A., Gattinoni, L. & Restifo, N. P. Sorting through subsets: Which T-cell populations mediate highly effective adoptive immunotherapy? *J. Immunother.* **35**, 651–660 (2012).
22. Gattinoni, L., Powell, D. J., Rosenberg, S. A. & Restifo, N. P. Adoptive immunotherapy for cancer: building on success. *Nat. Rev. Immunol.* **6**, 383–393 (2006).
23. Meidenbauer, N. *et al.* Survival and tumor localization of adoptively transferred Melan-A-specific T cells in melanoma patients. *J. Immunol.* **170**, 2161–2169 (2003).
24. Hunder, N. N. *et al.* Treatment of metastatic melanoma with autologous CD4+ T cells against NY-ESO-1. *N. Engl. J. Med.* **358**, 2698–2703 (2008).
25. Chapuis, A. G. *et al.* Transferred melanoma-specific CD8+ T cells persist, mediate tumor regression, and acquire central memory phenotype. *Proc. Natl. Acad. Sci. U. S. A.* **109**, 4592–4597 (2012).
26. Wolf, B. *et al.* Safety and Tolerability of Adoptive Cell Therapy in Cancer. *Drug Saf.* **42**, 315–334 (2019).
27. Eyquem, J. *et al.* Targeting a CAR to the TRAC locus with CRISPR/Cas9 enhances tumour rejection. *Nature* **543**, 113–117 (2017).
28. Massa, C. *et al.* Identification of patient-specific and tumor-shared T cell receptor

sequences in renal cell carcinoma patients. *Oncotarget* **8**, 21212–21228 (2017).

29. Garcia-Garijo, A., Fajardo, C. A. & Gros, A. Determinants for neoantigen identification. *Frontiers in Immunology* **10**, 1392 (2019).
30. Rizzuto, G. A. *et al.* Self-antigen–specific CD8+ T cell precursor frequency determines the quality of the antitumor immune response. *J. Exp. Med.* **206**, 849–866 (2009).
31. Rosenberg, S. A. & Restifo, N. P. Adoptive cell transfer as personalized immunotherapy for human cancer. *Science (80-.).* **348**, 62–68 (2015).
32. Pollack, S. M. *et al.* Tetramer guided, cell sorter assisted production of clinical grade autologous NY-ESO-1 specific CD8(+) T cells. *J. Immunother. cancer* **2**, 36 (2014).
33. Wherry, E. J. T cell exhaustion. *Nat. Immunol.* **131**, 492–499 (2011).
34. Rosenberg, S. A. *et al.* Use of Tumor-Infiltrating Lymphocytes and Interleukin-2 in the Immunotherapy of Patients with Metastatic Melanoma. *N. Engl. J. Med.* **319**, 1676–1680 (1988).
35. Dudley, M. E. *et al.* Cancer Regression and Autoimmunity in Patients After Clonal Repopulation with Antitumor Lymphocytes. *Science (80-.).* **298**, 850 LP – 854 (2002).
36. Rosenberg, S. A. *et al.* Durable Complete Responses in Heavily Pretreated Patients with Metastatic Melanoma Using T-Cell Transfer Immunotherapy. *Clin. Cancer Res.* **17**, 4550 LP – 4557 (2011).
37. Joseph, R. W. *et al.* Impact of Clinical and Pathologic Features on Tumor-Infiltrating Lymphocyte Expansion from Surgically Excised Melanoma Metastases

for Adoptive T-cell Therapy. *Clin. Cancer Res.* **17**, 4882 LP – 4891 (2011).

38. Fourcade, J. *et al.* Upregulation of Tim-3 and PD-1 expression is associated with tumor antigen-specific CD8+ T cell dysfunction in melanoma patients. *J. Exp. Med.* **207**, 2175–2186 (2010).

39. Baitsch, L. *et al.* Exhaustion of tumor-specific CD8+ T cells in metastases from melanoma patients. *J. Clin. Invest.* **121**, 2350–2360 (2011).

40. Zippelius, A. *et al.* Effector Function of Human Tumor-Specific CD8 T Cells in Melanoma Lesions: A State of Local Functional Tolerance. *Cancer Res.* **64**, 2865–2873 (2004).

41. Ahmadzadeh, M. *et al.* Tumor antigen-specific CD8 T cells infiltrating the tumor express high levels of PD-1 and are functionally impaired. *Blood* **114**, 1537–1544 (2009).

42. Gross, G., Waks, T. & Eshhar, Z. Expression of immunoglobulin-T-cell receptor chimeric molecules as functional receptors with antibody-type specificity. *Proc. Natl. Acad. Sci. U. S. A.* **86**, 10024–10028 (1989).

43. Khong, H. T. & Restifo, N. P. Natural selection of tumor variants in the generation of ‘tumor escape’ phenotypes. *Nat Immunol* **3**, 999–1005 (2002).

44. Lee, D. W. *et al.* Current concepts in the diagnosis and management of cytokine release syndrome. *Blood* **124**, 188–195 (2014).

45. Linette, G. P. *et al.* Cardiovascular toxicity and titin cross-reactivity of affinity-enhanced T cells in myeloma and melanoma. *Blood* **122**, 863–871 (2013).

46. Johnson, L. A. *et al.* Gene therapy with human and mouse T-cell receptors mediates cancer regression and targets normal tissues expressing cognate

antigen. *Blood* **114**, 535–546 (2009).

47. Morgan, R. A. *et al.* Cancer regression and neurologic toxicity following anti-MAGE-A3 TCR gene therapy. *J. Immunother.* **36**, 133–151 (2013).

48. Parkhurst, M. R. *et al.* T cells targeting carcinoembryonic antigen can mediate regression of metastatic colorectal cancer but induce severe transient colitis. *Mol. Ther.* **19**, 620–626 (2011).

49. Morgan, R. A. *et al.* Case report of a serious adverse event following the administration of t cells transduced with a chimeric antigen receptor recognizing ERBB2. *Mol. Ther.* **18**, 843–851 (2010).

50. Lamers, C. H. J. J. *et al.* Treatment of metastatic renal cell carcinoma with CAIX CAR-engineered T cells: Clinical evaluation and management of on-target toxicity. *Mol. Ther.* **21**, 904–912 (2013).

51. Kochenderfer, J. N. *et al.* Eradication of B-lineage cells and regression of lymphoma in a patient treated with autologous T cells genetically engineered to recognize CD19. *Blood* **116**, 4099–4102 (2010).

52. Maude, S. L. *et al.* Tisagenlecleucel in children and young adults with B-cell lymphoblastic leukemia. *N. Engl. J. Med.* **378**, 439–448 (2018).

53. Schuster, S. J. *et al.* Tisagenlecleucel in adult relapsed or refractory diffuse large B-cell lymphoma. *N. Engl. J. Med.* **380**, 45–56 (2019).

54. Ma, L. *et al.* Enhanced CAR–T cell activity against solid tumors by vaccine boosting through the chimeric receptor. *Science (80-.).* **365**, 162 LP – 168 (2019).

55. Gardner, R. *et al.* Acquisition of a CD19-negative myeloid phenotype allows immune escape of MLL-rearranged B-ALL from CD19 CAR-T-cell therapy. *Blood*

127, 2406–2410 (2016).

56. Orlando, E. J. *et al.* Genetic mechanisms of target antigen loss in CAR19 therapy of acute lymphoblastic leukemia. *Nat. Med.* **24**, 1504–1506 (2018).

57. O'Rourke, D. M. *et al.* A single dose of peripherally infused EGFRvIII-directed CAR T cells mediates antigen loss and induces adaptive resistance in patients with recurrent glioblastoma. *Sci. Transl. Med.* **9**, eaaa0984 (2017).

58. Jamal-Hanjani, M., Quezada, S. A., Larkin, J. & Swanton, C. Translational Implications of Tumor Heterogeneity. *Clin. Cancer Res.* **21**, 1258 LP – 1266 (2015).

59. Crowther, M. D. *et al.* Genome-wide CRISPR–Cas9 screening reveals ubiquitous T cell cancer targeting via the monomorphic MHC class I-related protein MR1. *Nat. Immunol.* **21**, 178–185 (2020).

60. Bird, L. MR1-restricted pan-cancer T cells. *Nat. Rev. Immunol.* **20**, 141 (2020).

61. Reinhard, K. *et al.* An RNA vaccine drives expansion and efficacy of claudin-CAR-T cells against solid tumors. *Science (80-.).* **367**, 446 LP – 453 (2020).

62. Chen, J. *et al.* NR4A transcription factors limit CAR T cell function in solid tumours. *Nature* **567**, 530–534 (2019).

63. Frigault, M. J. *et al.* Identification of Chimeric Antigen Receptors That Mediate Constitutive or Inducible Proliferation of T Cells. *Cancer Immunol. Res.* **3**, 356 LP – 367 (2015).

64. Milone, M. C. *et al.* Chimeric receptors containing CD137 signal transduction domains mediate enhanced survival of T cells and increased antileukemic efficacy in vivo. *Mol. Ther.* **17**, 1453–1464 (2009).

65. Rupp, L. J. *et al.* CRISPR/Cas9-mediated PD-1 disruption enhances anti-tumor efficacy of human chimeric antigen receptor T cells. *Sci. Rep.* **7**, 737 (2017).

66. Seo, H. *et al.* TOX and TOX2 transcription factors cooperate with NR4A transcription factors to impose CD8+ T cell exhaustion. *Proc. Natl. Acad. Sci.* **116**, 12410 LP – 12415 (2019).

67. Ghorashian, S. *et al.* Enhanced CAR T cell expansion and prolonged persistence in pediatric patients with ALL treated with a low-affinity CD19 CAR. *Nat. Med.* **25**, 1408–1414 (2019).

68. Mackensen, A. *et al.* Phase I study of adoptive T-cell therapy using antigen-specific CD8+ T cells for the treatment of patients with metastatic melanoma. *J. Clin. Oncol. Off. J. Am. Soc. Clin. Oncol.* **24**, 5060–5069 (2006).

69. Wölfl, M. & Greenberg, P. D. Antigen-specific activation and cytokine-facilitated expansion of naive, human CD8+ T cells. *Nat. Protoc.* **9**, 950–966 (2014).

70. Satthaporn, S. *et al.* Dendritic cells are dysfunctional in patients with operable breast cancer. *Cancer Immunol. Immunother.* **53**, 510–8 (2004).

71. Veglia, F. & Gabrilovich, D. I. Dendritic cells in cancer: the role revisited. *Curr. Opin. Immunol.* **45**, 43–51 (2017).

72. Hickey, J. W. *et al.* Adaptive Nanoparticle Platforms for High Throughput Expansion and Detection of Antigen-Specific T cells. *Nano Lett.* **20**, 6289–6298 (2020).

73. Hickey, J. W., Kosmides, A. K. & Schneck, J. P. Chapter Six - Engineering Platforms for T Cell Modulation. in *Biology of T Cells - Part A* (eds. Galluzzi, L. & Rudqvist, N.-P. B. T.-I. R. of C. and M. B.) **341**, 277–362 (Academic Press, 2018).

74. Snyder, J. E. *et al.* Measuring the frequency of mouse and human cytotoxic T cells by the Lysispot assay: independent regulation of cytokine secretion and short-term killing. *Nat. Med.* **9**, 231–236 (2003).

75. Bálint, Š. *et al.* Supramolecular attack particles are autonomous killing entities released from cytotoxic T cells. *Science (80-.).* **368**, 897 LP – 901 (2020).

76. Wang, C., Sun, W., Ye, Y., Bomba, H. N. & Gu, Z. Bioengineering of Artificial Antigen Presenting Cells and Lymphoid Organs. *Theranostics* **7**, 3504–3516 (2017).

77. Zhang, D. K. Y., Cheung, A. S. & Mooney, D. J. Activation and expansion of human T cells using artificial antigen-presenting cell scaffolds. *Nat. Protoc.* **15**, 773–798 (2020).

78. Tsai, S. J., Black, S. K. & Jewell, C. M. Leveraging the Modularity of Biomaterial Carriers to Tune Immune Responses. *Adv. Funct. Mater.* **n/a**, 2004119 (2020).

79. Ichikawa, J. *et al.* Rapid Expansion of Highly Functional Antigen-Specific T Cells from Patients with Melanoma by Nanoscale Artificial Antigen-Presenting Cells. *Clin. Cancer Res.* **26**, 3384–3396 (2020).

80. Perica, K. *et al.* Enrichment and Expansion with Nanoscale Artificial Antigen Presenting Cells for Adoptive Immunotherapy. *ACS Nano* **9**, 6861–6871 (2015).

81. Cheung, A. S., Zhang, D. K. Y. Y., Koshy, S. T. & Mooney, D. J. Scaffolds that mimic antigen-presenting cells enable ex vivo expansion of primary T cells. *Nat. Biotechnol.* **36**, 160–169 (2018).

82. Oelke, M. & Schneck, J. P. Overview of a HLA-Ig based 'Lego-like system' for T cell monitoring, modulation and expansion. *Immunol. Res.* **47**, 248–256 (2010).

83. Monette, A., Ceccaldi, C., Assaad, E., Lerouge, S. & Lapointe, R. Chitosan thermogels for local expansion and delivery of tumor-specific T lymphocytes towards enhanced cancer immunotherapies. *Biomaterials* **75**, 237–249 (2016).

84. Stephan, S. B. *et al.* Biopolymer implants enhance the efficacy of adoptive T-cell therapy. *Nat. Biotechnol.* **33**, 97–101 (2015).

85. Kosmides, A. K., Necochea, K., Hickey, J. W. & Schneck, J. P. Separating T Cell Targeting Components onto Magnetically Clustered Nanoparticles Boosts Activation. *Nano Lett.* **18**, 1916–1924 (2018).

86. Tang, L. *et al.* Enhancing T cell therapy through TCR-signaling-responsive nanoparticle drug delivery. *Nat. Biotechnol.* **36**, 707–716 (2018).

87. Kim, S. T. *et al.* The αβ T cell receptor is an anisotropic mechanosensor. *J. Biol. Chem.* **284**, 31028–31037 (2009).

88. Liu, B., Chen, W., Evavold, B. D. & Zhu, C. Accumulation of Dynamic Catch Bonds between TCR and Agonist Peptide-MHC Triggers T Cell Signaling. *Cell* **157**, 357–368 (2014).

89. Sibener, L. V *et al.* Isolation of a Structural Mechanism for Uncoupling T Cell Receptor Signaling from Peptide-MHC Binding. *Cell* **174**, 672-687.e27 (2018).

90. Lillemeier, B. F. *et al.* TCR and Lat are expressed on separate protein islands on T cell membranes and concatenate during activation. *Nat. Immunol.* **11**, 90–96 (2010).

91. Basu, R. & Huse, M. Mechanical Communication at the Immunological Synapse. *Trends Cell Biol.* **27**, 241–254 (2017).

92. Comrie, W. A., Li, S., Boyle, S. & Burkhardt, J. K. The dendritic cell cytoskeleton

promotes T cell adhesion and activation by constraining ICAM-1 mobility. *J. Cell Biol.* **208**, 457–473 (2015).

93. Herrmann, S. H. & Mescher, M. F. Secondary cytolytic T lymphocyte stimulation by purified H-2Kk in liposomes. *Proc. Natl. Acad. Sci.* **78**, 2488 LP – 2492 (1981).

94. Engelhard, V. H., Strominger, J. L., Mescher, M. & Burakoff, S. Induction of secondary cytotoxic T lymphocytes by purified HLA-A and HLA-B antigens reconstituted into phospholipid vesicles. *Proc. Natl. Acad. Sci.* **75**, 5688 LP – 5691 (1978).

95. Maus, M. V., Riley, J. L., Kwok, W. W., Nepom, G. T. & June, C. H. HLA tetramer-based artificial antigen-presenting cells for stimulation of CD4+T cells. *Clin. Immunol.* **106**, 16–22 (2003).

96. Mallet-Designe, V. I. *et al.* Detection of Low-Avidity CD4+ T Cells Using Recombinant Artificial APC: Following the Antiovalbumin Immune Response. *J. Immunol.* **170**, 123 LP – 131 (2003).

97. Vogt, A. B., Spindeldreher, S. & Kropshofer, H. Clustering of MHC–peptide complexes prior to their engagement in the immunological synapse: lipid raft and tetraspan microdomains. *Immunol. Rev.* **189**, 136–151 (2002).

98. Giannoni, F. *et al.* Clustering of T Cell Ligands on Artificial APC Membranes Influences T Cell Activation and Protein Kinase C θ Translocation to the T Cell Plasma Membrane. *J. Immunol.* **174**, 3204 LP – 3211 (2005).

99. Zappasodi, R. *et al.* The effect of artificial antigen-presenting cells with preclustered anti-CD28/-CD3/-LFA-1 monoclonal antibodies on the induction of ex vivo expansion of functional human antitumor T cells. *Haematologica* **93**, 1523–

1534 (2008).

100. Ding, Q. *et al.* RAFTsomes Containing Epitope-MHC-II Complexes Mediated CD4+ T Cell Activation and Antigen-Specific Immune Responses. *Pharm. Res.* **30**, 60–69 (2013).

101. Rogers, J. & Mescher, M. F. Augmentation of in vivo cytotoxic T lymphocyte activity and reduction of tumor growth by large multivalent immunogen. *J. Immunol.* **149**, 269–276 (1992).

102. Fang, R. H. *et al.* Cancer Cell Membrane-Coated Nanoparticles for Anticancer Vaccination and Drug Delivery. *Nano Lett.* **14**, 2181–2188 (2014).

103. Jiang, Y. *et al.* Engineered Cell-Membrane-Coated Nanoparticles Directly Present Tumor Antigens to Promote Anticancer Immunity. *Adv. Mater.* **32**, 2001808 (2020).

104. Cheng, S. *et al.* Artificial Mini Dendritic Cells Boost T Cell–Based Immunotherapy for Ovarian Cancer. *Adv. Sci.* **7**, 1903301 (2020).

105. Oelke, M. *et al.* Ex vivo induction and expansion of antigen-specific cytotoxic T cells by HLA-Ig–coated artificial antigen-presenting cells. *Nat. Med.* **9**, 619–625 (2003).

106. Ugel, S. *et al.* In vivo Administration of Artificial Antigen-Presenting Cells Activates Low-Avidity T Cells for Treatment of Cancer. *Cancer Res.* **69**, 9376–9385 (2009).

107. LEVINE, B. L. *et al.* Large-Scale Production of CD4+ T Cells from HIV-1-Infected Donors After CD3/CD28 Costimulation*. *J. Hematother.* **7**, 437–448 (1998).

108. Perica, K. *et al.* Magnetic field-induced t cell receptor clustering by nanoparticles enhances t cell activation and stimulates antitumor activity. *ACS Nano* **8**, 2252–

2260 (2014).

109. Hickey, J. W., Vicente, F. P., Howard, G. P., Mao, H.-Q. & Schneck, J. P. Biologically Inspired Design of Nanoparticle Artificial Antigen-Presenting Cells for Immunomodulation. *Nano Lett.* **17**, 7045–7054 (2017).

110. Hickey, J. W. *et al.* Efficient magnetic enrichment of antigen-specific T cells by engineering particle properties. *Biomaterials* **187**, 105–116 (2018).

111. Xia, F. *et al.* TCR and CD28 Concomitant Stimulation Elicits a Distinctive Calcium Response in Naive T Cells . *Frontiers in Immunology* **9**, 2864 (2018).

112. Fadel, T. R. *et al.* A carbon nanotube-polymer composite for T-cell therapy. *Nat. Nanotechnol.* **9**, 639–647 (2014).

113. Fadel, T. R. *et al.* Enhanced Cellular Activation with Single Walled Carbon Nanotube Bundles Presenting Antibody Stimuli. *Nano Lett.* **8**, 2070–2076 (2008).

114. Mescher, M. F. Surface contact requirements for activation of cytotoxic T lymphocytes. *J. Immunol.* **149**, 2402 LP – 2405 (1992).

115. Curtsinger, J., Deeths, M. J., Pease, P. & Mescher, M. F. Artificial cell surface constructs for studying receptor–ligand contributions to lymphocyte activation. *J. Immunol. Methods* **209**, 47–57 (1997).

116. Curtsinger, J. M. *et al.* Inflammatory Cytokines Provide a Third Signal for Activation of Naive CD4+ and CD8+ T Cells. *J. Immunol.* **162**, 3256 LP – 3262 (1999).

117. Deeths, M. J. & Mescher, M. F. B7-1-dependent co-stimulation results in qualitatively and quantitatively different responses by CD4+ and CD8+ T cells. *Eur. J. Immunol.* **27**, 598–608 (1997).

118. Deeths, M. J. & Mescher, M. F. ICAM-1 and B7-1 provide similar but distinct costimulation for CD8+ T cells, while CD4+ T cells are poorly costimulated by ICAM-1. *Eur. J. Immunol.* **29**, 45–53 (1999).

119. Steenblock, E. R. & Fahmy, T. M. A comprehensive platform for ex vivo T-cell expansion based on biodegradable polymeric artificial antigen-presenting cells. *Mol. Ther.* **16**, 765–772 (2008).

120. Steenblock, E. R., Fadel, T., Labowsky, M., Pober, J. S. & Fahmy, T. M. An artificial antigen-presenting cell with paracrine delivery of IL-2 impacts the magnitude and direction of the T cell response. *J. Biol. Chem.* **286**, 34883–34892 (2011).

121. Sunshine, J. C., Perica, K., Schneck, J. P. & Green, J. J. Particle shape dependence of CD8+ T cell activation by artificial antigen presenting cells. *Biomaterials* **35**, 269–277 (2014).

122. Meyer, R. a. *et al.* Biodegradable Nanoellipsoidal Artificial Antigen Presenting Cells for Antigen Specific T-Cell Activation. *Small* **11**, 1519–1525 (2015).

123. Schütz, C., Oelke, M., Schneck, J. P., Mackensen, A. & Fleck, M. Killer artificial antigen-presenting cells: the synthetic embodiment of a ‘guided missile’. *Immunotherapy* **2**, 539–550 (2010).

124. Perica, K. *et al.* Nanoscale artificial antigen presenting cells for T cell immunotherapy. *Nanomedicine Nanotechnology, Biol. Med.* **10**, 119–129 (2014).

125. Singha, S. *et al.* Peptide-MHC-based nanomedicines for autoimmunity function as T-cell receptor microclustering devices. *Nat. Nanotechnol.* **12**, 701–710 (2017).

126. Arechaga, I. *et al.* Structural characterization of the TCR complex by electron

microscopy. *Int. Immunol.* **22**, 897–903 (2010).

127. Chen, L. & Flies, D. B. Molecular mechanisms of T cell co-stimulation and co-inhibition. *Nat. Rev. Immunol.* **13**, 227–242 (2013).

128. Zappasodi, R. *et al.* Rational design of anti-GITR-based combination immunotherapy. *Nat. Med.* **25**, 759–766 (2019).

129. Waldman, A. D., Fritz, J. M. & Lenardo, M. J. A guide to cancer immunotherapy: from T cell basic science to clinical practice. *Nature Reviews Immunology* 1–18 (2020). doi:10.1038/s41577-020-0306-5

130. Willoughby, J. E. *et al.* Differential Impact of CD27 and 4-1BB Costimulation on Effector and Memory CD8 T Cell Generation following Peptide Immunization. *J. Immunol.* **193**, 244 LP – 251 (2014).

131. Hernandez-Chacon, J. A. *et al.* Costimulation through the CD137/4-1BB pathway protects human melanoma tumor-infiltrating lymphocytes from activation-induced cell death and enhances antitumor effector function. *J. Immunother.* **34**, 236–250 (2011).

132. Lee, S.-J. *et al.* 4-1BB and OX40 Dual Costimulation Synergistically Stimulate Primary Specific CD8 T Cells for Robust Effector Function. *J. Immunol.* **173**, 3002 LP – 3012 (2004).

133. Zeng, W., Su, M., Anderson, K. S. & Sasada, T. Artificial antigen-presenting cells expressing CD80, CD70, and 4-1BB ligand efficiently expand functional T cells specific to tumor-associated antigens. *Immunobiology* **219**, 583–592 (2014).

134. Maus, M. V *et al.* Ex vivo expansion of polyclonal and antigen-specific cytotoxic T lymphocytes by artificial APCs expressing ligands for the T-cell receptor, CD28

and 4-1BB. *Nat. Biotechnol.* **20**, 143–148 (2002).

135. Rudolf, D. *et al.* Potent costimulation of human CD8 T cells by anti-4-1BB and anti-CD28 on synthetic artificial antigen presenting cells. *Cancer Immunol. Immunother.* **57**, 175–183 (2008).

136. Zhang, L. *et al.* An Artificial Antigen-Presenting Cell Delivering 11 Immune Molecules Expands Tumor Antigen–Specific CTLs in Ex Vivo and In Vivo Murine Melanoma Models. *Cancer Immunol. Res.* **7**, 1188–1201 (2019).

137. Mossman, K. D., Campi, G., Groves, J. T. & Dustin, M. L. Altered TCR Signaling from Geometrically Repatterned Immunological Synapses. *Science (80-.).* **310**, 1191 LP – 1193 (2005).

138. Doh, J. & Irvine, D. J. Immunological synapse arrays: patterned protein surfaces that modulate immunological synapse structure formation in T cells. *Proc. Natl. Acad. Sci. U. S. A.* **103**, 5700–5705 (2006).

139. Bashour, K. T. *et al.* Cross talk between CD3 and CD28 is spatially modulated by protein lateral mobility. *Mol. Cell. Biol.* **34**, 955–964 (2014).

140. Shen, K., Thomas, V. K., Dustin, M. L. & Kam, L. C. Micropatterning of costimulatory ligands enhances CD4+ T cell function. *Proc. Natl. Acad. Sci.* **105**, 7791 LP – 7796 (2008).

141. Spatz, J. P. *et al.* Ordered Deposition of Inorganic Clusters from Micellar Block Copolymer Films. *Langmuir* **16**, 407–415 (2000).

142. Delcassian, D. *et al.* Nanoscale ligand spacing influences receptor triggering in T cells and NK cells. *Nano Lett.* **13**, 5608–5614 (2013).

143. Matic, J., Deeg, J., Scheffold, A., Goldstein, I. & Spatz, J. P. Fine Tuning and

Efficient T Cell Activation with Stimulatory aCD3 Nanoarrays. *Nano Lett.* **13**, 5090–5097 (2013).

144. Cai, H. *et al.* Full control of ligand positioning reveals spatial thresholds for T cell receptor triggering. *Nat. Nanotechnol.* **13**, 610–617 (2018).
145. Chang, V. T. *et al.* Initiation of T cell signaling by CD45 segregation at 'close contacts'. *Nat. Immunol.* **17**, 574–582 (2016).
146. Judokusumo, E., Tabdanov, E., Kumari, S., Dustin, M. L. & Kam, L. C. Mechanosensing in T Lymphocyte Activation. *Biophys. J.* **102**, L5–L7 (2012).
147. Saitakis, M. *et al.* Different TCR-induced T lymphocyte responses are potentiated by stiffness with variable sensitivity. *Elife* **6**, e23190 (2017).
148. O'Connor, R. S. *et al.* Substrate Rigidity Regulates Human T Cell Activation and Proliferation. *J. Immunol.* **189**, 1330 LP – 1339 (2012).
149. Majedi, F. S. *et al.* T-cell activation is modulated by the 3D mechanical microenvironment. *Biomaterials* **252**, 120058 (2020).
150. Hickey, J. W. *et al.* Engineering an Artificial T-Cell Stimulating Matrix for Immunotherapy. *Adv. Mater.* **31**, 1807359 (2019).
151. A Phase 1 Study in Patients With HPV+ Recurrent/ Metastatic Head and Neck Squamous Cell Carcinoma - Full Text View - ClinicalTrials.gov.
152. Sahin, U. *et al.* An RNA vaccine drives immunity in checkpoint-inhibitor-treated melanoma. *Nature* 1–6 (2020). doi:10.1038/s41586-020-2537-9
153. Wang, S., Sun, Z. & Hou, Y. Engineering Nanoparticles toward the Modulation of Emerging Cancer Immunotherapy. *Adv. Healthc. Mater.* 2000845 (2020). doi:10.1002/adhm.202000845

154. Adu-Berchie, K. & Mooney, D. J. Biomaterials as Local Niches for Immunomodulation. *Acc. Chem. Res.* acs.accounts.0c00341 (2020). doi:10.1021/acs.accounts.0c00341

155. Gu, L. & Mooney, D. J. Biomaterials and emerging anticancer therapeutics: engineering the microenvironment. *Nat. Rev. Cancer* **16**, 56–66 (2015).

156. De Gregorio, E. & Rappuoli, R. From empiricism to rational design: A personal perspective of the evolution of vaccine development. *Nature Reviews Immunology* **14**, 505–514 (2014).

157. McCarthy, E. F. The toxins of William B. Coley and the treatment of bone and soft-tissue sarcomas. *Iowa Orthop. J.* **26**, 154–158 (2006).

158. Gilbert, S. C. T-cell-inducing vaccines - what's the future. *Immunology* **135**, 19–26 (2012).

159. Schlom, J. *et al.* Therapeutic cancer vaccines. *Adv. Cancer Res.* **121**, 67–124 (2014).

160. Wang, J. *et al.* Choice of Nanovaccine Delivery Mode Has Profound Impacts on the Intralymph Node Spatiotemporal Distribution and Immunotherapy Efficacy. *Adv. Sci.* 2001108 (2020). doi:10.1002/advs.202001108

161. Irvine, D. J., Aung, A. & Silva, M. Controlling timing and location in vaccines. *Adv. Drug Deliv. Rev.* (2020). doi:10.1016/j.addr.2020.06.019

162. Reddy, S. T., Swartz, M. A. & Hubbell, J. A. Targeting dendritic cells with biomaterials: developing the next generation of vaccines. *Trends in Immunology* **27**, 573–579 (2006).

163. Liu, Z. & Roche, P. A. Macropinocytosis in phagocytes: Regulation of MHC class-

II-restricted antigen presentation in dendritic cells. *Frontiers in Physiology* **6**, (2015).

164. Foged, C., Brodin, B., Frokjaer, S. & Sundblad, A. Particle size and surface charge affect particle uptake by human dendritic cells in an in vitro model. in *International Journal of Pharmaceutics* **298**, 315–322 (Elsevier, 2005).
165. Henriksen-Lacey, M., Devitt, A. & Perrie, Y. The vesicle size of DDA:TDB liposomal adjuvants plays a role in the cell-mediated immune response but has no significant effect on antibody production. *J. Control. Release* **154**, 131–137 (2011).
166. Jarvis, C. M. *et al.* Antigen structure affects cellular routing through DC-SIGN. *Proc. Natl. Acad. Sci. U. S. A.* **116**, 14862–14867 (2019).
167. Chang, T. Z., Stadmiller, S. S., Staskevicius, E. & Champion, J. A. Effects of ovalbumin protein nanoparticle vaccine size and coating on dendritic cell processing. *Biomater. Sci.* **5**, 223–233 (2017).
168. Avraméas, A. *et al.* Expression of a mannose/fucose membrane lectin on human dendritic cells. *Eur. J. Immunol.* **26**, 394–400 (1996).
169. Shi, G. N. *et al.* Enhanced antitumor immunity by targeting dendritic cells with tumor cell lysate-loaded chitosan nanoparticles vaccine. *Biomaterials* **113**, 191–202 (2017).
170. Son, S. *et al.* Sugar-Nanocapsules Imprinted with Microbial Molecular Patterns for mRNA Vaccination. *Nano Lett.* **20**, 1499–1509 (2020).
171. Gulla, S. K. *et al.* In vivo targeting of DNA vaccines to dendritic cells using functionalized gold nanoparticles. *Biomater. Sci.* **7**, 773–788 (2019).

172. Hossain, M. K. & Wall, K. A. Use of dendritic cell receptors as targets for enhancing anti-cancer immune responses. *Cancers* **11**, (2019).

173. Zhou, J. J. *et al.* DEC205-DC targeted DNA vaccine against CX3CR1 protects against atherogenesis in mice. (2018). doi:10.1371/journal.pone.0195657

174. Schetters, S. T. T. *et al.* Mouse DC-SIGN/CD209a as target for antigen delivery and adaptive immunity. *Front. Immunol.* **9**, 1 (2018).

175. Picco, G., Beatson, R., Taylor-Papadimitriou, J. & Burchell, J. M. Targeting DNGR-1 (CLEC9A) with antibody/MUC1 peptide conjugates as a vaccine for carcinomas. *Eur. J. Immunol.* **44**, 1947–1955 (2014).

176. Park, H. Y. *et al.* Enhancing vaccine antibody responses by targeting Clec9A on dendritic cells. *npj Vaccines* **2**, 1–11 (2017).

177. Lu, L. *et al.* A Neonatal Fc Receptor-Targeted Mucosal Vaccine Strategy Effectively Induces HIV-1 Antigen-Specific Immunity to Genital Infection. *J. Virol.* **85**, 10542–10553 (2011).

178. Iborra, S. *et al.* The DC receptor DNGR-1 mediates cross-priming of CTLs during vaccinia virus infection in mice. *J. Clin. Invest.* **122**, 1628–1643 (2012).

179. Zelenay, S. *et al.* The dendritic cell receptor DNGR-1 controls endocytic handling of necrotic cell antigens to favor cross-priming of CTLs in virus-infected mice. *J. Clin. Invest.* **122**, 1615–1627 (2012).

180. Kamphorst, A. O., Guermonprez, P., Dudziak, D. & Nussenzweig, M. C. Route of Antigen Uptake Differentially Impacts Presentation by Dendritic Cells and Activated Monocytes. *J. Immunol.* **185**, 3426–3435 (2010).

181. Kim, C. G., Kye, Y. C. & Yun, C. H. The role of nanovaccine in cross-presentation

of antigen-presenting cells for the activation of CD8+ T cell responses. *Pharmaceutics* **11**, (2019).

182. Jones, K. S. Biomaterials as vaccine adjuvants. *Biotechnol. Prog.* **24**, 807–814 (2008).
183. Merad, M., Sathe, P., Helft, J., Miller, J. & Mortha, A. The dendritic cell lineage: Ontogeny and function of dendritic cells and their subsets in the steady state and the inflamed setting. *Annual Review of Immunology* **31**, 563–604 (2013).
184. Irvine, D. J., Hanson, M. C., Rakhra, K. & Tokatlian, T. Synthetic Nanoparticles for Vaccines and Immunotherapy. *Chemical Reviews* **115**, 11109–11146 (2015).
185. Ke, X. *et al.* Physical and chemical profiles of nanoparticles for lymphatic targeting. *Advanced Drug Delivery Reviews* **151**–**152**, 72–93 (2019).
186. Liu, H. *et al.* Structure-based programming of lymph-node targeting in molecular vaccines. *Nature* **507**, 519–522 (2014).
187. Schudel, A. *et al.* Programmable multistage drug delivery to lymph nodes. *Nat. Nanotechnol.* **15**, 491–499 (2020).
188. McLennan, D. N., Porter, C. J. H. & Charman, S. A. Subcutaneous drug delivery and the role of the lymphatics. *Drug Discovery Today: Technologies* **2**, 89–96 (2005).
189. Zhang, Y.-N., Poon, W., Sefton, E. & Chan, W. C. W. Suppressing Subcapsular Sinus Macrophages Enhances Transport of Nanovaccines to Lymph Node Follicles for Robust Humoral Immunity. *ACS Nano* (2020). doi:10.1021/acsnano.0c02240
190. Shakya, A. K. & Nandakumar, K. S. Antigen-Specific Tolerization and Targeted

Delivery as Therapeutic Strategies for Autoimmune Diseases. *Trends in Biotechnology* **36**, 686–699 (2018).

191. Li, X., Wang, X., Ito, A. & Tsuji, N. M. A nanoscale metal organic frameworks-based vaccine synergises with PD-1 blockade to potentiate anti-tumour immunity. *Nat. Commun.* **11**, 1–15 (2020).
192. Joffre, O. P., Segura, E., Savina, A. & Amigorena, S. Cross-presentation by dendritic cells. *Nature Reviews Immunology* **12**, 557–569 (2012).
193. Tsoras, A. N., Wong, K. M., Paravastu, A. K. & Champion, J. A. Rational Design of Antigen Incorporation Into Subunit Vaccine Biomaterials Can Enhance Antigen-Specific Immune Responses. *Front. Immunol.* **11**, 1547 (2020).
194. Duong, H. T. T. *et al.* Degradation-regulated architecture of injectable smart hydrogels enhances humoral immune response and potentiates antitumor activity in human lung carcinoma. *Biomaterials* **230**, 119599 (2020).
195. Kim, J. *et al.* Injectable, spontaneously assembling, inorganic scaffolds modulate immune cells in vivo and increase vaccine efficacy. *Nat. Biotechnol.* **33**, 64–72 (2015).
196. Shah, N. J. *et al.* A biomaterial-based vaccine eliciting durable tumour-specific responses against acute myeloid leukaemia. *Nat. Biomed. Eng.* **4**, 40–51 (2020).
197. Nguyen, T. L., Cha, B. G., Choi, Y., Im, J. & Kim, J. Injectable dual-scale mesoporous silica cancer vaccine enabling efficient delivery of antigen/adjuvant-loaded nanoparticles to dendritic cells recruited in local macroporous scaffold. *Biomaterials* **239**, 119859 (2020).
198. Li, W. A. *et al.* The effect of surface modification of mesoporous silica micro-rod

scaffold on immune cell activation and infiltration. *Biomaterials* **83**, 249–256 (2016).

199. Yan, J., Chen, R., Zhang, H. & Bryers, J. D. Injectable Biodegradable Chitosan-Alginate 3D Porous Gel Scaffold for mRNA Vaccine Delivery. *Macromol. Biosci.* **19**, e1800242 (2019).
200. González, F. E. *et al.* Tumor cell lysates as immunogenic sources for cancer vaccine design. *Hum. Vaccin. Immunother.* **10**, 3261–3269 (2014).
201. Aerts, J. G. J. V *et al.* Autologous Dendritic Cells Pulsed with Allogeneic Tumor Cell Lysate in Mesothelioma: From Mouse to Human. *Clin. Cancer Res.* **24**, 766 LP – 776 (2018).
202. Tanyi, J. L. *et al.* Personalized cancer vaccine effectively mobilizes antitumor T cell immunity in ovarian cancer. *Sci. Transl. Med.* **10**, eaao5931 (2018).
203. Bencherif, S. A. *et al.* Injectable cryogel-based whole-cell cancer vaccines. *Nat. Commun.* **6**, 7556 (2015).
204. Ali, O. a, Huebsch, N., Cao, L., Dranoff, G. & Mooney, D. J. Infection-mimicking materials to program dendritic cells in situ. *Nat. Mater.* **8**, 151–158 (2009).
205. Dendritic Cell Activating Scaffold in Melanoma. *ClinicalTrials.gov* (2017). Available at: https://clinicaltrials.gov/ct2/show/nct01753089.
206. Andorko, J. I., Hess, K. L., Pineault, K. G. & Jewell, C. M. Intrinsic immunogenicity of rapidly-degradable polymers evolves during degradation. *Acta Biomater.* **32**, 24–34 (2016).
207. Saung, M. T., Ke, X., Howard, G. P., Zheng, L. & Mao, H. Q. Particulate carrier systems as adjuvants for cancer vaccines. *Biomater. Sci.* **7**, 4873–4887 (2019).

208. Wang, H. & Mooney, D. J. Biomaterial-assisted targeted modulation of immune cells in cancer treatment. *Nat. Mater.* **17**, 761–772 (2018).

209. Hollingsworth, R. E. & Jansen, K. Turning the corner on therapeutic cancer vaccines. *npj Vaccines* **4**, 7 (2019).

210. Gajewski, T. F. & Cron, K. R. cDC1 dysregulation in cancer: An opportunity for intervention. *J. Exp. Med.* **217**, (2020).

211. Cervantes, J. L. & Doan, A. H. Discrepancies in the evaluation of the safety of the human papillomavirus vaccine. *Mem. Inst. Oswaldo Cruz* **113**, 1–4 (2018).

212. Martínez-Lavín, M. & Amezcua-Guerra, L. Serious adverse events after HPV vaccination: a critical review of randomized trials and post-marketing case series. *Clin. Rheumatol.* **36**, 2169–2178 (2017).

213. Kosmides, A. K. *et al.* Biomimetic biodegradable artificial antigen presenting cells synergize with PD-1 blockade to treat melanoma. *Biomaterials* **118**, 16–26 (2017).

214. Caserta, S., Alessi, P., Guarnerio, J., Basso, V. & Mondino, A. Synthetic CD4+ T Cell-Targeted Antigen-Presenting Cells Elicit Protective Antitumor Responses. *Cancer Res.* **68**, 3010–3018 (2008).

215. Schudel, A., Francis, D. M. & Thomas, S. N. Material design for lymph node drug delivery. *Nature Reviews Materials* **4**, 415–428 (2019).

216. Bahmani, B. *et al.* Targeted delivery of immune therapeutics to lymph nodes prolongs cardiac allograft survival. *J. Clin. Invest.* **128**, 4770–4786 (2018).

217. Sun, L. *et al.* DNA-Edited Ligand Positioning on Red Blood Cells to Enable Optimized T Cell Activation for Adoptive Immunotherapy. *Angew. Chemie Int. Ed.* **59**, 14842–14853 (2020).

218. Shen, C. *et al.* Latex bead-based artificial antigen-presenting cells induce tumor-specific CTL responses in the native T-cell repertoires and inhibit tumor growth. *Immunol. Lett.* **150**, 1–11 (2013).

219. Quayle, S. N. *et al.* Cue-101, a novel E7-pHLA-IL2-Fc fusion protein, enhances tumor antigen-specific T-cell activation for the treatment of HPV16-driven malignancies. *Clin. Cancer Res.* **26**, 1953 LP – 1964 (2020).

220. Vinay, D. S. & Kwon, B. S. 4-1BB (CD137), an inducible costimulatory receptor, as a specific target for cancer therapy. *BMB Rep.* **47**, 122–129 (2014).

221. Fam, S. Y. *et al.* Stealth Coating of Nanoparticles in Drug-Delivery Systems. *Nanomaterials* **10**, 787 (2020).

222. Weiden, J. *et al.* Injectable Biomimetic Hydrogels as Tools for Efficient T Cell Expansion and Delivery. *Front. Immunol.* **9**, (2018).

223. D'angelo, S. P. *et al.* Antitumor activity associated with prolonged persistence of adoptively transferred NY-ESO-1c259T cells in synovial sarcoma. *Cancer Discov.* **8**, 944–957 (2018).

224. Pérez del Río, E. *et al.* CCL21-loaded 3D hydrogels for T cell expansion and differentiation. *Biomaterials* **259**, 120313 (2020).

225. Suematsu, S. & Watanabe, T. Generation of a synthetic lymphoid tissue-like organoid in mice. *Nat. Biotechnol.* **22**, 1539–1545 (2004).

226. Okamoto, N., Chihara, R., Shimizu, C., Nishimoto, S. & Watanabe, T. Artificial lymph nodes induce potent secondary immune responses in naive and immunodeficient mice. *J. Clin. Invest.* **117**, 997–1007 (2007).

227. Kobayashi, Y. & Watanabe, T. Gel-trapped lymphorganogenic chemokines trigger

artificial tertiary lymphoid organs and mount adaptive immune responses in vivo. *Front. Immunol.* **7**, 316 (2016).

228. Shah, N. J. *et al.* An injectable bone marrow–like scaffold enhances T cell immunity after hematopoietic stem cell transplantation. *Nat. Biotechnol.* **37**, 293–302 (2019).
229. Robbins, P. F. *et al.* Cutting Edge: Persistence of Transferred Lymphocyte Clonotypes Correlates with Cancer Regression in Patients Receiving Cell Transfer Therapy. *J. Immunol.* **173**, 7125–7130 (2004).
230. Jafarzadeh, L., Masoumi, E., Fallah-Mehrjardi, K., Mirzaei, H. R. & Hadjati, J. Prolonged Persistence of Chimeric Antigen Receptor (CAR) T Cell in Adoptive Cancer Immunotherapy: Challenges and Ways Forward. *Frontiers in Immunology* **11**, 702 (2020).
231. Ochyl, L. J. & Moon, J. J. Dendritic Cell Membrane Vesicles for Activation and Maintenance of Antigen-Specific T Cells. *Adv. Healthc. Mater.* **8**, 1801091 (2018).
232. Smith, T. T. *et al.* Biopolymers codelivering engineered T cells and STING agonists can eliminate heterogeneous tumors. *J. Clin. Invest.* **127**, 2176–2191 (2017).
233. Zhang, Q. *et al.* Biomimetic Magnetosomes as Versatile Artificial Antigen-Presenting Cells to Potentiate T-Cell-Based Anticancer Therapy. *ACS Nano* **11**, 10724–10732 (2017).
234. Tzeng, S. Y. *et al.* In situ genetic engineering of tumors for long-lasting and systemic immunotherapy. *Proc. Natl. Acad. Sci. U. S. A.* **117**, 4043–4052 (2020).
235. Huang, K. W. *et al.* Highly efficient and tumor-selective nanoparticles for dual-

targeted immunogene therapy against cancer. *Sci. Adv.* **6**, eaax5032 (2020).

236. Hargadon, K. M., Johnson, C. E. & Williams, C. J. Immune checkpoint blockade therapy for cancer: An overview of FDA-approved immune checkpoint inhibitors. *International Immunopharmacology* **62**, 29–39 (2018).

237. Kato, D. *et al.* Prospects for personalized combination immunotherapy for solid tumors based on adoptive cell therapies and immune checkpoint blockade therapies. *Nihon Rinsho Meneki. Gakkai Kaishi* **40**, 68–77 (2017).

238. Schmid, D. *et al.* T cell-targeting nanoparticles focus delivery of immunotherapy to improve antitumor immunity. *Nat. Commun.* **8**, 1–12 (2017).

239. Luo, L. *et al.* Sustained release of anti-PD-1 peptide for perdurable immunotherapy together with photothermal ablation against primary and distant tumors. *J. Control. Release* **278**, 87–99 (2018).

240. Zhang, N. *et al.* Photothermal therapy mediated by phase-transformation nanoparticles facilitates delivery of anti-PD1 antibody and synergizes with antitumor immunotherapy for melanoma. *J. Control. Release* **306**, 15–28 (2019).

241. Ordikhani, F. *et al.* Targeting antigen-presenting cells by anti-PD-1 nanoparticles augments antitumor immunity. *JCI insight* **3**, (2018).

242. Kosmides, A. K., Sidhom, J.-W., Fraser, A., Bessell, C. A. & Schneck, J. P. Dual Targeting Nanoparticle Stimulates the Immune System To Inhibit Tumor Growth. *ACS Nano* **11**, 5417–5429 (2017).

243. Houot, R., Schultz, L. M., Marabelle, A. & Kohrt, H. T-cell-based Immunotherapy: Adoptive Cell Transfer and Checkpoint Inhibition. *Cancer Immunol. Res.* (2015). doi:10.1158/2326-6066.cir-15-0190

244. Foley, K. C., Nishimura, M. I. & Moore, T. V. Combination immunotherapies implementing adoptive T-cell transfer for advanced-stage melanoma. *Melanoma Research* **28**, 171–184 (2018).

245. Antigen-specific T Cell Therapy for Patients With Relapsed Refractory Multiple Myeloma. *ClinicalTrials.gov* (2020). Available at: https://www.clinicaltrials.gov/ct2/show/NCT04505813.

246. Antigen-specific T Cell Therapy for AML or MDS Patients With Relapsed Disease After Allo-HCT. *ClinicalTrials.gov* (2020). Available at: https://www.clinicaltrials.gov/ct2/show/NCT04284228.

247. Tsai, S. *et al.* Reversal of Autoimmunity by Boosting Memory-like Autoregulatory T Cells. *Immunity* **32**, 568–580 (2010).

248. Clemente-Casares, X. *et al.* Expanding antigen-specific regulatory networks to treat autoimmunity. *Nature* **530**, 434–440 (2016).

249. Riddell, S. R. *et al.* T–cell mediated rejection of gene–modified HIV–specific cytotoxic T lymphocytes in HIV–infected patients. *Nat. Med.* **2**, 216 (1996).

250. Walter, E. A. *et al.* Reconstitution of cellular immunity against cytomegalovirus in recipients of allogeneic bone marrow by transfer of T-cell clones from the donor. *N. Engl. J. Med.* **333**, 1038–1044 (1995).

251. Fesnak, A. D., June, C. H. & Levine, B. L. Engineered T cells: The promise and challenges of cancer immunotherapy. *Nat. Rev. Cancer* **16**, 566–581 (2016).

252. Rapoport, A. P. *et al.* NY-ESO-1–specific TCR–engineered T cells mediate sustained antigen-specific antitumor effects in myeloma. *Nat. Med.* **21**, 914 (2015).

253. Davis, M. M. & Bjorkman, P. J. T-cell antigen receptor genes and T-cell recognition. *Nature* **334**, 395 (1988).

254. Jenkins, M. K. & Moon, J. J. The role of naive T cell precursor frequency and recruitment in dictating immune response magnitude. *J. Immunol.* **188**, 4135–4140 (2012).

255. Newell, E. W. & Davis, M. M. Beyond model antigens: high-dimensional methods for the analysis of antigen-specific T cells. *Nat. Biotechnol.* **32**, 149 (2014).

256. Altman, J. D. *et al.* Phenotypic analysis of antigen-specific T lymphocytes. *Science (80-.).* **274**, 94–96 (1996).

257. Han, Q., Bradshaw, E. M., Nilsson, B., Hafler, D. A. & Love, J. C. Multidimensional analysis of the frequencies and rates of cytokine secretion from single cells by quantitative microengraving. *Lab Chip* **10**, 1391–1400 (2010).

258. Betts, M. R. *et al.* Sensitive and viable identification of antigen-specific CD8+ T cells by a flow cytometric assay for degranulation. *J. Immunol. Methods* **281**, 65–78 (2003).

259. Frentsch, M. *et al.* Direct access to CD4+ T cells specific for defined antigens according to CD154 expression. *Nat. Med.* **11**, 1118 (2005).

260. Newell, E. W., Sigal, N., Bendall, S. C., Nolan, G. P. & Davis, M. M. Cytometry by time-of-flight shows combinatorial cytokine expression and virus-specific cell niches within a continuum of CD8+ T cell phenotypes. *Immunity* **36**, 142–152 (2012).

261. Day, C. L. *et al.* Ex vivo analysis of human memory CD4 T cells specific for hepatitis C virus using MHC class II tetramers. *J. Clin. Invest.* **112**, 831–842

(2003).

262. Rodenko, B. *et al.* Generation of peptide–MHC class I complexes through UV-mediated ligand exchange. *Nat. Protoc.* **1**, 1120 (2006).

263. Hadrup, S. R. *et al.* Parallel detection of antigen-specific T-cell responses by multidimensional encoding of MHC multimers. *Nat. Methods* **6**, 520 (2009).

264. Newell, E. W., Klein, L. O., Yu, W. & Davis, M. M. Simultaneous detection of many T-cell specificities using combinatorial tetramer staining. *Nat. Methods* **6**, 497 (2009).

265. Gee, M. H. *et al.* Antigen identification for orphan T cell receptors expressed on tumor-infiltrating lymphocytes. *Cell* **172**, 549–563 (2018).

266. Inaba, K., Young, J. W. & Steinman, R. M. Direct activation of CD8+ cytotoxic T lymphocytes by dendritic cells. *J. Exp. Med.* **166**, 182–194 (1987).

267. Novy, P., Quigley, M., Huang, X. & Yang, Y. CD4 T Cells Are Required for CD8 T Cell Survival during Both Primary and Memory Recall Responses. *J. Immunol.* **179**, 8243 LP – 8251 (2007).

268. Bessell, C. A. *et al.* Commensal bacteria stimulate antitumor responses via T cell cross-reactivity. *JCI Insight* **5**, (2020).

269. Yarchoan, M., Johnson III, B. A., Lutz, E. R., Laheru, D. A. & Jaffee, E. M. Targeting neoantigens to augment antitumour immunity. *Nat. Rev. Cancer* **17**, 209 (2017).

270. Schumacher, T. N. & Schreiber, R. D. Neoantigens in cancer immunotherapy. *Science (80-.).* **348**, 69–74 (2015).

271. Abiko, K. *et al.* IFN-γ from lymphocytes induces PD-L1 expression and promotes

progression of ovarian cancer. *Br. J. Cancer* **112**, 1501 (2015).

272. Sahin, U. *et al.* Personalized RNA mutanome vaccines mobilize poly-specific therapeutic immunity against cancer. *Nature* **547**, 222–226 (2017).

273. González, S., Volkova, N., Beer, P. & Gerstung, M. Immuno-oncology from the perspective of somatic evolution. *Semin. Cancer Biol.* **52**, 75–85 (2018).

274. Sarkizova, S. & Hacohen, N. How T cells spot tumour cells. *Nature* **551**, 444–446 (2017).

275. Topalian, S. L., Taube, J. M., Anders, R. A. & Pardoll, D. M. Mechanism-driven biomarkers to guide immune checkpoint blockade in cancer therapy. *Nat. Rev. Cancer* **16**, 275–287 (2016).

276. Castle, J. C. *et al.* Exploiting the mutanome for tumor vaccination. *Cancer Res.* **72**, 1081–1091 (2012).

277. Hickey, J. W. & Schneck, J. P. Enrich and Expand Rare Antigen-specific T Cells with Magnetic Nanoparticles. *JoVE (Journal Vis. Exp.* e58640 (2018).

278. Kreiter, S. *et al.* Mutant MHC class II epitopes drive therapeutic immune responses to cancer. *Nature* **520**, 692–6 (2015).

279. Quezada, S. A. *et al.* Tumor-reactive CD4(+) T cells develop cytotoxic activity and eradicate large established melanoma after transfer into lymphopenic hosts. *J. Exp. Med.* **207**, 637–650 (2010).

280. Perez-diez, A. *et al.* CD4 cells can be more efficient at tumor rejection than CD8 cells. *Blood* **109**, 5346–5355 (2016).

281. Antony, P. A. *et al.* CD8+ T cell immunity against a tumor/self-antigen is augmented by CD4+ T helper cells and hindered by naturally occurring T

regulatory cells. *J. Immunol.* **174**, 2591–2601 (2005).

282. Bourgeois, C. & Tanchot, C. CD4 T cells are required for CD8 T cell memory generation. *Eur. J. Immunol.* **33**, 3225–3231 (2003).

283. Schietinger, A., Philip, M., Liu, R. B., Schreiber, K. & Schreiber, H. Bystander killing of cancer requires the cooperation of CD4(+) and CD8(+) T cells during the effector phase. *J. Exp. Med.* **207**, 2469–2477 (2010).

284. Li, K. *et al.* Adoptive cell therapy with CD4+ T helper 1 cells and CD8+ cytotoxic T cells enhances complete rejection of an established tumour, leading to generation of endogenous memory responses to non-targeted tumour epitopes. *Clin. Transl. Immunol.* **6**, e160 (2017).

285. Grupp, S. A. *et al.* Chimeric antigen receptor-modified T cells for acute lymphoid leukemia. *N. Engl. J. Med.* **368**, 1509–1518 (2013).

286. Porter, D. L., Levine, B. L., Kalos, M., Bagg, A. & June, C. H. Chimeric Antigen Receptor–Modified T Cells in Chronic Lymphoid Leukemia. *N. Engl. J. Med.* **365**, 725–733 (2011).

287. Isser, A., Livingston, N. K. & Schneck, J. P. Biomaterials to enhance antigen-specific T cell expansion for cancer immunotherapy. *Biomaterials* **268**, 120584 (2021).

288. Alspach, E. *et al.* MHC-II neoantigens shape tumour immunity and response to immunotherapy. *Nature* **574**, 696–701 (2019).

289. Mumberg, D. *et al.* CD4+ T cells eliminate MHC class II-negative cancer cells in vivo by indirect effects of IFN-γ. *Proc. Natl. Acad. Sci.* **96**, 8633 LP – 8638 (1999).

290. Hung, K. *et al.* The Central Role of CD4(+) T Cells in the Antitumor Immune

Response . *J. Exp. Med.* **188**, 2357–2368 (1998).

291. Borst, J., Ahrends, T., Bąbała, N., Melief, C. J. M. & Kastenmüller, W. CD4+ T cell help in cancer immunology and immunotherapy. *Nat. Rev. Immunol.* **18**, 635–647 (2018).

292. Sugata, K. *et al.* Affinity-matured HLA class II dimers for robust staining of antigen-specific CD4+ T cells. *Nat. Biotechnol.* **39**, 958–967 (2021).

293. Tay, R. E., Richardson, E. K. & Toh, H. C. Revisiting the role of CD4+ T cells in cancer immunotherapy—new insights into old paradigms. *Cancer Gene Ther.* **28**, 5–17 (2021).

294. Oelke, M. *et al.* Generation and purification of CD8+ melan-A-specific cytotoxic T lymphocytes for adoptive transfer in tumor immunotherapy. *Clin. Cancer Res.* **6**, 1997–2005 (2000).

295. Cameron, T. O., Cochran, J. R., Yassine-Diab, B., Sékaly, R.-P. & Stern, L. J. Cutting Edge: Detection of Antigen-Specific CD4+ T Cells by HLA-DR1 Oligomers Is Dependent on the T Cell Activation State. *J. Immunol.* **166**, 741 LP – 745 (2001).

296. Moon, J. J. *et al.* Naive CD4(+) T cell frequency varies for different epitopes and predicts repertoire diversity and response magnitude. *Immunity* **27**, 203–213 (2007).

297. Oh, D. Y. *et al.* Intratumoral CD4(+) T Cells Mediate Anti-tumor Cytotoxicity in Human Bladder Cancer. *Cell* **181**, 1612-1625.e13 (2020).

298. Cachot, A. *et al.* Tumor-specific cytolytic CD4 T cells mediate immunity against human cancer. *Sci. Adv.* **7**, eabe3348 (2021).

299. Melenhorst, J. J. *et al.* Decade-long leukaemia remissions with persistence of CD4+ CAR T cells. *Nature* **602**, 503–509 (2022).

300. Rhodes, K. R. *et al.* Biodegradable Cationic Polymer Blends for Fabrication of Enhanced Artificial Antigen Presenting Cells to Treat Melanoma. *ACS Appl. Mater. Interfaces* **13**, 7913–7923 (2021).

301. Zander, R. *et al.* CD4(+) T Cell Help Is Required for the Formation of a Cytolytic CD8(+) T Cell Subset that Protects against Chronic Infection and Cancer. *Immunity* **51**, 1028-1042.e4 (2019).

302. Gigante, M. *et al.* Dysfunctional DC subsets in RCC patients: ex vivo correction to yield an effective anti-cancer vaccine. *Mol. Immunol.* **46**, 893–901 (2009).

303. Wculek, S. K. *et al.* Dendritic cells in cancer immunology and immunotherapy. *Nat. Rev. Immunol.* **20**, 7–24 (2020).

304. Śledzińska, A. *et al.* Regulatory T Cells Restrain Interleukin-2- and Blimp-1-Dependent Acquisition of Cytotoxic Function by CD4+ T Cells. *Immunity* **52**, 151-166.e6 (2020).

305. Dennis, K. L., Blatner, N. R., Gounari, F. & Khazaie, K. Current status of interleukin-10 and regulatory T-cells in cancer. *Curr. Opin. Oncol.* **25**, 637–645 (2013).

306. Steinbrink, K., Graulich, E., Kubsch, S., Knop, J. & Enk, A. H. CD4+ and CD8+ anergic T cells induced by interleukin-10–treated human dendritic cells display antigen-specific suppressor activity. *Blood* **99**, 2468–2476 (2002).

307. Groux, H., Bigler, M., de Vries, J. E. & Roncarolo, M.-G. Inhibitory and Stimulatory Effects of IL-10 on Human CD8+ T Cells. *J. Immunol.* **160**, 3188 LP – 3193

(1998).

308. Naing, A. *et al.* PEGylated IL-10 (Pegilodecakin) Induces Systemic Immune Activation, CD8+ T Cell Invigoration and Polyclonal T Cell Expansion in Cancer Patients. *Cancer Cell* **34**, 775-791.e3 (2018).
309. Emmerich, J. *et al.* IL-10 Directly Activates and Expands Tumor-Resident CD8+ T Cells without De Novo Infiltration from Secondary Lymphoid Organs. *Cancer Res.* **72**, 3570 LP – 3581 (2012).
310. Mumm, J. B. *et al.* IL-10 Elicits IFNγ-Dependent Tumor Immune Surveillance. *Cancer Cell* **20**, 781–796 (2011).
311. Saxton, R. A. *et al.* Structure-based decoupling of the pro- and anti-inflammatory functions of interleukin-10. *Science (80-.).* **371**, eabc8433 (2021).
312. Drover, S., Karr, R. W., Fu, X.-T. & Marshall, W. H. Analysis of monoclonal antibodies specific for unique and shared determinants on HLA-DR4 molecules. *Hum. Immunol.* **40**, 51–60 (1994).
313. Lutz, M. B. *et al.* An advanced culture method for generating large quantities of highly pure dendritic cells from mouse bone marrow. *J. Immunol. Methods* **223**, 77–92 (1999).
314. Galeano Niño, J. L. *et al.* Cytotoxic T cells swarm by homotypic chemokine signalling. *Elife* **9**, e56554 (2020).
315. Hennecke, J., Carfi, A. & Wiley, D. C. Structure of a covalently stabilized complex of a human alphabeta T-cell receptor, influenza HA peptide and MHC class II molecule, HLA-DR1. *EMBO J.* **19**, 5611–5624 (2000).
316. Wagner, E. K. *et al.* Human cytomegalovirus-specific T-cell receptor engineered

for high affinity and soluble expression using mammalian cell display. *J. Biol. Chem.* **294**, 5790–5804 (2019).

317. Wrzesinski, C. *et al.* Increased intensity lymphodepletion enhances tumor treatment efficacy of adoptively transferred tumor-specific T cells. *J. Immunother. (Hagerstown, Md. 1997)* **33**, 1 (2010).

318. Sidhom, J.-W. *et al.* ImmunoMap: A Bioinformatics Tool for T-Cell Repertoire Analysis. *Cancer Immunol. Res.* canimm.0114.2017 (2017). doi:10.1158/2326-6066.CIR-17-0114

319. Isser, A., Yoshida, T., Ichikawa, J., Weber, J. & Schneck, J. A conserved MART-1 T cell receptor motif is predictive of responses to checkpoint blockade. in *JOURNAL FOR IMMUNOTHERAPY OF CANCER* **7**, (BMC CAMPUS, 4 CRINAN ST, LONDON N1 9XW, ENGLAND, 2019).

320. Dobson, C. S. *et al.* Antigen identification and high-throughput interaction mapping by reprogramming viral entry. *Nat. Methods* **19**, 449–460 (2022).

321. J., G. X. & J., E. S. V-CARMA: A tool for the detection and modification of antigen-specific T cells. *Proc. Natl. Acad. Sci.* **119**, e2116277119 (2022).

Curriculum Vitae

Ariel Isser was born in 1993 in Silver Spring, Maryland.

Ariel did his undergraduate work in Bioengineering at University of Maryland, where he received numerous honors including the *Most Outstanding Senior* award, researched in three laboratories, co-founded an *AEMB* Biomedical Engineering Honors Society Chapter, and established a departmental tutoring program.

In his Ph.D. in Biomedical Engineering at Johns Hopkins, Ariel received *NSF* and *NIH F31* Fellowships and was selected as a 2022 Siebel Scholar in Bioengineering. He mentored 12 students (three undergraduate and nine graduate) and together produced 8 publications and 10 national conference presentations, with multiple research awards.

Beyond research, Ariel designed and taught an undergraduate *Immunoengineering* course, mentored three Baltimore City high school students through P-TECH, and served as Education Chair for the Ph.D. Council. As an executive board member of BME EDGE, a student-run professional development organization, for four years and co-chair for two, Ariel helped implement department-wide changes to enhance professional development training.